Dissertation zur Erlangung des Doktorgrades

der Fakultät für Chemie und Pharmazie

der Ludwig-Maximilians-Universität München

The role of
integrins and cytoskeletal forces
in interstitial leukocyte migration

Tim Lämmermann

aus

Fürth

2009

1 Table of contents

2 List of Publications

The thesis is based on the following publications which are referred to in the text by their Roman numerals (I–VII):

I. Haiyan Chu, Ingo Thievessen, Michael Sixt, **Tim Lämmermann**, Ari Waisman, Attila Braun, Angelika A. Noegel, Reinhard Fässler.
γ-Parvin is dispensable for hematopoiesis, leukocyte trafficking, and T-cell-dependent antibody response.
Molecular and Cellular Biology. 2006 Mar; 26(5):1817-25.

II. Michael Sixt, Martina Bauer, **Tim Lämmermann**, Reinhard Fässler.
β1 integrins: zip codes and signaling relay for blood cells.
Current Opinion in Cell Biology. 2006 Oct; 18(5):482-90. Review.

III. Zerina Lokmic*, **Tim Lämmermann***, Michael Sixt, Susanna Cardell, Rupert Hallmann, Lydia Sorokin.
The extracellular matrix of the spleen as a potential organizer of immune cell compartments.
Seminars in Immunology. 2008 Feb; 20(1):4-13. Review.
* equally contributing first authors.

IV. **Tim Lämmermann**, Michael Sixt.
The microanatomy of T-cell responses.
Immunological Reviews. 2008 Feb; 221:26-43. Review.

V. **Tim Lämmermann**, Bernhard L. Bader, Susan J. Monkley, Tim Worbs, Roland Wedlich-Söldner, Karin Hirsch, Markus Keller, Reinhold Förster, David R. Critchley, Reinhard Fässler, Michael Sixt.
Rapid leukocyte migration by integrin-independent flowing and squeezing.
Nature. 2008 May 1; 453(7191):51-5.

VI. Kai Kessenbrock, Leopold Fröhlich, Michael Sixt, **Tim Lämmermann**, Andrew Bateman, Azzaq Belaaouaj, Johannes Ring, Markus Ollert, Reinhard Fässler, Dieter E. Jenne.
Proteinase 3 and neutrophil elastase enhance inflammation by inactivating anti-inflammatory progranulin.
Journal of Clinical Investigations. 2008 Jul; 118(7):2438-47.

VII. **Tim Lämmermann** , Jörg Renkawitz, Xunwei Wu, Karin Hirsch, Cord Brakebusch, Michael Sixt.
Cdc42-dependent leading edge coordination is essential for interstitial dendritic cell migration.
Blood. 2009 Jun 4; 113(23):5703-10. Epub 2009 Feb 3.

Reprints were made with permission from the publisher.

3   Abbreviations

2D	two-dimensional	LFA-1	lymphocyte function-associated antigen 1
3D	three-dimensional		
APC	antigen-presenting cell	LN	lymph node
Arp2/3	actin-related protein 2/3	Mac-1	macrophage antigen 1
BM	basement membrane	MAdCAM-1	mucosal vascular addressin cell adhesion molecule 1
CalDAG	Ca^{2+} and diacylglycerol-regulated guanine nucleotide exchange factor		
		MHC	major histocompatibility complex
CCL	CC-chemokine ligand	MMP	matrix metalloproteinase
CCR	CC-chemokine receptor	MSP	major sperm protein
CD	cluster of differentiation	PECAM-1	platelet/endothelial cell adhesion molecule 1
Cdc42	cell division cycle 42		
CLEVER-1	common lymphatic endothelial and vascular endothelial receptor 1	PGC	primordial germ cell
		PI3K	phosphoinositide-3 kinase
CXCL	CXC-chemokine ligand	PIP_3	phosphoinositol-3,4,5-triphosphate
CXCR	CXC-chemokine receptor	PNAd	peripheral lymph node addressin
DC	dendritic cell	PPs	Peyer's patches
dDC	dermal dendritic cell	PSGL-1	P-selectin glycoprotein ligand 1
ECM	extracellular matrix	PTB	phospho-tyrosine binding
ESAM	endothelial cell-selective adhesion molecule	Rac	ras-related C3 botulinum toxin substrate
FERM	4.1, ezrin, radixin, moesin	Rap1	Ras-associated protein 1
FRC	fibroblastic reticular cell	RAPL	regulator of cell polarization and adhesion enriched in lymphoid tissues
GDP	guanosine-5'-diphosphate		
GEF	guanine nucleotide exchange factor		
GTP	guanosine-5'-triphosphate	Rho	Ras-homologous
GTPase	guanine nucleoside triphosphatase	ROCK	Rho-associated kinase
HEV	high endothelial venule	S1P	sphingosine-1-phosphate
ICAM-1	intercellular adhesion molecule 1	SadA	substrate adhesion-deficient A
IL-1β	interleukin 1β	SLO	secondary lymphoid organ
JAM-A	junctional adhesion molecule A	VCAM-1	vascular cell adhesion molecule 1
LAD	leukocyte adhesion deficiency	VE-cadherin	vascular endothelial cadherin
LC	Langerhans cell	WASp	Wiskott-Aldrich syndrome protein
LEC	lymphatic endothelial cell		

4   Summary

Both innate and adaptive immune responses rely on rapid leukocyte trafficking. Most leukocytes continuously scan the body and recirculate between blood, peripheral tissues and the lymphatic system. Physiological leukocyte movement can be subdivided into two-dimensional (2D) and three-dimensional (3D) migratory events. The two migration modes likely differ mechanistically, although the precise differences were unknown and highly debated when I started my thesis work. During extravasation, leukocytes undergo a multistep adhesion cascade along the 2D surface of the blood endothelium. Here, selectin-mediated rolling along the endothelium promotes sensing of chemokines that are immobilized on the vascular lumen. This induces activation of integrin function which triggers leukocyte arrest and then crawling along the vessel wall. Integrin-mediated adhesion serves to couple the forces of actin polymerization and actomyosin contraction to 2D surfaces and thereby enables the cell to locomote. While integrin functions during extravasation have been studied in detail, it is controversial if integrin-mediated adhesion also contributes to 3D leukocyte movement in interstitial tissues (**reviewed in Paper II**). Although it is often equated with crawling of amoeboid-shaped cells on 2D surfaces where locomotion mechanics have been already assessed, leukocyte interstitial migration lacks a solid mechanical and molecular framework. Moreover, the generalization of findings in other amoeboid cells might cause problems, as the ambiguous definition of "amoeboid migration" comprises multiple locomotion modes, which range from contraction-based blebbing to entirely protrusive migration.

This Ph.D. thesis sought to study the interplay between adhesive, contractile and protrusive forces in the physiological interstitial movement of leukocytes. Dendritic cells (DCs) served as a model system as their migration route from the skin via afferent lymphatic vessels to the draining lymph node leads through different interstitial environments (**reviewed in Paper IV**). As DCs express at least eight integrin heterodimers and the molecular composition of the tissue compartments might favour adhesive interactions (**reviewed in Paper III and IV**), we hypothesized that DCs employ integrins to generate adhesion-mediated traction for 3D locomotion. To investigate the role integrins play during leukocyte migration, we employed a combinatorial mouse genetics approach to delete four integrin key subunits and thus deplete all integrin heterodimers from the surface of leukocytes (**Paper V**). Surprisingly, migration speeds of DCs, granulocytes and B cells in 3D collagen gels and DCs in dermal skin and lymph nodes were unaltered. In contrast, adhesion to 2D *in vitro* surfaces and leukocyte extravasation *in vivo* was severely impaired in the absence of integrins. We obtained similar

results when genetically deleting talin1, a major regulator of integrin activation (**Paper V**). Accordingly, after genetically deleting γ-parvin which contributes to a molecular complex linking integrins to the cytoskeleton, DC trafficking was also normal (**Paper I**). These experiments convincingly showed that for interstitial leukocyte migration integrin-mediated traction forces are dispensable. Pharmacological inhibition of actomyosin contraction and actin polymerisation revealed the major cellular forces that drive leukocyte migration through interstitial meshworks: The sole force of actin-network expansion at the leading edge is sufficient for 3D movement. Auxiliary myosin II-dependent contraction is only required on passage through narrow gaps, where a squeezing contraction of the trailing edge propels the rigid nucleus. Having established protrusive actin flow as a major driving force, we further addressed the question how coordination of actin flow influences 3D leukocyte migration (**Paper VII**). We therefore employed DCs lacking the small GTPase Cdc42. These cells still initiated actin flow and actomyosin contraction in response to chemotactic cues, but lacked temporal and spatial regulation of their protrusions. While migration on 2D surfaces was only mildly impaired, Cdc42 deficiency completely abrogated *in vivo* motility. This discrepancy was entirely caused by the geometrical complexity of the environment as multiple competing protrusions led to entanglement within 3D fibrillar scaffolds.

In summary, my Ph.D. thesis shows that leukocytes migrate in the absence of specific adhesive interactions through interstitial tissues. This is in contrast to the general cell migration paradigm of integrin-mediated traction on 2D surfaces. Instead, actin-network expansion at the leading edge and auxiliary actomyosin contraction at the cell rear appear to directly transduce the intracellular force onto the 3D matrix. Therefore, we conclude that internal stabilization of polarity and coordinated cytoskeletal flow rather than transmembrane force coupling are decisive for 3D leukocyte migration. Adhesion-independent movement renders leukocytes autonomous from the tissue context and allows them to quickly and flexibly navigate through any organ without adaptations to alternating extracellular ligands. Moreover, substrate independency favours migration along paths of least resistance that does not necessitate proteolytic degradation of the interstitial matrix which we confirmed for granulocytes (**Paper VI**).

The results of my Ph.D. thesis provide insights into basic questions of cell motility and cytoskeletal regulation which underlie leukocyte trafficking and thus immunological function. Furthermore, the results might have implications for dendritic cell-based tumor vaccination strategies.

5   Introduction

5.1   Leukocyte migration in general

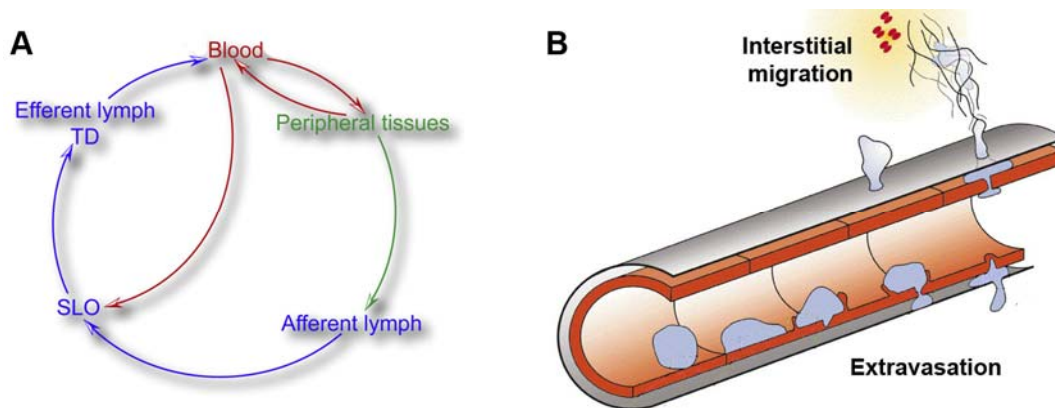### 5.1.1   Principle trafficking processes

Figure 1: Leukocyte trafficking. (A) Leukocyte circulation through the body involves trafficking through different tissue compartments (scheme adapted from Alvarez et al. [1]). (B) Leukocytes exit the blood by adhering to and transmigrating across an endothelial cell layer. Movement within tissues is characterized by crawling through interstitial matrix (scheme adapted from Sixt et al. [2]).

The innate and adaptive immune system protects the vertebrate's body from foreign invaders. Specialized leukocyte subsets cooperate perfectly in time and space to become the cellular counterforce in a healthy organism. After their generation in the bone marrow or the thymus, they emigrate into the blood and circulate through the body. Leukocyte migration comprises three different processes: i) exit from the blood vessel into the tissue (extravasation), ii) migration within peripheral tissues and lymphoid organs (interstitial migration) and iii) entry into blood sinuses or lymphatic vessels (egress from tissues) (Fig. 1A).

Extravasation from the blood allows entry into different organs (Fig. 1B). For instance, innate immune cells (neutrophils, monocytes) rapidly exit blood vessels at sites of acute inflammation. Naïve lymphocytes as part of the adaptive immune system recirculate constantly between blood, secondary lymphoid organs (SLOs) and lymph. To enter lymph nodes (LNs) and Peyer's patches (PPs), they must actively traverse high endothelial venules (HEVs), whereas entry of the spleen occurs passively. Each leukocyte subtype carries characteristic sets of trafficking molecules (adhesion receptors and chemokine receptors) on its surfaces to specifically direct its recruitment to the correct anatomical site [3, 4].

During interstitial migration leukocytes scan the tissue for an infectious source in the body (Fig. 1B). At sites of acute injury, neutrophils rapidly release cytotoxic mediators to eliminate the invader. Monocytes differentiate to macrophages or dendritic cells (DCs) and establish a tissue-resident defence at peripheral sites. In contrast, naïve antigen-specific T lymphocytes search for antigen-presenting DCs in SLOs. After cellular encounter, T cells acquire activation signals and differentiate to effector T cells. As a consequence, they then change expression of trafficking molecules which enable LN exit and migration to peripheral sites. Trafficking molecules might not be as specific for leukocyte interstitial migration as for extravasation. While leukocyte-specific chemokine receptors were shown to determine directed migration, it is not clear if leukocytes require a characteristic set of adhesion receptors for navigating through interstitial tissues.

Leukocyte exit organs either by entering blood sinuses (in bone marrow or spleen), lymphatic vessels (in peripheral tissues) or lymphatic sinuses (in LNs). As these processes have not been investigated in the course of this thesis, I will not further discuss them.

5.1.2   Trafficking molecules
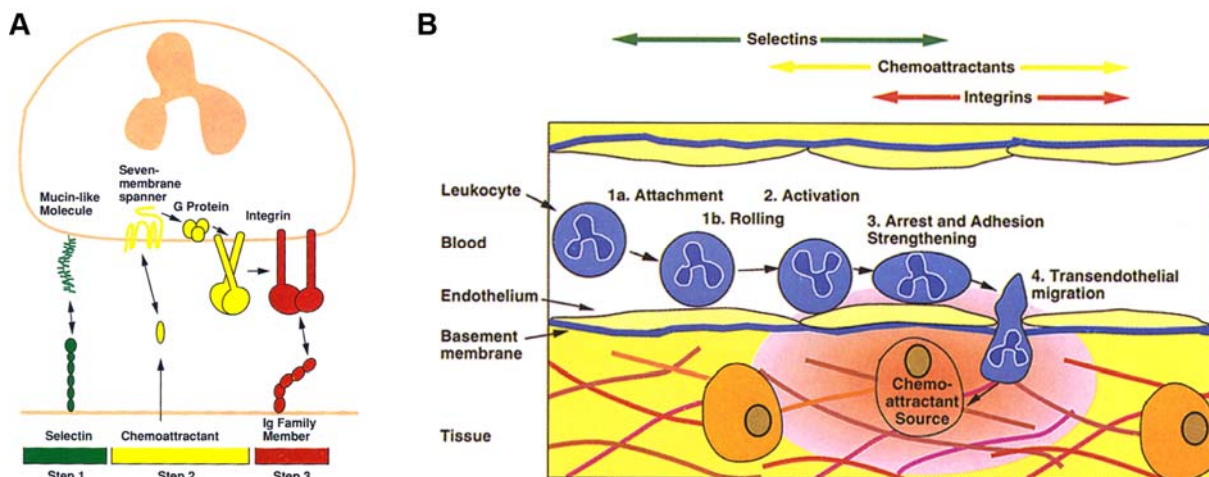
Figure 2: Trafficking molecules. (A) Leukocyte-specific recruitment to peripheral tissues requires the concerted action of trafficking molecules (selectins, chemokines, integrins). (B) In the course of extravasation, trafficking molecules enable leukocytes to undergo a multistep adhesion cascade along the endothelium (schemes taken from Springer [5]).

Leukocyte migration has been mostly and extensively studied in the context of the extravasation process through the endothelial cell layer [6]. To overcome both the high shear

force within the blood vessel and the tight seal of the endothelial cells, leukocytes undergo a sequence of distinct adhesive and signalling events which has been termed the multistep adhesion cascade (Fig. 2B). Traditionally, leukocyte emigration has been described as a three-step model based on three molecular interactions: (i) selectin-mediated tethering and rolling along the inner vessel, followed by (ii) chemokine-induced leukocyte activation leading subsequently to (iii) integrin-dependent leukocyte firm arrest [5, 7]. Therefore, selectins, integrins and chemokine receptors are also termed "trafficking molecules" as their combinatorial expression on the plasma membrane gives leukocytes a unique identity and ability to home to vascular beds with specific "area codes" [5] (Fig. 2A). This principle provides an enormous combinatorial diversity for leukocyte recruitment. It allows continuity for steady-state leukocyte homing, but also flexibility upon inflammation when leukocytes and endothelial cells activate or newly synthesize trafficking molecules. In the following, I will briefly outline the functional principles of selectins and chemokines and then introduce the family of integrin receptors and their functions on leukocytes in more detail.

Selectins constitute a family of highly conserved C-type lectins, which bind sialyl-Lewis X-like carbohydrate ligands that are presented by sialomucin-like surface molecules such as PSGL-1 [6, 8]. Ligand binding occurs with exceptionally high on- and off-rates and facilitates initial leukocyte capturing and rolling under heavy blood flow [5, 9, 10]. Three members participate in the early extravasation steps: L-selectin is expressed on most circulating leukocytes and is especially important for transmigration across HEVs and peripheral inflamed vessels [11, 12]. Upon inflammation, endothelial cells upregulate the expression of P- and E-selectin and determine recruitment of several immune cells by interacting with PSGL-1 on the leukocyte surface [13].

While rolling, leukocytes sense chemokines that are immobilized by heparan sulphate residues or silent chemokine receptors on the endothelial cells' luminal side [14, 15]. Chemokines bind to G-protein coupled chemokine receptors and initiate diverse signalling pathways [16, 17]. Ligated chemokine receptors exchange GDP against GTP at the Gα subunit of heterotrimeric G proteins. Gα (with Gi as major regulator of chemokine signalling) and Gβγ subunits dissociate from each other, which triggers an intracellular calcium flux. The resulting activation of signalling molecules such as PI3K or small RhoGTPases induces several molecular pathways [18, 19]. One outcome is integrin activation on the leukocyte surface. Circulating leukocytes carry integrins in a non-activated conformation that, upon chemokine

signalling, changes to an active state. The structural basis of this event and the key molecules involved in this process will be described in the next paragraph.

5.2 Integrins on leukocytes

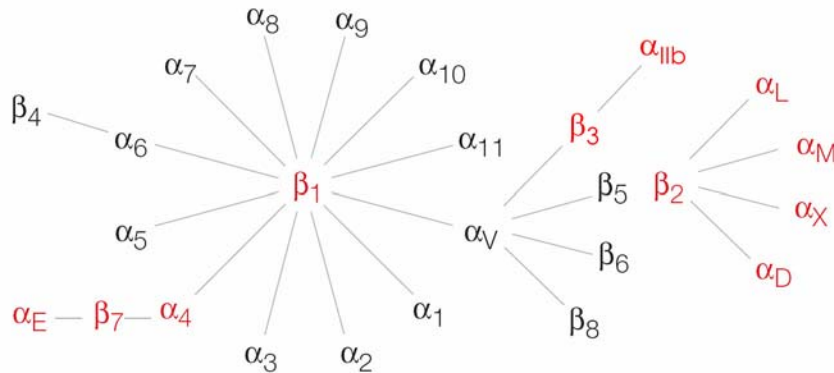### 5.2.1 Integrin structure and functions

Figure 3: The integrin family. The various associations between α subunits and β subunits allow formation of at least 24 integrin heterodimers. The most intensively studied integrins on platelets and leukocytes are highlighted in red (scheme adapted from Kinashi[20]).

In metazoans, integrins represent the major adhesion receptors binding both extracellular and cellular ligands [21]. They are heterodimeric type I transmembrane glycoproteins that are composed of non-covalently associated α and β subunits. 18 α and 8 β chains can differently combine to form 24 integrin receptors [22]. Each subunit is composed of a large extracellular domain (N-terminus of >700 residues), a single transmembrane domain (>20 residues) and a usually small cytoplasmic domain (C-terminus of 13-70 residues) [23]. While the cytoplasmic domain is linked to the actin cytoskeleton, the extracellular domain binds to extracellular matrix molecules (ECM) and/or cellular counter-receptors. Several integrins can bind to the same extracellular ligand, but also several ligands are bound by the same integrin. The family of integrins can be subdivided into four major subfamilies according to key subunits that assemble multiple heterodimers [22] (Fig. 3). Analysis of expression patterns and studies of mice with homozygous null mutations revealed their physiological function and significance [24, 25]. The β1 subfamily is the largest family with 12 α chains that assemble with the β1 chain. Homozygous null mutations of the β1 gene in mice result in peri-implantation lethality at day E5.5 due to an inner cell mass failure [26, 27]. The αv subfamily comprises five integrin heterodimers that all, together with the integrins α5β1 and αIIBβ3, recognize the tri-peptide

arginine-glycine-aspartic acid (RGD). The αv knockout mice survive until E12 and occasionally develop to birth. These mice show cleft palate and die from massive CNS or gastrointestinal hemorrhage [28]. The four integrins that share the β2 subunit are exclusively expressed on leukocytes. Consequently, β2 null mice are viable and show most of the features of the human leukocyte adhesion deficiency type I (LAD-I) [29]. LAD-I patients harbour inactivating mutations in the β2 chain and suffer from leukocytosis, and spontaneous and recurrent infections due to impaired emigration of neutrophils [30]. Two other leukocyte-restricted integrin dimers share the β7 chain and null mutations of the β7 gene result in viable mice with abnormal development of the PPs and reduced numbers of intraepithelial lymphocytes [31]. In summary, integrins have been shown to play crucial roles in embryonic development, tissue maintenance and repair, host defence and hemostasis [32].
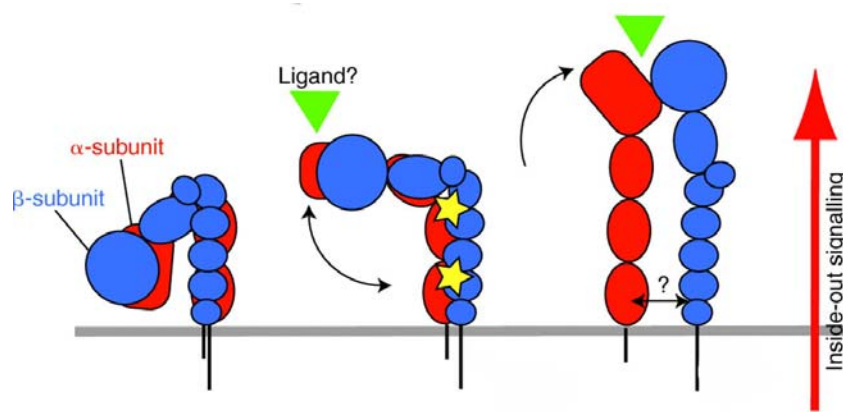
Figure 4: A model of integrin conformation-function relationships. The three major conformational states that have been identified so far are shown (from left to right): bent form (inactive), extended with closed head-piece (primed) and extended with open head-piece and separated legs (ligand bound) (scheme adapted from Askari et al.[33]).

Integrins signal bidirectionally across the plasma membrane, integrating signals from the extracellular ligands to the intracellular cytoskeleton and signalling adaptors [22]. "Inside-out signalling" refers to the process by which cellular activation results in increase of the adhesive properties of the integrin, a process also called "integrin inside-out activation" [34]. Studies on the integrins αIIBβ3, αvβ3 and αLβ2 (LFA-1) showed that integrins undergo conformational changes reflecting different stages of activation. There are three major integrin conformations that have been identified so far: the bent form (low affinity), the extended form with a closed ligand-binding head (intermediate affinity) and the extended form with an open head-piece for ligand binding and separated legs (high affinity) [35] (Fig. 4). It is established that upon cellular activation, integrins undergo a conformational change that involves unbending and extension

of the receiver. However, a spectrum of conformations seems likely and accumulating evidence suggests that the degree of extension might be both specific for a particular integrin and for a specific activation stimulus [33].

In particular reported for LFA-1, initial binding to multivalent ligands results in clustering of integrin receptors and stabilising an extended integrin, strengthening adhesion, and transmitting signals to the cell interior ("outside-in signalling") [34, 36]. The corresponding signals determine aspects of cell adherence, spreading, migration, but also differentiation, survival and leukocyte-specific processes such as degranulation and cytokine secretion.

5.2.2 Integrin activation in leukocytes

The short cytoplasmic domains of both α and β subunits harbour conserved amino acid sequences that contribute to the different conformational states of integrin activity. The α integrin cytoplasmic tails contain a GFFKR sequence that is believed to be critical for a salt bridge-mediated interaction with the β chain. This association is thought to prevent integrin activation by stabilizing the low-affinity state [23, 36]. However, this issue is still under debate. The β chain cytoplasmic domain contains two NPXY (NPXF in the β2 chain) motifs that mediate talin and kindlin binding leading to separation of the α and β tails [36]. This unclasping might be propagated across the plasma membrane by alterations in the interaction of the transmembrane segments and changes in the membrane insertions of the membrane-proximal domains of the cytoplasmic tails, but this has not yet been fully understood [23, 33]. The ultimate consequence of inside-out signals is the change of the extracellular ectodomains to a high affinity conformation leading to integrin activation.

Talin (~ 270 kDa) was the first protein shown to interact with integrin cytoplasmic tails [37, 38] and constitutes an essential mediator of integrin activation [39]. Two talin isoforms exist in vertebrates (talin-1 and talin-2) with talin-1 as the predominant isoform in hematopoietic cells [40, 41]. Talins consist of a globular N-terminal head region and a flexible rod domain. The talin head contains a FERM domain that is subdivided into F1, F2 and F3 domain. Upon intracellular activation, the auto-inhibited talin undergoes conformational change exposing the phosphotyrosin-binding (PTB) domain of the F3 domain [41]. Binding of the PTB domain to the membrane-proximal NPXY motif is believed to disrupt the salt bridge between the α and β subunit and thus leads to separation of the cytoplasmic domains [42]. However, additional

interactions with the β chain cytoplasmic domain are most likely required, as other PTB-containing proteins can bind to the NPXY motif, but cannot activate the integrin [43]. The physiological significance of talin-mediated integrin activation has been previously reported in two studies. Mice with a conditional deletion of the *Tln1* gene showed spontaneous bleeding and lack of activation of the platelet integrins α2β1 and αIIBβ3 [44, 45]. For leukocytes, binding of talin to high affinity LFA-1 in T cells suggests a similar role in integrin activation [46], but this has not yet been confirmed *in vivo*.

Recent data demonstrated that talin alone is not sufficient to activate integrins and requires kindlins for integrin activation [47]. Kindlins are a novel family of FERM domain-containing proteins [48]. They generally interact with the membrane-distal NPXY motif of the β chain cytoplasmic domain [47, 49-52]. Their FERM domain shows high levels of sequence similarity to that of talin [53]. In the absence of kindlins, integrin activation cannot occur [47, 50, 52, 54]. It is meanwhile clear that both kindlins and talin are required for integrin activation. As they bind distinct regions of the integrin β cytoplasmic tail, they may cooperate to mediate integrin activation. The exact sequence of protein binding events remains further investigation. There are three kindlin family members in mammals with kindlin-3 exclusively expressed in cells of hematopoietic origin [55]. Kindlin-3 has been shown to activate β1, β2 and β3 integrins on platelets and leukocytes [47, 54]. Kindlin-3 null mice show severe bleedings and lack of platelet and neutrophil firm adhesion [47, 54]. Recently, mutations in kindlin-3 were implicated with human LAD-III, which is associated with severe defects in leukocyte and platelet integrin activation [56-59]. For years, the causes of LAD-III have been connected to another regulatory pathway of integrin activation. Some LAD-III patients had a mutation in CalDAG-GEF1, a guanine nucleotide exchange factor (GEF) for the small GTPase Rap1 [60, 61]. This was mirrored in mice with homozygous null mutations of CalDAG-GEF1 showing a LAD-III-like phenotype [62]. However, recent in-depth analysis showed that Kindlin-3, but not CalDAG-GEF1, restored the adhesive deficiencies in LAD-III cell lines and provided strong evidence that Kindlin-3 deficiency underlies LAD-III [56, 57].

In hematopoietic cells Rap1 activates β1, β2 and β3 integrins [63]. Several pathways of Rap1 activation have been described in platelets and leukocytes. The activity of Rap1 is regulated by GDP-GTP exchange through GEFs [63]. To exert its function, active Rap1 needs to be recruited to the plasma membrane and protein kinase C has been shown to induce a complex of protein kinase D1 and Rap1 with the surface-expressed integrin β1 chain [64]. Active Rap1 can modulate integrin affinity via two Rap1 effectors that act independently, but maybe also cooperatively [34]. Rap1 induces the formation of a complex containing talin and the Rap1

effector RIAM that facilitates talin binding to the β2 cytoplasmic domain [65]. RAPL, another Rap1 effector is most likely specific for the integrin LFA-1. RAPL associates with active Rap1 and binds to two lysine residues that are only found in the αL chain distal to the common GFFKR motif [66]. Taken together, kindlin and talin binding to integrin β cytoplasmic tails represent essential steps in integrin activation. How protein recruitment to α cytoplasmic tails influences integrin activation requires further investigation.

Another recently emerging concept has been observed for integrin α4β1 and suggests external force as an additional factor in integrin activation on leukocytes. It has been shown that moderately applied force on ligand-bound integrin α4β1 leads to nanosecond transitions to the high-affinity state [67, 68]. Leukocytes might physiologically face low forces as shear flow of the blood stream. Hereby, it has been proposed that already extended integrins anchored to the inner cortical cytoskeleton undergo rapid ligand-induced integrin activation [9]. Thus, force might strengthen integrin-ligand bonds and accelerate outside-in signals.

5.2.3   Functions of integrins in leukocyte migration

5.2.3.1   Extravasation

Most knowledge about leukocyte integrins has been derived from studies of the extravasation process. Over the years and with the help of intravital microscopy, the classical three-step model has been refined by adding several separate events, including slow rolling, adhesion strengthening, intraluminal crawling, and paracellular and transcellular migration [6] (Fig. 5). In almost all steps, integrins have been proven or at least discussed to play major roles. In consideration of the vast amount of existing data, the following section will primarily focus on specific roles of distinct integrin heterodimers that have been observed *in vivo*. Extravasation of lymphocytes, neutrophils/monocytes and other blood cells will be discussed separately, as leukocyte subtypes differently employ integrin heterodimers.
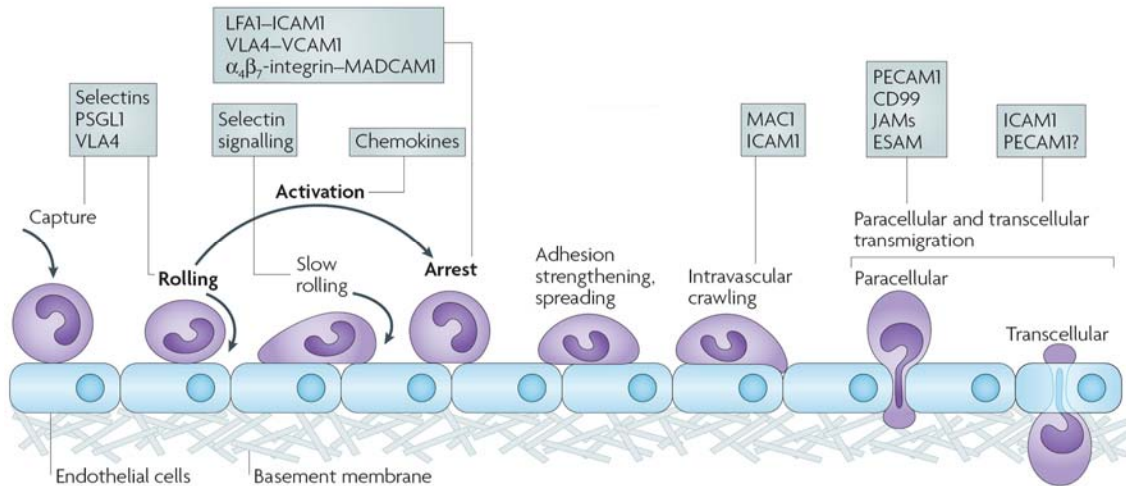
Figure 5: The updated leukocyte adhesion cascade. The classical three steps are shown in bold letters. Additional steps that have been identified recently are shown in regular letters. The involvement of different integrin heterodimers at each step are indicated (VLA4: integrin α4β1) (scheme adapted from Ley et al.[6]).

Integrins in the adhesion cascade

Naïve lymphocytes activate integrins upon chemokine sensing at the HEV [69]. Under homoestatic conditions, HEVs express VCAM-1 [70] and ICAM-1 [71], the ligands for α4β1 and LFA-1, respectively. HEVs in PPs, but not in peripheral LNs, express additionally MadCAM-1, the ligand for the integrin α4β7 [72] and results in different integrin employment during firm lymphocyte arrest. LFA-1 predominantly determines an abrupt arrest in peripheral LNs with a compensating role for integrin α4β1 [70, 73, 74]. In contrast, lymphocyte subsets expressing α4β7 are preferentially recruited to PPs, where LFA-1-dependent adhesion plays only a minor role [70, 72]. Apart from firm arrest, integrins have also been implicated in earlier steps of lymphocyte extravasation. In HEVs of rat PPs, integrin α4β1 seems to facilitate both rolling and arrest [75]. The integrin α4β1 is also part of a feedback loop that amplifies the homing process: Binding of α4β1 to autotaxin, a HEV-expressed lipase, generates lysophosphatic acid which in turn amplifies the chemokine receptor response [76].

Neutrophils and monocytes differ from lymphocytes as they additionally express high amounts of the integrin αMβ2 (Mac-1) that binds several ligands including ICAM-1, ICAM-2 and fibrinogen. In inflamed postcapillary venules, neutrophils and monocytes employ distinct integrins for extravasation. Whereas LFA-1 mediates neutrophil rolling and adhesion, Mac-1 allows subsequent crawling along the endothelium to search for the optimal emigration site [77, 78]. By contrast, monocyte extravasation seems to depend largely on the integrin α4β1 [79], which has also been suggested for T cells [80-82]. An interesting phenomenon has been observed

in non-inflamed postcapillary venules. Here, monocytes perform long-range crawling along the resting endothelium which is 10 to 1000 times slower than rolling and independent of the blood midstream flow. This patrolling behaviour depends on LFA-1 and serves rapid tissue invasion in an early innate immune response [83].

Integrin-dependent homing to other organs follows the general scheme of rolling, activation and arrest. Hereby, extravasation of common lymphoid progenitors in corticomedullary vessels of the thymus depends on α4β1 and LFA-1 [84], while homing of stem cells and progenitor cells to the bone marrow requires only the α4β1-VCAM1 interaction [85-88]. However, lymphocyte extravasation can also occur in the absence of rolling in a α4β1-VCAM1-dependent manner in liver sinusoids [89] and in inflamed vessels of the central nervous system [90-93].

Integrins during transmigration

After the sequential adhesion cascade leukocytes cross the endothelial layer in a process termed transendothelial migration or transmigration or diapedesis (Fig. 5). Leukocytes can enter the tissue either via the paracellular (through endothelial cell junctions) [94] or the transcellular (through the endothelial cell itself) route [95]. The percentage of transcellular migrating cells ranges from 10% to 90% among the different sudies. Therefore, it is not clear which conditions and vascular beds might favour one or the other route [96]. For instance, neutrophils crawl laterally in a Mac-1-ICAM-1-dependent manner along the endothelium and before emigrating paracellularly [78, 97]. When depleting Mac-1 on neutrophils, transmigration is delayed and occurs preferentially transcellularly [78].

Integrins might be involved in the actual transmigration process, as integrin ligands are expressed on the apical side of the endothelium and laterally in the junction [98]. During transcellular migration, both VCAM-1 and ICAM-1 are found on so-called docking structures or transmigratory cups on endothelial cells [99, 100]. After contact with leukocytes, ligand clusters might form and trigger signalling events in the endothelial cells. These might then capture and guide the leukocyte through intercellular junctions or transcytose it directly through the endothelial cell body [101, 102]. Podosomes on the leukocyte's ventral side protrude into the underlying endothelium to test at which site to penetrate the endothelial layer [95].

A role for ICAMs in the diapedesis step has been suggested, but is not entirely established yet. By contrast, other junctional proteins such as PECAM-1, CD99, JAM-A and VE-cadherin seem to collaborate in a sequential opening of the endothelial junction [94]. However, paracellular transmigration might still influence integrin functions on extravasating

leukocytes. In a particular experimental setting (IL-1β-induced inflamed venule of the cremasteric muscle, peritonitis model), transient homophilic PECAM-1 interactions between leukocyte and endothelial cells upregulate the expression of integrin α6β1 on neutrophils [103]. The α6β1 integrin, a major receptor for the basement membrane (BM) component laminin, has been shown to be important for BM passage [103]. This interaction might be required when neutrophils face the BM before migrating through preformed openings (also called low expression sites as they show low levels of laminins and collagen IV) of the endothelial BM that correspond with gaps in the pericyte sheet without creating defects [104]. However, this is not a general phenomenon as neutrophil migration in another setting does not require PECAM-1-induced integrin upregulation [105].

5.2.3.2 Interstitial migration

The subsequent steps after extravasation and passage of the endothelial BM have been poorly addressed and little is known about the adhesive interactions that mediate leukocyte migration in extravascular spaces. Migration outside blood vessels is commonly referred to as interstitial migration and ranges from movement through the loosely packed and fibrillar-collagen-dominated connective tissue of the mesenchymal interstitium to trafficking within the cell-rich environment of SLOs. Intravital microscopy data on this aspect of leukocyte migration are limited, as blocking integrin functions in most cases already interferes with leukocyte entry into tissues. The few existing studies propose integrin-independent lymphocyte migration in the LN (see also 5.4.2.4) [106], but also integrin-dependent neutrophil migration in the mesenteric interstitium [107]. The latter conclusion derives from a series of studies that observed a partial inhibition (speed reduction of only 30%) of neutrophils by blocking antibodies against the collagen-binding β1 and α2 integrin chains [107, 108]. Static observations in a series of studies employing blocking antibodies and genetic inactivation suggested that collagen receptors α2β1 and α1β1 play a role in integrin-mediated retention of T cells during cutaneous hypersensitivity, experimental arthritis, colitis and virus infection by localizing T cells within the interstitium [109-112].

Artificial 3D gels consisting of ECM components, predominantly collagens I and III, have been extensively used to mimic the porous and fibrillar environment of the dermal interstitium (see also 5.4.2.2). They provide a defined migration scaffold to follow leukocyte migration by video microscopy. Employing this and related settings, several groups addressed

the question if adhesion contributes to migration within interstitial matrices. Leukocytes were shown to interact with extracellular matrix molecules in 2D settings [113] and chemotactic locomotion of T cells within 3D collagen gels depended on integrins of the β1 family [114]. However, early reports already favoured a non-adhesive migration mode of neutrophils and lymphocytes through 3D matrices [115, 116]. Along the same line, granulocytes of LAD-I patients and after blocking integrin β2 function only showed a motility reduction in 2D, but not in 3D settings [117, 118]. When migrating in the spatially confined space between two closely adjacent glass surfaces, granulocytes can switch to biophysical mechanisms of translocation (squeezing or "chimneying") that are independent of integrin binding. By contrast, on 2D surfaces granulocytes were completely dependent on integrins to generate traction forces [119]. Ultimately, antibody blocking studies showed that random T cell migration in the gel can occur in the complete absence of integrin-mediated binding [120] and proteolytic activity [121].

Leukocytes are often compared with migrating cells of an "amoeboid" shape. Some tumor cell lines show amoeboid morphology during 3D migration, but it is unclear if they engage integrins or not. While few reports claim amoeboid migration of single tumor cells to be integrin-independent [122, 123], others observe just reductions in tumor migration when blocking integrins [124-126].

5.3   Amoeboid migration of leukocytes

5.3.1   Amoeboid migration

Leukocyte movement in interstitial environments is commonly referred to as *amoeboid* migration and owes its name from the protozoon *Amoeba proteus (amoibè* (αμοιβή) as the Greek word for "change", and Proteus as the Greek god of change) [127, 128]. The group of amoeboid migrating cells is heterogenous and comprises different unicellular eukaryotes which vary in size, compactness and their habitat, but all share the one morphological feature that defines them as "amoeboid": During movement they undergo a constant shape change forming extensions (originally described as pseudopods or "false feet") that rapidly protrude and retract. However, it is nowadays clear that different amoeboid cells employ various locomotion mechanisms resulting in variants of amoeboid phenotypes ranging from contraction-based blebbing to entirely protrusive migration. The term "amoeboid migration" often reflects and summarizes all kinds of "non-mesenchymal migration" modes (Fig. 6).

Mesenchymal cells such as fibroblasts, smooth muscle and endothelial cells have an elongated morphology with slow migration rates. Tight coupling to the environment through long-lasting, highly adhesive focalized contact sites (focal contacts, focal and fibrillar adhesions) aligns the cell along the substrate. As a consequence of substrate-dependent migration, mesenchymal cells cannot circumvent matrix-dense regions. To overcome these barriers in fibrillar tissues, they proteolytically degrade the environment and move forward [129, 130]. Amoeboid cells by contrast show only weak adhesion to substrates and lack prominent adhesion sites. Thus, only low adhesive forces counteract the inherent cortical contractility explaining the roundish amoeboid morphology. The transient interactions with the environment allow substrate-independent, highly dynamic migration with high speeds and extreme deformability. This enables the cells to move along paths of least external resistance without proteolysis [121, 131].
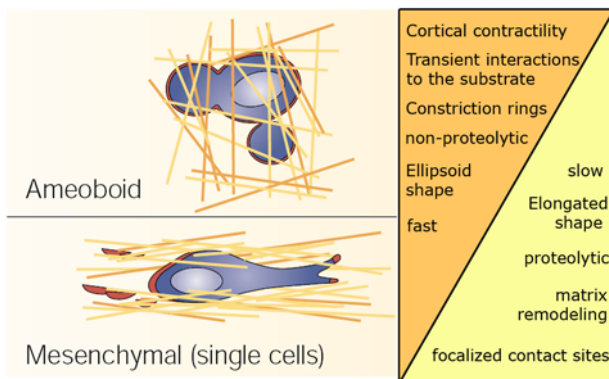
Figure 6: The phenotypic hallmarks of amoeboid and mesenchymal migration (see also text) (scheme adapted from Friedl and Weigelin [132] and Friedl [129]).

As described above, leukocyte migration in the context of extravasation requires integrin-mediated adhesion, whereas locomotion in confined and 3D environments might depend less on adhesion. Therefore, leukocytes might differently generate internal forces for migration. In the following section, I will introduce the basic force-generating principles (contraction and protrusion) and discuss their interrelation and dependence on adhesion for cell movement. I will further compare leukocytes with other amoeboid cells and highlight similarities and differences in their crawling behaviour.

5.3.2   Cellular forces in amoeboid migration

Once cell polarity is established, protrusive forces at the cell front and contractile forces behind the leading edge orchestrate cell migration [133, 134]. Protrusive forces can be driven by polymer-network expansion or internal hydrostatic pressure and both principles serve to

"push" the plasma membrane outward (Fig. 7). Polymerizing actin moves beads, bacteria and virus intracellularly [135]. When acting at the cell front, polymerization and elongation of actin filaments extend the plasma membrane [136]. This results in protrusive structures with sheet-like lamellipodia and needle-like filopodia [137, 138] (Fig. 7A).

Figure 7: Formation of cellular protrusions. (A) Actin polymerization "pushes" the membrane at the leading edge and forms lamellipodia and fil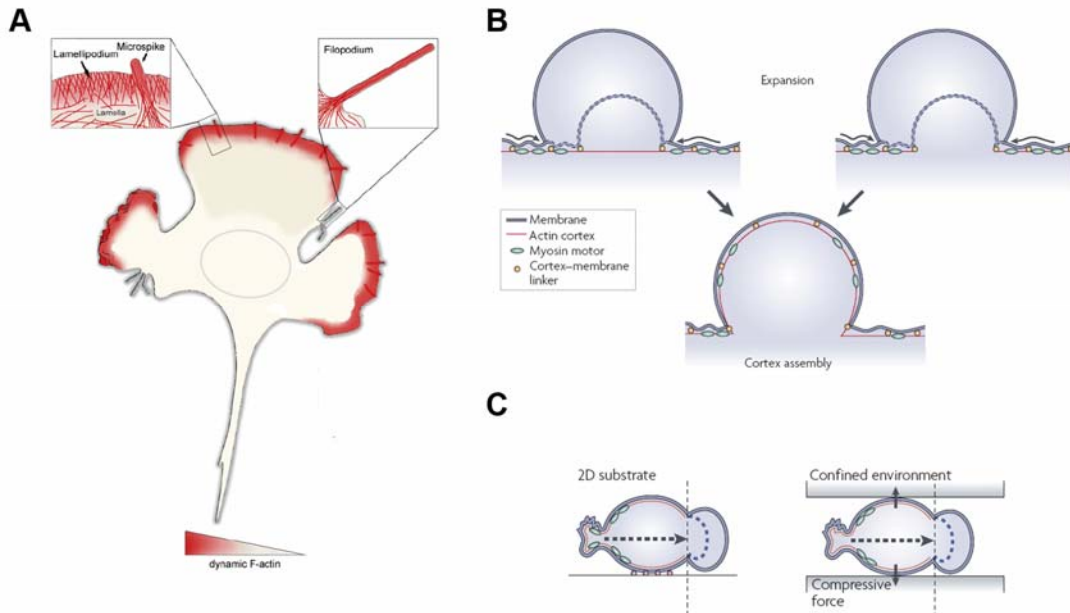opodia (scheme adapted from Ladwein and Rottner [139]). (B) Alternatively, internal hydrostatic pressure leads to detachment of the membrane from the actin cortex (left) or ruptures in the actin cortex (right). (C) The resulting cytoplasm-filled, actin-devoid blebs have been suggested to mediate migration (schemes taken from Charras and Paluch [140]).

"Pseudopodia" termed historically all cellular protrusions, but is nowadays only referred to finger-like projections of *Dyctiostelium* and leukocytes [141]. Alternatively, internal hydrostatic pressure generates cytosol-filled blebs. In contrast to polymer network expansion, bleb formation requires contractile forces. Myosin II produces tension in actin networks by pulling actin filaments past one another. This causes a rise in pressure leading either to ruptures in the cortical actin with plasma membrane anchored actin-binding proteins [142] or local detachment of the plasma membrane from the cortical cytoskeleton [143, 144] (Fig. 7B). In both cases, a flow of cytosol generates a growing bulge that displaces the membrane. After cytosol inflation slows down, the sequential recruitment of actin, actin-binding proteins and myosin II leads to bleb retraction [145]. Contractile forces behind the leading edge can only produce traction on the surface, when the cell front is fixed in some way (Fig. 8). Whereas actin-devoid blebs are likely not coupled extracellularly, actin-rich protrusions adhere to the environment. Then, actomyosin contraction in front of the nucleus generates "pulling" forces to translocate the

14

cell body. To allow retraction and detachment on high adhesive surfaces, cells must additionally contract their actin cortex at the back [146] (Fig. 8). In general, tight coordination of protrusive, contractile and adhesive forces determines cell migration and altering their individual strength results in differently shaped cells with individual migration strategies.

5.3.2.1 Balancing adhesion and contraction

For some amoeboid cells the nature of adhesion structure is still not known (*Amoeba proteus*, nematode sperm). In *Dictyostelium*, SadA was identified as putative membrane receptor that mediates firm adhesion [147], but it is unclear if it contributes to eupodia and actin foci, two described actin-containing structures that mechanically link the cells to the substratum [148, 149]. Leukocytes carry adhesion receptors such as integrins diffusely distributed on their plasma membrane [120]. While some leukocytes (naïve lymphocytes, unstimulated neutrophils, mature dendritic cells) already detach from 2D surfaces by the flux of culture medium, others (activated lymphocytes, monocytes and neutrophils) crawl integrin-dependently against high shear forces along blood vessels (as described above) [78, 83, 150]. Adhesive structures initially confine amoeboid cells to surfaces, a function that is not necessarily correlated to the generation of traction. Studies on human T lymphocytes suggest a dual role for adhesions: A highly adhesive mid-cell region, the so-called focal zone, confines T cell migration along endothelial and lipid bilayers [46]. To allow migration, weaker adhesions at the T cells' leading edges might act in concert with contractile forces and mediate horizontal movement on the substrate [151].
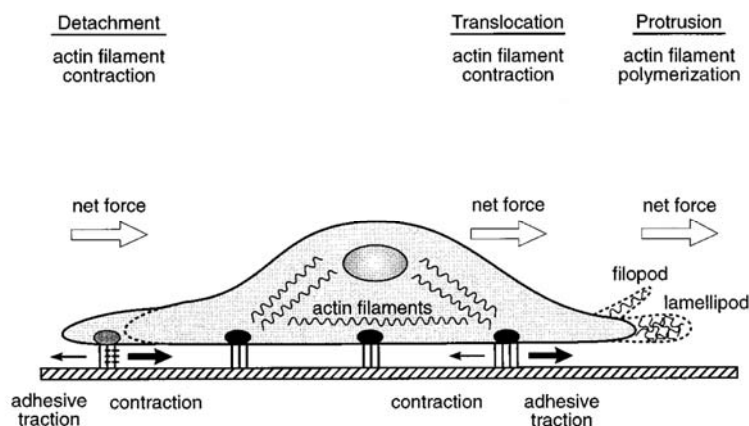

Figure 8: Contractile and protrusive forces during cell migration on 2D surfaces. Contractile forces behind the leading edge generate traction forces on the underlying surface. On high adhesive surfaces, contraction at the back is required to detach the cell (scheme adapted from Lauffenburger and Horwitz [146]).

Amoeboid cell movement requires adhesion-mediated traction to transduce internal contractile forces onto the 2D substratum (Fig. 8). The third Newton's law of motion predicts that contractile forces of the cell body will always result in rearward traction forces at the adhesive cell front. Traction force measurements revealed high stresses at the trailing edge of *Dictyostelium* [152-154] and the uropod of neutrophils [155]. Rearward traction forces at the leading edge have been demonstrated in aggregation-prone *Dictyostelium* cells [152], but could rarely be detected in vegetative *Dictyostelium* cells [153] and neutrophils [155]. Thus, lacking prominent adhesion sites at the leading edge favours a distributed pattern of single very small rearward forces at the leading edge that each might fall under the limit of detection.

High traction stresses at the cell rear are myosin II-dependent [152, 154]. Inhibiting myosin II activity during migration on "high" adhesive surfaces leads to reduced velocities in *Dictyostelium* [156] and an elongated morphology of neutrophils [157] and T lymphocytes [158, 159]. Hence, actomyosin contraction at the posterior part of the cell facilitates detachment and retraction.

When migrating on "low" adhesive surfaces, amoeboid crawling is independent of myosin II-based contraction as has been demonstrated for *Dictyostelium* cells [160], neutrophils [157] and T lymphocytes [161]. Despite the lack of myosin II activity, *Dictyostelium* cells still displayed unchanged rearward traction forces at the leading edge [152], suggesting actin polymerization as the only force-generating principle. Myosin II-independent locomotion is reminiscent of the migration of nematode (*Ascaris suum*) sperm that lack kinesins such as myosin II and crawl by the sole force of an expanding polymer network. Instead of actin, they utilize major sperm protein (MSP) as filament-forming polymer. Nematode protrusions result from pH-dependent polymerization and bundling of MSP filaments pushing against the membrane and a volume expansion caused by a decreased density of filament packing [162, 163]. How can these cells retract their cell body in the absence of contraction? While the polymer network at the leading edge assembles and branches, the ongoing rearrangement and disassembly of the network at the posterior part is sufficient to rupture adhesion points and cause retraction [164, 165]. Similar principles are likely to account for the expansion of actin networks [162], although this has not been proven. Instead, protrusion at the leading edge might create membrane tension pulling the back of the cell forward without the need for contraction.

As described in section 5.2.3.2, leukocyte migration within confined and 3D environments might not depend on adhesive forces, but relies predominantly on contractile forces and polymer network expansion. Early observations of constriction rings [166, 167] and lateral pseudopods that insert into matrix footholds [168, 169] were all morphological expressions of

dynamic cytoskeletal changes (Fig. 6). Although 3D leukocyte movement has often been termed "biophysical migration", this ambiguous definition lacks any mechanistical framework. Only little is known about the interplay of contractile forces and polymer network expansion in leukocytes. Therefore, I will summarize current data that has been obtained in other amoeboid migrating cells.

5.3.2.2 Balancing contraction and polymer network expansion

Cellular protrusions might result from contraction-based internal pressure (blebs) or polymer network expansion (lamellipodia, filopodia). While truly polymerization-driven lamellipodia were observed in myosin II-independent migration of *Dictyostelium*, neutrophils and T lymphocytes [157, 160, 161, 170] or nematode sperm [162], it is unknown how and if bleb formation alone transduces migratory force to a substrate (Fig. 7C). Protrusive bleb formation occurs during migration of *Dictyostelium* [170, 171], but blocking myosin II ceases blebbing and results in actin-rich filopodia-lamellipodia at the leading edge [170]. This clearly showed that both forces can act at the same time and questions if retracting blebs or residual adhesive actin-rich protrusions generate traction. Similar to *Dictyostelium* on 2D, zebrafish primordial germ cells (PGCs) *in vivo* also show a biased formation of protrusive blebs at the leading edge. Chemokine receptor signalling increases free calcium and activation of myosin II at the cell front, which favours a blebbing model of focalized contraction and local pressure increase [143, 172].

Some tumor cell lines (e.g. A375m melanoma, LS174T colon carcinoma) also show inherent amoeboid appearance [124], while some mesenchymal-type cell lines (e.g. HT-1080 fibrosarcoma, MDA-MB-231 mammary carcinoma) switch to amoeboid morphology after protease inhibition [124, 126, 131]. As formation of blebs often coincides with the amoeboid phenotype and enhanced invasion or migration, blebbing movement has been widely promoted as a tumor cell migration strategy [140, 173]. However, unlike PGCs, most amoeboid tumor cells are not polarized and form cellular blebs in an uncontrolled fashion in all directions. As they appear stationary in most 3D assay, it is unknown if blebbing contributes to tumor cell migration at all. Together with the missing knowledge about the role of adhesion, it cannot be ruled out that amoeboid-shaped tumor cells might still move by traction through residual adhesive protrusions. In recent years, tremendous progress has been achieved in understanding the molecular switch from mesenchymal to amoeboid morphology [129]. While the mesenchymal-type mode is promoted by signals that activate the small GTPase Rac and

thus formation of F-actin-rich protrusions, the amoeboid mode results from enhanced contraction. Hereby, activation of the small GTPase RhoA leads to ROCK-dependent myosin light chain phosphorylation and myosin II activation [124]. Thus, Rac and RhoA signalling have opposing effects and reciprocally regulate each other [125]. Inhibiting one pathway will automatically activate the other signalling module and consequently change the mode of movement.

How leukocytes generate force during interstitial migration has not been well investigated. Interpretations and conclusions of available data were not fully convincing due to technical drawbacks (antibody blocking of integrins, artificial *in vitro* assays, leukocyte cell lines). DCs were only rarely employed, although they serve as a perfect model to study leukocyte mechanics during physiological interstitial migration. In the last part, I will briefly introduce DCs and describe in detail the migratory environment and chemotactic cues that guide DCs from the skin to the lymph node. I will further depict molecular players (adhesion receptors, cytoskeletal regulators) that have been suggested to facilitate DC migration.

5.4 Dendritic cell migration

5.4.1 Dendritic cells in general

DCs are the most potent antigen-presenting cells (APCs) that induce adaptive immune responses to pathogens, but also maintain self-tolerance of T cells [174]. They act as sentinels by continuously sampling the tissue for foreign particles. Once an antigen is taken up, it is proteolytically processed and peptide fragments presented on the APC surface in the context of major histocompatility complex (MHC) molecules. Hereby, presentation via MHC class I and MHC class II (MHC-II) molecules induce the activation, proliferation and differentiation of naïve $CD8^+$ T cells (cross-presentation) and $CD4^+$ T cells, respectively [175]. Several DC subsets have meanwhile been defined by differential expression of surface molecules with conventional DCs ($CD11c^{high}$, MHC-II^+) and type I interferon-producing plasmacytoid DCs ($CD11c^{low}$ MHC-II^{low}) as the two most prominent subtypes [176].

Almost present in all organs, DCs are enriched at peripheral sites of microbial entry (such as skin and mucosal tissue) and in SLOs where they initiate T cell priming. Most studies have focussed thereby on the function of skin DCs and their trafficking from the skin via lymphatic vessels to the draining cutaneous LNs [1, 177].

5.4.2 Dendritic cell trafficking from the skin to the lymph node

5.4.2.1 Mobilization and principle guidance cues

Two populations of resident DCs exist in the skin: the Langerhans cells (LCs) of the epidermis and the dermal DCs (dDCs) residing within the interstitium [178, 179]. As immature DCs they constantly scan the skin for internal (damage) and external (microbes) danger signals (Fig. 9A). Upon inflammatory stimuli, DCs first undergo a brief period of immobility and increased antigen uptake followed by so-called maturation [180]. This includes the upregulated expression of: (i) co-stimulatory molecules (MHC-II, CD40, CD80, CD86) to initiate T cell priming, and (ii) the CC-chemokine receptor 7 (CCR7) to follow chemotactic cues to the draining lymph nodes (Fig. 9). Even under non-inflammatory conditions, a small number of DCs traffics to the LN (steady-state migration) [181, 182].
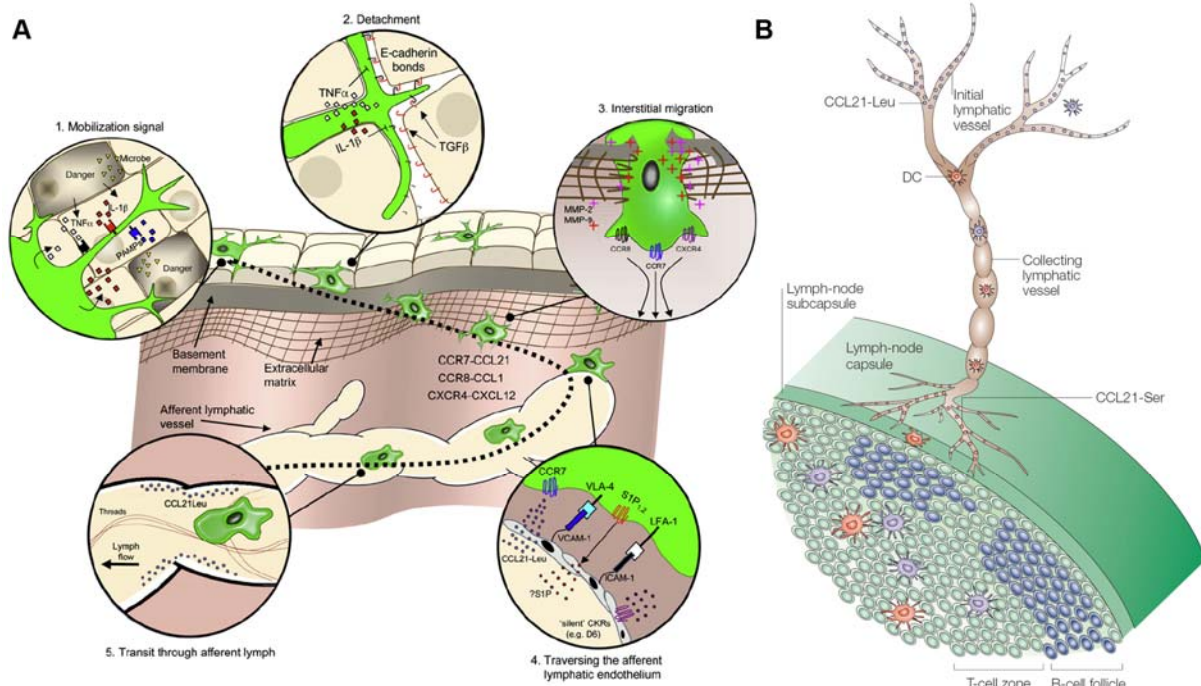
Figure 9: Dendritic cell trafficking. (A) Dendritic cells migrate from the skin (epidermis and dermis) into lymphatic vessels. The molecular processes and sequence of migration events are highlighted (described in detail in the text) (scheme taken from Alvarez et al. [1]). (B) Expression of chemoattractant guidance cues along the route from the lymphatic vessel to the lymph node (scheme adapted from Randolph et al. [177]).

DC migration from the skin to the LN is predominantly guided by CCR7-binding chemokines [183]. During *in vitro* maturation CCR7 is highly upregulated on DCs, while other chemokine receptors are downregulated [184, 185]. The ligands for CCR7 were detected along the migration

route (Fig. 9B): (i) Lymphatic endothelial cells (LECs) of the afferent lymph vessels constitutively produce CCL21-Leu and CCL21-Ser, the two existing isoforms of CCL21, and upregulate their expression during inflammation [186, 187]. (ii) Stroma cells in the LN paracortex express both CCL19 and CCL21-Ser [187]. In several studies, steady-state and inflammatory DCs lacking CCR7 did not enter afferent lymphatics and were thus absent in the LN [183, 186, 188]. This was in line with findings in *plt/plt* mice (paucity of lymph node T cells) that have a naturally occurring deletion of CCL21-Ser and CCL19 [189]. DCs still entered lymphatics, but did not traverse into the LNs [189, 190]. Expression of CCR7 alone might not be sufficient to induce DC migration, as additional signals such as lipid mediators were shown to sensitize CCR7 for its ligands [191, 192]. DC migration might also be influenced by other chemotactic molecules in a CCR7-independent fashion. Upon inflammation, enhanced expression of CXCR4 on DCs and its ligand CXCL12 on inflamed vessels was reported [193]. Moreover, DCs express all five known sphingosine-1-phosphate (S1P) receptors and might also be attracted by high amounts of S1P in the lymph fluid [194-196]. Indeed, small molecule antagonists against S1P receptors interfered with DC migration to the LN [195, 197].

While the chemotactic guidance cues are well-defined, it is unclear by which mechanisms DCs (i) migrate through the interstitium of the dermis and the lymph node or (ii) overcome potential anatomical barriers.

5.4.2.2 Dendritic cell trafficking in the skin

Skin architecture

The skin consists of the epidermis and the underlying dermis joined and maintained together by a basement membrane [198]. In the epidermis, multiple layers of keratinocytes at distinct stages of differentiation form a thin layer of stratified squamous epithelium. They rest on the epidermal BM, a dense sheet of tightly interconnected molecules such as laminins, collagen IV, nidogens and heparan sulphate proteoglycans [199, 200]. The mesenchymally derived dermis is composed of scattered fibroblasts and their deposited ECM. The dense ECM scaffold can be functionally divided into the fibrillar fraction (fibrillar collagen bundles, elastic fibers, and microfibrils) and the non-fibrillar fraction (mainly glycosaminoglycans and proteoglycans). While the fibrillar fraction is mechanically stable and counteracts the tension produced by contracting fibroblasts [201], the non-fibrillar fraction fills the volume between the fibers and behaves like a viscous fluid [202].

Migration within the skin

Under non-inflammatory conditions, LCs in the epidermis appear as branched immobile cells with dendrites that intermingle with neighbouring keratinocytes and occasionally show repetitive movement [203-205]. They owe their sessile phenotype to homophilic E-cadherin contacts with keratinocytes [206]. After antigenic stimulation, LCs disrupt these junctions and detach which already leads to DC maturation [207, 208]. During exit from the epidermis, LCs face the structural dense epidermal BM which requires specialized mechanisms for transmigration [209]. Studies on ear explants indicated matrix metalloproteinase (MMP) 2- and 9-mediated proteolytic degradation [210] and integrin α6-dependent adhesion to be involved in this process [211]. In a psoriasis model, integrin α1-deficient T cells were unable to traverse the epidermal BM which further implicated a role of integrins [212]. Besides integrins, the hyaluronat receptor CD44 has been suggested to participate in LC migration [213]. In this scenario, enhanced expression of osteopontin in the inflamed skin fosters chemotactic migration via CD44 and αv integrins [214]. However, another study confirmed impaired migration of CD44-deficient DCs to the LN, but LC migration was not affected [215].

Once LCs have overcome the epidermal BM, they migrate similar to dDCs in the mesenchymal interstitium. As described above (see section 5.2.3.2), 3D collagen gels simulate fibrillar scaffolds of the dermis and have also been used for the study of DC migration and DC-T cell interaction [120, 121, 216]. Thereby, it has been noted that DCs migrate with a speed of 5 μm/min up to 50-times faster than mesenchymal cells such as fibroblasts (0.1-0.5 μm/min) [217]. Only recently, employing intravital multiphoton microscopy on ear dermis of CD11c-YFP reporter mice, dDC interstitial migration was observed for the first time *in vivo* [204]. In healthy mice, immature dDCs were actively crawling at a mean velocity of 4 μm/min. Moreover, translocation through the interstitial space was pertussis toxin sensitive suggesting a role for chemokines. Up to 4 h after LPS challenge, dDC migration speed significantly decreased, but increased again after 6 to 8 h. The mechanisms behind this phenomenon are unclear, but insights may come from *in vitro* studies. Immature DCs are highly adhesive on 2D substrata and form invasive, integrin-containing adhesive structures, called podosomes [218, 219]. While immature DCs rely on integrin α5β1-mediated adhesion, maturing DCs disassemble podosomes and become highly migratory [220, 221]. If interstitial migration depends on proteolytic activity remains still controversial. In contrast to the meanwhile accepted dogma of non-proteolytic amoeboid leukocyte migration [121], MMP9-deficient DCs showed impaired migration *in vivo* and in dermal explants [210, 222]. However, this

defect might also result from alterations in the dermal chemokine milieu, as MMPs are known to process chemokines [223].

5.4.2.3 Dendritic cell trafficking into the lymphatic vessel

Lymphatic vessel architecture
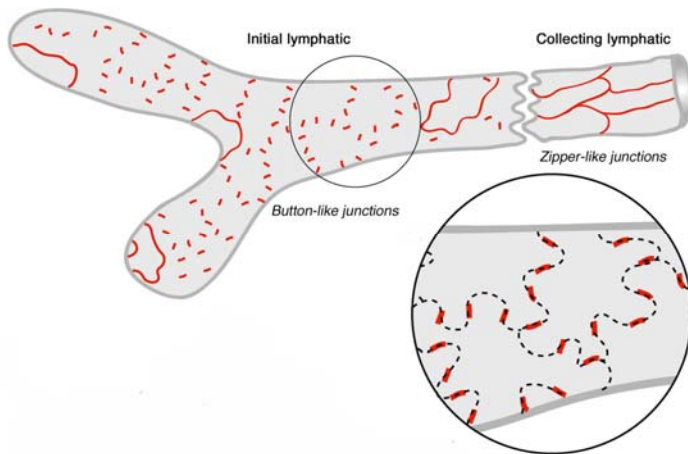
Figure 10: Lymphatic vessel architecture. Initial lymphatics form discontinuous button-like junctions, collecting lymphatics form continuous zipper-like junctions between lymphatic endothelial cells. The detailed view shows oak-leaf-shaped lymphatic endothelial cells (dashed line) with lateral buttons (red) (scheme taken from Baluk et al. [226]).

Lymphatic vessels openly communicate with the interstitium and actively pump interstitial fluid unidirectional out of the tissue towards the LN [177]. The distal blind endings of initial lymphatics pass into the proximal part, the lymphatic collector vessels (Fig. 10). Initials are composed of oak-leaf-shaped LECs which form overlapping flap valves to allow entry, but prevent exit of interstitial fluid [224, 225]. LECs are anchored laterally by discontinuous button-like junctions forming 3 μm-sized openings in the initials [226] (Fig. 10). The thin BM surrounding the initials is also discontinuous and does not restrict solute movement [227, 228]. Lymphatic collector vessels form continuous, zipper-like endothelial cell-cell junctions similar to blood vessels. As they harbour semilunar valves and a surrounding smooth muscle layer that periodically contracts, they consequently push fluid toward the draining lymph node. Furthermore, elastic fibers connect the abluminal side of the lymph vessels to the fibrillar matrix of the dermal interstitium. When the interstitial pressure increases and as such the interstitial ECM enlarges during edema, the elastic fibers pull the lumen of the lymphatics open and allow more fluid to pass [224].

Migration into lymphatic vessels

Several adhesive ligands are expressed on the lymphatic BM or LECs and might facilitate entry into the lymphatic vessels. Upon inflammation, VCAM-1 and ICAM-1 are highly expressed on LECs. Systemic administration of blocking antibodies against VCAM-1 or ICAM-1 suggested a role for the integrins LFA-1 and α4β1 on DCs [229]. Accordingly, DC migration in ICAM-1-deficient mice [230] and in mice deficient for RAPL was impaired [231]. RAPL is required for activation of the integrins α4β1 and LFA-1 by the small GTPase Rap1 [66]. In contrast, integrin β2-deficient mice showed normal DC migration [232]. Hence, if integrins contribute to lymphatic is still an open question. Interestingly, the button-like junctions of lymphatic initials contain VE-cadherin and tight junction proteins including occludins, claudins, zonula occludens-1, ESAM and JAM-A [226]. Similar proteins are found in blood vessel endothelial junctions and have been implicated in leukocyte diapedesis. Of note, JAM-A-deficient DCs display increased migration to lymph nodes suggesting a role for JAM-A as gatekeeper for DC entry into the afferent lymphatics [233]. It is unclear how DCs traverse the lymphatic endothelium. Transient gap opening and lateral interaction with molecules of the button-like junctions might allow paracellular passage, but also transcellular migration is possible [234]. In addition, LECs highly express other surface molecules which might support DC entry: mannose receptor (ligand for L-selectin) [235], CLEVER-1 [236] and podoplanin [237]. Podoplanin is of particular interest as its tissue expression is associated with CCL21 expression [238, 239]. As lymphatic vessels express high levels of CCL21 [186, 240], podoplanin might influence CCL21 presentation and as such chemotactic migration. Alternatively, a model termed 'autologous chemotaxis' was suggested for tumor cell guidance into lymph vessels [241]. Some tumor cell lines, similar to DCs, co-express CCR7 and its ligand CCL19, which seems paradox at first sight. However, within the interstitium, the unidirectional flow convection toward the lymph vessel might drag the secreted chemokine and thereby create a gradient that could then be followed by the same cell. Although this concept appears appealing, the individual contributions of CCL19 and CCL21 remain to be challenged *in vivo*. Transport of DCs within the lymphatic vessels is most likely the same than for solutes. Thereby, a passive flowing with the stream of interstitial fluid is powered by the periodic contractions of the lymphatic vessels [242]. DCs and fluid are then pumped directly into the subcapsular sinus of the LN [243].

5.4.2.4   Dendritic cell trafficking within the lymph node

Lymph node architecture

Lymph vessels from different peripheral drainage areas often congregate at one LN. The LN is composed of (i) the outer subcapsular sinus (entry side for afferent lymphatic vessels), (ii) the B cell follicles (zone of B cell activation beneath the sinus), (iii) the inner T cell paracortex (zone of T cell activation), and (iiii) the medullary sinus (exit site for leukocytes) [244] (Fig. 11).
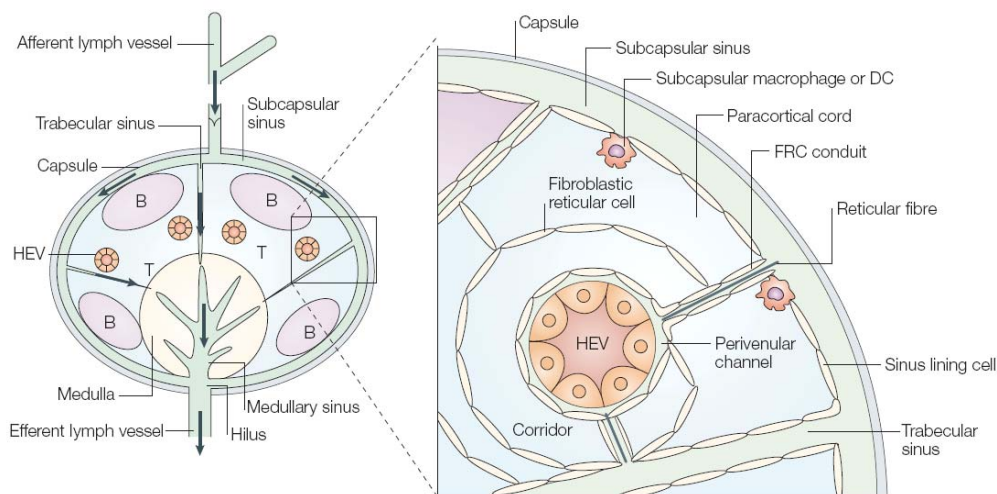
Figure 11: Lymph node architecture. Lymph fluid and dendritic cells arrive via afferent lymphatic vessels. Dendritic cells pass the sinus and area between B cell follicles (B) before entering the T cell cortex (T). Arrows indicate the route of soluble antigen along fibroblastic reticular cell (FRC) conduits. The detailed view indicates FRC conduits bridging the sinus with the HEV (scheme taken from von Andrian and Mempel [69]).

The subcapsular sinus is populated by different resident cell types. Stromal retothelial cells build a 3D sponge-like structure resting on a floor consisting of sinus-lining cells and a discontinuous BM. Subcapsular macrophages settle between the retothelial cells and contribute to the extremely cell-rich composition of the sinus encasing the LN parenchyma [245].

Both follicles and paracortex comprise immune cell types that reside in a stromal cell network. While follicles bear B cells in the follicular dendritic cell network, the paracortex is densely packed with T cells and few DCs in the sponge-like scaffold of fibroblastic reticular cells (FRCs) [246]. FRCs reside on and continuously enwrap highly ordered ECM tubes termed conduits, according to their function in channelling small molecules through the cortex (Fig. 11). The conduit, varying in diameter from 200 nm to 3 μm, consists of an inner core of parallel collagen (type I and III) bundles intermingled with microfibrils and an outer core of

fibronectin and typical BM membrane proteins such as laminins, collagen IV and nidogens [247, 248]. Although more than 95% of the conduit is covered with FRCs, gaps remain that are covered by hematopoietic cells [249, 250]. Mainly resident DCs localize close to FRCs enabling them to rapidly uptake (within minutes) subcutaneously injected small molecules that percolate exclusively in the LN conduits [248]. The FRC fiber network is qualitatively homogenous throughout the T cell paracortex, but is described as more densely packed in a zone called "cortical ridge". Here, in close vicinity to the B cell follicles, a high density of HEVs ensures entry of leukocytes from the blood stream into the LN [251]. Of note, FRC networks and conduits are not exclusive to the LN T cell paracortex, but are found in almost similar composition in the splenic white pulp and the thymic medulla [252, 253].

Migration into and within the lymph node

The mechanisms of DC migration through the cell-rich subcapsular sinus have not been investigated so far. Locomotion kinetics obtained from intravital microscopy studies suggested that the sinus might not represent a major anatomical barrier for DCs [254]. This is in line with observations on T cells that effortlessly glide into the subcapsular sinus, when exposed to an artificial chemokine gradient [255].

Unlike in the sinus, FRCs of the T cell paracortex abundantly express CCL19 and CCL21 suggesting a chemokine gradient along the sinus-cortex border. When both chemokines are absent in the cortex (as observed in *plt/plt* mice), DCs do not enter the LN parenchyma, arguing for a dominant role of CCR7 in LN entry [189, 190]. Our knowledge about paracortical DC migration is mainly based on multiphoton microscopy studies and is still descriptive. Bone-marrow derived DCs entered the T cell paracortex and congregated close to HEVs 18 to 20 h after subcutaneous injection, before at later time points DCs were more evenly distributed [256, 257]. One day after injection, DCs showed remarkable motility with average speeds of 6-7 µm/min [257, 258], before velocities decreased again and DCs integrated into a dense network of sessile DCs [259]. Interestingly, endogenous dDCs also travelled close to HEVs 24 h after ear inflammation, while epidermal LCs required 72 h to localize to deeper cortex areas [203]. The underlying mechanisms of this phenomenon are not clear, but differential expression of chemokine receptors such as CXCR5 might play a role [260].

How DC motility in the lymph node is sustained and how DCs generate traction for locomotion are open questions, but studies on T cell migration revealed some intriguing principles that might also hold true for DCs. Early intravital microscopy work suggested that

T cells perform a dynamic random walk in the LN and encounters with DCs were regarded as random collisions [69, 261]. However, when simultaneously visualising the stromal FRC network, T cell paths led preferentially along the reticular fiber network and turned out to be deterministic and not random [262, 263]. Similar to DCs, naïve T cells express CCR7 and it appeared appealing that its ligands CCL19 and CCL21 are expressed along FRCs and might contribute to deterministic T cell migration [106, 240]. Indeed, interference with CCR7 signalling on T cells decreased the basal motility almost by half [255, 264, 265]. Hence, FRCs appear to be a chemokinetic and adhesive surface. Surprisingly, simultaneous functional blockade of the major integrins α4β1, α4β7 and LFA-1 on T cells did not influence T cell motility [106]. This contrasts with studies on NK cells, another leukocyte subset, which required integrin α2β1-mediated close contact to FRCs for effective migration in the LN [266].

In summary, T cell motility in the paracortex requires signalling through CCR7 ligands expressed on FRCs. Although T cells migrate along the FRC network, current data argues against adhesion-mediated traction as force-generating principle for T cell movement in the LN. However, it is unknown how an alternative migration mode might mechanistically work and if adhesion-independent migration is general for all leukocytes.

5.4.3   Cytoskeletal regulation of dendritic cell migration

As outlined in section 5.2.3.2, 3D leukocyte migration is non-proteolytic and might not require strong adhesive interactions with the environment [119-121]. Hence, the constant shape change of locomoting leukocytes relies largely on internal cytoskeletal forces (contraction, polymer network expansion). The small GTPases Rac, Rho and Cdc42 represent key switches for determining cytoskeletal dynamics [267]. In tumor cells, they regulate the switch from mesenchymal to amoeboid shape (see section 5.3.2.2) [124, 268]. How Rho GTPases influence leukocyte interstitial migration has not been investigated in detail. Most data rely on migration studies on 2D surfaces that do not reflect the complexity of 3D or *in vivo* environments [269]. Only few studies addressed cytoskeletal dynamics during physiological DC migration. Rac1/Rac2-double deficient DCs showed completely abrogated actin polymerization which resulted in cell rounding and concomitant immobility of the cells. Thus, DC migration from the skin to the LN was severely impaired [270]. Although RhoA's function in regulating actomyosin rear end contraction is established in leukocytes [271], its relevance for migration in 3D environments has not been tested yet.

Cdc42 stabilizes and maintains spatial and temporal asymmetries in many cell types [269, 272] and polarity also determines directional movement of leukocytes. Accordingly, loss of chemotactic path finding was observed upon intervention with Cdc42 in neutrophils [271, 273], macrophages [274], hematopoietic stem cells [275] and *Drosophila melanogaster* hemocytes [276]. Although Cdc42 has not been deleted in DCs until to date, studies using dominant-negative versions of the molecule revealed defects in the endocytotic pathway [277], antigen presentation [278], podosome formation [279] and dendrite formation [280] of immature DCs. The impact of Cdc42 on DC cytoskeletal dynamics and migration in 3D interstitial environments is unknown, but work on upstream activators and downstream effectors provided indirect hints. PI3Kγ is a lipid kinase mainly expressed in leukocytes and involved in the production of PIP_3. This second messenger is recruited to the plasma membrane and activates primarily protein kinases with a pleckstrin homology motif, but mediates also assembly of GTPase regulators [281]. In neutrophils, inhibition of PIP_3 accumulation prevents the activation of Cdc42 and reduces Rac activity leading to the formation of unstable pseudopods [271]. Interestingly, PI3Kγ-deficient DCs showed impaired migration from the periphery to draining LNs [282]. However, this defect might not be entirely caused by cytoskeletal disorganization. As PI3Kγ gets directly activated from βγ subunits of activated G protein coupled receptors, it might also influence chemokine sensing [281]. A key Cdc42 effector is WASp that activates the Arp2/3 complex and thus contributes to organized actin polymerization [283]. WASp-depleted DCs showed several cytoskeletal abnormalities including impaired membrane projections and podosomes [279]. Moreover, migration of injected bone marrow-derived DCs and LCs to the LN was compromised [284, 285]. However, it is unclear if Cdc42-mediated WASp function accounted for these defects, as WASp can also be regulated independent of Cdc42. In summary, regulation of cytoskeletal dynamics seems to determine DC migration. Future studies will now have to address the underlying cell biological events fostering interstitial movement and the physiological level where this regulation might be relevant.

6   Aim of the thesis

Leukocyte migration has been studied in detail in the context of extravasation. Interstitial migration, however, remains poorly investigated and might fundamentally differ in its molecular mechanisms (reviewed in Paper II). It is still an open question if physiological interstitial migration requires transmembrane adhesion receptors. Moreover, the amoeboid shape change of leukocytes still lacks a mechanical and molecular framework. Therefore, this Ph.D. thesis sought to study the interplay between adhesive, contractile and protrusive forces during interstitial leukocyte chemotaxis *in vivo* and *in vitro*. In the course of the thesis, the following questions were experimentally targeted:

i)   Does leukocyte migration require integrins and adhesion-mediated traction? (**Paper I and V**)

ii)   How do actomyosin contraction and actin network expansion regulate interstitial migration? (**Paper V**)

iii) Which role does the coordination of leading edge protrusions play? (**Paper VII**)

iv)   Does lack of two specific serine proteases impair granulocyte extravasation and interstitial migration? (**Paper VI**)

To monitor leukocyte interstitial migration by time-lapse video microscopy, *in vitro* (2D and 3D) chemotaxis and *ex vivo* skin explant assays were established that allowed reproducible and manipulable experimental settings. As primary model system, bone-marrow derived dendritic cells (DCs) were employed. The bone marrow was derived from different mouse strains: γ-parvin-deficient mice (Paper I), proteinase 3/neutrophil elastase-double-deficient mice (Paper VI) and mice that were genetically depleted in the hematopoietic system for all integrins (Paper V), talin (Paper V) and Cdc42 (Paper VII). Dendritic cell movement from the dermis of the skin via lymphatics to the lymph node (reviewed in Paper IV) was further tested and migratory dynamics visualized by two-photon microscopy of the lymph node (Paper V). To generalize findings, results obtained with dendritic cells were confirmed with granulocytes and B lymphoblasts (Paper V and VI). Chemical inhibitors were employed to interfere with actomyosin contraction and actin polymerization (Paper V).

7 Brief summaries of the publications

7.1 Summary Paper I

Chu, H. et al. (2006). γ-Parvin is dispensable for hematopoiesis, leukocyte trafficking, and T-cell-dependent antibody response. *Mol. Cell Biol.* 26, 1817-25.

Parvins consist of three members (α-, β-, γ-parvin) which are components of a multiprotein complex that assembles at the cytoplasmic domain of integrin receptors at sites of cell adhesion. Together with integrin-linked kinase (ILK) and PINCH, parvins form a functional complex that links integrins to the cytoskeleton. While α- and β-parvins are widely expressed, γ-parvin has been reported to be restricted to hematopoietic cells. In this study, the expression pattern of the parvins in hematopoietic cells and the phenotype of γ-parvin-deficient mice were analyzed. Mice lacking γ-parvin were viable and fertile. Surprisingly, loss of γ-parvin expression had no effect on blood cell differentiation, proliferation, and survival and no consequence for the T-cell-dependent antibody response and for the migration of lymphocytes and dendritic cells. These data indicate that despite high expression of γ-parvin in hematopoietic cells it must play a more subtle role for blood cell homeostasis.

I contributed to this study by assisting in leukocyte homing assays and flow cytometry analysis of apoptosis.

7.2 Summary Paper II (Review)

Sixt, M. et al. (2006). β1 integrins: zip codes and signaling relay for blood cells. *Curr. Opin. Cell Biol.* 18, 882-90.

β1 integrins comprise the largest integrin receptor family. At least eight of the twelve known heterodimers of the β1 integrin family are expressed on hematopoietic cells. Among these, the VCAM-1 receptor α4β1 has been studied most thoroughly during the process of blood cell extravasation. In this review, we summarize and discuss the confirmed and speculative roles of β1 integrins in leukocyte extravasation, transmigration, movement and retention in interstitial tissues and cell-cell interactions between immune cells. We further give a short overview how targeting integrin interactions might be beneficial in anti-inflammatory therapies.

7.3 Summary Paper III (Review)

Lokmic, Z.*, Lämmermann, T.* et al. (2006). The extracellular matrix of the spleen as a potential organizer of immune cell compartments. *Sem. in Immunol.* 20, 4-13.
* equally contributing first authors.

Blood cells and blood-derived pathogens constantly pass through the open vascular system of the spleen. To exert its dual role as secondary lymphoid organ and site of erythrocyte removal, the spleen is highly organized into different compartments (white pulp, red pulp and marginal zone). While their immune cell composition has been studied in detail over the years, the fibroblastic reticular cell network has only gained little attention. This stromal backbone consists of reticular fibroblasts and extracellular matrix (ECM). In this review, we summarize how distinctly expressed ECM molecules define splenic compartments and speculate about their impact on immune cell localization and structural support. In particular, we highlight the unique molecular structure of the reticular fiber network in the white pulp that, as in the T cell cortex of the lymph node, serves as a conduit for fluid and small particle transport.

7.4 Summary Paper IV (Review)

Lämmermann, T. and Sixt, M. (2008). The microanatomy of T-cell responses. *Immunol. Rev.* 221, 26-43.

Soluble and cell-bound antigens are delivered from the periphery through lymphatic vessels into the lymph node where they initiate adaptive immune responses. In this review, we describe the non-hematopoietic infrastructure of the lymphatic system with a focus on antigen transport from the skin to the draining lymph node. Dendritic cells (DCs) are the major antigen-presenting cells in the periphery. After antigen uptake, they migrate in the dermis, enter the lymphatic vessels and pass the subcapsular sinus of the lymph node. In the cortex, they meet T cells that move along the fibroblastic reticular cell (FRC) network, the stromal backbone of secondary lymphoid organs. Here, we describe the functional anatomy of these compartments and the molecular requirements for DC migration. In contrast to cell-bound antigen, soluble antigen is rapidly transported by dermal fluid to the lymph node where it is directly drained into the inner core of the FRC network serving as conduit system. We discuss the molecular similarities between the conduit system and the dermis and suggest that the conduits can be viewed as a compacted peripheral interstitium.

7.5 Summary Paper V

Lämmermann, T. et al. (2008). Rapid leukocyte migration by integrin-independent flowing and squeezing. *Nature*. 453, 51-55.

According to the general cell migration paradigm, locomoting cells generate traction by coupling contractile forces and actin polymerization to an adhesive surface. In agreement with this principle, rapidly migrating leukocytes use integrin-mediated adhesion when moving over two-dimensional surfaces or along blood vessels. By contrast, the contribution of integrins during three-dimensional (3D) movement of leukocytes within tissues has remained controversial. While blocking integrin function with antibodies might have produced unspecific side effects, single genetic depletion of integrin subunits could not rule out a compensating role for other integrin heterodimers. In this study, we genetically ablated all integrin heterodimers from murine leukocytes and show that functional integrins do not contribute to migration in 3D *in vitro* networks. By studying dendritic cell migration in the dermis, entry into the lymphatics and movement within the lymph node, we show that leukocyte migration *in vivo* is dispensable of integrins. Instead, leukocytes can migrate by the sole force of actin-network expansion, which promotes protrusive flowing of the leading edge. Myosin II-dependent contraction is only required upon passage through narrow gaps, where a squeezing contraction of the trailing edge propels the rigid nucleus. We conclude that non-adhesive migration renders leukocytes autonomous from the tissue context and allows them to quickly and flexibly navigate through any organ without adaptations to alternating extracellular ligands.

7.6   Summary Paper VI

Kessenbrock, K. et al. (2008). Proteinase 3 and neutrophil elastase enhance inflammation by inactivating anti-inflammatory progranulin. *J. Clin. Invest.*. 118, 2438-47.

Neutrophils represent the first line of defense during infectious inflammation, but also contribute to non-infectious chronic inflammation. In this study, mice that were depleted of two very similar neutrophil serine proteases, proteinase 3 (PR3) and neutrophil elastase (NE), showed reduced neutrophil infiltration in a model of subcutaneous formation of antigen-antibody immune complexes (Arthus reaction). This was not a generalized defect in neutrophil extravasation or migration, as neutrophil infiltration in response to application of phorbol esters to the skin and migration in a fibrillar interstitium was not impaired. Instead, NE and PR3 cleaved the anti-inflammatory molecule progranulin (PGRN) and administrating PGRN to wild-type mice inhibited neutrophil influx in the course of the Arthus reaction. In conclusion, NE and PR3 mediate local pro-inflammatory effects by degrading PGRN.

My contribution to this study was design and analysis of the phorbol ester-mediated inflammation model and analysis of neutrophil chemotaxis in 3D collagen gels.

7.7   Summary Paper VII

Lämmermann, T. et al. (2009). Cdc42-dependent leading edge coordination is essential for interstitial dendritic cell migration. *Blood*. Prepublished online February 3, 2009.

Interstitial leukocyte migration is independent of adhesive forces and pericellular proteolysis. Instead, the protrusive flow of the actin cytoskeleton directly drives a basal mode of locomotion that is occasionally supported by actomyosin contractions at the trailing edge to propel the cell's rigid nucleus. In this study, we address the question how coordination of actin flow influences leukocyte migration in a three-dimensional (3D) environment. We employed DCs lacking the small GTPase Cdc42 that still initiated actin flow and actomyosin contraction in response to chemotactic cues, but failed to temporally and spatially regulate their protrusions. While this defect still allowed the cells to move on two-dimensional surfaces, their *in vivo* motility was completely abrogated. This difference was entirely caused by the geometrical complexity of the environment as multiple competing protrusions led to instantaneous entanglement within 3D matrix scaffolds. We conclude that the decisive factor for migrating DCs is internal stabilization of polarity and adequate coordination of cytoskeletal flow.

8   Acknowledgements

Ideas, knowledge and help from many people contributed to and influenced the outcome of this thesis. I would like to express my sincere gratitude to all of them and highlight two persons in particular:

Dr. Michael Sixt, for believing in me and choosing me as his first Ph.D. student. I would like to thank for excellent supervision and support, brilliant ideas, a lot of fun and lasting friendship.

Prof. Dr. Reinhard Fässler, for believing in the Sixt lab and supporting it in any thinkable way. I would like to thank for continuous intellectual, financial and technical support and for providing stimulating and inspiring working conditions and atmosphere.

I would like to thank the members of the thesis committee for reviewing my work: Prof. Dr. Reinhard Fässler as first referee, Prof. Dr. Markus Sperandio as second referee, Prof. Dr. Angelika Vollmar, Prof. Dr. Christian Wahl, Prof. Dr. Martin Biel and Prof. Dr. Karl-Peter Hopfner.

Special thanks to collaborating scientists for invaluable help and discussions: Prof. Dr. Reinhold Förster, Dr. Tim Worbs, Prof. Dr. Cord Brakebusch, Prof. Dr. David Critchley, Dr. Susan Monkley, Prof. Dr. Bernhard Bader, Dr. Markus Keller, Dr. Kai Kessenbrock, Prof. Dr. Dieter Jenne, Prof. Dr. Lydia Sorokin and Dr. Zerina Lokmic.

Special thanks also to Karin Hirsch for tremendous help in the lab, Dr. Sylvia Cremer for evaluating statistical data, Dr. Marc Schmidt-Supprian and Dr. Markus Moser for fruitful discussions.

Furthermore, my thanks go to members of the Sixt lab, Kathrin, Jörg, Fabian and Holger, all present and former members of the department, in particular Martina, Aurelia, Ola, Michi, Karsten, Sebastian and Raphael for companion and friendship, a very comfortable working atmosphere, fruitful discussions and experimental help. I would also like to thank Dr. Walter Göhring for constant technical and administrative support, Sylvia Zehner and Carmen Schmitz for help with administrative work and the animal caretakers for help in mouse breeding, in particular Diana Schmidt and Jens Päßler.

Most importantly, I would like to thank my family, in particular my mother Renate, my brother Lutz and my sunshine Geli, for support, confidence and encouragement throughout my thesis – even though science can be big fun, it will never replace life with you.

9 Curriculum Vitae

PERSONAL INFORMATION

Name	Tim Lämmermann
Nationality	German
Date and place of birth	27.11.1978, Fürth, Germany
Marital status	Single, no children
Address	Gräfelfinger Str. 121, 81375 München

EDUCATION

11/2004-07/2009   **Max-Planck Institute of Biochemistry**, Martinsried, Germany
Department of Molecular Medicine, Prof. Dr. Reinhard Fässler
Ph.D. student with Dr. Michael Sixt

09/2003-04/2004   **Lund University**, Lund, Sweden
Department of Experimental Pathology, Prof. Dr. Lydia Sorokin
Diploma thesis ("The extracellular matrix of the spleen")

09/1998-04/2004   **Friedrich Alexander University**, Erlangen-Nuremberg, Germany
Studies in molecular medicine
Majors: cell biology, minors: immunology, pharmacology, neuroscience
Master of science (Dipl. Mol. Med.), final grade: with excellence (1.0)

10/1988-06/1997   **Hardenberg Gymnasium**, Fürth, Germany
Allgemeine Hochschulreife (university entrance qualification)
Final grade: very good (1.0)

10/1984-09/1988   **Adalbert-Stifter Grundschule**, Fürth, Germany
Primary school

CIVIL SERVICE

07/1997-09/1998   Civil service in old people's home, Nuremberg, Germany

München, den 20.4.2009

10 References

1. Alvarez, D., Vollmann, E.H. & von Andrian, U.H. Mechanisms and consequences of dendritic cell migration. *Immunity* **29**, 325-42 (2008).
2. Sixt, M., Bauer, M., Lammermann, T. & Fassler, R. Beta1 integrins: zip codes and signaling relay for blood cells. *Curr Opin Cell Biol* **18**, 482-90 (2006).
3. Luster, A.D., Alon, R. & von Andrian, U.H. Immune cell migration in inflammation: present and future therapeutic targets. *Nat Immunol* **6**, 1182-90 (2005).
4. Bromley, S.K., Mempel, T.R. & Luster, A.D. Orchestrating the orchestrators: chemokines in control of T cell traffic. *Nat Immunol* **9**, 970-80 (2008).
5. Springer, T.A. Traffic signals for lymphocyte recirculation and leukocyte emigration: the multistep paradigm. *Cell* **76**, 301-14 (1994).
6. Ley, K., Laudanna, C., Cybulsky, M.I. & Nourshargh, S. Getting to the site of inflammation: the leukocyte adhesion cascade updated. *Nat Rev Immunol* **7**, 678-89 (2007).
7. Butcher, E.C. Leukocyte-endothelial cell recognition: three (or more) steps to specificity and diversity. *Cell* **67**, 1033-6 (1991).
8. McEver, R.P. Selectins. *Curr Opin Immunol* **6**, 75-84 (1994).
9. Alon, R. & Dustin, M.L. Force as a facilitator of integrin conformational changes during leukocyte arrest on blood vessels and antigen-presenting cells. *Immunity* **26**, 17-27 (2007).
10. Alon, R. & Ley, K. Cells on the run: shear-regulated integrin activation in leukocyte rolling and arrest on endothelial cells. *Curr Opin Cell Biol* **20**, 525-32 (2008).
11. Rosen, S.D. Ligands for L-selectin: homing, inflammation, and beyond. *Annu Rev Immunol* **22**, 129-56 (2004).
12. Sperandio, M. et al. P-selectin glycoprotein ligand-1 mediates L-selectin-dependent leukocyte rolling in venules. *J Exp Med* **197**, 1355-63 (2003).
13. McEver, R.P. Selectins: lectins that initiate cell adhesion under flow. *Curr Opin Cell Biol* **14**, 581-6 (2002).
14. Middleton, J. et al. Transcytosis and surface presentation of IL-8 by venular endothelial cells. *Cell* **91**, 385-95 (1997).
15. Pruenster, M. et al. The Duffy antigen receptor for chemokines transports chemokines and supports their promigratory activity. *Nat Immunol* **10**, 101-8 (2009).
16. Rot, A. & von Andrian, U.H. Chemokines in innate and adaptive host defense: basic chemokinese grammar for immune cells. *Annu Rev Immunol* **22**, 891-928 (2004).
17. Thelen, M. & Stein, J.V. How chemokines invite leukocytes to dance. *Nat Immunol* **9**, 953-9 (2008).
18. Kehrl, J.H. Chemoattractant receptor signaling and the control of lymphocyte migration. *Immunol Res* **34**, 211-27 (2006).
19. Viola, A. & Luster, A.D. Chemokines and their receptors: drug targets in immunity and inflammation. *Annu Rev Pharmacol Toxicol* **48**, 171-97 (2008).
20. Kinashi, T. Intracellular signalling controlling integrin activation in lymphocytes. *Nat Rev Immunol* **5**, 546-59 (2005).
21. Hynes, R.O. & Zhao, Q. The evolution of cell adhesion. *J Cell Biol* **150**, F89-96 (2000).
22. Hynes, R.O. Integrins: bidirectional, allosteric signaling machines. *Cell* **110**, 673-87 (2002).
23. Banno, A. & Ginsberg, M.H. Integrin activation. *Biochem Soc Trans* **36**, 229-34 (2008).
24. Bouvard, D. et al. Functional consequences of integrin gene mutations in mice. *Circ Res* **89**, 211-23 (2001).
25. Sheppard, D. In vivo functions of integrins: lessons from null mutations in mice. *Matrix Biol* **19**, 203-9 (2000).
26. Fassler, R. & Meyer, M. Consequences of lack of beta 1 integrin gene expression in mice. *Genes Dev* **9**, 1896-908 (1995).
27. Stephens, L.E. et al. Deletion of beta 1 integrins in mice results in inner cell mass failure and peri-implantation lethality. *Genes Dev* **9**, 1883-95 (1995).
28. Bader, B.L., Rayburn, H., Crowley, D. & Hynes, R.O. Extensive vasculogenesis, angiogenesis, and organogenesis precede lethality in mice lacking all alpha v integrins. *Cell* **95**, 507-19 (1998).
29. Scharffetter-Kochanek, K. et al. Spontaneous skin ulceration and defective T cell function in CD18 null mice. *J Exp Med* **188**, 119-31 (1998).
30. Etzioni, A. & Alon, R. Leukocyte adhesion deficiency III: a group of integrin activation defects in hematopoietic lineage cells. *Curr Opin Allergy Clin Immunol* **4**, 485-90 (2004).
31. Wagner, N. et al. Critical role for beta7 integrins in formation of the gut-associated lymphoid tissue. *Nature* **382**, 366-70 (1996).

32. Harburger, D.S. & Calderwood, D.A. Integrin signalling at a glance. *J Cell Sci* **122**, 159-63 (2009).
33. Askari, J.A., Buckley, P.A., Mould, A.P. & Humphries, M.J. Linking integrin conformation to function. *J Cell Sci* **122**, 165-70 (2009).
34. Mor, A., Dustin, M.L. & Philips, M.R. Small GTPases and LFA-1 reciprocally modulate adhesion and signaling. *Immunol Rev* **218**, 114-25 (2007).
35. Luo, B.H., Carman, C.V. & Springer, T.A. Structural basis of integrin regulation and signaling. *Annu Rev Immunol* **25**, 619-47 (2007).
36. Abram, C.L. & Lowell, C.A. The diverse functions of Src family kinases in macrophages. *Front Biosci* **13**, 4426-50 (2008).
37. Burridge, K. & Connell, L. Talin: a cytoskeletal component concentrated in adhesion plaques and other sites of actin-membrane interaction. *Cell Motil* **3**, 405-17 (1983).
38. Horwitz, A., Duggan, K., Buck, C., Beckerle, M.C. & Burridge, K. Interaction of plasma membrane fibronectin receptor with talin--a transmembrane linkage. *Nature* **320**, 531-3 (1986).
39. Calderwood, D.A. Integrin activation. *J Cell Sci* **117**, 657-66 (2004).
40. Monkley, S.J., Pritchard, C.A. & Critchley, D.R. Analysis of the mammalian talin2 gene TLN2. *Biochem Biophys Res Commun* **286**, 880-5 (2001).
41. Critchley, D.R. & Gingras, A.R. Talin at a glance. *J Cell Sci* **121**, 1345-7 (2008).
42. Campbell, I.D. & Ginsberg, M.H. The talin-tail interaction places integrin activation on FERM ground. *Trends Biochem Sci* **29**, 429-35 (2004).
43. Wegener, K.L. et al. Structural basis of integrin activation by talin. *Cell* **128**, 171-82 (2007).
44. Petrich, B.G. et al. Talin is required for integrin-mediated platelet function in hemostasis and thrombosis. *J Exp Med* **204**, 3103-11 (2007).
45. Nieswandt, B. et al. Loss of talin1 in platelets abrogates integrin activation, platelet aggregation, and thrombus formation in vitro and in vivo. *J Exp Med* **204**, 3113-8 (2007).
46. Smith, A. et al. A talin-dependent LFA-1 focal zone is formed by rapidly migrating T lymphocytes. *J Cell Biol* **170**, 141-51 (2005).
47. Moser, M., Nieswandt, B., Ussar, S., Pozgajova, M. & Fassler, R. Kindlin-3 is essential for integrin activation and platelet aggregation. *Nat Med* **14**, 325-30 (2008).
48. Siegel, D.H. et al. Loss of kindlin-1, a human homolog of the Caenorhabditis elegans actin-extracellular-matrix linker protein UNC-112, causes Kindler syndrome. *Am J Hum Genet* **73**, 174-87 (2003).
49. Ma, Y.Q., Qin, J., Wu, C. & Plow, E.F. Kindlin-2 (Mig-2): a co-activator of beta3 integrins. *J Cell Biol* **181**, 439-46 (2008).
50. Montanez, E. et al. Kindlin-2 controls bidirectional signaling of integrins. *Genes Dev* **22**, 1325-30 (2008).
51. Shi, M. et al. A structural hypothesis for the transition between bent and extended conformations of the leukocyte beta2 integrins. *J Biol Chem* **282**, 30198-206 (2007).
52. Ussar, S. et al. Loss of Kindlin-1 causes skin atrophy and lethal neonatal intestinal epithelial dysfunction. *PLoS Genet* **4**, e1000289 (2008).
53. Kloeker, S. et al. The Kindler syndrome protein is regulated by transforming growth factor-beta and involved in integrin-mediated adhesion. *J Biol Chem* **279**, 6824-33 (2004).
54. Moser, M. et al. Kindlin-3 is required for beta2 integrin-mediated leukocyte adhesion to endothelial cells. *Nat Med* **15**, 300-5 (2009).
55. Ussar, S., Wang, H.V., Linder, S., Fassler, R. & Moser, M. The Kindlins: subcellular localization and expression during murine development. *Exp Cell Res* **312**, 3142-51 (2006).
56. Svensson, L. et al. Leukocyte adhesion deficiency-III is caused by mutations in KINDLIN3 affecting integrin activation. *Nat Med* **15**, 306-12 (2009).
57. Malinin, N.L. et al. A point mutation in KINDLIN3 ablates activation of three integrin subfamilies in humans. *Nat Med* **15**, 313-8 (2009).
58. Mory, A. et al. Kindlin-3: a new gene involved in the pathogenesis of LAD-III. *Blood* **112**, 2591 (2008).
59. Kuijpers, T.W. et al. LAD-1/variant syndrome is caused by mutations in FERMT3. *Blood* (2008).
60. Pasvolsky, R. et al. A LAD-III syndrome is associated with defective expression of the Rap-1 activator CalDAG-GEFI in lymphocytes, neutrophils, and platelets. *J Exp Med* **204**, 1571-82 (2007).
61. Alon, R. & Etzioni, A. LAD-III, a novel group of leukocyte integrin activation deficiencies. *Trends Immunol* **24**, 561-6 (2003).
62. Bergmeier, W. et al. Mice lacking the signaling molecule CalDAG-GEFI represent a model for leukocyte adhesion deficiency type III. *J Clin Invest* **117**, 1699-707 (2007).
63. Bos, J.L. Linking Rap to cell adhesion. *Curr Opin Cell Biol* **17**, 123-8 (2005).
64. Medeiros, R.B. et al. Protein kinase D1 and the beta 1 integrin cytoplasmic domain control beta 1 integrin function via regulation of Rap1 activation. *Immunity* **23**, 213-26 (2005).
65. Lafuente, E.M. et al. RIAM, an Ena/VASP and Profilin ligand, interacts with Rap1-GTP and mediates Rap1-induced adhesion. *Dev Cell* **7**, 585-95 (2004).

66. Katagiri, K., Maeda, A., Shimonaka, M. & Kinashi, T. RAPL, a Rap1-binding molecule that mediates Rap1-induced adhesion through spatial regulation of LFA-1. *Nat Immunol* **4**, 741-8 (2003).

67. Puklin-Faucher, E., Gao, M., Schulten, K. & Vogel, V. How the headpiece hinge angle is opened: New insights into the dynamics of integrin activation. *J Cell Biol* **175**, 349-60 (2006).

68. Astrof, N.S., Salas, A., Shimaoka, M., Chen, J. & Springer, T.A. Importance of force linkage in mechanochemistry of adhesion receptors. *Biochemistry* **45**, 15020-8 (2006).

69. von Andrian, U.H. & Mempel, T.R. Homing and cellular traffic in lymph nodes. *Nat Rev Immunol* **3**, 867-78 (2003).

70. Berlin-Rufenach, C. et al. Lymphocyte migration in lymphocyte function-associated antigen (LFA)-1-deficient mice. *J Exp Med* **189**, 1467-78 (1999).

71. Prieto, J. et al. MALA-2, mouse homologue of human adhesion molecule ICAM-1 (CD54). *Eur J Immunol* **19**, 1551-7 (1989).

72. Hamann, A., Andrew, D.P., Jablonski-Westrich, D., Holzmann, B. & Butcher, E.C. Role of alpha 4-integrins in lymphocyte homing to mucosal tissues in vivo. *J Immunol* **152**, 3282-93 (1994).

73. Brakebusch, C. et al. Beta1 integrin is not essential for hematopoiesis but is necessary for the T cell-dependent IgM antibody response. *Immunity* **16**, 465-77 (2002).

74. Shamri, R. et al. Lymphocyte arrest requires instantaneous induction of an extended LFA-1 conformation mediated by endothelium-bound chemokines. *Nat Immunol* **6**, 497-506 (2005).

75. Tsuzuki, Y. et al. alpha 4 integrin plays a critical role in early stages of T lymphocyte migration in Peyer's patches of rats. *Int Immunol* **8**, 287-95 (1996).

76. Kanda, H. et al. Autotaxin, an ectoenzyme that produces lysophosphatidic acid, promotes the entry of lymphocytes into secondary lymphoid organs. *Nat Immunol* **9**, 415-23 (2008).

77. Henderson, R.B. et al. The use of lymphocyte function-associated antigen (LFA)-1-deficient mice to determine the role of LFA-1, Mac-1, and alpha4 integrin in the inflammatory response of neutrophils. *J Exp Med* **194**, 219-26 (2001).

78. Phillipson, M. et al. Intraluminal crawling of neutrophils to emigration sites: a molecularly distinct process from adhesion in the recruitment cascade. *J Exp Med* **203**, 2569-75 (2006).

79. Henderson, R.B., Hobbs, J.A., Mathies, M. & Hogg, N. Rapid recruitment of inflammatory monocytes is independent of neutrophil migration. *Blood* **102**, 328-35 (2003).

80. Arroyo, A.G., Yang, J.T., Rayburn, H. & Hynes, R.O. Differential requirements for alpha4 integrins during fetal and adult hematopoiesis. *Cell* **85**, 997-1008 (1996).

81. Siegelman, M.H., Stanescu, D. & Estess, P. The CD44-initiated pathway of T-cell extravasation uses VLA-4 but not LFA-1 for firm adhesion. *J Clin Invest* **105**, 683-91 (2000).

82. Singbartl, K. et al. A CD2-green fluorescence protein-transgenic mouse reveals very late antigen-4-dependent CD8+ lymphocyte rolling in inflamed venules. *J Immunol* **166**, 7520-6 (2001).

83. Auffray, C. et al. Monitoring of blood vessels and tissues by a population of monocytes with patrolling behavior. *Science* **317**, 666-70 (2007).

84. Scimone, M.L., Aifantis, I., Apostolou, I., von Boehmer, H. & von Andrian, U.H. A multistep adhesion cascade for lymphoid progenitor cell homing to the thymus. *Proc Natl Acad Sci U S A* **103**, 7006-11 (2006).

85. Mazo, I.B. et al. Bone marrow is a major reservoir and site of recruitment for central memory CD8+ T cells. *Immunity* **22**, 259-70 (2005).

86. Potocnik, A.J., Brakebusch, C. & Fassler, R. Fetal and adult hematopoietic stem cells require beta1 integrin function for colonizing fetal liver, spleen, and bone marrow. *Immunity* **12**, 653-63 (2000).

87. Priestley, G.V., Scott, L.M., Ulyanova, T. & Papayannopoulou, T. Lack of alpha4 integrin expression in stem cells restricts competitive function and self-renewal activity. *Blood* **107**, 2959-67 (2006).

88. Qian, H., Tryggvason, K., Jacobsen, S.E. & Ekblom, M. Contribution of alpha6 integrins to hematopoietic stem and progenitor cell homing to bone marrow and collaboration with alpha4 integrins. *Blood* **107**, 3503-10 (2006).

89. Bonder, C.S. et al. Rules of recruitment for Th1 and Th2 lymphocytes in inflamed liver: a role for alpha-4 integrin and vascular adhesion protein-1. *Immunity* **23**, 153-63 (2005).

90. Bauer, M. et al. Beta1 integrins differentially control extravasation of inflammatory cell subsets into the CNS during autoimmunity. *Proc Natl Acad Sci U S A* **106**, 1920-5 (2009).

91. Kerfoot, S.M. et al. Reevaluation of P-selectin and alpha 4 integrin as targets for the treatment of experimental autoimmune encephalomyelitis. *J Immunol* **176**, 6225-34 (2006).

92. Vajkoczy, P., Laschinger, M. & Engelhardt, B. Alpha4-integrin-VCAM-1 binding mediates G protein-independent capture of encephalitogenic T cell blasts to CNS white matter microvessels. *J Clin Invest* **108**, 557-65 (2001).

93. Yednock, T.A. et al. Prevention of experimental autoimmune encephalomyelitis by antibodies against alpha 4 beta 1 integrin. *Nature* **356**, 63-6 (1992).

94. Vestweber, D. Adhesion and signaling molecules controlling the transmigration of leukocytes through endothelium. *Immunol Rev* **218**, 178-96 (2007).

95. Carman, C.V. et al. Transcellular diapedesis is initiated by invasive podosomes. *Immunity* **26**, 784-97 (2007).

96. Petri, B., Phillipson, M. & Kubes, P. The physiology of leukocyte recruitment: an in vivo perspective. *J Immunol* **180**, 6439-46 (2008).

97. Schenkel, A.R., Mamdouh, Z. & Muller, W.A. Locomotion of monocytes on endothelium is a critical step during extravasation. *Nat Immunol* **5**, 393-400 (2004).

98. Oppenheimer-Marks, N., Davis, L.S., Bogue, D.T., Ramberg, J. & Lipsky, P.E. Differential utilization of ICAM-1 and VCAM-1 during the adhesion and transendothelial migration of human T lymphocytes. *J Immunol* **147**, 2913-21 (1991).

99. Barreiro, O. et al. Dynamic interaction of VCAM-1 and ICAM-1 with moesin and ezrin in a novel endothelial docking structure for adherent leukocytes. *J Cell Biol* **157**, 1233-45 (2002).

100. Carman, C.V. & Springer, T.A. A transmigratory cup in leukocyte diapedesis both through individual vascular endothelial cells and between them. *J Cell Biol* **167**, 377-88 (2004).

101. Nieminen, M. et al. Vimentin function in lymphocyte adhesion and transcellular migration. *Nat Cell Biol* **8**, 156-62 (2006).

102. Millan, J. et al. Lymphocyte transcellular migration occurs through recruitment of endothelial ICAM-1 to caveola- and F-actin-rich domains. *Nat Cell Biol* **8**, 113-23 (2006).

103. Dangerfield, J., Larbi, K.Y., Huang, M.T., Dewar, A. & Nourshargh, S. PECAM-1 (CD31) homophilic interaction up-regulates alpha6beta1 on transmigrated neutrophils in vivo and plays a functional role in the ability of alpha6 integrins to mediate leukocyte migration through the perivascular basement membrane. *J Exp Med* **196**, 1201-11 (2002).

104. Wang, S. et al. Venular basement membranes contain specific matrix protein low expression regions that act as exit points for emigrating neutrophils. *J Exp Med* **203**, 1519-32 (2006).

105. Dangerfield, J.P., Wang, S. & Nourshargh, S. Blockade of alpha6 integrin inhibits IL-1beta- but not TNF-alpha-induced neutrophil transmigration in vivo. *J Leukoc Biol* **77**, 159-65 (2005).

106. Woolf, E. et al. Lymph node chemokines promote sustained T lymphocyte motility without triggering stable integrin adhesiveness in the absence of shear forces. *Nat Immunol* **8**, 1076-85 (2007).

107. Werr, J., Xie, X., Hedqvist, P., Ruoslahti, E. & Lindbom, L. beta1 integrins are critically involved in neutrophil locomotion in extravascular tissue In vivo. *J Exp Med* **187**, 2091-6 (1998).

108. Werr, J. et al. Integrin alpha(2)beta(1) (VLA-2) is a principal receptor used by neutrophils for locomotion in extravascular tissue. *Blood* **95**, 1804-9 (2000).

109. Andreasen, S.O. et al. Expression and functional importance of collagen-binding integrins, alpha 1 beta 1 and alpha 2 beta 1, on virus-activated T cells. *J Immunol* **171**, 2804-11 (2003).

110. de Fougerolles, A.R. et al. Regulation of inflammation by collagen-binding integrins alpha1beta1 and alpha2beta1 in models of hypersensitivity and arthritis. *J Clin Invest* **105**, 721-9 (2000).

111. Fiorucci, S. et al. Importance of innate immunity and collagen binding integrin alpha1beta1 in TNBS-induced colitis. *Immunity* **17**, 769-80 (2002).

112. Ray, S.J. et al. The collagen binding alpha1beta1 integrin VLA-1 regulates CD8 T cell-mediated immune protection against heterologous influenza infection. *Immunity* **20**, 167-79 (2004).

113. Shimizu, Y. & Shaw, S. Lymphocyte interactions with extracellular matrix. *Faseb J* **5**, 2292-9 (1991).

114. Franitza, S., Alon, R. & Lider, O. Real-time analysis of integrin-mediated chemotactic migration of T lymphocytes within 3-D extracellular matrix-like gels. *J Immunol Methods* **225**, 9-25 (1999).

115. Brown, A.F. Neutrophil granulocytes: adhesion and locomotion on collagen substrata and in collagen matrices. *J Cell Sci* **58**, 455-67 (1982).

116. Haston, W.S., Shields, J.M. & Wilkinson, P.C. Lymphocyte locomotion and attachment on two-dimensional surfaces and in three-dimensional matrices. *J Cell Biol* **92**, 747-52 (1982).

117. Saltzman, W.M., Livingston, T.L. & Parkhurst, M.R. Antibodies to CD18 influence neutrophil migration through extracellular matrix. *J Leukoc Biol* **65**, 356-63 (1999).

118. Schmalstieg, F.C., Rudloff, H.E., Hillman, G.R. & Anderson, D.C. Two-dimensional and three-dimensional movement of human polymorphonuclear leukocytes: two fundamentally different mechanisms of locomotion [corrected]. *J Leukoc Biol* **40**, 677-91 (1986).

119. Malawista, S.E. & de Boisfleury Chevance, A. Random locomotion and chemotaxis of human blood polymorphonuclear leukocytes (PMN) in the presence of EDTA: PMN in close quarters require neither leukocyte integrins nor external divalent cations. *Proc Natl Acad Sci U S A* **94**, 11577-82 (1997).

120. Friedl, P., Entschladen, F., Conrad, C., Niggemann, B. & Zanker, K.S. CD4+ T lymphocytes migrating in three-dimensional collagen lattices lack focal adhesions and utilize beta1 integrin-independent strategies for polarization, interaction with collagen fibers and locomotion. *Eur J Immunol* **28**, 2331-43 (1998).

121. Wolf, K., Muller, R., Borgmann, S., Brocker, E.B. & Friedl, P. Amoeboid shape change and contact guidance: T-lymphocyte crawling through fibrillar collagen is independent of matrix remodeling by MMPs and other proteases. *Blood* **102**, 3262-9 (2003).

122.   Friedl, P. & Wolf, K. Tumour-cell invasion and migration: diversity and escape mechanisms. *Nat Rev Cancer* **3**, 362-74 (2003).

123.   Hegerfeldt, Y., Tusch, M., Brocker, E.B. & Friedl, P. Collective cell movement in primary melanoma explants: plasticity of cell-cell interaction, beta1-integrin function, and migration strategies. *Cancer Res* **62**, 2125-30 (2002).

124.   Sahai, E. & Marshall, C.J. Differing modes of tumour cell invasion have distinct requirements for Rho/ROCK signalling and extracellular proteolysis. *Nat Cell Biol* **5**, 711-9 (2003).

125.   Sanz-Moreno, V. et al. Rac activation and inactivation control plasticity of tumor cell movement. *Cell* **135**, 510-23 (2008).

126.   Zaman, M.H. et al. Migration of tumor cells in 3D matrices is governed by matrix stiffness along with cell-matrix adhesion and proteolysis. *Proc Natl Acad Sci U S A* **103**, 10889-94 (2006).

127.   Bory. *Dictionnaire classique d'histoire naturelle*, 158 (1826).

128.   Rösel von Rosenhof, A.J. *Insecten-Belustigung* **3**, 622-623,223-224 (1755).

129.   Friedl, P. Prespecification and plasticity: shifting mechanisms of cell migration. *Curr Opin Cell Biol* **16**, 14-23 (2004).

130.   Wolf, K. et al. Multi-step pericellular proteolysis controls the transition from individual to collective cancer cell invasion. *Nat Cell Biol* **9**, 893-904 (2007).

131.   Wolf, K. et al. Compensation mechanism in tumor cell migration: mesenchymal-amoeboid transition after blocking of pericellular proteolysis. *J Cell Biol* **160**, 267-77 (2003).

132.   Friedl, P. & Weigelin, B. Interstitial leukocyte migration and immune function. *Nat Immunol* **9**, 960-9 (2008).

133.   Krummel, M.F. & Macara, I. Maintenance and modulation of T cell polarity. *Nat Immunol* **7**, 1143-9 (2006).

134.   Xu, J. et al. Divergent signals and cytoskeletal assemblies regulate self-organizing polarity in neutrophils. *Cell* **114**, 201-14 (2003).

135.   Merz, A.J. & Higgs, H.N. Listeria motility: biophysics pushes things forward. *Curr Biol* **13**, R302-4 (2003).

136.   Mogilner, A. & Oster, G. Polymer motors: pushing out the front and pulling up the back. *Curr Biol* **13**, R721-33 (2003).

137.   Chhabra, E.S. & Higgs, H.N. The many faces of actin: matching assembly factors with cellular structures. *Nat Cell Biol* **9**, 1110-21 (2007).

138.   Mitchison, T.J. & Cramer, L.P. Actin-based cell motility and cell locomotion. *Cell* **84**, 371-9 (1996).

139.   Ladwein, M. & Rottner, K. On the Rho'd: the regulation of membrane protrusions by Rho-GTPases. *FEBS Lett* **582**, 2066-74 (2008).

140.   Charras, G. & Paluch, E. Blebs lead the way: how to migrate without lamellipodia. *Nat Rev Mol Cell Biol* **9**, 730-6 (2008).

141.   Kay, R.R., Langridge, P., Traynor, D. & Hoeller, O. Changing directions in the study of chemotaxis. *Nat Rev Mol Cell Biol* **9**, 455-63 (2008).

142.   Paluch, E., Piel, M., Prost, J., Bornens, M. & Sykes, C. Cortical actomyosin breakage triggers shape oscillations in cells and cell fragments. *Biophys J* **89**, 724-33 (2005).

143.   Charras, G.T., Yarrow, J.C., Horton, M.A., Mahadevan, L. & Mitchison, T.J. Non-equilibration of hydrostatic pressure in blebbing cells. *Nature* **435**, 365-9 (2005).

144.   Mitchison, T.J., Charras, G.T. & Mahadevan, L. Implications of a poroelastic cytoplasm for the dynamics of animal cell shape. *Semin Cell Dev Biol* **19**, 215-23 (2008).

145.   Charras, G.T., Hu, C.K., Coughlin, M. & Mitchison, T.J. Reassembly of contractile actin cortex in cell blebs. *J Cell Biol* **175**, 477-90 (2006).

146.   Lauffenburger, D.A. & Horwitz, A.F. Cell migration: a physically integrated molecular process. *Cell* **84**, 359-69 (1996).

147.   Fey, P., Stephens, S., Titus, M.A. & Chisholm, R.L. SadA, a novel adhesion receptor in Dictyostelium. *J Cell Biol* **159**, 1109-19 (2002).

148.   Fukui, Y. & Inoue, S. Amoeboid movement anchored by eupodia, new actin-rich knobby feet in Dictyostelium. *Cell Motil Cytoskeleton* **36**, 339-54 (1997).

149.   Uchida, K.S. & Yumura, S. Dynamics of novel feet of Dictyostelium cells during migration. *J Cell Sci* **117**, 1443-55 (2004).

150.   Shulman, Z. et al. Lymphocyte crawling and transendothelial migration require chemokine triggering of high-affinity LFA-1 integrin. *Immunity* **30**, 384-96 (2009).

151.   Stanley, P. et al. Intermediate-affinity LFA-1 binds alpha-actinin-1 to control migration at the leading edge of the T cell. *Embo J* **27**, 62-75 (2008).

152.   Iwadate, Y. & Yumura, S. Actin-based propulsive forces and myosin-II-based contractile forces in migrating Dictyostelium cells. *J Cell Sci* **121**, 1314-24 (2008).

153. Lombardi, M.L., Knecht, D.A., Dembo, M. & Lee, J. Traction force microscopy in Dictyostelium reveals distinct roles for myosin II motor and actin-crosslinking activity in polarized cell movement. *J Cell Sci* **120**, 1624-34 (2007).

154. Uchida, K.S., Kitanishi-Yumura, T. & Yumura, S. Myosin II contributes to the posterior contraction and the anterior extension during the retraction phase in migrating Dictyostelium cells. *J Cell Sci* **116**, 51-60 (2003).

155. Smith, L.A., Aranda-Espinoza, H., Haun, J.B., Dembo, M. & Hammer, D.A. Neutrophil traction stresses are concentrated in the uropod during migration. *Biophys J* **92**, L58-60 (2007).

156. Wessels, D. et al. Cell motility and chemotaxis in Dictyostelium amebae lacking myosin heavy chain. *Dev Biol* **128**, 164-77 (1988).

157. Eddy, R.J., Pierini, L.M., Matsumura, F. & Maxfield, F.R. Ca2+-dependent myosin II activation is required for uropod retraction during neutrophil migration. *J Cell Sci* **113 (Pt 7)**, 1287-98 (2000).

158. Morin, N.A. et al. Nonmuscle myosin heavy chain IIA mediates integrin LFA-1 de-adhesion during T lymphocyte migration. *J Exp Med* **205**, 195-205 (2008).

159. Smith, A., Bracke, M., Leitinger, B., Porter, J.C. & Hogg, N. LFA-1-induced T cell migration on ICAM-1 involves regulation of MLCK-mediated attachment and ROCK-dependent detachment. *J Cell Sci* **116**, 3123-33 (2003).

160. Jay, P.Y., Pham, P.A., Wong, S.A. & Elson, E.L. A mechanical function of myosin II in cell motility. *J Cell Sci* **108 (Pt 1)**, 387-93 (1995).

161. Jacobelli, J., Bennett, F.C., Pandurangi, P., Tooley, A.J. & Krummel, M.F. Myosin-IIA and ICAM-1 regulate the interchange between two distinct modes of T cell migration. *J Immunol* **182**, 2041-50 (2009).

162. Bottino, D., Mogilner, A., Roberts, T., Stewart, M. & Oster, G. How nematode sperm crawl. *J Cell Sci* **115**, 367-84 (2002).

163. Miao, L. et al. The role of filament-packing dynamics in powering amoeboid cell motility. *Proc Natl Acad Sci U S A* **105**, 5390-5 (2008).

164. Joanny, J.F., Julicher, F. & Prost, J. Motion of an adhesive gel in a swelling gradient: a mechanism for cell locomotion. *Phys Rev Lett* **90**, 168102 (2003).

165. Miao, L., Vanderlinde, O., Stewart, M. & Roberts, T.M. Retraction in amoeboid cell motility powered by cytoskeletal dynamics. *Science* **302**, 1405-7 (2003).

166. de Bruyn, P.P.H. The amoeboid movement of the mammalian leucocyte in tissue culture. *Anat Rec* **95**, 117-192 (1946).

167. Lewis, W.H. Locomotion of lymphocytes *Bull Johns Hopkins Hosp* **49**, 29-36 (1931).

168. Friedl, P., Borgmann, S. & Brocker, E.B. Amoeboid leukocyte crawling through extracellular matrix: lessons from the Dictyostelium paradigm of cell movement. *J Leukoc Biol* **70**, 491-509 (2001).

169. Mandeville, J.T., Lawson, M.A. & Maxfield, F.R. Dynamic imaging of neutrophil migration in three dimensions: mechanical interactions between cells and matrix. *J Leukoc Biol* **61**, 188-200 (1997).

170. Yoshida, K. & Soldati, T. Dissection of amoeboid movement into two mechanically distinct modes. *J Cell Sci* **119**, 3833-44 (2006).

171. Langridge, P.D. & Kay, R.R. Mutants in the Dictyostelium Arp2/3 complex and chemoattractant-induced actin polymerization. *Exp Cell Res* **313**, 2563-74 (2007).

172. Blaser, H. et al. Migration of zebrafish primordial germ cells: a role for myosin contraction and cytoplasmic flow. *Dev Cell* **11**, 613-27 (2006).

173. Fackler, O.T. & Grosse, R. Cell motility through plasma membrane blebbing. *J Cell Biol* **181**, 879-84 (2008).

174. Steinman, R.M. & Banchereau, J. Taking dendritic cells into medicine. *Nature* **449**, 419-26 (2007).

175. Lopez-Bravo, M. & Ardavin, C. In vivo induction of immune responses to pathogens by conventional dendritic cells. *Immunity* **29**, 343-51 (2008).

176. Shortman, K. & Naik, S.H. Steady-state and inflammatory dendritic-cell development. *Nat Rev Immunol* **7**, 19-30 (2007).

177. Randolph, G.J., Angeli, V. & Swartz, M.A. Dendritic-cell trafficking to lymph nodes through lymphatic vessels. *Nat Rev Immunol* **5**, 617-28 (2005).

178. Kaplan, D.H., Kissenpfennig, A. & Clausen, B.E. Insights into Langerhans cell function from Langerhans cell ablation models. *Eur J Immunol* **38**, 2369-76 (2008).

179. Merad, M., Ginhoux, F. & Collin, M. Origin, homeostasis and function of Langerhans cells and other langerin-expressing dendritic cells. *Nat Rev Immunol* **8**, 935-47 (2008).

180. Reis e Sousa, C. Dendritic cells in a mature age. *Nat Rev Immunol* **6**, 476-83 (2006).

181. Brand, C.U., Hunziker, T. & Braathen, L.R. Studies on human skin lymph containing Langerhans cells from sodium lauryl sulphate contact dermatitis. *J Invest Dermatol* **99**, 109S-110S (1992).

182. Tomura, M. et al. Monitoring cellular movement in vivo with photoconvertible fluorescence protein "Kaede" transgenic mice. *Proc Natl Acad Sci U S A* **105**, 10871-6 (2008).

183. Forster, R. et al. CCR7 coordinates the primary immune response by establishing functional microenvironments in secondary lymphoid organs. *Cell* **99**, 23-33 (1999).

184. Sallusto, F. et al. Rapid and coordinated switch in chemokine receptor expression during dendritic cell maturation. *Eur J Immunol* **28**, 2760-9 (1998).

185. Sozzani, S. et al. Differential regulation of chemokine receptors during dendritic cell maturation: a model for their trafficking properties. *J Immunol* **161**, 1083-6 (1998).

186. MartIn-Fontecha, A. et al. Regulation of dendritic cell migration to the draining lymph node: impact on T lymphocyte traffic and priming. *J Exp Med* **198**, 615-21 (2003).

187. Vassileva, G. et al. The reduced expression of 6Ckine in the plt mouse results from the deletion of one of two 6Ckine genes. *J Exp Med* **190**, 1183-8 (1999).

188. Ohl, L. et al. CCR7 governs skin dendritic cell migration under inflammatory and steady-state conditions. *Immunity* **21**, 279-88 (2004).

189. Gunn, M.D. et al. A chemokine expressed in lymphoid high endothelial venules promotes the adhesion and chemotaxis of naive T lymphocytes. *Proc Natl Acad Sci U S A* **95**, 258-63 (1998).

190. Mori, S. et al. Mice lacking expression of the chemokines CCL21-ser and CCL19 (plt mice) demonstrate delayed but enhanced T cell immune responses. *J Exp Med* **193**, 207-18 (2001).

191. Kabashima, K. et al. Thromboxane A2 modulates interaction of dendritic cells and T cells and regulates acquired immunity. *Nat Immunol* **4**, 694-701 (2003).

192. Scandella, E., Men, Y., Gillessen, S., Forster, R. & Groettrup, M. Prostaglandin E2 is a key factor for CCR7 surface expression and migration of monocyte-derived dendritic cells. *Blood* **100**, 1354-61 (2002).

193. Kabashima, K. et al. CXCL12-CXCR4 engagement is required for migration of cutaneous dendritic cells. *Am J Pathol* **171**, 1249-57 (2007).

194. Cyster, J.G. Chemokines, sphingosine-1-phosphate, and cell migration in secondary lymphoid organs. *Annu Rev Immunol* **23**, 127-59 (2005).

195. Czeloth, N. et al. Sphingosine-1 phosphate signaling regulates positioning of dendritic cells within the spleen. *J Immunol* **179**, 5855-63 (2007).

196. Maeda, Y. et al. Migration of CD4 T cells and dendritic cells toward sphingosine 1-phosphate (S1P) is mediated by different receptor subtypes: S1P regulates the functions of murine mature dendritic cells via S1P receptor type 3. *J Immunol* **178**, 3437-46 (2007).

197. Gollmann, G. et al. Sphingosine-1-phosphate receptor type-1 agonism impairs blood dendritic cell chemotaxis and skin dendritic cell migration to lymph nodes under inflammatory conditions. *Int Immunol* **20**, 911-23 (2008).

198. Fuchs, E. & Raghavan, S. Getting under the skin of epidermal morphogenesis. *Nat Rev Genet* **3**, 199-209 (2002).

199. Rowe, R.G. & Weiss, S.J. Breaching the basement membrane: who, when and how? *Trends Cell Biol* **18**, 560-74 (2008).

200. Timpl, R. Macromolecular organization of basement membranes. *Curr Opin Cell Biol* **8**, 618-24 (1996).

201. Griffith, L.G. & Swartz, M.A. Capturing complex 3D tissue physiology in vitro. *Nat Rev Mol Cell Biol* **7**, 211-24 (2006).

202. Swartz, M.A. & Fleury, M.E. Interstitial flow and its effects in soft tissues. *Annu Rev Biomed Eng* **9**, 229-56 (2007).

203. Kissenpfennig, A. et al. Dynamics and function of Langerhans cells in vivo: dermal dendritic cells colonize lymph node areas distinct from slower migrating Langerhans cells. *Immunity* **22**, 643-54 (2005).

204. Ng, L.G. et al. Migratory dermal dendritic cells act as rapid sensors of protozoan parasites. *PLoS Pathog* **4**, e1000222 (2008).

205. Vishwanath, M. et al. Development of intravital intermittent confocal imaging system for studying Langerhans cell turnover. *J Invest Dermatol* **126**, 2452-7 (2006).

206. Tang, A., Amagai, M., Granger, L.G., Stanley, J.R. & Udey, M.C. Adhesion of epidermal Langerhans cells to keratinocytes mediated by E-cadherin. *Nature* **361**, 82-5 (1993).

207. Schwarzenberger, K. & Udey, M.C. Contact allergens and epidermal proinflammatory cytokines modulate Langerhans cell E-cadherin expression in situ. *J Invest Dermatol* **106**, 553-8 (1996).

208. Jiang, A. et al. Disruption of E-cadherin-mediated adhesion induces a functionally distinct pathway of dendritic cell maturation. *Immunity* **27**, 610-24 (2007).

209. Hotary, K., Li, X.Y., Allen, E., Stevens, S.L. & Weiss, S.J. A cancer cell metalloprotease triad regulates the basement membrane transmigration program. *Genes Dev* **20**, 2673-86 (2006).

210. Ratzinger, G. et al. Matrix metalloproteinases 9 and 2 are necessary for the migration of Langerhans cells and dermal dendritic cells from human and murine skin. *J Immunol* **168**, 4361-71 (2002).

211. Price, A.A., Cumberbatch, M., Kimber, I. & Ager, A. Alpha 6 integrins are required for Langerhans cell migration from the epidermis. *J Exp Med* **186**, 1725-35 (1997).

212. Conrad, C. et al. Alpha1beta1 integrin is crucial for accumulation of epidermal T cells and the development of psoriasis. *Nat Med* **13**, 836-42 (2007).

213. Weiss, J.M. et al. An essential role for CD44 variant isoforms in epidermal Langerhans cell and blood dendritic cell function. *J Cell Biol* **137**, 1137-47 (1997).

214. Weiss, J.M. et al. Osteopontin is involved in the initiation of cutaneous contact hypersensitivity by inducing Langerhans and dendritic cell migration to lymph nodes. *J Exp Med* **194**, 1219-29 (2001).

215. Mummert, D.I., Takashima, A. & Mummert, M.E. Langerhans cells in CD44-deficient mice emigrate from the epidermis but fail to reach the lymph nodes after hapten application. *J Invest Dermatol* **122**, 846-7 (2004).

216. Gunzer, M. et al. Antigen presentation in extracellular matrix: interactions of T cells with dendritic cells are dynamic, short lived, and sequential. *Immunity* **13**, 323-32 (2000).

217. Friedl, P., Zanker, K.S. & Brocker, E.B. Cell migration strategies in 3-D extracellular matrix: differences in morphology, cell matrix interactions, and integrin function. *Microsc Res Tech* **43**, 369-78 (1998).

218. Linder, S. & Kopp, P. Podosomes at a glance. *J Cell Sci* **118**, 2079-82 (2005).

219. West, M.A. et al. TLR ligand-induced podosome disassembly in dendritic cells is ADAM17 dependent. *J Cell Biol* **182**, 993-1005 (2008).

220. De Vries, I.J. et al. Effective migration of antigen-pulsed dendritic cells to lymph nodes in melanoma patients is determined by their maturation state. *Cancer Res* **63**, 12-7 (2003).

221. van Helden, S.F. et al. A critical role for prostaglandin E2 in podosome dissolution and induction of high-speed migration during dendritic cell maturation. *J Immunol* **177**, 1567-74 (2006).

222. Yen, J.H., Khayrullina, T. & Ganea, D. PGE2-induced metalloproteinase-9 is essential for dendritic cell migration. *Blood* **111**, 260-70 (2008).

223. Van Lint, P. & Libert, C. Chemokine and cytokine processing by matrix metalloproteinases and its effect on leukocyte migration and inflammation. *J Leukoc Biol* **82**, 1375-81 (2007).

224. Schmid-Schonbein, G.W. Microlymphatics and lymph flow. *Physiol Rev* **70**, 987-1028 (1990).

225. Trzewik, J., Mallipattu, S.K., Artmann, G.M., Delano, F.A. & Schmid-Schonbein, G.W. Evidence for a second valve system in lymphatics: endothelial microvalves. *Faseb J* **15**, 1711-7 (2001).

226. Baluk, P. et al. Functionally specialized junctions between endothelial cells of lymphatic vessels. *J Exp Med* **204**, 2349-62 (2007).

227. Sauter, B., Foedinger, D., Sterniczky, B., Wolff, K. & Rappersberger, K. Immunoelectron microscopic characterization of human dermal lymphatic microvascular endothelial cells. Differential expression of CD31, CD34, and type IV collagen with lymphatic endothelial cells vs blood capillary endothelial cells in normal human skin, lymphangioma, and hemangioma in situ. *J Histochem Cytochem* **46**, 165-76 (1998).

228. Vainionpaa, N. et al. Basement membrane protein distribution in LYVE-1-immunoreactive lymphatic vessels of normal tissues and ovarian carcinomas. *Cell Tissue Res* **328**, 317-28 (2007).

229. Johnson, L.A. et al. An inflammation-induced mechanism for leukocyte transmigration across lymphatic vessel endothelium. *J Exp Med* **203**, 2763-77 (2006).

230. Xu, H. et al. The role of ICAM-1 molecule in the migration of Langerhans cells in the skin and regional lymph node. *Eur J Immunol* **31**, 3085-93 (2001).

231. Katagiri, K. et al. Crucial functions of the Rap1 effector molecule RAPL in lymphocyte and dendritic cell trafficking. *Nat Immunol* **5**, 1045-51 (2004).

232. Grabbe, S. et al. Beta2 integrins are required for skin homing of primed T cells but not for priming naive T cells. *J Clin Invest* **109**, 183-92 (2002).

233. Cera, M.R. et al. Increased DC trafficking to lymph nodes and contact hypersensitivity in junctional adhesion molecule-A-deficient mice. *J Clin Invest* **114**, 729-38 (2004).

234. Johnson, L.A. & Jackson, D.G. Cell traffic and the lymphatic endothelium. *Ann N Y Acad Sci* **1131**, 119-33 (2008).

235. Irjala, H. et al. Mannose receptor is a novel ligand for L-selectin and mediates lymphocyte binding to lymphatic endothelium. *J Exp Med* **194**, 1033-42 (2001).

236. Salmi, M., Koskinen, K., Henttinen, T., Elima, K. & Jalkanen, S. CLEVER-1 mediates lymphocyte transmigration through vascular and lymphatic endothelium. *Blood* **104**, 3849-57 (2004).

237. Breiteneder-Geleff, S. et al. Angiosarcomas express mixed endothelial phenotypes of blood and lymphatic capillaries: podoplanin as a specific marker for lymphatic endothelium. *Am J Pathol* **154**, 385-94 (1999).

238. Banas, B. et al. Roles of SLC/CCL21 and CCR7 in human kidney for mesangial proliferation, migration, apoptosis, and tissue homeostasis. *J Immunol* **168**, 4301-7 (2002).

239. Kriehuber, E. et al. Isolation and characterization of dermal lymphatic and blood endothelial cells reveal stable and functionally specialized cell lineages. *J Exp Med* **194**, 797-808 (2001).

240. Luther, S.A., Tang, H.L., Hyman, P.L., Farr, A.G. & Cyster, J.G. Coexpression of the chemokines ELC and SLC by T zone stromal cells and deletion of the ELC gene in the plt/plt mouse. *Proc Natl Acad Sci U S A* **97**, 12694-9 (2000).

241. Shields, J.D. et al. Autologous chemotaxis as a mechanism of tumor cell homing to lymphatics via interstitial flow and autocrine CCR7 signaling. *Cancer Cell* **11**, 526-38 (2007).

242. Swartz, M.A. The physiology of the lymphatic system. *Adv Drug Deliv Rev* **50**, 3-20 (2001).

243. Witte, M.H. et al. Structure function relationships in the lymphatic system and implications for cancer biology. *Cancer Metastasis Rev* **25**, 159-84 (2006).

244. Junt, T., Scandella, E. & Ludewig, B. Form follows function: lymphoid tissue microarchitecture in antimicrobial immune defence. *Nat Rev Immunol* **8**, 764-75 (2008).

245. Lammermann, T. et al. Rapid leukocyte migration by integrin-independent flowing and squeezing. *Nature* **453**, 51-5 (2008).

246. Ushiki, T., Ohtani, O. & Abe, K. Scanning electron microscopic studies of reticular framework in the rat mesenteric lymph node. *Anat Rec* **241**, 113-22 (1995).

247. Gretz, J.E., Norbury, C.C., Anderson, A.O., Proudfoot, A.E. & Shaw, S. Lymph-borne chemokines and other low molecular weight molecules reach high endothelial venules via specialized conduits while a functional barrier limits access to the lymphocyte microenvironments in lymph node cortex. *J Exp Med* **192**, 1425-40 (2000).

248. Sixt, M. et al. The conduit system transports soluble antigens from the afferent lymph to resident dendritic cells in the T cell area of the lymph node. *Immunity* **22**, 19-29 (2005).

249. Anderson, A.O. & Shaw, S. Conduit for privileged communications in the lymph node. *Immunity* **22**, 3-5 (2005).

250. Hayakawa, M., Kobayashi, M. & Hoshino, T. Direct contact between reticular fibers and migratory cells in the paracortex of mouse lymph nodes: a morphological and quantitative study. *Arch Histol Cytol* **51**, 233-40 (1988).

251. Katakai, T. et al. A novel reticular stromal structure in lymph node cortex: an immuno-platform for interactions among dendritic cells, T cells and B cells. *Int Immunol* **16**, 1133-42 (2004).

252. Drumea-Mirancea, M. et al. Characterization of a conduit system containing laminin-5 in the human thymus: a potential transport system for small molecules. *J Cell Sci* **119**, 1396-405 (2006).

253. Nolte, M.A. et al. A conduit system distributes chemokines and small blood-borne molecules through the splenic white pulp. *J Exp Med* **198**, 505-12 (2003).

254. Sumen, C., Mempel, T.R., Mazo, I.B. & von Andrian, U.H. Intravital microscopy: visualizing immunity in context. *Immunity* **21**, 315-29 (2004).

255. Worbs, T., Mempel, T.R., Bolter, J., von Andrian, U.H. & Forster, R. CCR7 ligands stimulate the intranodal motility of T lymphocytes in vivo. *J Exp Med* **204**, 489-95 (2007).

256. Bajenoff, M., Granjeaud, S. & Guerder, S. The strategy of T cell antigen-presenting cell encounter in antigen-draining lymph nodes revealed by imaging of initial T cell activation. *J Exp Med* **198**, 715-24 (2003).

257. Mempel, T.R., Henrickson, S.E. & Von Andrian, U.H. T-cell priming by dendritic cells in lymph nodes occurs in three distinct phases. *Nature* **427**, 154-9 (2004).

258. Bousso, P. & Robey, E. Dynamics of CD8+ T cell priming by dendritic cells in intact lymph nodes. *Nat Immunol* **4**, 579-85 (2003).

259. Lindquist, R.L. et al. Visualizing dendritic cell networks in vivo. *Nat Immunol* **5**, 1243-50 (2004).

260. Saeki, H., Wu, M.T., Olasz, E. & Hwang, S.T. A migratory population of skin-derived dendritic cells expresses CXCR5, responds to B lymphocyte chemoattractant in vitro, and co-localizes to B cell zones in lymph nodes in vivo. *Eur J Immunol* **30**, 2808-14 (2000).

261. Wei, S.H., Parker, I., Miller, M.J. & Cahalan, M.D. A stochastic view of lymphocyte motility and trafficking within the lymph node. *Immunol Rev* **195**, 136-59 (2003).

262. Bajenoff, M. et al. Stromal cell networks regulate lymphocyte entry, migration, and territoriality in lymph nodes. *Immunity* **25**, 989-1001 (2006).

263. Mempel, T.R., Junt, T. & von Andrian, U.H. Rulers over randomness: stroma cells guide lymphocyte migration in lymph nodes. *Immunity* **25**, 867-9 (2006).

264. Asperti-Boursin, F., Real, E., Bismuth, G., Trautmann, A. & Donnadieu, E. CCR7 ligands control basal T cell motility within lymph node slices in a phosphoinositide 3-kinase-independent manner. *J Exp Med* **204**, 1167-79 (2007).

265. Okada, T. & Cyster, J.G. CC chemokine receptor 7 contributes to Gi-dependent T cell motility in the lymph node. *J Immunol* **178**, 2973-8 (2007).

266. Garrod, K.R., Wei, S.H., Parker, I. & Cahalan, M.D. Natural killer cells actively patrol peripheral lymph nodes forming stable conjugates to eliminate MHC-mismatched targets. *Proc Natl Acad Sci U S A* **104**, 12081-6 (2007).

267. Etienne-Manneville, S. & Hall, A. Rho GTPases in cell biology. *Nature* **420**, 629-35 (2002).

268. Gadea, G., Sanz-Moreno, V., Self, A., Godi, A. & Marshall, C.J. DOCK10-mediated Cdc42 activation is necessary for amoeboid invasion of melanoma cells. *Curr Biol* **18**, 1456-65 (2008).

269. Heasman, S.J. & Ridley, A.J. Mammalian Rho GTPases: new insights into their functions from in vivo studies. *Nat Rev Mol Cell Biol* **9**, 690-701 (2008).

270. Benvenuti, F. et al. Requirement of Rac1 and Rac2 expression by mature dendritic cells for T cell priming. *Science* **305**, 1150-3 (2004).

271. Van Keymeulen, A. et al. To stabilize neutrophil polarity, PIP3 and Cdc42 augment RhoA activity at the back as well as signals at the front. *J Cell Biol* **174**, 437-45 (2006).

272. Etienne-Manneville, S. Cdc42--the centre of polarity. *J Cell Sci* **117**, 1291-300 (2004).

273. Srinivasan, S. et al. Rac and Cdc42 play distinct roles in regulating PI(3,4,5)P3 and polarity during neutrophil chemotaxis. *J Cell Biol* **160**, 375-85 (2003).

274. Allen, W.E., Zicha, D., Ridley, A.J. & Jones, G.E. A role for Cdc42 in macrophage chemotaxis. *J Cell Biol* **141**, 1147-57 (1998).

275. Yang, L. et al. Rho GTPase Cdc42 coordinates hematopoietic stem cell quiescence and niche interaction in the bone marrow. *Proc Natl Acad Sci U S A* **104**, 5091-6 (2007).

276. Stramer, B. et al. Live imaging of wound inflammation in Drosophila embryos reveals key roles for small GTPases during in vivo cell migration. *J Cell Biol* **168**, 567-73 (2005).

277. Garrett, W.S. et al. Developmental control of endocytosis in dendritic cells by Cdc42. *Cell* **102**, 325-34 (2000).

278. Shurin, G.V. et al. Small rho GTPases regulate antigen presentation in dendritic cells. *J Immunol* **174**, 3394-400 (2005).

279. Burns, S., Thrasher, A.J., Blundell, M.P., Machesky, L. & Jones, G.E. Configuration of human dendritic cell cytoskeleton by Rho GTPases, the WAS protein, and differentiation. *Blood* **98**, 1142-9 (2001).

280. Swetman, C.A. et al. Extension, retraction and contraction in the formation of a dendritic cell dendrite: distinct roles for Rho GTPases. *Eur J Immunol* **32**, 2074-83 (2002).

281. Wymann, M.P. et al. Phosphoinositide 3-kinase gamma: a key modulator in inflammation and allergy. *Biochem Soc Trans* **31**, 275-80 (2003).

282. Del Prete, A. et al. Defective dendritic cell migration and activation of adaptive immunity in PI3Kgamma-deficient mice. *Embo J* **23**, 3505-15 (2004).

283. Higgs, H.N. & Pollard, T.D. Activation by Cdc42 and PIP(2) of Wiskott-Aldrich syndrome protein (WASp) stimulates actin nucleation by Arp2/3 complex. *J Cell Biol* **150**, 1311-20 (2000).

284. de Noronha, S. et al. Impaired dendritic-cell homing in vivo in the absence of Wiskott-Aldrich syndrome protein. *Blood* **105**, 1590-7 (2005).

285. Pulecio, J. et al. Expression of Wiskott-Aldrich syndrome protein in dendritic cells regulates synapse formation and activation of naive CD8+ T cells. *J Immunol* **181**, 1135-42 (2008).

11 Supplements

The supplemental information and supplemental videos for Paper V, Paper VI and Paper VII are provided in the online versions of the publisher's homepage.

In the following, papers I to VII are reprinted.

Paper I: Reprinted from *Molecular and Cellular Biology,* 26(5), Haiyan Chu, Ingo Thievessen, Michael Sixt, Tim Lämmermann, Ari Waisman, Attila Braun, Angelika A. Noegel, Reinhard Fässler. γ-Parvin is dispensable for hematopoiesis, leukocyte trafficking, and T-cell-dependent antibody response, Copyright (2006), with permission from the American Society of Microbiology.

Paper II: Reprinted from *Current Opinion in Cell Biology,* 18(5), Michael Sixt, Martina Bauer, Tim Lämmermann, Reinhard Fässler. β1 integrins: zip codes and signaling relay for blood cells, 482-90, Copyright (2006), with permission from Elsevier.

Paper III: Reprinted from *Seminars in Immunology,* 20(1), Zerina Lokmic, Tim Lämmermann, Michael Sixt, Susanna Cardell, Rupert Hallmann, Lydia Sorokin. The extracellular matrix of the spleen as a potential organizer of immune cell compartments, 4-13, Copyright (2008), with permission from Elsevier.

Paper IV: Reprinted from *Immunological Reviews,* 221:26-43, Tim Lämmermann, Michael Sixt. The microanatomy of T-cell responses, 26-43, Copyright (2008), with permission from Wiley-Blackwell.

Paper V: Reprinted from *Nature,* 453(7191), Tim Lämmermann, Bernhard L. Bader, Susan J. Monkley, Tim Worbs, Roland Wedlich-Söldner, Karin Hirsch, Markus Keller, Reinhold Förster, David R. Critchley, Reinhard Fässler, Michael Sixt. Rapid leukocyte migration by integrin-independent flowing and squeezing, 51-5, Copyright (2008), with permission from the Nature Publishing Group.

Paper VI: Reprinted from *Journal of Clinical Investigations,* 118(7), Kai Kessenbrock, Leopold Fröhlich, Michael Sixt, Tim Lämmermann, Andrew Bateman, Azzaq Belaaouaj, Johannes Ring, Markus Ollert, Reinhard Fässler, Dieter E. Jenne. Proteinase 3 and neutrophil elastase enhance inflammation by inactivating anti-inflammatory progranulin, 2438-47, Copyright (2008), with permission from the American Society of Clinical Investigation.

Paper VII: Reprinted from *Blood Journal*, 113(23), Tim Lämmermann , Jörg Renkawitz, Xunwei Wu, Karin Hirsch, Cord Brakebusch, Michael Sixt. Cdc42-dependent leading edge coordination is essential for interstitial dendritic cell migration., 5703-10, Copyright (2009), with permission from the American Society of Hematology. Prepublished online February 3, 2009; DOI 10.1182/blood-2008-11-191882.

γ-Parvin Is Dispensable for Hematopoiesis, Leukocyte Trafficking, and T-Cell-Dependent Antibody Response†

Haiyan Chu,[1] Ingo Thievessen,[1] Michael Sixt,[1] Tim Lämmermann,[1] Ari Waisman,[2]‡
Attila Braun,[1] Angelika A. Noegel,[3] and Reinhard Fässler[1]*

*Department of Molecular Medicine, Max Planck Institute for Biochemistry, Am Klopferspitz 18, 82152 Martinsried, Germany[1];
Laboratory of Molecular Immunology, Institute for Genetics, University of Cologne, Zülpicher Str. 47,
50674 Cologne, Germany[2]; and Center for Biochemistry, Medical Faculty, University of Cologne,
Joseph-Stelzmann-Str. 52, 50931 Cologne, Germany[3]*

Integrins regulate cell behavior through the assembly of multiprotein complexes at the site of cell adhesion. Parvins are components of such a multiprotein complex. They consist of three members (α-, β-, and γ-parvin), form a functional complex with integrin-linked kinase (ILK) and PINCH, and link integrins to the actin cytoskeleton. Whereas α- and β-parvins are widely expressed, γ-parvin has been reported to be expressed in hematopoietic organs. In the present study, we report the expression pattern of the parvins in hematopoietic cells and the phenotypic analysis of γ-parvin-deficient mice. Whereas α-parvin is not expressed in hematopoietic cells, β-parvin is only found in myeloid cells and γ-parvin is present in both cells of the myeloid and lymphoid lineages, where it binds ILK. Surprisingly, loss of γ-parvin expression had no effect on blood cell differentiation, proliferation, and survival and no consequence for the T-cell-dependent antibody response and lymphocyte and dendritic cell migration. These data indicate that despite the high expression of γ-parvin in hematopoietic cells it must play a more subtle role for blood cell homeostasis.

Cell extracellular matrix (ECM) adhesions are crucial for various biological processes, including cell migration, proliferation, and cell survival (12, 15, 17). Integrins connect the ECM to the actin cytoskeleton at cellular attachment plaques that contain focal adhesion (FA)-associated proteins (8). A family of proteins consisting of actopaxin/CH-ILKBP/α-parvin, affixin/β-parvin, and γ-parvin, collectively called the parvins, has been recently identified in humans and mice (22, 23, 31, 34). In lower organisms such as *Caenorhabditis elegans* and *Drosophila melanogaster*, there is only a single parvin protein (19, 23). Parvins are composed of an N-terminal polypeptide stretch, followed by a single actin-binding domain, which consists of two in tandem arranged calponin homology domains. α- and β-parvin share a high homology (23), and both bind to integrin-linked kinase (ILK), paxillin, and F-actin at FAs (1, 9, 22, 23, 31, 34). In addition, β-parvin also binds α-PIX, a guanine exchange factor for Rac and Cdc42 (21, 25), and α-actinin (35). Both α- and β-parvin associate with ILK and PINCH to form the ILK-PINCH-parvin complexes (37, 39, 40). Disruption of the complex in mammalian cells alters cell shape and impairs cell motility and survival (7, 36, 38, 39). In *C. elegans* disruption of the complex causes muscle detachment and a PAT (paralyzed at the four-cell stage) phenotype (19).

γ-Parvin consists of 331 amino acids and shares the same protein structure as α- and β-parvin. The mouse γ-parvin only shows 40% identity and 60% similarity to the α- or β-parvin at the amino acid level. No γ-parvin binding partners have been identified thus far. In contrast to the wide expression pattern of α- and β-parvin, γ-parvin mRNA is predominantly found in hematopoietic and lymphoid tissues (16, 22, 23, 34). These features of the γ-parvin raise the question of whether γ-parvin mediates integrin signaling via association with ILK and thereby regulates events, including cell differentiation, migration, and positioning in the hematopoietic system. In the present study, we described the expression pattern of the parvin protein family in hematopoietic organs and hematopoietic cells. To directly test the function of γ-parvin in vivo, we generated γ-parvin-deficient mice. Our study shows that γ-parvin is highly expressed in myeloid and lymphoid cells and that neither hematopoiesis nor T-cell-dependent antibody response, nor lymphocyte or dendritic cell (DC) migration is abnormal in the absence of γ-parvin.

MATERIALS AND METHODS

Antibodies. Rabbit anti-PINCH1 and PINCH2 polyclonal antibodies were described (18). Monoclonal anti-ILK antibody was from BD Transduction Laboratory, rabbit anti-α-actin and mouse antitalin antibodies were from Sigma Aldrich, rat anti-B220 (RA3-6B2), rat anti-Thy1.2, anti-rabbit or -mouse immunoglobulin G (IgG) (H+L)–horseradish peroxidase, anti-IgM (R6-60.2), rat anti-IgD (11-26c.2a), rat anti-CD19 (1D3), anti-CD4 (H129.19), anti-CD8 (53-6.2), rat anti-CD3 (17A2), anti-Gr-1 (RB6-8C5), anti-Mac-1 (M1-70), anti-Ter-119, hamster anti-CD11c (HL3), CD86 (GL1), and major histocompatibility complex (MHC) II (M5/114.15.2) were from BD Pharmingen (San Jose, CA). Alexa 488 phalloidin was from Molecular Probes (Leiden, The Netherlands).

Antibodies were conjugated with fluorescein isothiocyanate (FITC), phycoerythrin (PE), or biotin and used at a 1:200 dilution. FITC-conjugated goat anti-rat or -mouse IgGs and streptavidin Cy-5 were from Jackson Immunoresearch (West Grove, PA). Rabbit pan-laminin antibody was described in Sorokin et al. (28). Annexin V-FITC was a gift from Ernst Pöschl (University of Erlangen-Nürnberg, Erlangen-Nürnberg, Germany) and was used at a 1:1,000 dilution.

* Corresponding author. Mailing address: Department of Molecular Medicine, Max Planck Institute for Biochemistry, Am Klopferspitz 18, 82152 Martinsried, Germany. Phone: (49) 89-8578-2424. Fax: (49) 89-8578-2422. E-mail: faessler@biochem.mpg.de.

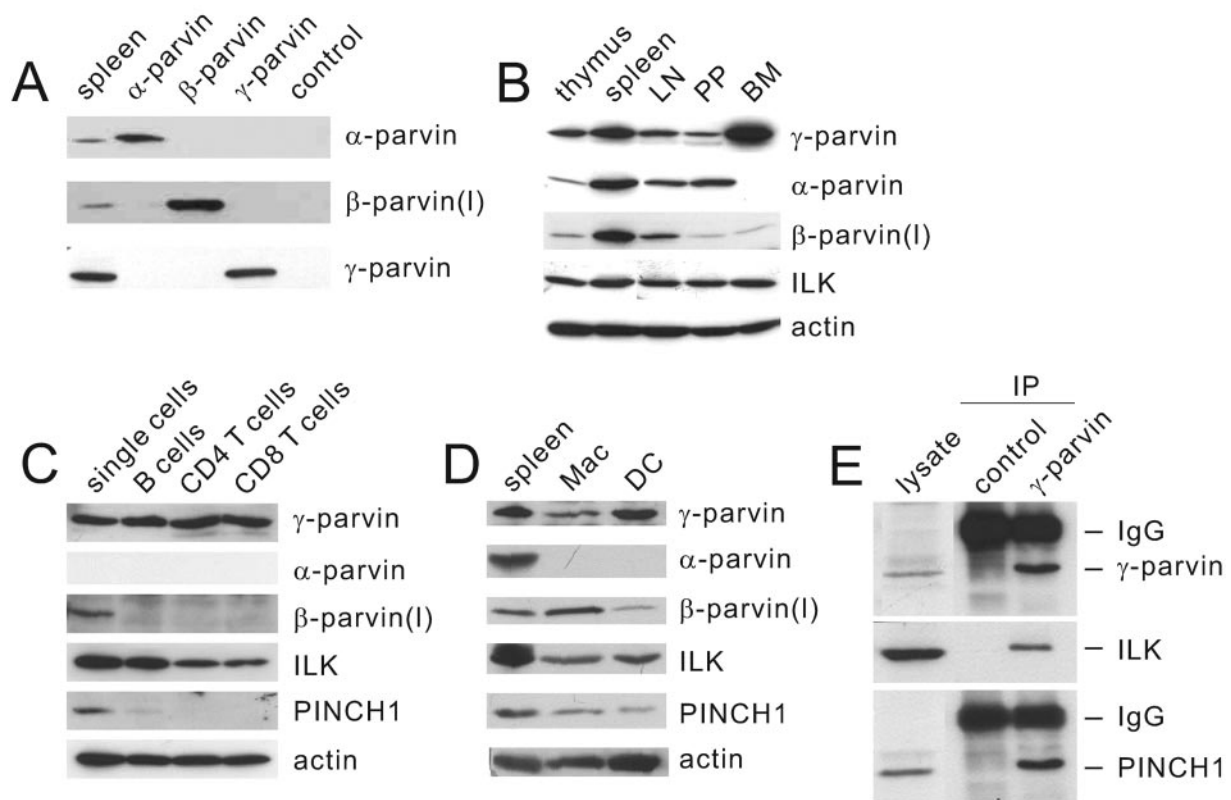‡ Present address: Medizinsche Klinik und Poliklinik, Johannes Gutenberg-Universitat Mainz, 55131 Mainz, Germany.

FIG. 1. Expression of parvins in the hematopoietic system (A) Peptide antisera were generated against α-parvin, the long isoform of β- and γ-parvin. Spleen lysate and in vitro-translated α-, β-, and γ-parvin proteins were subjected to sodium dodecyl sulfate-polyacrylamide gel electrophoresis and probed with the antisera. (B) Thymus, spleen, lymph nodes (LN), Peyer's (PP), and bone marrow (BM) were isolated, lysed, and immunoblotted with anti-γ-, α-, and β-parvin and anti-ILK antibodies. (C) B220-, CD4-, and CD8-positive cells were sorted from adult mouse splenic single cell suspensions and analyzed by Western blotting with antiparvin, anti-ILK, and anti-PINCH1 antibodies. (D) BM-derived macrophages (Mac) and dendritic cells (DCs) were lysed and immunoblotted with antiparvin, -ILK, and -PINCH1 antibodies. (E) BM-derived DC lysate was immunoprecipitated with anti-γ-parvin antibody and with control preimmune serum. The immunoprecipitates were immunoblotted with γ-parvin, ILK and PINCH1 antibodies, respectively.

Generation of parvin peptide antibodies. To generate specific antibodies, N-terminal peptides corresponding to α-parvin amino acid residues 5 to 19 (PQKSPLVPKSPTPKS), β-parvin residues 3 to 16 (SAPPRSPTPRAPKM), and γ-parvin residues 2 to 17 (ELEFLYDLLQLPKEVA) were synthesized, coupled to the carrier protein KLH (Imject Maleimide Activated mc KLH; Pierce), and used to immunize rabbits. The antisera were further purified by using the SulfoLink kit (Pierce) and tested on in vitro translated α-, β-, and γ-parvin proteins, respectively (Fig. 1A).

Generation of γ-parvin-deficient mice. A γ-parvin cDNA fragment derived from EST clone AA981356 was used to screen a 129/Sv mouse P1-derived artificial chromosome library (27). P1-derived artificial chromosome 656L16 (from the Human Genome Mapping Project Center, Cambridge, United Kingdom) was used to generate the targeting vector. A 5.5-kb fragment was used as 5′ flanking arm and a 2.3-kb fragment as a 3′ flanking arm (Fig. 2A). An internal ribosome entry site-lacZ reporter cassette, followed by a PKG-driven neo gene (27), was inserted between the two arms. The targeting vector was electroporated into passage 15 R1 embryonic stem (ES) cells and selected with G418 (3). Southern blots from 360 EcoRV-digested ES cell clones were hybridized with an external 700-bp SphI-HindIII fragment derived from intron 10 (Fig. 2A). Nine recombinant ES clones were identified by detection of a 4.9-kb recombinant band, in addition to the 5.7-kb wild-type band. Three targeted ES clones were injected into blastocysts to generate germ line chimeras, which were then mated with C57BL/6 females. Genotyping of γ-parvin mutant mice was performed by Southern blot or by PCR using a wild-type allele primer pair (forward, GTTTGAAGAACTGCA GAAGG; reverse, GTTGATCCATTCCATCAGCA) and a recombinant allele-specific primer pair derived from the lacZ gene (forward, CTGGGTAATAAG CGTTGGCAAT; reverse, CCAACTGGTAATGGTAGCGAC).

In vitro translation. α-, β-, and γ-parvin cDNAs (16) were amplified with Vent DNA polymerase (New England Biolabs, United Kingdom) and cloned into a modified pCS2+ mammalian SP6 promoter driven expression vector. In vitro translation reactions were performed with TNT Coupled Transcription/Translation Systems (Promega, Mannheim, Germany) using rabbit reticulocyte lysate and subsequently analyzed by Western assay.

Western analysis and immunoprecipitation. Cells were lysed in 150 mM NaCl–5 mM EDTA–1% Triton X-100 (pH 7.4) in the presence of protease inhibitors (Roche, Mannheim, Germany). Alternatively, tissues were homogenized in radioimmunoprecipitation assay buffer (150 mM NaCl, 50 mM Tris-HCl [pH 7.4], 5 mM EDTA, 0.1% sodium dodecyl sulfate, 1% sodium deoxycholate, 1% Triton X-100) containing protease inhibitors. For Western analysis, 30 to 50 μg of protein were gel separated, blotted, and probed with the primary and the secondary horseradish peroxidase-conjugated antibodies.

For immunoprecipitation, cells were lysed in ice-cold buffer (150 mM NaCl, 1 mM EGTA, 1% Triton X-100, 100 mM NaF, 10% glycerol, 50 mM HEPES [pH 7.5], 10 mM Na$_4$P$_2$O$_7$) supplemented with protease inhibitors. Then, 500 μg of protein was incubated with 0.8 mg of protein A (Sigma) in 50 μl of lysis buffer and with 1 μg of purified γ-parvin antibody or 1 μg of preimmune serum as a negative control at 4°C overnight. The protein-antibody-containing pellet was washed with lysis buffer and subjected to immunoblotting.

Northern blot assay, reverse transcription-PCR (RT-PCR), and immunostaining. Preparation, gel separation, blotting, and hybridization of total RNA from spleen and thymus was performed as previously described (3). γ-Parvin cDNA (nucleotides 269 to 865) was used as probes.

For RT-PCR, total RNA was reverse-transcribed with iScript cDNA Synthesis Kit (Bio-Rad, Germany) and amplified with a β-parvin forward primer located in exon 5 (GGAAGCCGTGCAAGACCTGC) and a reverse primer located in exon 6 (CCCTGAAGTGCATGGCCAGG). An HPRT1 primer pair was used as a control (forward, TCAGTCAACGGGGGACATAAA; reverse, GGGGCT GTACTGCTTAACCAG).
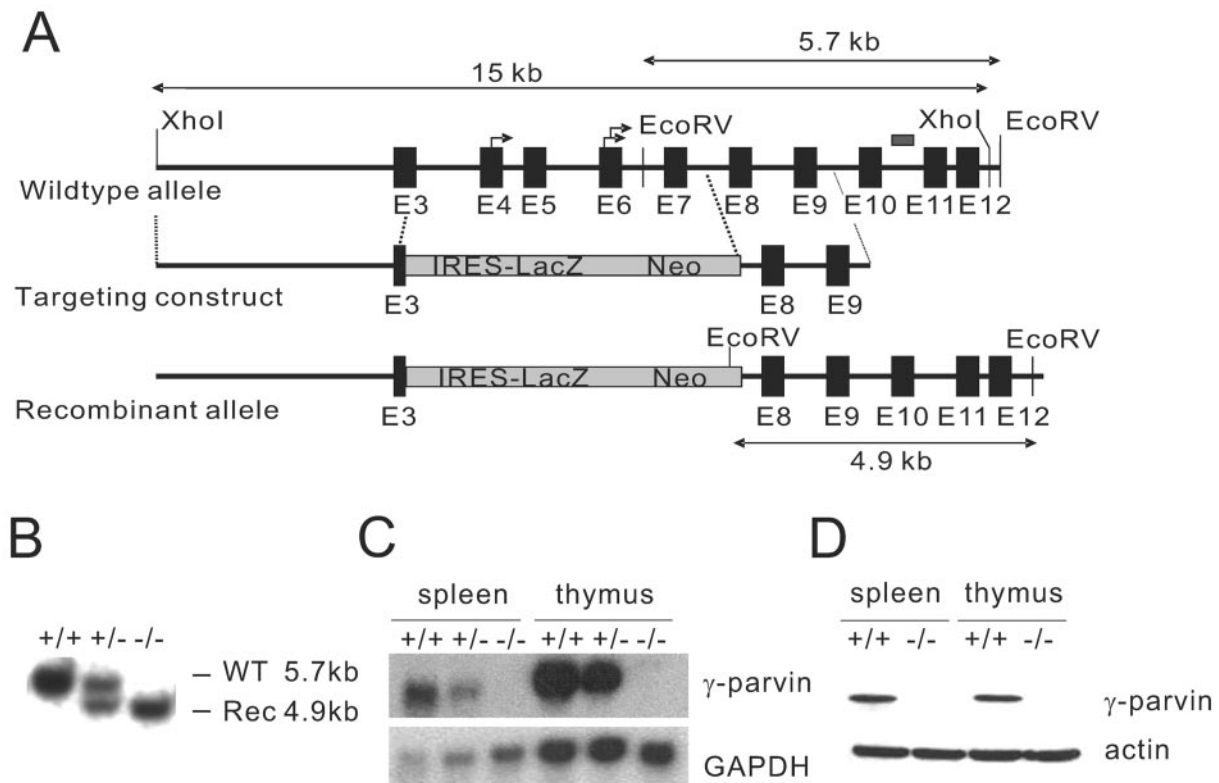
FIG. 2. Generation of γ-parvin-deficient mice. (A) An internal ribosome entry site (IRES)-LacZ neomycin cassette was inserted into the γ-parvin gene by replacing a 5.4-kb genomic fragment spanning exon 3 to intron 7, including both ATG-containing exons. The arrow indicates ATG triplets. (B) Homozygous mice were genotyped by Southern blot. (C) Loss of γ-parvin mRNA was shown by Northern blot in mouse thymus and spleen tissues. GAPDH cDNA probe was used to control mRNA loading. (D) Loss of γ-parvin expression was determined by Western blotting. The blots were reprobed with antiactin as loading control. Single cells, spleen single-cell suspension; WT, wild type; Rec, recombinant.

Immunofluorescence studies of tissue sections and cells were performed as described previously (3).

Flow cytometry analysis (FACS) and magnetic cell sorting. Single-cell suspensions were prepared by gently pushing the dissected organs through 70-mm cell strainers (BD). Fluorescence-activated cell sorting (FACS) analysis was performed as described previously (24). For magnetic cell sorting, 10^7 spleen cells were mixed with FITC-conjugated anti-B220, CD4, CD8, or CD3 antibodies (BD Biosciences), respectively; incubated with anti-FITC microbeads; and sorted out according to the instructions of the manufacturer (Miltenyi Biotech, Inc.). Sorted cells were analyzed by FACS to test purities and analyzed by Western blotting or RT-PCR.

Generation of bone marrow (BM)-derived DC and macrophages were carried out as described previously (20, 26). Cells were immunostained (DCs for CD11c and Gr-1, macrophages for Mac-1) and analyzed by FACS.

For apoptosis assay, macrophages were harvested on day 8, stained with annexin V-FITC, and analyzed by FACS to determine the percentage of the apoptotic cells.

DC migration in vivo. On days 8 to 10 of DC culture, the medium was supplemented with 200 ng of lipopolysaccharide (LPS; Sigma)/ml to induce maturation. For fluorescence labeling, cells in phosphate-buffered saline were incubated for 10 min with 3 mM CFSE or 10 μM TAMRA (Molecular Probes) at room temperature. A 1:1 mixture of each 10^6 CFSE- and TAMRA-labeled DC was injected into the hind footpad of recipient mice in a volume of 30 ml of phosphate-buffered saline. After 48 h, the popliteal lymph nodes (LN) were dissected and immunostained with pan-laminin antibody, or single-cell suspensions were prepared and analyzed by flow cytometry.

Lymphocyte homing in vivo. Spleen single-cell suspensions of knockout and control animals were prepared and erythrocytes were lysed. For fluorescence labeling, cells were incubated for 10 min with 1 mM CFSE or 20 μM TAMRA (Molecular Probes) at room temperature. A 1:1 mixture of each 2×10^7 CFSE- and TAMRA-labeled cells was injected intravenously. After 90 min and 24 h, lymphocytes were isolated from spleen and peripheral LN (inguinal, axial), and

the ratio of control to mutant cells in these organs was determined by FACS using simultaneous staining with antibodies to B220 or CD3.

Immunization. Mice were immunized via the intraperitoneal route with 100 μg of alum-precipitated NP$_{23}$-CG) and boosted with 10 mg/mouse 6 weeks after the first immunization. A total of 50 μl of blood was collected from each mouse at the indicated time points. Enzyme-linked immunosorbent assays (ELISAs) were carried out as described previously (10).

Statistics. The statistical analyzes of FACS and ELISA data were performed by using the Student t test. The P value for significance was set at 0.05.

RESULTS

Expression of the parvin family members in the hematopoietic system. To determine the expression of the individual parvin family members, we generated peptide antisera that exclusively recognized the corresponding in vitro translated protein (Fig. 1A). The β-parvin mRNA can generate three isoforms depending on which translation initiation codon is used for protein translation (34). The peptide we used to generate our anti-β-parvin antibody is not present in the two shorter isoforms called β-parvin(s) and β-parvin(ss). Hence, the anti-β-parvin antibody exclusively recognizes the long β-parvin(l) isoform.

Western blot analysis of lysates derived from thymus, spleen, LN and Peyer's patch (PP) revealed that α-parvin, β-parvin, and γ-parvin are expressed at the expected molecular masses (around 42 kDa for α- and β-parvin and 37 kDa for γ-parvin) (Fig. 1B). BM lysates showed high expression levels of γ-par-

vin, low levels of β-parvin and no detectable α-parvin (Fig. 1B). In addition to the BM, we detected the γ-parvin protein in thymus, spleen, LN, and PP on Western blot (Fig. 1B). In addition to these hematopoietic organs, we found very weak γ-parvin signal in lung and hardly detectable signal in testis lysates (data not shown). To further determine the cell-type-specific expression of the parvin family members, we sorted B cells and CD4- and CD8-positive T cells from adult mouse spleen by using magnetic microbeads. The purities of the sorted cells ranged between 92 and 99% as analyzed with cell-type-specific antibodies by FACS (data not shown). γ-Parvin was expressed at similar levels in all three cell populations (Fig. 1C). α- and β-parvin(l) were absent from B and T cells (Fig. 1C). Lysates from a splenic single-cell suspension showed γ- and β-parvin(l) expression but no detectable α-parvin. BM-derived macrophages and DCs expressed γ- and β-parvin but no detectable α-parvin protein (Fig. 1D).

α- and β-parvin can bind ILK and together with PINCH1 form an ILK-PINCH-parvin complex (39, 40). To test whether γ-parvin has similar properties, lysates from DCs were immunoprecipitated with anti-γ-parvin antibody or preimmune serum. Subsequent Western blotting detected ILK, PINCH1, and γ-parvin in the anti-γ-parvin immunoprecipitates but not in the preimmune serum control (Fig. 1E), indicating that γ-parvin can also bind ILK and form a ternary complex with ILK and PINCH1.

Mice lacking γ-parvin expression are viable and fertile. To directly analyze γ-parvin in vivo, we introduced a constitutive null mutation into the γ-parvin gene of mice (Fig. 2A). Southern blot or PCR based genotyping of tail biopsies from 159 3-month-old mice revealed the presence of homozygous mice at the expected Mendelian ratio (Fig. 2B and data not shown). Northern and Western blot analysis confirmed the absence of γ-parvin in homozygous mutant mice (Fig. 2C and D). Both heterozygous and homozygous γ-parvin mutant mice were indistinguishable from their wild-type littermate controls. They were fertile and had a normal life span.

Normal hematopoiesis in γ-parvin-deficient mice. α- and β-parvin have been shown to modulate cell migration and cell survival (6, 31, 34, 40). To test whether γ-parvin has a similar function in vivo, we first determined the cellularity and the population sizes of different cell lineages in BM, thymus, spleen, LN, and PP of 5-month-old control and γ-parvin-null mice. The average cell numbers were similar between control and γ-parvin-deficient BM, thymus, and spleen. They were $(29.8 \pm 8.1) \times 10^6$ in control BM and $(35.1 \pm 11.1) \times 10^6$ in γ-parvin-null BM, $(37.1 \pm 10.6) \times 10^6$ in control thymus and $(40.2 \pm 12.1) \times 10^6$ in γ-parvin-null thymus and $(104.0 \pm 33.5) \times 10^6$ in control spleen and $(107.6 \pm 30.8) \times 10^6$ in γ-parvin-null spleen.

To determine the population sizes of different cell lineages we prepared single cell suspensions from lymphoid organs, immunostained them with different lineage markers (B-cell markers B220, IgM, IgD, and CD19; T-cell markers CD4, CD8, and CD3; erythrocyte marker Ter119; granulocyte marker Gr-1; macrophage marker Mac-1; natural killer cell markers Dx5 and NK1.1) and analyzed them by FACS. The relative numbers of the different cell types were similar in BM, thymus, spleen, LN, and PP between control and γ-parvin-null mice of 4, 8, and 20 weeks of age (Fig. 3A to C and data not shown).

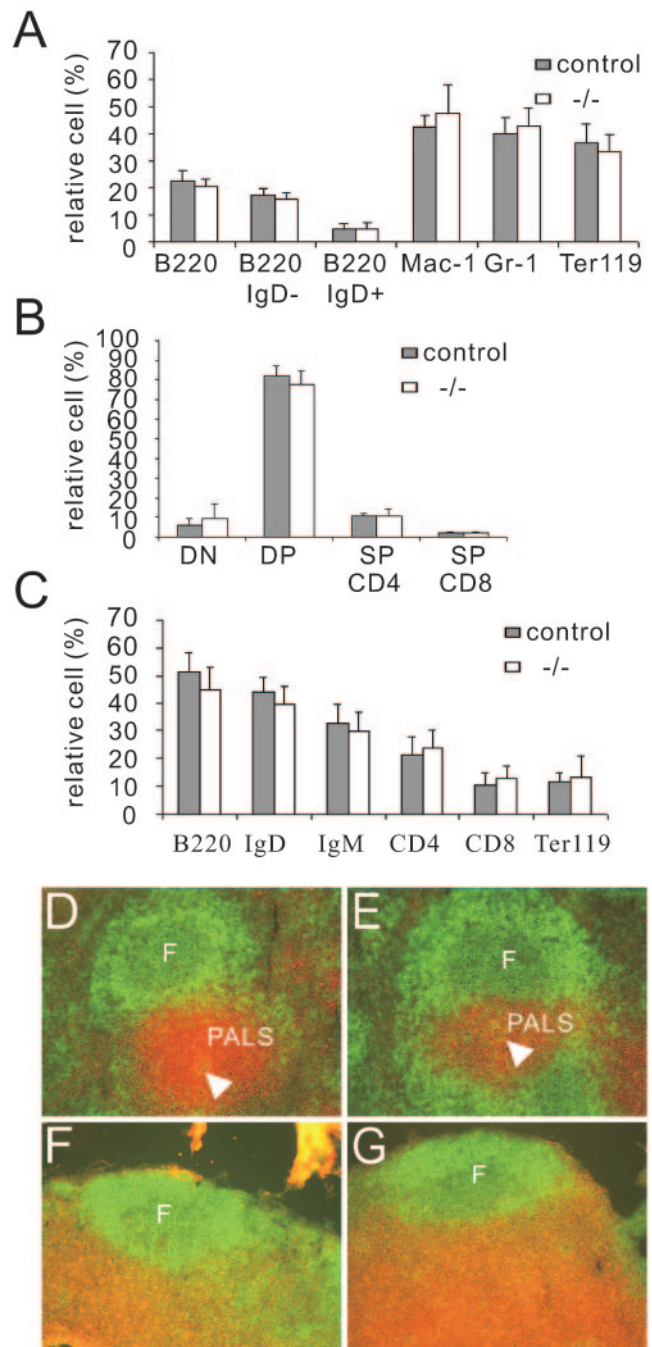

FIG. 3. Composition and architecture of lymphoid organs in γ-parvin-deficient mice. (A to C) Single-cell suspensions derived from primary and secondary lymphoid tissues (BM [A], thymus [B], spleen [C]) were immunostained with different hematopoietic lineage makers and analyzed by FACS. The relative cell numbers are shown ($n = 5/5$, 5-month-old mice). (D to G) Immunostaining of spleen (D and E) and LN (F and G) with anti-B220 (FITC) and anti-Thy1.2 (Cy3) antibodies showed normal distribution of B and T cells. F, B-cell follicle; PALS, periarteriolar lymphoid sheath. Magnification, ×200.

To test whether γ-parvin-null hematopoietic organs have a normal architecture and distribution of the different cell populations, we performed histochemistry and immunostainings of tissue sections derived from hematopoietic organs. Hematox-
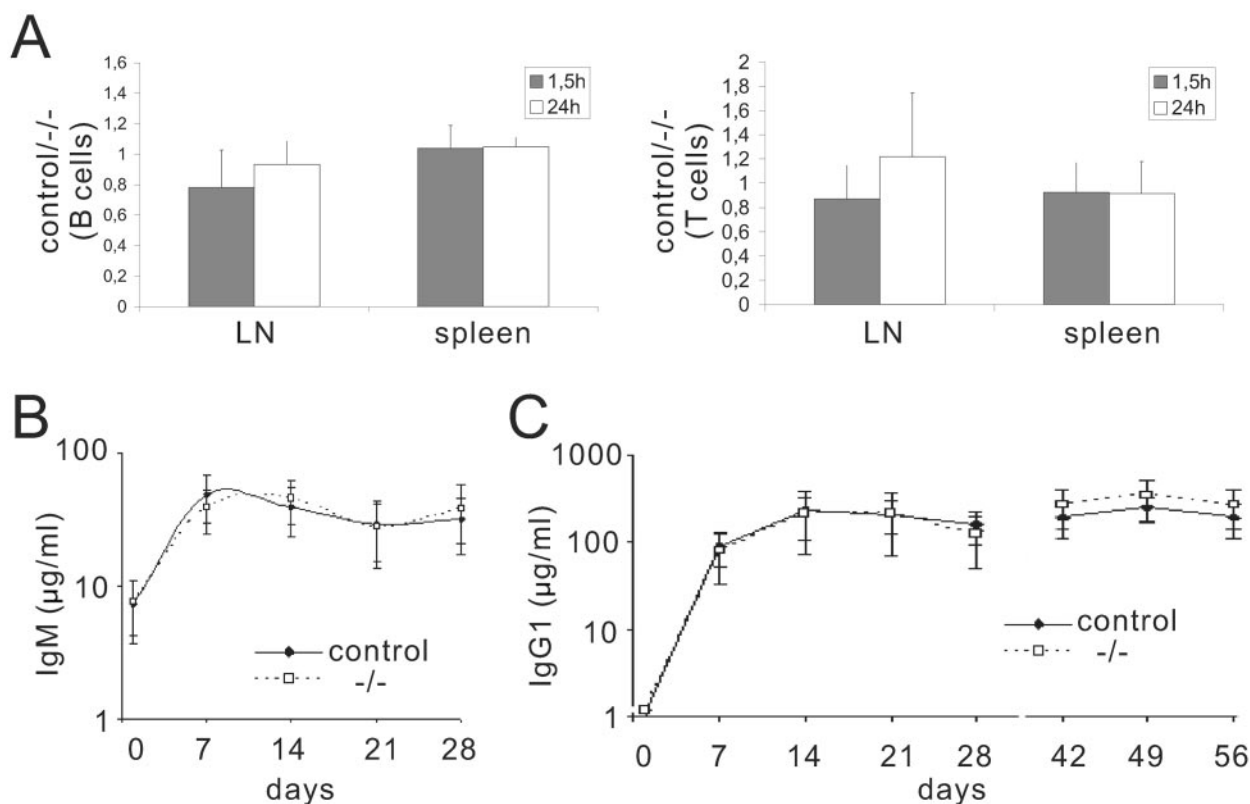
FIG. 4. Lymphocyte homing and T-cell-dependent antibody responses in γ-parvin-deficient mice. (A and B) Spleen single cell suspensions of γ-parvin-deficient and control mice were labeled with TAMRA and CFSE, mixed 1:1, and injected intravenously into wild-type mice. Half of the experiments were performed with inverted labeling. The ratio of knockout to control B and T cells in LN and spleen was determined by FACS. Values are the means of three independent experiments with three to six animals ± the standard error of the mean. (B and C) Mice were immunized with the T-cell-dependent antigen NP-CG, and the anti-NP IgM (B) and IgG1 (C) responses were measured by ELISA. (*n* = 7).

ylin-eosin staining revealed a normal architecture of thymus, spleen, LN, and PP derived from γ-parvin-null mice (data not shown). Immunostaining of spleen, LN, and PP with the B-cell marker B220 and the T-cell marker Thy1.2 showed normal T- and B-cell distribution in the mutant tissues (Fig. 3D and data not shown).

Normal lymphocyte homing and T-cell-dependent antibody response in γ-parvin-deficient mice. The association of γ-parvin with integrins and the actin cytoskeleton in hematopoietic cells suggested a potential role of γ-parvin in leukocyte trafficking. We therefore tested whether short and long-term homing of B and T cells was altered in the absence of γ-parvin. Single cell suspensions of spleens from knockout and control mice were labeled with different fluorescent dyes and a 1:1 mixture of both genotypes was injected intravenously into wild-type recipients. After 90 min and 24 h the ratio of fluorescent cells that homed into spleen and peripheral lymph nodes was determined for B220 positive B cells and CD3 positive T cells, respectively. No significant difference in homing frequency could be observed between mutant and control cells (Fig. 4A).

To more generally test for a role of γ-parvin in adaptive immune responses, we first measured the levels of total immunoglobulins (IgM, IgA, IgG1, IgG2a, IgG2b, and IgG3) and found that they were similar between γ-parvin-null and control animals (data not shown). Next, we investigated whether the T-cell-dependent antibody response differs between control

and γ-parvin-null mice. Mice were immunized with the T-cell-specific antigen NP-CG and the anti-NP antibody heavy chain isotypes (IgM and IgG1), as well as light-chain isotypes (Igκ and Igλ) were measured 1, 2, 3, and 4 weeks later by ELISA. No significant differences were found in any of these anti-NP isotypes between γ-parvin-null and control mice (Fig. 4B and C; see Fig. S1 in the supplemental material). Moreover, when mice were boosted with NP-CG antigens 6 weeks after the immunization, γ-parvin-null mice showed a similar memory antibody response as control mice (Fig. 4C and Fig. S1 in the supplemental material; data for IgG2a and IgG3 are not shown).

Differentiation of macrophages and maturation and migration of DCs are normal in γ-parvin-deficient mice. To test for a possible role of γ-parvin in the myeloid lineage, we differentiated DCs from BM precursors in vitro and induced maturation by adding LPS to the culture medium. Efficiency of DC generation was identical in γ-parvin-deficient and control cultures (Fig. 5A). Morphology as determined by bright-field microscopy was unchanged in this cell type (data not shown). To more specifically address possible cytoskeletal alterations, we performed immunostaining of adherent immature DC for F-actin and the integrin-associated proteins talin (Fig. 5B) and vinculin (not shown). Independent of the genotype, we found the typical podosome structure containing an actin core surrounded by a ring of talin and vinculin.
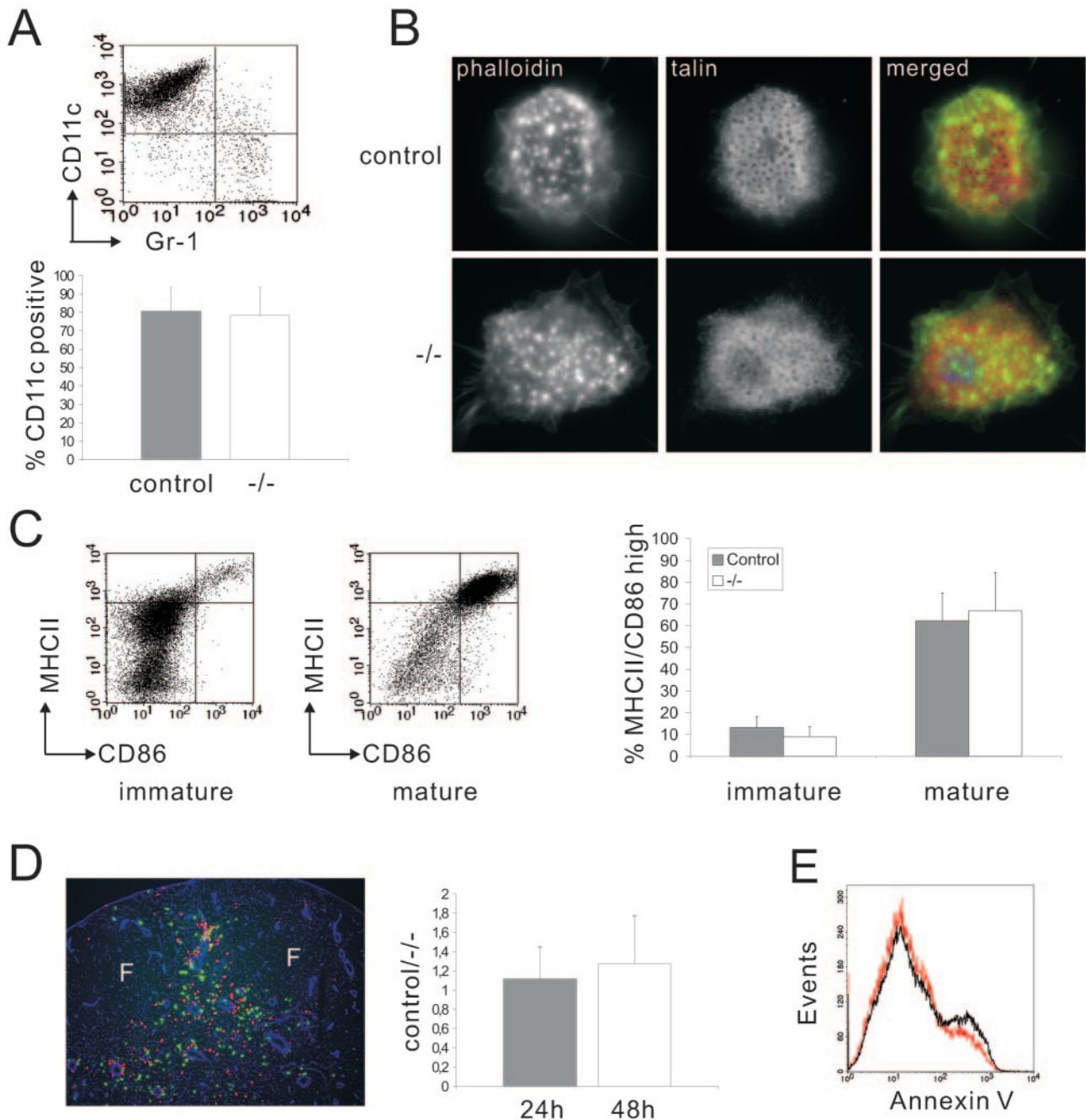
FIG. 5. Differentiation, maturation, and migration of BM-derived DCs. (A) γ-Parvin control and null BM-derived DCs were analyzed by FACS with CD11c and Gr-1 antibodies. Quantification shows mean values of three independent experiments. (B) Immature DC were plated on coverslips, fixed, and immunostained. (C) FACS analysis of MHCII and CD86 on the BM-derived DCs (upper panel) and mature DCs stimulated with LPS overnight (lower panel). The quantification shows mean values of three independent experiments ± the SD. (D) BM-derived DCs from both control and γ-parvin-deficient mice were stimulated with LPS overnight, labeled with TAMRA and CFSE, respectively, mixed in a 1:1 ratio, and subsequently injected into the hind footpad of mice. After 48 h, the popliteal LNs were dissected and immunostained with pan-laminin antibody. F, B-cell follicle. Magnification, ×200. Quantitative data were obtained by FACS analysis of popliteal lymph nodes. Values are means of five independent experiments with three to six mice each ± the standard error of the mean. (E) BM-derived macrophages were harvested (including the cells in suspension) on day 8 and stained with FITC-conjugated annexin V. Data for control cells are shown in black line; those for γ-parvin-null cells are shown in red.

After maturation, γ-parvin-deficient DCs upregulated MHC II and the costimulatory molecules CD86 and CD40 to a similar extent as control DCs (Fig. 5C and data not shown). In vivo, these mature DCs actively migrate via the afferent lym-

phatics into the draining LNs where they encounter and activate naive T cells. To test migration and positioning of DC in vivo, we performed competitive migration experiments. In vitro generated γ-parvin-deficient, and control DCs were la-
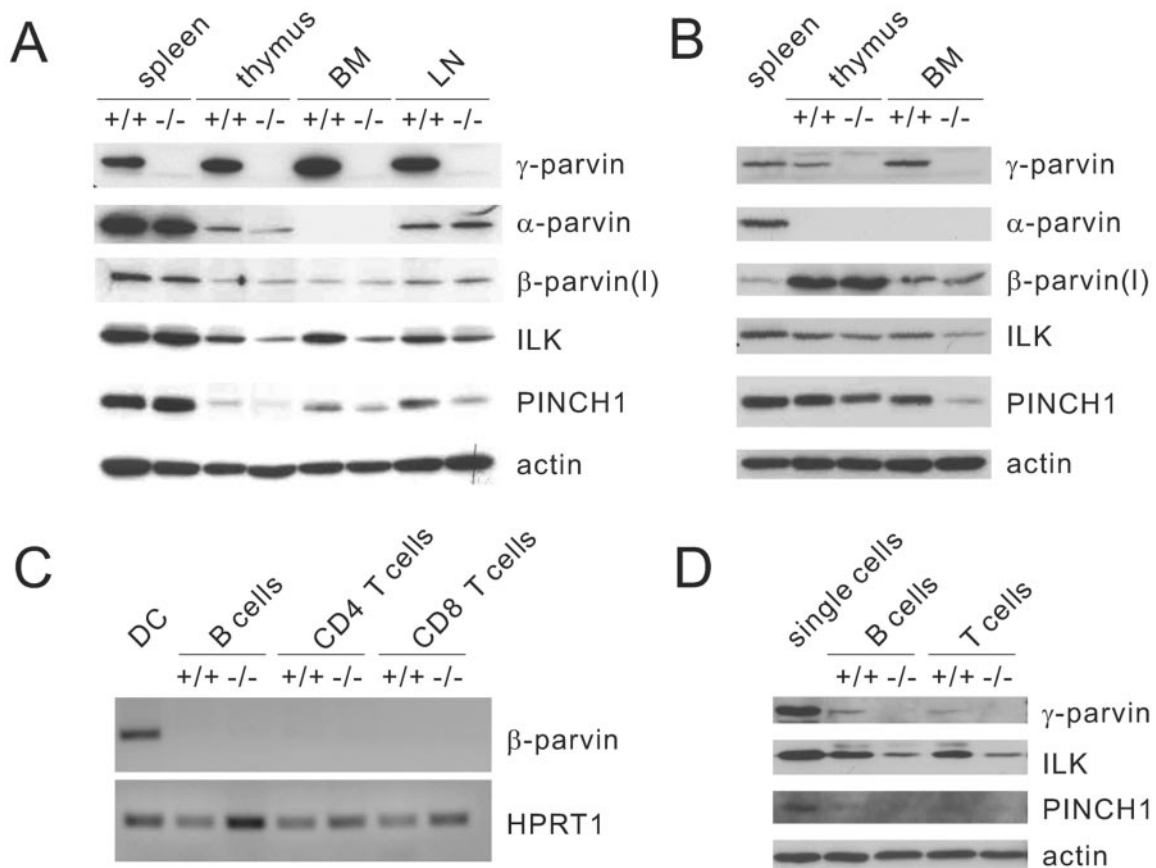
FIG. 6. Levels of α- or β-parvin in γ-parvin-deficient mice. (A) The lysates derived from spleen, thymus, BM, and LN from both control and γ-parvin-deficient mice were immunoblotted with anti-parvin, ILK, and PINCH1 antibodies. (B) BM-derived macrophages and DCs from both control and γ-parvin-deficient mice were immunoblotted with antiparvin, anti-ILK, and anti-PINCH1 antibodies. (C) B220-, CD4-, and CD8-positive cells were sorted from adult splenic single cells and analyzed by RT-PCR for β-parvin mRNA. HPRT1 was used as a control. (D) B220- and CD3-positive cells were sorted from adult splenic single cells and analyzed by Western blotting with anti-γ-parvin, -ILK, and -PINCH1 antibodies. BM, bone marrow; LN, lymph nodes; Mac, macrophages; DC, dendritic cells.

beled with different fluorescent dyes, mixed at a 1:1 ratio, and injected into the footpads of wild-type mice. Histological examination of the draining LNs 24 and 48 h after injection revealed that both γ-parvin-null and control DCs migrated into the T-cell cortex where they located in the same areas (Fig. 5D and data not shown). For quantification, LN suspensions were analyzed by flow cytometry revealing no significant differences between knockout and control cells. These data indicate that myelopoiesis, terminal maturation, and migration of DCs are unaltered in the absence of γ-parvin.

It has been shown that deletion of ILK in a macrophage cell line resulted in increased apoptosis due to decreased levels of PKB/Akt phosphorylation (29). To test whether this effect could be due to the absence of the ILK-PINCH-γ-parvin complex, we differentiated primary macrophages from BM precursor cells in vitro and stained for annexin V to determine the percentage of apoptotic cells in the cultures. Our data showed that γ-parvin-null BM precursors could differentiate into macrophages, as well as heterozygous control cells, and both purities were more than 98% (FACS data not shown). No difference in apoptosis could be

observed between γ-parvin-null and heterozygous control cells (data not shown and Fig. 5E).

Loss of γ-parvin is not compensated by an upregulation of α- or β-parvin expression. It is possible that the lack of an obvious phenotype in the hematopoietic organs and in T and B cells, and DCs of mutant mice is due to compensation by other parvin family members. To test this hypothesis, we determined the expression of all parvins in hematopoietic organs and myeloid and lymphoid lineages. The level of the β-parvin(l) isoform (that is detected by our antibody) was unchanged in the γ-parvin-deficient BM, thymus, spleen, and LN (Fig. 6A), as well as in macrophages and DCs (Fig. 6B). To exclude expression of the shorter isoforms in T and B cells, we performed RT-PCR and found that β-parvin mRNA was not detectable in both control and γ-parvin-deficient cells (Fig. 6C), indicating that also the smaller isoforms are not compensating for the loss of γ-parvin. The level of α-parvin protein was neither increased in lysates from mutant thymus nor mutant LN nor spleen (Fig. 6A), and undetectable in γ-parvin-deficient, as well as wild-type BM, DCs, and macrophages (Fig. 6B).

Next we tested whether the absence of γ-parvin had an impact on the ternary protein complex with ILK and PINCH1. Western blot analyzes showed that ILK and PINCH1 proteins were reduced in the γ-parvin-deficient BM, thymus, spleen, and LN (Fig. 6A), as well as in γ-parvin-deficient macrophages and DCs (Fig. 6B). In B and T lymphocytes, ILK protein was also reduced, while PINCH1 was undetectable in B and T cells in the absence of γ-parvin (Fig. 6D).

DISCUSSION

In the present study we report the hematopoietic expression pattern of the parvin family members, show that γ-parvin can form a ternary complex with ILK and PINCH1, and describe the first analysis of γ-parvin-deficient mice.

To determine the expression of the individual parvin members in hematopoietic organs and cells, we used peptides to generate highly specific antibodies against α-, β-, and γ-parvin. Western analysis with these antibodies showed that γ-parvin was the only parvin family member that was expressed in all hematopoietic organs and cells tested. γ-Parvin is highly expressed in B and T lymphocytes, DCs, and, to a lesser extent, in macrophages. β-Parvin was expressed in all hematopoietic organs, in myeloid cells but not in lymphocytes. Finally, our Western blot studies showed that α-parvin was present in whole organ lysates derived from spleen, thymus and LN but absent in splenic single cells, BM-derived cells, and myeloid (DCs and macrophages) and lymphoid cells (T and B lymphocytes). These findings suggest that α-parvin is likely expressed in stromal and/or endothelial cells of hematopoietic organs and may have, if at all, a rather indirect role on the development and function of hematopoietic cells.

It has been shown in several studies that α- and β-parvins localize to focal adhesion sites and tensin-rich fibrillar adhesions (11, 23, 31, 34). A central player for recruiting α- and β-parvin to focal adhesions is ILK, which binds with its kinase domain to the second calponin homology domain of the α- or β-parvins and with its N-terminal ankyrin repeat to the LIM only protein PINCH (30, 31, 34). The ternary protein complex of ILK, PINCH, and α- or β-parvin forms prior to cell adhesion and is anchored through ILK to the cytoplasmic domain of the β1 integrin upon adhesion (33, 34, 39, 40). γ-Parvin shares approximately 40% identity and 60% similarity with the paralogous α- and β-parvins, and it was not known whether γ-parvin is also capable of binding ILK and forming a complex with PINCH. To resolve this question, we performed coimmunoprecipitation experiments with lysates from DCs, which express high levels of ILK, PINCH1, and γ-parvin. The results revealed that immunoprecipitation of γ-parvin efficiently pulled down ILK and PINCH1, indicating that γ-parvin can, like the other parvins, form and stabilize a ternary complex with ILK and PINCH1.

The specific expression of γ-parvin in hematopoietic cells suggests a potential role in hematopoiesis and/or the immune response. Furthermore, the ability to associate with ILK and PINCH1 makes γ-parvin and the entire ternary protein complex a candidate for transducing β1 and β3 integrin functions in hematopoietic cells. β1 integrins are expressed on almost all hematopoietic cells and perform functions during the embryonic and adult hematopoiesis. During embryogenesis β1 integrins control trafficking of embryonic and extra-embryonic hematopoietic stem cells into the fetal liver (13, 24) and induce the formation of PPs by enabling the interaction of a unique subset of hematopoietic cells that is expressing CD4 and lacking CD3 with stromal cells in the gut (4). Postnatally, β1 integrins are essential for the homing of adult hematopoietic stem cells into the BM and the regulation of the T-cell-dependent antibody response (1, 2, 24). β3 integrins have an essential role for platelet aggregation (14) and play a more subtle role during monocyte migration (32). The role of ILK and PINCH1 in blood cells is less well studied. In one report it has been demonstrated that ILK plays an important role for monocyte/macrophage survival by regulating the activation of PKB/Akt (29), and another study suggested that ILK may regulate trans-endothelial migration of monocytes (5). To test whether γ-parvin contributes, at least in part, to the transduction of the β1 and/or β3 integrin function(s) in the hematopoietic system, we disrupted the γ-parvin gene in mice. Surprisingly, the γ-parvin-deficient mice were born at the expected Mendelian distribution, were fertile, and displayed no obvious phenotype. Moreover, the cell numbers and the proportion of different myeloid and lymphoid cells in BM, thymus, spleen, LN, and PP were normal in mice lacking γ-parvin expression. Similarly, differentiation of BM precursors to macrophages occurred normally and without signs of increased apoptosis. This indicates that γ-parvin has no rate-limiting function for the homing of hematopoietic stem cells during development, as well as for their potential to give rise to the different blood cell lineages. Furthermore, the recirculation through lymphatic organs is also normal in the absence of γ-parvin. Finally, functional assays such as T-cell-dependent antibody response and the in vivo migration of BM-derived DCs to LN are also independent of the expression of γ-parvin.

An explanation for the lack of phenotype in γ-parvin-deficient mice is compensation or redundancy by other parvin family members. Although this could explain the normal migration of DCs and the absence of apoptosis in macrophages, which both express in addition to γ-parvin significant levels of β-parvin, it does not explain the normal T-cell-dependent antibody response, since both T and B cells express γ-parvin only and neither upregulate α- nor β-parvin expression in the absence of γ-parvin. In line with previous studies on the stability of the ILK/PINCH/parvin complex, the loss of γ-parvin expression reduced the levels of ILK and PINCH in T cells (33). Interestingly, the reduction of ILK and PINCH1 in γ-parvin-deficient T and B cells suggests that the ILK/PINCH1/γ-parvin complex plays most likely a more subtle role for regulating the T-cell-dependent antibody response and that β1 integrins use another signaling complex to fulfill this task. Such functions can be tested by deleting individual members of the ILK/PINCH/parvin complex specifically in T cells using the Cre/loxP system.

In summary, our study shows that mouse development and postnatal aging can proceed normally when the γ-parvin gene is disrupted. Although the γ-parvin gene seems to be dispensable in vivo, we cannot rule out that γ-parvin serves specific tasks that we have not been investigated here. It is also possible that there is a certain degree of compensation between γ-parvin and β-parvin. This possibility will be difficult to analyze, since the γ-parvin and β-parvin genes are separated by only

around 12 kb and the generation of compound mutant mice is only possible by targeting both genes in the same ES cell line.

REFERENCES

1. **Brakebusch, C., and R. Fässler.** 2003. The integrin-actin connection, an eternal love affair. EMBO J. **22:**2324–2333.
2. **Brakebusch, C., S. Fillatreau, A. J. Potocnik, G. Bungartz, P. Wilhelm, M. Svensson, P. Kearney, H. Korner, D. Gray, and R. Fässler.** 2002. β1 integrin is not essential for hematopoiesis but is necessary for the T cell-dependent IgM antibody response. Immunity **16:**465–477.
3. **Fässler, R., M. Pfaff, J. Murphy, A. A. Noegel, S. Johansson, R. Timpl, and R. Albrecht.** 1995. Lack of β1 integrin gene in embryonic stem cells affects morphology, adhesion, and migration but not integration into the inner cell mass of blastocysts. J. Cell Biol. **128:**979–988.
4. **Finke, D., H. Acha-Orbea, A. Mattis, M. Lipp, and J. Kraehenbuhl.** 2002. CD4+ CD3− cells induce Peyer's patch development: role of alpha4beta1 integrin activation by CXCR5. Immunity **17:**363–373.
5. **Friedrich, E. B., S. Sinha, L. Li, S. Dedhar, T. Force, A. Rosenzweig, and R. E. Gerszten.** 2002. Role of integrin-linked kinase in leukocyte recruitment. J. Biol. Chem. **277:**16371–16375.
6. **Fukuda, T., L. Guo, X. Shi, and C. Wu.** 2003. CH-ILKBP regulates cell survival by facilitating the membrane translocation of protein kinase B/Akt. J. Cell Biol. **160:**1001–1008.
7. **Fukuda, T., K. Chen, X. Shi, and C. Wu.** 2003. PINCH-1 is an obligate partner of integrin-linked kinase (ILK) functioning in cell shape modulation, motility, and survival. J. Biol. Chem. **278:**51324–51333.
8. **Geiger, B., A. Bershadsky, R. Pankov, and K. M. Yamada.** 2001. Transmembrane crosstalk between the extracellular matrix-cytoskeleton crosstalk. Nat. Rev. Mol. Cell. Biol. **2:**793–805.
9. **Grashoff, C., I. Thievessen, K. Lorenz, S. Ussar, and R. Fässler.** 2004. Integrin-linked kinase: integrin's mysterious partner. Curr. Opin. Cell Biol. **16:**565–571.
10. **Gray, D., P. Dullforce, and S. Jainandunsing.** 1994. Memory B-cell development but not germinal center formation is impaired by in vivo blockade of CD40-CD40 ligand interaction. J. Exp. Med. **180:**141–155.
11. **Guo, L., and C. Wu.** 2002. Regulation of fibronectin matrix deposition and cell proliferation by the PINCH-ILK-CH-ILKBP complex. FASEB J. **16:**1298–1300.
12. **Guo, W., and F. G. Giancotti.** 2004. Integrin signalling during tumour progression. Nat. Rev. Mol. Cell. Biol. **5:**816–826.
13. **Hirsch, E., A. Iglesias, A. J. Potocnik, U. Hartmann, and R. Fässler.** 1996. Impaired migration but not differentiation of hematopoietic stem cells in the absence of β1 integrins. Nature **380:**171–175.
14. **Hodiva-Dilke, K. M., K. P. McHugh, D. A. Tsakiris, H. Rayburn, D. Crowley, M. Ullman-Cullere, F. P. Ross, B. S. Coller, S. Teitelbaum, and R. O. Hynes.** 1999. β3-Integrin-deficient mice are a model for Glanzmann thrombasthenia showing placental defects and reduced survival. J. Clin. Investig. **103:**229–238.
15. **Hynes, R. O.** 2002. Integrins: bidirectional, allosteric signaling machines. Cell **110:**673–687.
16. **Korenbaum, E., T. M. Olski, and A. A. Noegel.** 2001. Genomic organization and expression profile of the parvin family of focal adhesion proteins in mice and humans. Gene **279:**69–79.
17. **Lee, J. W., and R. Juliano.** 2004. Mitogenic signal transduction by integrin-and growth factor receptor-mediated pathways. Mol. Cells **17:**188–202.
18. **Li, S., R. Bordoy, F. Stanchi, M. Moser, A. Braun, O. Kudlacek, U. M. Wewer, P. D. Yurchenco, and R. Fässler.** 2005. PINCH1 regulates cell-matrix and cell-cell adhesions, cell polarity and cell survival during the peri-implantation stage. J. Cell Sci. **118:**2913–2921.
19. **Lin, X., H. Qadota, D. G. Moerman, and B. D. Williams.** 2003. *Caenorhabditis elegans* PAT-6/actopaxin plays a critical role in the assembly of integrin adhesion complexes in vivo. Curr. Biol. **13:**922–932.
20. **Lutz, M. B., N. Kukutsch, A. L. Ogilvie, S. Rossner, F. Koch, N. Romani, and G. Schuler.** 1999. An advanced culture method for generating large quantities of highly pure dendritic cells from mouse bone marrow. J. Immun. Methods **223:**77–92.
21. **Mishima, W., A. Suzuki, S. Yamaji, R. Yoshimi, A. Ueda, T. Kaneko, J. Tanaka, Y. Miwa, S. Ohno, and Y. Ishigatsubo.** 2004. The first CH domain of affixin activates Cdc42 and Rac1 through αPIX, a Cdc42/Rac1-specific guanine nucleotide exchanging factor. Genes Cells **9:**193–204.
22. **Nikolopoulos, S. N., and C. E. Turner.** 2000. Actopaxin, a new focal adhesion protein that binds paxillin LD motifs and actin and regulates cell adhesion. J. Cell Biol. **151:**1435–1448.
23. **Olski, T. M., A. A. Noegel, and E. Korenbaum.** 2001. Parvin, a 42 kDa focal adhesion protein, related to the α-actinin superfamily J. Cell Sci. **114:**525–538.
24. **Potocnik, A. J., C. Brakebusch, and R. Fässler.** 2000. Fetal and adult hematopoietic stem cells require β1 integrin function for colonizing fetal liver, spleen, and bone marrow. Immunity **12:**653–663.
25. **Rosenberger, G., I. Jantke, A. Gal, and K. Kutsche.** 2003. Interaction of alphaPIX (ARHGEF6) with beta-parvin (PARVB) suggests an involvement of alphaPIX in integrin-mediated signaling. Hum. Mol. Genet. **12:**155–167.
26. **Rutherford, M. S., and L. B. Schook.** 1992. Differential immunocompetence of macrophages derived using macrophage or granulocyte-macrophage colony-stimulating factor. J. Leukoc. Biol. **51:**69–76.
27. **Sakai, T., S. Li, D. Docheva, C. Grashoff, K. Sakai, K. Kostka, A. Braun, A. Pfeifer, P. D. Yurchenco, and R. Fässler.** 2003. Integrin-linked kinase (ILK) is required for polarizing the epiblast, cell adhesion, and controlling actin accumulation. Genes Dev. **17:**926–940.
28. **Sorokin, L., A. Sonnenberg, M. Aumailley, R. Timpl, and P. Ekblom.** 1990. Recognition of the laminin E8 cell-binding site by an integrin possessing the alpha 6 subunit is essential for epithelial polarization in developing kidney tubules. J. Cell Biol. **111:**1265–1273.
29. **Troussard, A. A., N. M. Mawji, C. Ong, A. Mui, R. St. Arnaud, and S. Dedhar.** 2003. Conditional knockout of integrin-linked kinase demonstrates an essential role in protein kinase B/Akt activation. J. Biol. Chem. **278:**22374–22378.
30. **Tu, Y., F. Li, S. Goicoechea, and C. Wu.** 1999. The LIM-only protein PINCH directly interacts with integrin-linked kinase and is recruited to integrin-rich sites in spreading cells. Mol. Cell. Biol. **19:**2425–2434.
31. **Tu, Y., Y. Huang, Y. Zhang, Y. Hua, and C. Wu.** 2001. A new focal adhesion protein that interacts with integrin-linked kinase and regulates cell adhesion and spreading. J. Cell Biol. **153:**585–598.
32. **Weerasinghe, D., K. P. McHugh, F. P. Ross, E. J. Brown, R. H. Gisler, and B. A. Imhof.** 1998. A role for the αvβ3 integrin in the transmigration of monocytes. J. Cell Biol. **142:**595–607.
33. **Wu, C.** 2004. The PINCH-ILK-parvin complexes: assembly, functions, and regulation. Biochim. Biophys. Acta **1692:**55–62.
34. **Yamaji, S., A. Suzuki, Y. Sugiyama, Y. Koide, M. Yoshida, H. Kanamori, H. Mohri, S. Ohno, and Y. Ishigatsubo.** 2001. A novel integrin-linked kinase-binding protein, affixin, is involved in the early stage of cell-substrate interaction. J. Cell Biol. **153:**1251–1264.
35. **Yamaji, S., A. Suzuki, H. Kanamori, W. Mishima, R. Yoshimi, H. Takasaki, M. Takabayashi, K. Fujimaki, S. Fujisawa, S. Ohno, and Y. Ishigatsubo.** 2004. Affixin interacts with α-actinin and mediates integrin signaling for reorganization of F-actin induced by initial cell-substrate interaction. J. Cell Biol. **165:**539–551.
36. **Yang, Y., L. Guo, S. M. Blattner, P. Mundel, M. Kretzler, and C. Wu.** 2005. Formation and phosphorylation of the PINCH-1-integrin linked kinase–α-parvin complex are important for regulation of renal glomerular podocyte adhesion, architecture, and survival. J. Am. Soc. Nephrol. **16:**1966–1976.
37. **Zhang, Y., K. Chen, L. Guo, and C. Wu.** 2002. Characterization of PINCH-2, a new focal adhesion protein that regulates the PINCH-1-ILK interaction, cell spreading, and migration. J. Biol. Chem. **277:**38328–38333.
38. **Zhang, Y., L. Guo, K. Chen, and C. Wu.** 2002. A critical role of the PINCH-integrin-linked kinase interaction in the regulation of cell shape change and migration. J. Biol. Chem. **277:**318–326.
39. **Zhang, Y., K. Chen, Y. Tu, A. Velyvis, Y. Yang, J. Qin, and C. Wu.** 2002. Assembly of the PINCH-ILK-CH-ILKBP complex precedes and is essential for localization of each component to cell-matrix adhesion sites. J. Cell Sci. **115:**4777–4786.
40. **Zhang, Y., K. Chen, Y. Tu, and C. Wu.** 2004. Distinct roles of two structurally closely related focal adhesion proteins, α-parvins and β-parvins, in regulation of cell morphology and survival. J. Biol. Chem. **279:**41695–41705.

β1 integrins: zip codes and signaling relay for blood cells

Michael Sixt, Martina Bauer, Tim Lämmermann and Reinhard Fässler

At least eight of the twelve known members of the β1 integrin family are expressed on hematopoietic cells. Among these, the VCAM-1 receptor α4β1 has received most attention as a main factor mediating firm adhesion to the endothelium during blood cell extravasation. Therapeutic trials are ongoing into the use of antibodies and small molecule inhibitors to target this interaction and hence obtain anti-inflammatory effects. However, extravasation is only one possible process that is mediated by β1 integrins and there is evidence that they also mediate leukocyte retention and positioning in the tissue, lymphocyte activation and possibly migration within the interstitium. Genetic mouse models where integrins are selectively deleted on blood cells have been used to investigate these functions and further studies will be invaluable to critically evaluate therapeutic trials.

Addresses
Department of Molecular Medicine, Max Planck Institute of Biochemistry, Martinsried, Germany

Corresponding author: Fässler, Reinhard (faessler@biochem.mpg.de)

Introduction

To fulfill their surveillance function immune cells continuously patrol the organism, shuttling back and forth between the blood stream, the lymphatic fluid, secondary lymphatic organs and peripheral tissues [1]. This mobile life style requires flexible switching between passive transport and various cell-to-cell and cell-to-extracellular matrix (ECM) interactions to arrest, migrate and become activated.

The current paradigm of cell locomotion within tissues and along cell surfaces involves integrin-mediated adhesion to ECM or cellular counter-receptors, which generates traction forces necessary for translocation of the cell body [2]. Integrins are perfectly suited to this task since they link the cytoskeleton with the extracellular environment. Integrins are heterodimeric cell surface receptors made up of α and β subunits. The combination of 18 known α and 8 β subunits in mammals can give rise to 24

different receptors [3]. Antibody blocking studies, gene targeting approaches in mice and investigation of human diseases have unambiguously revealed that integrins are essential for intact hematopoietic development, homeostasis and inflammation. However, integrin ligand binding can affect several cellular events in addition to adhesion and migration, including cell differentiation, polarization, activation and survival [3]. A drawback of most studies manipulating integrin functions on blood cells *in vivo* is that the cell-biological process affected by the manipulation is not exactly defined. This is especially evident when complex inflammatory models (for example for autoimmune diseases) are studied and clinical symptoms or histological parameters are used as readout. A further critical issue is that within recent years an increasing number of mouse knockout studies have been published that address the *in vivo* function of cytoplasmic proteins involved in integrin signaling without explicitly investigating which integrins are affected.

In this review we focus on the largest integrin family which contains the β1 chain. The blood-cell-specific β2 integrin subfamily has been extensively reviewed by others [4]. We will try to dissect the different cell-biological functions that β1 integrins mediate when leukocytes emerge from the blood vessels, locate within tissues, become activated and re-enter the blood circulation.

Extravasation from the blood circulation

One of the best-established concepts in leukocyte biology is the extravasation paradigm. When hematopoietic cells leave the blood stream they go through a sequential adhesion cascade to overcome both the high shear forces within the blood vessel and the tight seal of the endothelial cells (see Figure 1). Transient selectin–carbohydrate interactions cause hematopoietic cells to begin to roll along an activated endothelium. While rolling, the cells sense chemokines that are immobilized on heparan sulfate residues on the luminal side of the endothelial cells. The ligated chemokine receptors then transmit signals into the leukocyte that lead to the rapid activation of integrins (inside-out signaling — see Box 1), which results in the integrins adhering firmly to their counter receptors on the endothelial cell. Although adhesion during extravasation is an essential step during leukocyte trafficking, it has little in common with cell migration in the true sense. It is rather a cell adhesion event of the hematopoietic cell to the two-dimensional surface of the endothelial lumen.

The crucial β1 integrin family member involved in extravasation is α4β1, which binds to the endothelial Ig

Box 1 Regulation of β1 integrin activation

On circulating leukocytes, integrins are locked in the low-affinity state. Only upon 'inside out' signaling (triggered, for example, by chemokines, growth factors or T cell receptor activation) integrins adopt a high-affinity conformation (termed integrin activation) facilitating ligand binding and subsequent cell adhesion. Ligand binding in turn induces integrin 'outside in' signaling that (among many other effects) further consolidates cell binding by clustering the integrins and thereby increasing binding avidity. Cytoplasmic key players mediating 'inside-out' signaling are the small GTPases of the Rap family and talin.

Rap1: Several recent *in vitro* studies have proven that Rap1, the best-characterized member of the five Rap proteins, is essential for β1 integrin activation on leukocytes. Studies with cell lines revealed that activated Rap1 increases β1 integrin-mediated adhesion and migration on VCAM-1 via α4β1 and on fibronectin via α4β1 and α5β1 [57,58]. The same was shown for primary thymocytes of transgenic mice expressing the constitutively active Rap1-mutant Rap1V12 [59], whereas T and B cells derived from Rap1-deficient mice show impaired adhesion on fibronectin [60]. Rap1 is recruited to the plasma membrane by PKD1, where it is activated upon integration into a complex containing the β1 integrin cytoplasmic tail [61,62]. For Rap1-mediated inside-out signaling, the two Rap1 binding effectors RIAM and RAPL are essential. Accordingly, T cells and dendritic cells from RAPL-deficient mice show impaired adhesion to β1 integrin ligands and reduced transmigration through endothelial monolayers [63]. Overexpression of RIAM enhances Rap1-mediated T cell adhesion to fibronectin. Through its interaction with profilin and ENA/Vasp proteins, RIAM probably links Rap1–GTP to the actin cytoskeleton [64].

Talin: Talin is a large rod-like molecule that binds via its globular head domain to the membrane proximal NPXY motif of β integrins in a phosphorylation-regulated manner. Talin acts as a physical link between integrins and the actin cytoskeleton and its binding to integrin β chains is regarded as the final common step in integrin activation [65]. Two recent studies assessed the *in vivo* role of the β1 integrin NPXY motifs by employing mouse genetic models. They revealed that the intact conformation of the NPXY motifs are essential, as substitution of the tyrosines by alanine abolishes β1 integrin function and leads to a β1 integrin-null phenotype [66,67]. Accordingly, chimeric mice with alanine substitutions, similar to a β1 integrin-null chimera, fail to develop hematopoietic cells, probably as a result of impaired talin binding [67]. Both studies, however, challenged the former view that tyrosine phosphorylation is essential for affinity regulation of β1 integrins, as replacement of both cytoplasmic tyrosines with phenylalanine did not result in an obvious phenotype, indicating that tyrosine phosphorylation is dispensable for the physiological β1 integrin function *in vivo*.

superfamily cell surface receptor VCAM-1 (vascular cell adhesion molecule 1). This interaction is conserved in many different physiological settings where extravasation occurs. In the steady state, lymphocyte recirculation via high endothelial venules [5], T cell precursor entry into the thymus [6] and T cell and stem cell homing into the bone marrow [7–9] are regulated via this pathway. During inflammation, lymphocytes and monocytes use α4β1 to immigrate into the skin, lung, peritoneum and liver [10,11,12•]. For several cell types it has also been shown that VCAM-1-α4β1 binding can mediate not only firm adhesion but also rolling along the endothelium [12•]. In a somewhat controversial deviation from the paradigm,

there is evidence that extravasation of lymphocytes into the central nervous system during autoimmune inflammation is possible in the absence of previous rolling [13,14•]. Here the cells can be rather abruptly captured by VCAM-1 exposed on the endothelial lumen.

In most cases the function of α4β1 is partially redundant with that of β2 integrins and α4β7, which bind the endothelial counter-receptors intercellular adhesion molecule (ICAM-1) and mucosal addressin cell adhesion molecule-1 (MAdCAM-1), respectively. An impressive example of this redundancy is lymphocyte recirculation into lymph nodes, which is only partially affected by β2 and β7 elimination [5] and unimpaired in the absence of β1 integrin [15]. Combined blockade, however, results in almost 100% reduction of lymphocyte recirculation [5]. Many details concerning the overlapping functions of these integrins remain to be clarified using genetic models in which the separate families are targeted simultaneously.

Important exceptions to this redundancy are T cell trafficking into the CNS, which is largely inhibitable by α4β1 blockade [16], stem cell homing into the bone marrow, which is completely defective in the absence of β1 integrin [7], and the migration of hematopoietic progenitor cells from the fetal blood into the fetal liver during early development. In early hematopoietic development, we could show that genetic deletion of the β1 integrin gene in progenitor cells leads to their accumulation in the fetal blood and hence the inability to populate hematopoietic tissues [7,17]. Although it is likely that α4 is of major importance in this setting, other α chains may be involved. A possible candidate is the largely neglected integrin α9β1, which is highly expressed on granulocytes and binds to VCAM-1 and the ECM proteins tenascin, osteopontin and fibronectin. α9β1 has been shown to mediate transendothelial migration *in vitro* via interaction with VCAM-1 [18]. Interestingly, α4 and α9 chain are closely related and together form a sub-family that binds to the cytoplasmic adaptor paxillin [19].

Migration through the endothelium
Tight adhesion to the endothelium is followed by a cascade of migration events that probably successively trigger each other. First the cells have to pass through the endothelial monolayer. There is no *in vivo* evidence that this process — called 'diapedesis' — is directly dependent on β1 integrins. It is rather mediated by cell adhesion molecules of the JAM family, CD99 and PECAM-1 [1]. Nevertheless, ligation of endothelial VCAM-1 via α4β1 seems to be a prerequisite for diapedesis, as it triggers a signal within the endothelial cell that is transmitted via the cytoplasmic tail of VCAM [20]. The endothelial cell then reacts by actively extending protrusions to capture and guide the extravasating cell through intercellular junctions or by transcytosing it directly

Figure 1
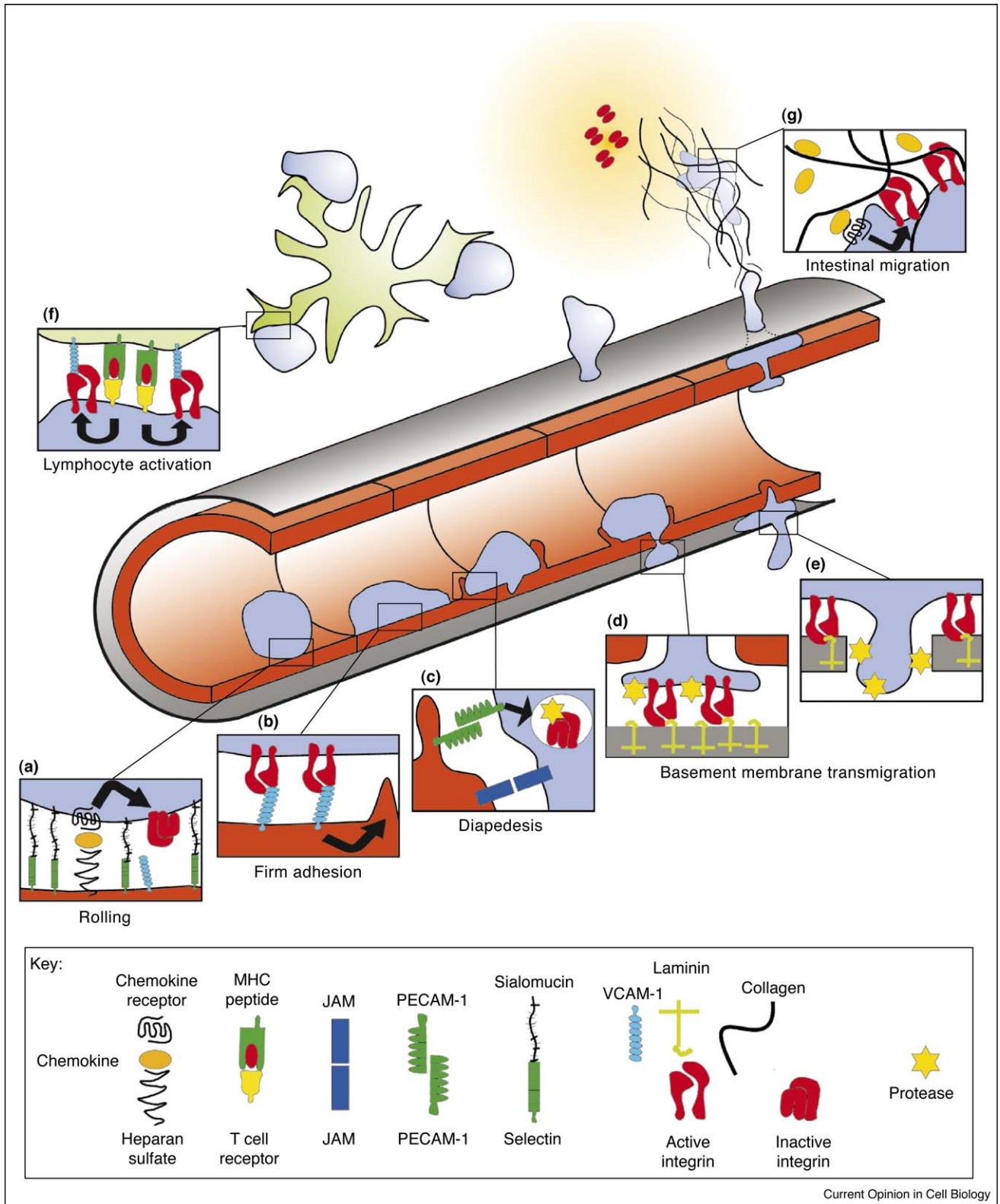
Roles of β1 integrins during extravasation, interstitial migration and lymphocyte activation. **(a)** During selectin-mediated rolling, the extravasating cell senses chemokines that are immobilized on the surface of the endothelium, leading to the inside-out activation of integrin α4β1. **(b)** The α4β1–VCAM-1 interaction mediates firm adhesion and triggers a reverse signal via VCAM-1 that induces the extension of endothelial protrusions,

through the endothelial cell body — called emperipolesis [20,21].

Transmigration through the basement membrane

All the events following diapedesis are far less characterized, which is mainly due to their experimental inaccessibility and the lack of established *in vitro* models to study molecular interactions. Directly after passing through the endothelium, the transmigrating cells face a seemingly impermeable barrier of ECM: the endothelial basement membrane (BM). BMs are tightly interconnected and thin (∼50–100 nm) sheets of specialized ECM components of the laminin and collagen IV family [22]. It is possible that β1 integrins play an active role during this passage and *in vitro* studies have demonstrated that leukocytes can actively bind BM components [23]. If BM transmigration is selectively blocked *in vivo* one would expect that extravasating leukocytes become trapped between the endothelial cell layer and the underlying BM. Indeed this phenomenon was observed when extravasation of granulocytes triggered by interleukin (IL)-1 was studied in mice in which platelet endothelial cell adhesion molecule-1 (PECAM-1) was functionally inactivated by blocking antibodies or genetic deletion [24]. The homophilic interaction between PECAM-1 on granulocyte and endothelium induced the up-regulation of the laminin binding α6β1 integrin on the granulocyte surface, which in turn was necessary for BM transmigration [25]. Although this sequence of events was well demonstrated in this specific experimental setting, it is not a general phenomenon, as granulocyte extravasation in response to tumor necrosis factor (TNF)α occurred independently of PECAM-1 and α6β1 [26]. Another recently reported example of the possible involvement of a BM binding integrin during extravasation is the reduced homing of hematopoietic stem cells into the bone marrow after antibody blockade of α6β1 [27].

A physiologically distinct situation where leukocytes cross a BM occurs during the emigration of Langerhans cells from the epidermis. Their penetration through the epidermal BM (which is biochemically distinct from blood vessel BMs [28]) can also be inhibited by antibody blockade of α6 integrin [29]. Although in this case it remains to be shown which β chain (β1 or β4) pairs with α6, laminin is the likely ligand.

Apart from these fragmentary data about molecular players, the progression of physiological events that leads to BM transmigration is completely enigmatic. Proteolytic digestion via proteases, especially by the matrix metalloproteinase (MMP) family, has been suggested in several *ex vivo* models [30,31]. In this context it is interesting that ligation of integrins can lead to the induction of MMPs on leukocytes [31,32]. It remains to be shown if integrins merely signal the presence of a BM to induce proteolytic cascades or other events leading to the BM's local disassembly, or if integrin-mediated adhesion is also a physical requirement for the translocation of the cell body through the BM.

Migration through the interstitium

The diverse extracellular environments that leukocytes face upon passaging through the BM range from the loosely packed and fibrillar-collagen-dominated connective tissue of the mesenchymal interstitium to the cell-rich environment of secondary lymphatic organs. At this stage, true directed migration takes over and it is assumed that leukocytes navigate along gradients of chemotactic agents towards their destinations. Despite numerous *in vitro* studies using artificial settings such as transwell filters coated with ECM components, it is still controversial if this directed migration depends on integrins at all *in vivo*. The most direct experimental evidence for integrin involvement is provided by a series of intravital microscopy studies revealing that migration of granulocytes through the mesenteric interstitium can be partially inhibited by blocking antibodies against the collagen-binding β1 and α2 integrin chains [33–35]. However, measured reductions in speed of only ∼30% raise the question of whether the remaining migratory activity is mediated by compensating (β2 or αv) integrins or whether it is completely integrin-independent. *In vitro* experimental approaches using three-dimensional gels of the fibrillar collagens I and III, which mimic the interstitial ECM, can be utilized as migration matrices and studied by video microscopy. Even in this artificial and very defined setting, the results obtained with integrin-blocking antibodies are controversial. By combined antibody blockade of αv, β2 and β1 integrins, it was shown that random T cell migration in the gel can occur in an 'ameboid' fashion in the complete absence of integrin-mediated binding [36] and proteolytic activity [37]. However, others demonstrated that in the presence of chemotactic agents, T cells utilize β1 (α1, α2, α6) integrins for locomotion within collagen gels [38]. Although the issue of interstitial migration remains to be clarified using genetic approaches in combination with intravital microscopy, it is evident that it is essential to define not only the nature of the ECM ligand but also the spatial configuration of the extracellular environment in order to establish

---

(Figure Legend 1 continued) establishing a 'docking structure'. **(c)** Diapedesis is mediated via PECAM-1, JAMs, CD99 and β2 integrins (not shown). Signals from the endothelium induce surface expression of α6β1 and proteases on the transmigrating cell. **(d,e)** In some cases the laminin-binding integrin α6β1 and cell surface proteases mediate passage of the basement membrane. **(f)** α4β1 localizes to synapses between follicular dendritic cells and B cells and dendritic cells and T cells where it promotes lymphocyte activation. **(g)** Interstitial migration along chemotactic gradients is possibly mediated by the collagen-binding α2β1 integrin.

---

integrin dependency. In an elegant study, Malawista *et al.* [39] showed that in the spatially constrained environment of a narrow space between two closely adjacent glass surfaces, granulocytes can switch to biophysical mechanisms of translocation (squeezing or 'chimneying') that are independent of integrin binding. By contrast, on two dimensional surfaces granulocytes are completely dependent on integrins to generate traction forces [39]. These findings impressively demonstrate the importance of using 3-dimensional model systems to study interstitial blood cell migration.

In the light of these diverse and partially controversial data, it seems possible that within the 3-dimensional environment of the interstitium the quickly migrating blood cells employ adhesive mechanisms that are fundamentally different from the integrin-dependent migration strategies used by mesenchymal cells.

Retention and positioning within the tissue

While it still remains to be clarified to what extent integrins are involved in interstitial leukocyte migration, there is solid evidence that integrin-mediated binding can define the position of hematopoietic cells by immobilizing and retaining them in their niches. Owing to the poor knowledge about the spatial configuration and molecular composition of these niches, it is not known if retention simply reflects integrin-mediated cell binding or if more complex processes are triggered via integrin signaling that ultimately lead to retention. Two prominent examples of integrin-mediated retention are illustrated by studies involving marginal zone B cells and hematopoietic progenitor cells.

Several studies revealed that different precursors can be released from the bone marrow by antibody blockade or genetic inactivation of the α4 integrin [40,41]. Similar results were obtained with mice lacking the α4β1 ligand VCAM-1 [42]. It has been proposed that in the bone marrow the stroma-derived chemokine CXCL12 triggers a sustained signal that keeps the integrin in the active state and therefore immobilizes the cells to VCAM-1 and fibronectin on stroma cells [43].

Marginal zone B cells are part of the first line defense system against circulating soluble antigens. As such, they are located in a defined ring area around the white pulp follicles of the spleen, where they capture blood-borne antigens. Only upon activation by microbial stimuli or antigen do they downregulate integrin avidity, detach from the marginal zone and follow a chemotactic gradient of the chemokine CXCL13 that guides them into the follicle, where they produce immunoglobulins. The retention of marginal zone B cells is redundantly mediated by α4β1 and αLβ2 integrin, and blockade or genetic ablation of these integrins causes the cells to dislocate from the marginal zone [44]. In marginal zone

B cells, integrin affinity was shown to be regulated via the GTPase RhoA and the exchange factor lsc, as in the absence of lsc these cells are unable to leave their niche following stimulation owing to an insufficient down-modulation of integrin avidity [45•].

An interesting series of studies that suggests a role for integrin-mediated retention during pathological processes has been performed by de Fougerolles and co-workers. Using antibody blockade and genetic inactivation, they demonstrated that the collagen receptors α1β1 and α2β1 are critically involved in the course of cutaneous hypersensitivity, experimental arthritis and colitis by localizing T cells within the interstitium [46–48]. Furthermore, in two models of murine virus infection, the number of virus-specific CD8 memory T cells in the lung of infected animals could be reduced by anti-α1β1 administration without affecting T cell recruitment during primary infection [49,50•]. Therefore it is likely that α1β1 is needed for the long term retention of CD8 memory T cells in the lung.

Cell–cell interactions and activation of lymphocytes

The initiating step in all T-cell-dependent immune responses is the formation of an immunological synapse — the contact between an antigen-presenting cell (B cell or dendritic cell) and a T cell. A main functional constituent of the synapse is a sealing zone (the peripheral supramolecular activation cluster or pSMAC), which is defined and maintained by the interaction of LFA1 on the T cell with ICAM 1 on the antigen presenting cell.

Although early *in vitro* studies already suggested that β1 integrins have potent co-stimulatory functions, conditional knockout mice lacking β1 integrins on hematopoietic cells showed a relatively weak immunological phenotype: T-cell-dependent immune responses were grossly unaffected with the surprising exception that IgM production was severely decreased [15]. However, recent data suggest that members of the β1 integrin family might play a more subtle regulatory role during immune synapse formation. Mittelbrunn *et al.* showed that α4β1, like αLβ2, localizes within the pSMAC of synapses between T cells and dendritic cells/B cells. Furthermore, they could demonstrate that this interaction is important for shifting of the T cells towards a Th1-type cellular immune response [51••]. Another recent study showed that B cells utilize α4β1 to bind VCAM-1 co-expressed with antigen on the surface of fibroblasts *in vitro*, which might reflect B cell interaction with follicular dendritic cells in the lymph node [52,53•]. Moreover, it could be shown that this interaction synergizes with the B cell receptor signal and triggers B cell activation. It will be important to test if integrins assist T/B cell receptor signaling only indirectly, by establishing and maintaining

the cell–cell contact, or if active cross talk occurs between the signaling pathways triggered by both receptors.

Members of the β1 integrin subfamily as anti-inflammatory drug targets

Pharmacological interference with leukocyte extravasation is an attractive strategy for anti-inflammatory therapies that was sparked off by the discovery of the extravasation paradigm in the late 1980s. Table 1 lists some selected diseases where blockade of β1 integrins showed beneficial effects, together with a proposed mechanism of action. Although the intended therapeutic effect of most of these therapeutic approaches involves the inhibition of firm adhesion to the endothelium, it is not clear whether other processes, for example lymphocyte activation, could be affected as well. A prominent example of this uncertainty is autoimmune inflammation of the central nervous system. It is well established that the binding of lymphocytes to inflamed brain blood vessels during experimental autoimmune encephalomyelitis in rodents is inhibited by antibodies against α4β1 and that these antibodies prevent the development of the disease [16]. This therapeutic principle was used in a clinical trial to treat patients suffering from the equivalent human disease, multiple sclerosis [54]. Despite very promising results, approximately one out of thousand patients acquired a deadly opportunistic viral infection of the

CNS during chronic treatment [55]. These could have been caused either by impaired trafficking of non-pathogenic lymphocytes that are essential for normal CNS immunosurveillance or by a more general immunosuppression. Indeed it has been shown in rodent EAE that an anti-α4 antibody which does not inhibit lymphocyte homing *in vivo* still ameliorates EAE [56]. This argues in favor of an additional role for α4β1 apart from mediating extravasation. In this context the recent data suggesting a role for α4β1 in T cell activation are of special interest.

Conclusions

Advances in the field of intravital imaging make it now possible to track the dynamic behavior of cells in most tissues of living animals. In combination with genetic models where integrins are specifically deleted on defined blood cell lineages, this approach will allow the pinpointing of many of the cell biological roles of β1 integrins on hematopoietic cells. This knowledge will be decisive to predict side effects when pharmacological approaches are developed in which integrins are targeted in a non-cell-type-specific manner. Investigating cytoplasmic players involved in the activation of the β1 integrins will further teach us to what extent the signaling pathways are cell-type- and α-chain-specific and will eventually reveal new drug targets to inhibit extravasation in a more cell- and tissue-type-specific manner.

Table 1

Model system	Involved integrin dimer and mode of inhibition	Effects of integrin inhibition	Proposed mode of action	References
EAE, multiple sclerosis (Lewis rat, mouse, human)	α4β1 Anti-α4 mAb	Reduced clinical signs of disease, reduced inflammatory infiltrate	Blockade of firm adhesion to endothelium and thereby extravasation	[16,54,56]
Morbus Crohn (human)	α4 integrins Humanized anti-α4 mAb	Reduced clinical signs and lowered C-reactive protein levels	Not addressed, probably extravasation blockade	[68]
Arthritis (mouse)	α4β1 S18407: synthetic α4β1 inhibitor	Reduced clinical signs, reduced inflammatory infiltrate and mediators; bacterial clearance not affected.	Interference with neutrophil activation, cellular trafficking not severely affected	[69]
Hepatitis (mouse)	α1β1, α2β1 Anti-α1/α2 mAb, α1 deficiency	Reduced clinical signs, reduced inflammatory infiltrate	Unclear; either migration in tissue or activation of cells	[46]
	α4β1 Anti-α4 mAb, anti-VCAM-1 mAb	Reduced clinical signs of disease	Interference with α4β- mediated rolling, adhesion in sinusoids	[12•]
Peritonitis (mouse)	α4 integrins Y991A mutation in α4, blocks paxillin binding	Defective recruitment of lymphocytes and monocytes to the peritoneum	Probably extravasation blockade	[70]
Influenza (mouse)	α1β1 α1 deficiency; anti-α1 mAb	No inhibition of the recruitment to the lung during primary infection; reduced number of memory CD8+ T cells in the tissue and compromised secondary immunity	Inhibition of long term retention of CD8 memory T cells in the lung	[50•]
Colitis (mouse)	α1β1 α1 deficiency; anti-α1 mAb	Reduced clinical symptoms, reduced inflammatory infiltrate, decreased IFN-γ and TNF-α production	Reduced extravasation, migration or retention of monocytes; reduced cytokine production	[48]

CNS, central nervous system; EAE, experimental autoimmune encephalomyelitis; TNBS, 2, 4, 6-trinitrobenzene sulfonic acid.

Acknowledgements

References and recommended reading

• of special interest
•• of outstanding interest

1. Luster AD, Alon R, von Andrian UH: **Immune cell migration in inflammation: present and future therapeutic targets**. *Nat Immunol* 2005, **6**:1182-1190.

2. Ridley AJ, Schwartz MA, Burridge K, Firtel RA, Ginsberg MH, Borisy G, Parsons JT, Horwitz AR: **Cell migration: integrating signals from front to back**. *Science* 2003, **302**:1704-1709.

3. Hynes RO: **Integrins: bidirectional, allosteric signaling machines**. *Cell* 2002, **110**:673-687.

4. Dustin ML, Bivona TG, Philips MR: **Membranes as messengers in T cell adhesion signaling**. *Nat Immunol* 2004, **5**:363-372.

5. Berlin-Rufenach C, Otto F, Mathies M, Westermann J, Owen MJ, Hamann A, Hogg N: **Lymphocyte migration in lymphocyte function-associated antigen (LFA)-1-deficient mice**. *J Exp Med* 1999, **189**:1467-1478.

6. Scimone ML, Aifantis I, Apostolou I, von Boehmer H, von Andrian UH: **A multistep adhesion cascade for lymphoid progenitor cell homing to the thymus**. *Proc Natl Acad Sci USA* 2006, **103**:7006-7011.

7. Potocnik AJ, Brakebusch C, Fassler R: **Fetal and adult hematopoietic stem cells require β1 integrin function for colonizing fetal liver, spleen, and bone marrow**. *Immunity* 2000, **12**:653-663.

8. Priestley GV, Scott LM, Ulyanova T, Papayannopoulou T: **Lack of α4 integrin expression in stem cells restricts competitive function and self-renewal activity**. *Blood* 2006, **107**:2959-2967.

9. Mazo IB, Honczarenko M, Leung H, Cavanagh LL, Bonasio R, Weninger W, Engelke K, Xia L, McEver RP, Koni PA *et al.*: **Bone marrow is a major reservoir and site of recruitment for central memory CD8+ T cells**. *Immunity* 2005, **22**:259-270.

10. Issekutz AC, Issekutz TB: **The role of E-selectin, P-selectin, and very late activation antigen-4 in T lymphocyte migration to dermal inflammation**. *J Immunol* 2002, **168**:1934-1939.

11. Nandi A, Estess P, Siegelman M: **Bimolecular complex between rolling and firm adhesion receptors required for cell arrest; CD44 association with VLA-4 in T cell extravasation**. *Immunity* 2004, **20**:455-465.

12. Bonder CS, Norman MU, Swain MG, Zbytnuik LD, Yamanouchi J,
• Santamaria P, Ajuebor M, Salmi M, Jalkanen S, Kubes P: **Rules of recruitment for Th1 and Th2 lymphocytes in inflamed liver: a role for α-4 integrin and vascular adhesion protein-1**. *Immunity* 2005, **23**:153-163.
This paper shows that two types of T helper cells use entirely different mechanisms to extravasate into the same tissue.

13. Vajkoczy P, Laschinger M, Engelhardt B: **α4-integrin-VCAM-1 binding mediates G protein-independent capture of encephalitogenic T cell blasts to CNS white matter microvessels**. *J Clin Invest* 2001, **108**:557-565.

14. Kerfoot SM, Norman MU, Lapointe BM, Bonder CS, Zbytnuik L,
• Kubes P: **Reevaluation of P-Selectin and α4 Integrin as targets for the treatment of experimental autoimmune encephalomyelitis**. *J Immunol* 2006, **176**:6225-6234.
A critical reevaluation of receptor usage during lymphocyte infiltration into the CNS. It is suggested that previous antibody blocking studies might have over-estimated the effect of integrin blockade on extravasation and underestimated effects on T cell priming or CNS infiltration.

15. Brakebusch C, Fillatreau S, Potocnik AJ, Bungartz G, Wilhelm P, Svensson M, Kearney P, Korner H, Gray D, Fassler R: **β1 integrin is not essential for hematopoiesis but is necessary for the T cell-dependent IgM antibody response**. *Immunity* 2002, **16**:465-477.

16. Yednock TA, Cannon C, Fritz LC, Sanchez-Madrid F, Steinman L, Karin N: **Prevention of experimental autoimmune encephalomyelitis by antibodies against α4β1 integrin**. *Nature* 1992, **356**:63-66.

17. Hirsch E, Iglesias A, Potocnik AJ, Hartmann U, Fassler R: **Impaired migration but not differentiation of haematopoietic stem cells in the absence of β1 integrins**. *Nature* 1996, **380**:171-175.

18. Taooka Y, Chen J, Yednock T, Sheppard D: **The integrin α9β1 mediates adhesion to activated endothelial cells and transendothelial neutrophil migration through interaction with vascular cell adhesion molecule-1**. *J Cell Biol* 1999, **145**:413-420.

19. Liu S, Slepak M, Ginsberg MH: **Binding of paxillin to the α9 integrin cytoplasmic domain inhibits cell spreading**. *J Biol Chem* 2001, **276**:37086-37092.

20. Barreiro O, Yanez-Mo M, Serrador JM, Montoya MC, Vicente-Manzanares M, Tejedor R, Furthmayr H, Sanchez-Madrid F: **Dynamic interaction of VCAM-1 and ICAM-1 with moesin and ezrin in a novel endothelial docking structure for adherent leukocytes**. *J Cell Biol* 2002, **157**:1233-1245.

21. Carman CV, Springer TA: **A transmigratory cup in leukocyte diapedesis both through individual vascular endothelial cells and between them**. *J Cell Biol* 2004, **167**:377-388.

22. Timpl R: **Macromolecular organization of basement membranes**. *Curr Opin Cell Biol* 1996, **8**:618-624.

23. Sixt M, Hallmann R, Wendler O, Scharffetter-Kochanek K, Sorokin LM: **Cell adhesion and migration properties of β2-integrin negative polymorphonuclear granulocytes on defined extracellular matrix molecules. Relevance for leukocyte extravasation**. *J Biol Chem* 2001, **276**:18878-18887.

24. Thompson RD, Noble KE, Larbi KY, Dewar A, Duncan GS, Mak TW, Nourshargh S: **Platelet-endothelial cell adhesion molecule-1 (PECAM-1)-deficient mice demonstrate a transient and cytokine-specific role for PECAM-1 in leukocyte migration through the perivascular basement membrane**. *Blood* 2001, **97**:1854-1860.

25. Dangerfield J, Larbi KY, Huang MT, Dewar A, Nourshargh S: **PECAM-1 (CD31) homophilic interaction up-regulates α6β1 on transmigrated neutrophils *in vivo* and plays a functional role in the ability of α6 integrins to mediate leukocyte migration through the perivascular basement membrane**. *J Exp Med* 2002, **196**:1201-1211.

26. Dangerfield JP, Wang S, Nourshargh S: **Blockade of α6 integrin inhibits IL-1β- but not TNF-α-induced neutrophil transmigration *in vivo***. *J Leukoc Biol* 2005, **77**:159-165.

27. Qian H, Tryggvason K, Jacobsen SE, Ekblom M: **Contribution of α6 integrins to hematopoietic stem and progenitor cell homing to bone marrow and collaboration with α4 integrins**. *Blood* 2006, **107**:3503-3510.

28. Hallmann R, Horn N, Selg M, Wendler O, Pausch F, Sorokin LM: **Expression and function of laminins in the embryonic and mature vasculature**. *Physiol Rev* 2005, **85**:979-1000.

29. Price AA, Cumberbatch M, Kimber I, Ager A: **α6 integrins are required for Langerhans cell migration from the epidermis**. *J Exp Med* 1997, **186**:1725-1735.

30. Ratzinger G, Stoitzner P, Ebner S, Lutz MB, Layton GT, Rainer C, Senior RM, Shipley JM, Fritsch P, Schuler G *et al.*: **Matrix metalloproteinases 9 and 2 are necessary for the migration of Langerhans cells and dermal dendritic cells from human and murine skin**. *J Immunol* 2002, **168**:4361-4371.

31. Graesser D, Mahooti S, Haas T, Davis S, Clark RB, Madri JA: **The interrelationship of α4 integrin and matrix metalloproteinase-2 in the pathogenesis of experimental autoimmune encephalomyelitis**. *Lab Invest* 1998, **78**:1445-1458.

32. Segarra M, Vilardell C, Matsumoto K, Esparza J, Lozano E, Serra-Pages C, Urbano-Marquez A, Yamada KM, Cid MC: **Dual function of focal adhesion kinase in regulating integrin-induced MMP-2 and MMP-9 release by human T lymphoid cells**. *FASEB J* 2005, **19**:1875-1877.

33. Werr J, Xie X, Hedqvist P, Ruoslahti E, Lindbom L: **β1 integrins are critically involved in neutrophil locomotion in extravascular tissue *In vivo***. *J Exp Med* 1998, **187**:2091-2096.

34. Werr J, Johansson J, Eriksson EE, Hedqvist P, Ruoslahti E, Lindbom L: **Integrin α2β1 (VLA-2) is a principal receptor used by neutrophils for locomotion in extravascular tissue**. *Blood* 2000, **95**:1804-1809.

35. Lundberg S, Lindholm J, Lindbom L, Hellstrom PM, Werr J: **Integrin α2β1 regulates neutrophil recruitment and inflammatory activity in experimental colitis in mice**. *Inflamm Bowel Dis* 2006, **12**:172-177.

36. Friedl P, Entschladen F, Conrad C, Niggemann B, Zanker KS: **CD4+ T lymphocytes migrating in three-dimensional collagen lattices lack focal adhesions and utilize β1 integrin-independent strategies for polarization, interaction with collagen fibers and locomotion**. *Eur J Immunol* 1998, **28**:2331-2343.

37. Wolf K, Muller R, Borgmann S, Brocker EB, Friedl P: **Amoeboid shape change and contact guidance: T-lymphocyte crawling through fibrillar collagen is independent of matrix remodeling by MMPs and other proteases**. *Blood* 2003, **102**:3262-3269.

38. Franitza S, Alon R, Lider O: **Real-time analysis of integrin-mediated chemotactic migration of T lymphocytes within 3-D extracellular matrix-like gels**. *J Immunol Methods* 1999, **225**:9-25.

39. Malawista SE, de Boisfleury Chevance A: **Random locomotion and chemotaxis of human blood polymorphonuclear leukocytes (PMN) in the presence of EDTA: PMN in close quarters require neither leukocyte integrins nor external divalent cations**. *Proc Natl Acad Sci USA* 1997, **94**:11577-11582.

40. Qin G, Ii M, Silver M, Wecker A, Bord E, Ma H, Gavin M, Goukassian DA, Yoon YS, Papayannopoulou T *et al.*: **Functional disruption of α4 integrin mobilizes bone marrow-derived endothelial progenitors and augments ischemic neovascularization**. *J Exp Med* 2006, **203**:153-163.

41. Papayannopoulou T, Priestley GV, Nakamoto B, Zafiropoulos V, Scott LM, Harlan JM: **Synergistic mobilization of hemopoietic progenitor cells using concurrent β1 and β2 integrin blockade or β2-deficient mice**. *Blood* 2001, **97**:1282-1288.

42. Leuker CE, Labow M, Muller W, Wagner N: **Neonatally induced inactivation of the vascular cell adhesion molecule 1 gene impairs B cell localization and T-cell-dependent humoral immune response**. *J Exp Med* 2001, **193**:755-768.

43. Glodek AM, Honczarenko M, Le Y, Campbell JJ, Silberstein LE: **Sustained activation of cell adhesion is a differentially regulated process in B lymphopoiesis**. *J Exp Med* 2003, **197**:461-473.

44. Lu TT, Cyster JG: **Integrin-mediated long-term B cell retention in the splenic marginal zone**. *Science* 2002, **297**:409-412.

45. Rubtsov A, Strauch P, Digiacomo A, Hu J, Pelanda R, Torres RM:
• **Lsc regulates marginal-zone B cell migration and adhesion and is required for the IgM T-dependent antibody response**. *Immunity* 2005, **23**:527-538.
This study shows that in the absence of the exchange factor lsc, marginal zone B cells are locked in their niche as a result of their inability to detach from the integrin ligands.

46. de Fougerolles AR, Sprague AG, Nickerson-Nutter CL, Chi-Rosso G, Rennert PD, Gardner H, Gotwals PJ, Lobb RR, Koteliansky VE: **Regulation of inflammation by collagen-binding integrins α1β1 and α2β1 in models of hypersensitivity and arthritis**. *J Clin Invest* 2000, **105**:721-729.

47. Krieglstein CF, Cerwinka WH, Sprague AG, Laroux FS, Grisham MB, Koteliansky VE, Senninger N, Granger DN, de Fougerolles AR: **Collagen-binding integrin α1β1 regulates intestinal inflammation in experimental colitis**. *J Clin Invest* 2002, **110**:1773-1782.

48. Fiorucci S, Mencarelli A, Palazzetti B, Sprague AG, Distrutti E, Morelli A, Novobrantseva TI, Cirino G, Koteliansky VE, de Fougerolles AR: **Importance of innate immunity and collagen binding integrin α1β1 in TNBS-induced colitis**. *Immunity* 2002, **17**:769-780.

49. Andreasen SO, Thomsen AR, Koteliansky VE, Novobrantseva TI, Sprague AG, de Fougerolles AR, Christensen JP: **Expression and functional importance of collagen-binding integrins, α1β1 and α2β1, on virus-activated T cells**. *J Immunol* 2003, **171**:2804-2811.

50. Ray SJ, Franki SN, Pierce RH, Dimitrova S, Koteliansky V,
• Sprague AG, Doherty PC, de Fougerolles AR, Topham DJ: **The collagen binding α1β1 integrin VLA-1 regulates CD8 T cell-mediated immune protection against heterologous influenza infection**. *Immunity* 2004, **20**:167-179.
The latest of a series of studies demonstrating that α1 and α2β1 integrins are decisive for leukocyte positioning within the tissue during inflammatory responses.

51. Mittelbrunn M, Molina A, Escribese MM, Yanez-Mo M, Escudero E,
•• Ursa A, Tejedor R, Mampaso F, Sanchez-Madrid F: **VLA-4 integrin concentrates at the peripheral supramolecular activation complex of the immune synapse and drives T helper 1 responses**. *Proc Natl Acad Sci USA* 2004, **101**:11058-11063.
The first *in vivo* evidence that β1 integrins are involved in the priming of naïve T cells.

52. Fleire SJ, Goldman JP, Carrasco YR, Weber M, Bray D, Batista FD: **B cell ligand discrimination through a spreading and contraction response**. *Science* 2006, **312**:738-741.

53. Carrasco YR, Batista FD: **B-cell activation by membrane-bound
• antigens is facilitated by the interaction of VLA-4 with VCAM-1**. *EMBO J* 2006, **25**:889-899.
This study shows how β 1 integrins assist B cell activation by establishing a synapse between the antigen-carrying cell and the B cell that is equivalent to the immunological synapse seen between antigen-presenting cells and T cells.

54. Polman CH, O'Connor PW, Havrdova E, Hutchinson M, Kappos L, Miller DH, Phillips JT, Lublin FD, Giovannoni G, Wajgt A *et al.*: **A randomized, placebo-controlled trial of natalizumab for relapsing multiple sclerosis**. *N Engl J Med* 2006, **354**:899-910.

55. Langer-Gould A, Atlas SW, Green AJ, Bollen AW, Pelletier D: **Progressive multifocal leukoencephalopathy in a patient treated with natalizumab**. *N Engl J Med* 2005, **353**:375-381.

56. Engelhardt B, Laschinger M, Schulz M, Samulowitz U, Vestweber D, Hoch G: **The development of experimental autoimmune encephalomyelitis in the mouse requires α4-integrin but not α4β7-integrin**. *J Clin Invest* 1998, **102**:2096-2105.

57. McLeod SJ, Shum AJ, Lee RL, Takei F, Gold MR: **The Rap GTPases regulate integrin-mediated adhesion, cell spreading, actin polymerization, and Pyk2 tyrosine phosphorylation in B lymphocytes**. *J Biol Chem* 2004, **279**:12009-12019.

58. Shimonaka M, Katagiri K, Nakayama T, Fujita N, Tsuruo T, Yoshie O, Kinashi T: **Rap1 translates chemokine signals to integrin activation, cell polarization, and motility across vascular endothelium under flow**. *J Cell Biol* 2003, **161**:417-427.

59. Sebzda E, Bracke M, Tugal T, Hogg N, Cantrell DA: **Rap1A positively regulates T cells via integrin activation rather than inhibiting lymphocyte signaling**. *Nat Immunol* 2002, **3**:251-258.

60. Duchniewicz M, Zemojtel T, Kolanczyk M, Grossmann S, Scheele JS, Zwartkruis FJ: **Rap1A-deficient T and B cells show impaired integrin-mediated cell adhesion**. *Mol Cell Biol* 2006, **26**:643-653.

61. Medeiros RB, Dickey DM, Chung H, Quale AC, Nagarajan LR, Billadeau DD, Shimizu Y: **Protein kinase D1 and the β1 integrin cytoplasmic domain control β1 integrin function via regulation of Rap1 activation**. *Immunity* 2005, **23**:213-226.

62. Bivona TG, Wiener HH, Ahearn IM, Silletti J, Chiu VK, Philips MR: **Rap1 up-regulation and activation on plasma membrane regulates T cell adhesion**. *J Cell Biol* 2004, **164**:461-470.

63. Katagiri K, Maeda A, Shimonaka M, Kinashi T: **RAPL, a Rap1-binding molecule that mediates Rap1-induced adhesion**

through spatial regulation of LFA-1. *Nat Immunol* 2003, **4**:741-748.

64. Lafuente EM, van Puijenbroek AA, Krause M, Carman CV, Freeman GJ, Berezovskaya A, Constantine E, Springer TA, Gertler FB, Boussiotis VA: **RIAM, an Ena/VASP and Profilin ligand, interacts with Rap1-GTP and mediates Rap1-induced adhesion**. *Dev Cell* 2004, **7**:585-595.

65. Tadokoro S, Shattil SJ, Eto K, Tai V, Liddington RC, de Pereda JM, Ginsberg MH, Calderwood DA: **Talin binding to integrin β tails: a final common step in integrin activation**. *Science* 2003, **302**:103-106.

66. Czuchra A, Meyer H, Legate K, Brakebusch C, Fassler R: **Genetic analysis of β1 integrin activation motivs in mice.** *J Biol Cell* 2006. in press.

67. Chen H, Zou Z, Sarratt KL, Zhou D, Zhang M, Sebzda E, Hammer DA, Kahn ML: *In vivo* **β1 integrin function requires**

phosphorylation-independent regulation by cytoplasmic tyrosines. *Genes Dev* 2006, **20**:927-932.

68. Ghosh S, Goldin E, Gordon FH, Malchow HA, Rask-Madsen J, Rutgeerts P, Vyhnalek P, Zadorova Z, Palmer T, Donoghue S: **Natalizumab for active Crohn's disease**. *N Engl J Med* 2003, **348**:24-32.

69. Glasner J, Blum H, Wehner V, Stilz HU, Humphries JD, Curley GP, Mould AP, Humphries MJ, Hallmann R, Rollinghoff M *et al.*: **A small molecule α4β1 antagonist prevents development of murine Lyme arthritis without affecting protective immunity**. *J Immunol* 2005, **175**:4724-4734.

70. Feral CC, Rose DM, Han J, Fox N, Silverman GJ, Kaushansky K, Ginsberg MH: **Blocking the α4 integrin-paxillin interaction selectively impairs mononuclear leukocyte recruitment to an inflammatory site**. *J Clin Invest* 2006, **116**:715-723.

Paper III

Review

The extracellular matrix of the spleen as a potential organizer of immune cell compartments

Zerina Lokmic [a,1], Tim Lämmermann [b,1], Michael Sixt [b], Susanna Cardell [c],
Rupert Hallmann [a], Lydia Sorokin [a,*]

[a] *Physiological Chemistry and Pathobiochemistry, Muenster University, Waldeyerstrasse 15,
48149 Muenster, Germany*
[b] *Max-Planck Institute for Biochemistry, Martinsried, Munich, Germany*
[c] *Immunology Department, Gothenburg University, Gothenburg, Sweden*

Abstract

Until recently little information was available on the molecular details of the extracellular matrix (ECM) of secondary lymphoid tissues. There is now growing evidence that these ECMs are unique structures, combining characteristics of basement membranes and interstitial or fibrillar matrices, resulting in scaffolds that are strong and highly flexible and, in certain secondary lymphoid compartments, also forming conduit networks for rapid fluid transport. This review will address the structural characteristics of the ECM of the murine spleen and its potential role as an organizer of immune cell compartments, with reference to the lymph node where relevant.
© 2007 Elsevier Ltd. All rights reserved.

Keywords: Extracellular matrix; Spleen; Reticular fibres

1. Introduction

Cellular compartmentalisation within secondary lymphoid organs is essential for normal immune function. Over the past years, the complex relationship between cell–cell adhesion molecules, cytokines and chemotactic factors involved in the maintenance of immune cell compartments within lymph nodes and the spleen has started to be elucidated [1–3]. Only recently, however, has attention turned to stromal cells, the cellular part of the non-hematopoietic scaffold, and their impact on establishing the milieu in which immune reactions take place. Even though the acellular component of this scaffold, the reticular fibre network, has long been recognised to form the backbone of secondary lymphoid organs, relatively little is know of this acellular compartment and whether it does more than support the fibroblastic reticular cells of secondary lymphoid organs.

Historically, electron microscopic studies have been employed to decipher the nature of the extracellular matrix (ECM) of secondary lymphoid tissues, revealing the reticular fibre network or "reticulum" [4], but details on molecular composition remained sparse not only due to the strong focus on immunology and cellular composition of secondary lymphoid tissues, but also due to the absence of specific tools for the detection of defined ECM molecules. Several isolated studies on the spleen demonstrated the presence of both interstitial matrix molecules (collagen types I, II and III, fibronectin, tenascin-C) and basement membrane components (laminins, collagen type IV, heparan sulfate proteoglycans, nidogen) (summarised in Table 1). However, the generic nature of these studies together with the species differences observed in spleen architecture [5,6] has made it difficult to draw conclusions apart from the presence or absence of defined molecules in certain sites. It is only recently, as a consequence of systematic analyses of the localisation of defined basement membrane versus interstitial matrix molecules with respect to immune cell populations, that the existence of distinct matrices associated with different immune cell compartments has become apparent [7]. This review gives an overview on how the differential expression of ECM molecules defines lymphoid compartments, with focus on the spleen, and will provide a framework for future studies

---

* Corresponding author. Tel.: +49 251 83 55581; fax: +49 251 83 55596.
E-mail address: sorokin@uni-muenster.de (L. Sorokin).
[1] Equal contributors.

Table 1
Summary of studies performed on extracellular matrix molecules expressed in the spleen

ECM type	ECM molecule	Mouse	Rat	Human	Guinea fowl
Interstitial matrix	Collagen I	[38]		[33]	[77]
	Collagen II			[78]	
	Collagen III			[33,79]	[77]
	Fibronectin	[50]		[33]	[77]
	Tenascin	[46,51]		[79]	[77]
	Vitronectin			[33]	
Basement membrane	Laminins	[42,48,80]	[80]	[7,33,79]	[77]
	Collagen IV			[7,33,60,79]	
	Perlecan			[81]	
	Heparan sulfates	[49]	[49]		
	Hyaluronan			[82]	

elucidating the influence of the non-immunological scaffold on immune cell function.

2. Extracellular matrices

Two structurally and functionally distinct extracellular matrices can be distinguished in most tissues, the loose connective tissue of the interstitial matrix and the thin sheet-like structure of the basement membrane. The interstitial matrix represents a network that loosely connects mesenchymal cells or fibroblasts and is typically composed of the fibrillar-forming collagens (such as collagen types I, II, III, V and XI), which convey great flexibility and tensile strength to these matrices, plus non-collagenous glycoproteins (such as tenascin, fibronectin, vitronectin, chondroitin-, dermatan-, keratan-sulfate proteoglycans), which are highly charged molecules with a high capacity for intermolecular interactions not only with other ECM molecules but also with growth factors and cytokines [8–11]. Specialised interstitial matrix molecules associated with highly elastic tissues include the microfibrillar proteins, such as fibrillin 1 and 2, and elastin. In contrast, basement membranes are highly interconnected glycoprotein networks that act principally to separate tissue compartments. They consist of a scaffold of collagen type IV that is interconnected to a laminin network via molecules such as the heparan sulfate proteoglycan, perlecan, and the nidogens. Apart from these four main components, molecules such as agrin, fibulin-1 and -2, BM-40/osteonectin/SPARC, collagen types VII, VIII, XV and XVIII are minor components of some basement membranes, which nevertheless have distinct functional roles [12].

Laminins, heterotrimeric glycoproteins composed of α, β, and γ chains, are considered to represent the biologically active component of basement membranes, with the α chains carrying distinct cell binding sites that signal specific information to different cell types that controls their growth, migration and differentiation. To date 5α, 4β and 3γ laminin chains have been identified that may combine to form at least 16 different isoforms [13] that are named according to their αβγ chain composition. For example, laminin 111 is composed of laminin α1, β1 and γ1 chains [14]. The major receptors for the laminins include β1 and β3 integrins, and α-dystroglycan of the dystrophin-glycoprotein complex (as reviewed by [15]), all of which interact only with

laminin α chains. Apart from direct signalling to cells via such receptors, laminins and other basement membrane components, in particular the highly charged heparan sulfate proteoglycans, perlecan and agrin, can also function as storage sites for growth factors and cytokines as described for the interstitial matrix glycoproteins above.

Reticular fibres have long been known as argyrophilic structures that are highlighted by silver staining and commonly found in parenchymal tissues such as the liver, bone marrow, lung and kidney, typically underlying epithelia or covering the surface of muscle, adipose and Schwann cells [4,16,17]. Ultrastructurally, these fibres consist of both basement membrane and interstitial matrix components [4,18,19]. Particularly prominent reticular fibres occur in secondary lymphoid organs where, because of their fluid draining function (described below), they have also been termed "conduits". Conduits in this context are, therefore, reticular fibres with an unusually large diameter (1–2 μm), characterised by an outer basement membrane layer, and a central fibrillar collagen core as a defined substructure. In the following paragraph, we describe the ECM of the spleen, which is particular due to the heterogenity of molecularly distinct reticular fibres that define different lymphoid compartments.

3. Types of ECM in the spleen

The main splenic structures that contain ECM components are the capsule, trabecules, vascular walls and reticular fibres. A dense connective tissue layer of fibrillar collagen, a typical interstitial matrix, and elastic fibres surround the spleen and encapsulate trabecules and incoming arteries. The functional compartments of the spleen are the white pulp and red pulp which are connected by the marginal zone. Endothelial cell basement membranes are found in the vascular walls of the central artery and branching capillaries of the white pulp, as well as in the venous sinuses of the red pulp. In addition, the endothelial cell basement membrane of the marginal sinus, underlying the marginal zone, shows unique characteristics that are discussed below. Apart from their identification by the immune cells residing in these niches, each of the three splenic compartments – white pulp, red pulp and marginal zone – can also be distinguished by the organization and composition of the basement membrane of the reticular fibre network. This becomes appar-
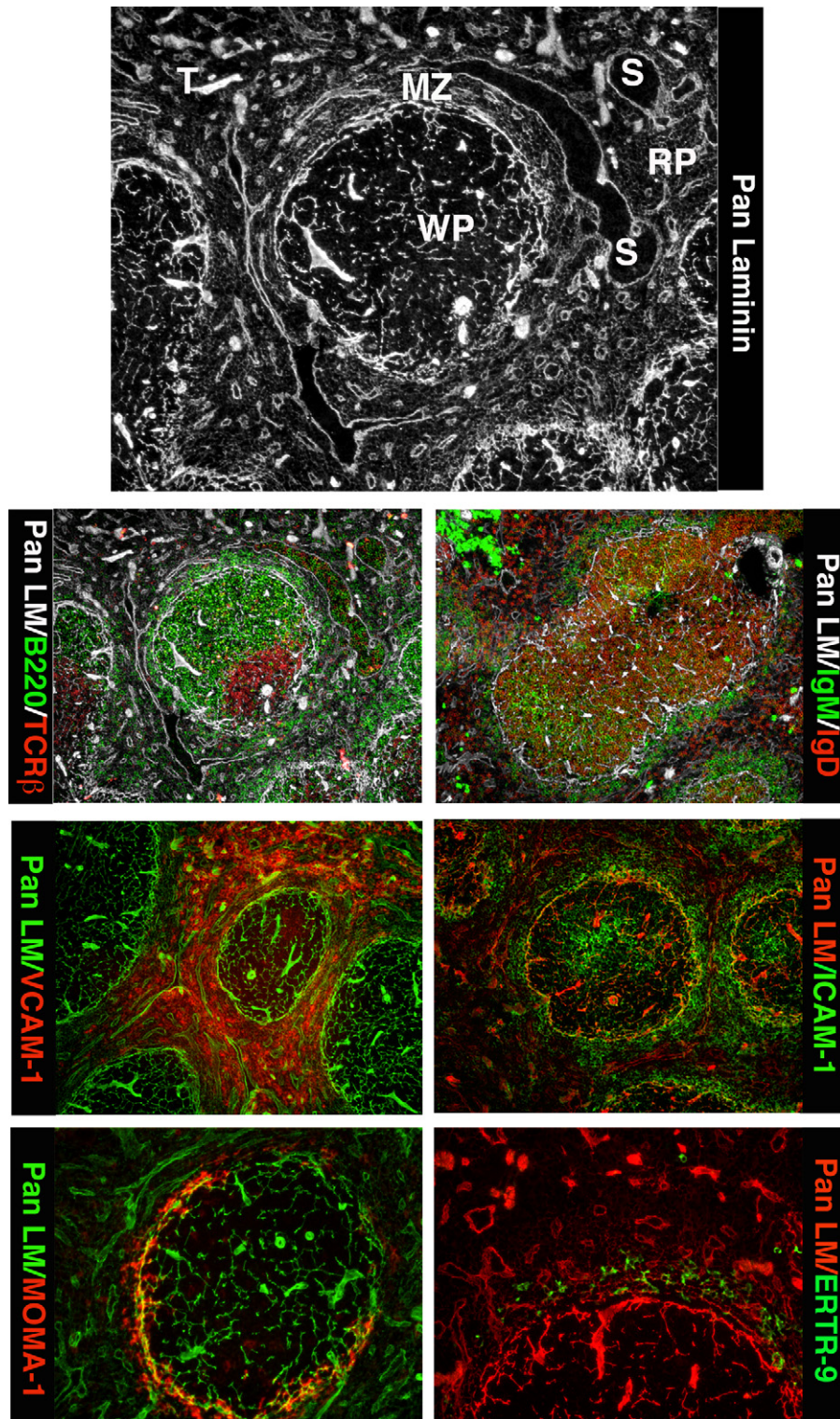
Fig. 1. Pan-laminin immunofluorescence (Pan LM) staining of adult murine spleen in combination with markers of specific immune cell compartments, including B220 for B cells, T cell receptor β (TCRβ) for T cells, IgM/IgD to distinguish MZ B cells (IgM^{high}/IgD^{low}) from follicular B cells (IgM^{low}/IgD^{high}), VCAM-1 and ICAM-1 as markers of stromal cell compartments, MOMA-1 as a marker of the metallophilic sinus-lining macrophages, and ERTR-9 as a marker of marginal zone macrophages. The sinus-lining basement membrane appears as quasi-continuous pan-laminin staining surrounding the white pulp. MZ is marginal zone; WP is white pulp; RP is red pulp; S is venous sinus, T is trabeculae.

	Fibre diameter	Collagen core	Microfibril layer	Basement membrane	Fibroblastic reticular cell
LN	1-2μm	Coll I/III	ERTR-7	LM 511/411/332	gp38, αSM, Des
Spleen WP/PALS	1-2μm	Coll I/III	ERTR-7	LM 511/411/332	gp38, αSM, Des
WP/B cell	1-2μm	Coll I	-	LM 511/411/211	αSM, Des
MZ	<1μm	-	ERTR-7	LM 521/ Agrin	Des
RP	30-50nm	-	ERTR-7	LM ?	gp38, Des

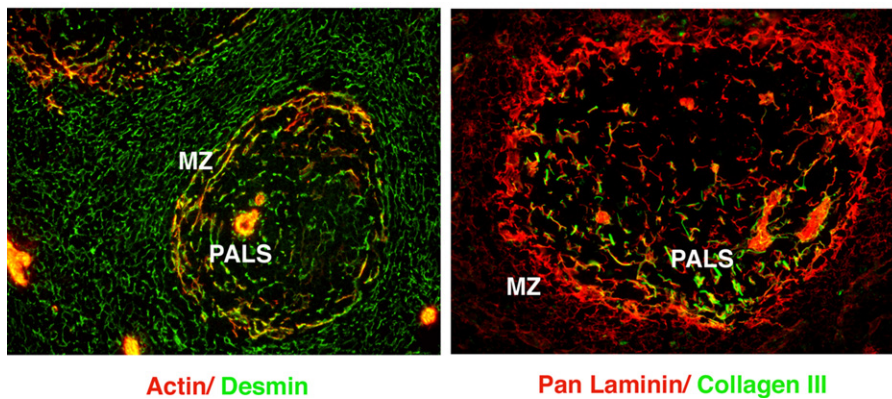**Actin/ Desmin**   **Pan Laminin/ Collagen III**

Fig. 2. Schematic representation of the typical structure of a reticular fibre found in the lymph node. Table lists significant differences between reticular fibre networks found in lymph nodes and at different sites in the spleen. In addition to the molecules listed, in all tissues the microfibrillar layer also contains collagen type VI and fibrillins 1 and/or 2, while the basement membrane layer contains collagen type IV, perlecan and nidogens 1 and/or 2. Immunofluorescence images illustrate examples of molecular differences in reticular fibre networks in the spleen. PALS is periarterial lymphoid sheath; MZ is marginal zone.

ent by staining of adult murine spleen sections with antibodies specific for one of the major basement membrane components, such as pan-laminin antibody. Even at low magnifications, the splenic compartmentalisation is evident: The white pulp, delineated by the quasi-continuous marginal sinus-lining basement membrane, contains a network of larger diameter reticular fibres that show wider spacing compared to the filigran, dense reticular fibre network of the marginal zone and red pulp (Fig. 1). Co-staining for basement membranes and markers of B- and T-lymphocytes, and/or macrophage populations specific for the marginal zone and marginal sinus demonstrates a correlation between localisation of immune cells and distinct ECM compartments (Fig. 1), which are explained in detail below.

3.1. White pulp reticular networks (conduits)

The reticular fibres of the T cell area of the splenic white pulp, the periarteriolar lymphoid sheath (PALS), closely resemble the well-described reticular fibres of the T cell cortex of lymph node (Fig. 2). The basement membrane layer of these reticular fibres is characterised by the presence of laminin isoforms 511, 411 and 332, the heparan sulfate proteoglycan, perlecan, collagen type IV and nidogen 1, while the fibrillar core typically contains collagen types I [20–22] and III [23,24]. These two distinct ECM layers are interconnected by a microfibrillar layer [19,25] characterised by fibrillin 1 and/or fibrillin 2, collagen type VI and, the yet to be defined, ER-TR7 antigen [20,23] (Fig. 2). The entire ECM core is largely ensheathed by reticular fibroblasts that may interdigitate with other cells types, such as dendritic cells as has been shown in the lymph node [20], but also remains naked in certain regions [26].

Although the overall multilayered structure is similar, the reticular fibres of the lymphoid follicle (B cell area) of the white pulp have several unique characteristics that distinguish them from reticular fibres of lymph nodes and PALS. Most notably they show little or no ERTR-7 antigen expression and they lack collagen type III in their core; apart from the characteristic laminins 511 and 411 in the basement membrane layer they also express laminin 211 and not laminin 332 found in the PALS and lymph nodes (Fig. 2) (manuscript in preparation).

The differential expression of collagen types I and III in the reticular fibre core is likely to control fibre diameter, and strength and flexibility of the network. While collagen type I fibrils can form long-range, highly stable structures, the inclusion of collagen type III into these fibrils confers increased elasticity and is associated with reduced fibril diameter [16,17,27]. Collagen type VI, found in the microfibrillar mantle, is a short-chained collagen that forms filamentous networks commonly found in elastic tissues [28,29]. Collagen type VI and the fibrillins have been postulated to interact with both basement membrane and interstitial matrix components and thereby probably form an elastic link between the collagen core and the outer basement membrane of the reticular fibre [30].

The outer basement membrane is most likely to act as an adhesive substrate for the ensheathing fibroblastic reticular cells. Why different laminin isoforms occur in this basement membrane in different reticular fibres is not clear, but several possibilities exist. Laminins 511, 211, 411 and 332 are not only biochemically distinct molecules but are also structurally distinct, as shown by rotary shadowing [15]. This results in large variations in their abilities to form interactions both within a laminin network and with other basement membrane components [15,31], which may influence the tightness of the barrier formed by the basement membrane and thereby influence the conduit function of reticular fibre networks. In addition, these different laminin isoforms impart different cellular signals via several receptors, many of which have been identified on fibroblastic reticular cells [32,33], that control cell growth, differentiation and migration [13,31]. The laminin composition of the basement membrane underlying the fibroblastic reticular cells may, therefore, influence their differentiation state and/or the expression of defined marker molecules, contributing to the observed heterogeneity of this cell population (reviewed in Allen and Cyster, this volume; [34–36].

Basement membranes normally restrict the movement of large (>70 kDa) and positively charged molecules. This selective barrier to soluble molecules both into and out of the reticular fibre contributes to the fluid-conduction or so-called conduit function that has been demonstrated for reticular fibres of lymph nodes [20–22,37]. Tracer injection experiments in mice [38] have revealed that low molecular weight tracers accumulate in the core of reticular fibres of the B cell area of the splenic white pulp in a similar manner as has been described for the lymph node [20,37], suggesting that it may also provide a fluid transport mechanism. In the lymph node this conduit system has been shown to be connected to the afferent lymphatics and to transport both chemokines (CCL21, CCL19) and small molecular weight antigens [21,22,37] from peripheral sites of inflammation to the high endothelial cell venules (HEVs). Resident dendritic cells which interdigitate with the reticular fibroblasts within T cell areas of lymph nodes are capable of taking up antigen from the core of the conduit, presumably for the presentation to local T cells although this has not yet been conclusively demonstrated [20]. Unlike the lymph node, the splenic conduit system is not connected to an afferent lymphatic system. Rather, there is most likely a tight connection between the vascular system and the conduit system. The central collagen core of the white pulp reticular fibre emerges from the interstitial matrix of the trabecular arteries (unpublished observation). Time course tracer experiments have shown that small molecular weight tracers (<70 kDa) arriving in the bloodstream are deposited in the marginal zone and move rapidly to the red pulp. A small proportion of the incoming tracer, however, moves from the marginal zone in the direction of the center of the follicle within the reticular fibre, where it colocalises with chemokines such as CXCL13 (in the B cell area) and CCL21 (in the PALS) in the conduit core [38]. The white pulp reticular fibre network may, therefore, provide a means of transport of blood borne factors from the blood stream which may influence immune interactions in the lymphoid follicles.

Apart from the conduit function, the reticular fibre network of the lymph node has recently been shown to provide a scaffold which supports the migration of naive T cells and B cells between the afferent lymphatics and HEVs and border of the B cell areas [39]. It is unlikely that the ECM of the reticular fibre network plays a role in this migration process, rather that lymphocytes migrate on the fibroblastic reticular cell layer, which in turn is anchored to the ECM scaffold. The reticular fibroblasts that enfold the splenic conduit fibres have been suggested to bind and present chemokines in the PALS (CCL21) and in the lymphoid follicles (CXCL13) [38], consistent with a role in migration of lymphocytes. As the white pulp reticular fibre network interconnects the marginal sinus with the white pulp and PALS, and the outer sheath of the central artery [18,38] it is possible that, as in lymph node, it provides a route for lymphocytes moving either into or out of the white pulp.

3.2. Red pulp reticular networks

Within the spleen, the reticular fibre network of the red pulp differs from that of the white pulp in several ways: reticular fibres of the red pulp have a considerably smaller diameter (30–50 nm) than those of the white pulp (1–2 μm) [4,40] and they lack the characteristic pronounced fibrillar collagen core (Fig. 2). Rather, the red pulp reticular fibre network consists of a typical basement membrane component (containing collagen type IV, perlecan, nidogen 1 and an as yet undefined laminin isoform), plus an extensive microfibrillar layer containing ERTR-7 antigen, collagen type VI and fibrillin 2 (Fig. 2) (manuscript in preparation). The spatial organization of these two ECM layers to each other and to the stromal cells of red pulp is not clear, due to the absence of appropriate electron microscopic studies. Apart from its function in the retention of aging erythrocytes, the dense red pulp fibre network may provide the stable backbone for red pulp macrophages and other red pulp stromal cells. Its impact on proliferation and differentiation of these cells as well as its direct influence on recirculating lymphocytes remains to be elucidated.

3.3. Marginal sinus and marginal zone reticular networks

The marginal zone is described as a layer surrounding the B cell follicles, with the marginal sinus facing to the WP
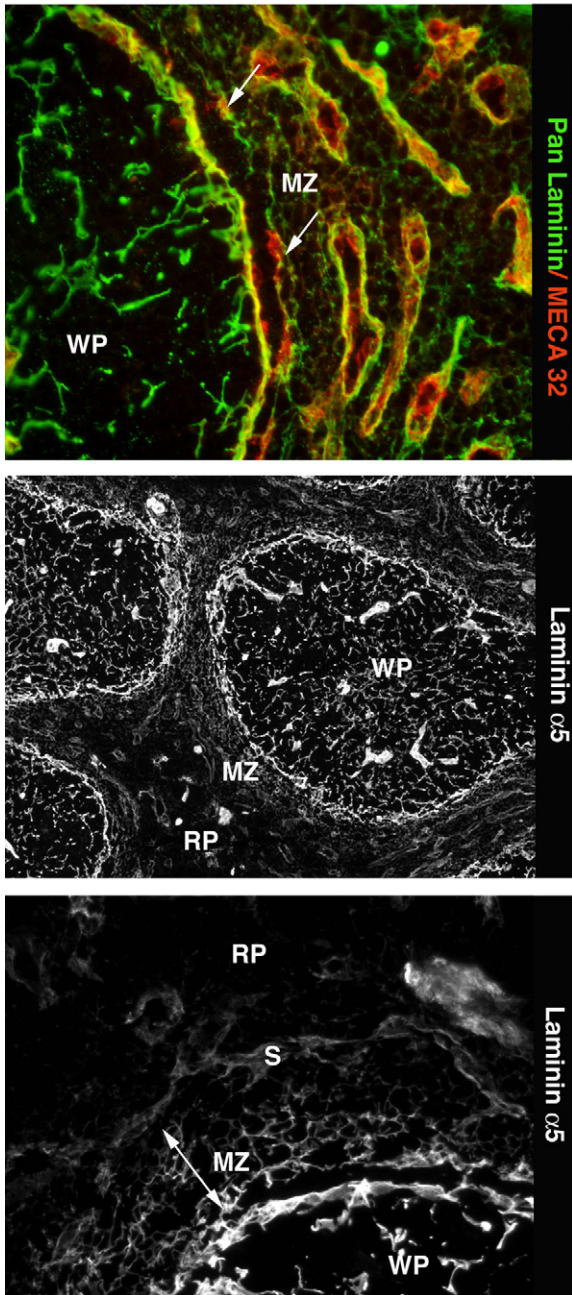
Fig. 3. Immunofluorescence staining for pan-laminin and the endothelial cell marker, MECA-32, showing the sinus-lining basement membrane delineating the border to the white pulp and an outer basement membrane underlying the MECA-32+ endothelial cells of the marginal sinus (marked with arrows). Black and white images illustrate laminin α5 immunofluorescence staining which occurs predominantly in the reticular fibre network of the white pulp and in a diffuse manner in the surrounding marginal zone. The higher magnification image shows the staining of laminin α5 in the marginal zone but not red pulp stroma. Basement membranes of the venous sinus in the red pulp also contain laminin α5. The gap between sinus-lining basement membrane and marginal zone is the outer basement membrane of the marginal sinus vessels as also seen in the uppermost panel.

defining its innermost border and the RP its outermost border and is the only B cell-dependent area in the body where B lymphocytes are not organized in a follicular structure (Figs. 1 and 3).

3.4. Marginal sinus

In the spleen all incoming cells arrive via the central artery. The capillaries of splenic follicles are branches of the central artery in the white pulp that anastomose to form a vascular net covering the white pulp and terminate in the marginal sinus. The contents of the marginal sinus pass into the marginal zone, while the flat sinus-lining reticular fibroblasts characterised by expression of the mucosal addressin cell adhesion molecule (MAdCAM) [41] and the Ig superfamily adhesion molecule member, L1 [42], are located at the inner border of the marginal sinus and separate the white pulp from the marginal zone. A sinus-lining basement membrane occurs at this site containing all components that are typically present in basement membranes, including: laminins (isoforms laminin 511, 521 and some laminin 411 and 421), collagen type IV, perlecan and nidogens 1 and 2 (Fig. 3).

The basement membrane at this site in rats and humans has been described to have a double layered structure, with one basement membrane underlying the endothelial cells of the incoming blood vessels, separating the marginal sinus from the marginal zone, while the other forms the inner border between marginal sinus and white pulp and underlies the MAdCAM positive sinus-lining reticular cells [43–46]. Electron microscopy has identified discontinuities in the two basement membranes: Pores sufficiently large to allow the passage of cells occur in the basement membrane layer bordering the marginal zone which correspond to gaps between adjacent endothelial cells, thereby, permitting the free passage of blood borne leukocytes. In contrast, smaller discontinuities, which would not permit the easy passage of cells, occur both in the basement membrane layer and the sinus-lining reticular cells on the inner border to the white pulp [43–46]. The marginal sinus is discontinuous and varies in width. In the regions where there are discontinuities in the marginal sinus, the white pulp is separated from the marginal zone by the sinus-lining basement membrane alone. It has been speculated that these sites of direct connection also represent sites of lymphocyte migration from the marginal zone into the lymphoid follicle. Pan-basement membrane staining (Fig. 3) suggests a close association between the sinus-lining basement membrane and subjacent white pulp reticular fibre network [43,44], potentially forming a route for lymphocyte migration from the marginal zone into the follicle as described above.

3.5. Marginal zone reticular networks

The marginal zone is described as a region surrounding the B cell follicles, with the marginal sinus defining its innermost border and the red pulp its outermost border and is the only B cell-dependent area in the body where B lymphocytes are not organized in a follicular structure (Figs. 1 and 3). The inner border can be clearly defined by MAdCAM expressing sinus-lining reticular cells and the underlying basement membrane, while the outer border is defined by the distribution of IgM^{high}/IgD^{low} B cells. The reticular fibre network of the marginal zone is characteristically much denser than that in the red pulp or the

white pulp [47] (Fig. 3) and has a unique expression of laminin 521 [7] and heparan sulfate proteoglycan, agrin (manuscript in preparation), plus a dense expression of other basement membrane molecules including collagen type IV, nidogen 1 [48] and perlecan [49]. Some interstitial matrix molecules occur here, including fibronectin [50,51] and the ERTR-7 antigen, but not fibrillar collagens or the typical microfibrillar molecules (fibrillin 1 and 2), indicating an important structural difference to the matrices of the white pulp and red pulp [7,46,52,53]. Unpublished confocal microscopy data suggests that the ECM of the marginal zone does not share the conduit-like structure of white pulp reticular fibre network but rather more closely resembles a classical basement membrane structure, which encases individual cells or groups of cells, resulting in a basket-like structure (Fig. 3). Electron microscopic studies have suggested that there is frequent contact between the reticular fibres of the marginal zone and lymphocytes [46], further substantiating the concept that the reticular fibre network is distinct at this site.

The function of the specialised ECM in the marginal zone is unclear, as is the precise spatial relationship between the ECM and the cells resident at this site, including reticular cells and the VCAM-1+/ICAM-1+ stromal cells [54], marginal zone B cells (MZ B cells), and the ERTR-9+ [55] and MOMA-1+/SER-4+ [56,57] macrophages. The ECM may either provide an adhesive niche for one or more of these cell populations, or it may indirectly influence these cell populations by trapping specific chemokines or cytokines at this site.

It is known that resident stromal cells in the marginal zone constitutively express the cell adhesion molecules, ICAM-1 and VCAM-1. Interactions with these adhesion molecules and $\alpha4\beta1$ and LFA-1 expressed on MZ and follicular B lymphocytes play important roles in the long-term retention of MZ B cells at this site [54], and for B- and T-lymphocyte migration into the white pulp [50]. In addition to these adhesive events, a balance between sphingosine-1-phosphate (S1P) and CXCL13 is required for maintaining MZ B cells in the marginal zone. Normally, S1P interactions with S1P-1 receptor are associated with egression of lymphocytes from lymph nodes. However, in the case of MZ B cells, which have high levels of S1P-1 receptor, engagement of the receptor is required for their retention in the marginal zone [58]. This effect is partially due to failure to respond to the chemoattractant, CXCL13, produced in the lymphoid follicle, and upregulation of ICAM-1/VCAM-1-mediated adhesion. However, molecules other than S1P are involved in retention of MZ B cells in the marginal zone, since in the absence of S1P and CXCR5 (the receptor for CXCL13) MZ B cells are still maintained at this site [58]. Whether the specialised ECM of the marginal zone contributes either directly or indirectly to any of the events described above remains to be investigated.

4. Potential function of ECM in the spleen

The close correlation between immune cell localisation and structurally and biochemically distinct ECM compartments in the spleen leads to the question whether the reticular fibre networks of the spleen have an impact on immune cell reactions. A major direct effect on the trafficking of the highly dynamic recirculating lymphocytes is unlikely, as most of the reticular fibres are covered by the cellular processes of reticular fibroblasts and/or endothelial cells [18,45,59–61]. However, the few sites where the ECM is exposed [26] it may provide anchorage for sessile leukocyte populations such as MZ B cells, macrophages in marginal zone and red pulp, or resident dendritic cells in the marginal zone and white pulp. In addition, it is likely that the ECM exerts indirect effects on immune cells of the spleen by 1) storage or presentation of cytokines, growth factors or chemokines (as discussed above), and/or 2) as a major element for survival, proliferation and differentiation of mesenchymal and endothelial stromal cells which have been shown to influence trafficking [62–64], differentiation [65,66] and commitment [67] of immune cells in the spleen.

4.1. Cellular sources of ECM in the spleen

There is growing evidence for the heterogenity of splenic stromal cells with the identification of new markers (reviewed in Allen and Cyster, this volume; [34,35]) Fibroblastic reticular cell populations can be distinguished by antibodies against gp38 (white pulp PALS), smooth muscle actin (white pulp), desmin (white pulp and red pulp) (see Fig. 2), BP-1 (white pulp follicle), ICAM-1 (marginal zone and white pulp), VCAM-1 (marginal zone and red pulp) and antibodies IBL-10 (white pulp) and IBL-11 (white pulp PALS) against unknown epitopes [36]. In the B cell follicle, follicular dendritic cells (FDC) represent another mesenchymal FRC which is not tightly associated with the ECM [68,69]. Also endothelial cells show heterogeneity: Apart from the ubiquitous endothelial expression of MECA-32Ag, Endomucin and PECAM-1 (not sinus-lining endothelium) (unpublished observations), antibodies have been generated that define distinct endothelial cell compartments in the spleen [70,71]. Investigation of correlations between stromal cell and ECM markers will contribute to the understanding of which cells produce the matrix of the reticular fibres in the red pulp, marginal zone and white pulp.

In vitro data from fibroblastic reticular cell lines derived from lymph nodes has shown that these cells are capable of synthesising ERTR-7 antigen, laminins and fibronectin, and that their extracellular deposition is strongly promoted by either contact with lymphocytes or exogenously added TNFα/LTα [63], indicating an interplay between immune cells and stromal cells. Macrophages are an additional immune cell located within the stroma that have been postulated to secrete ECM molecules and are certainly sources of ECM modifying proteases and cytokines that can alter ECM secretion by other cells [72,73].

Whether additional stromal cells exist in either the white pulp or red pulp of the spleen which may contribute to ECM structures is not clear. Indeed, studies identifying the precise cells responsible for synthesis of individual matrix components and regulating the ECM deposition and remodelling during secondary lymphoid organ development and homeostasis remain to be performed.

4.2. Animal models for splenic ECM investigation

As discussed above, spleen compartments can now be characterised not only by their immune cell composition, but also by their ECM structure and molecular composition. However, the relationship between ECM and immune cell function remains entirely open to investigation. Due to the complexity of different ECM types and the difficulty in reconstituting extracellular matrices *in vitro* that faithfully reflect the *in vivo* situation, such analyses will require the use of transgenic mice deficient in defined ECM molecules, but also investigation of ECM molecules in mice known to lack specific splenic immune cell or stromal cell populations. Not only will structural analyses be important in these mice, but also studies of chemokine and/or cytokine localisation.

Several transgenic mouse strains exist, which lack ECM molecules normally expressed in different splenic compartments that are viable but have not been examined from point of view of spleen structure or function. These include mice lacking the microfibrillar molecules collagen type VI and fibrillin 1, the small leucine-rich proteoglycans, fibromodulin, biglycan and decorin, expressed in the collagen core of reticular fibres [20], or specific isoforms of basement membrane components such as nidogens 1 and 2, and laminin α2 which occurs exclusively in the reticular fibre network of the B cell area of the white pulp (as described above) (ECM mouse mutants are reviewed in Refs. [74,75]. Although complete elimination of the major basement membrane or interstitial matrix components, such as the laminins, collagen type IV, perlecan and fibronectin (see Refs. [74,75]) results in mouse embryoes that do not survive sufficiently long for investigation of the spleen, several tissue-specific knockout mice are currently being generated that will not only provide models for investigation of the significance of splenic ECM but also identification of their cellular source.

Non-ECM transgenic mice which will be particularly important to investigate with respect to ECM expression include mice deficient in the TNF superfamily members, which show anatomical abnormalities in the formation of distinct B and T cell areas as well as the marginal zone [76]. In particular, mice lacking lymphotoxin (LT) α in which T and B cells have no separate areas and are completely intermingled, and LTβ deficient mice which show B cells localized in a ring around a central T cell area [76] are likely to provide information on whether ECM is directly or indirectly involved in immune cell compartmentalisation.

5. Conclusion

The spleen is traditionally characterised by its complex immune cell compartmentalisation, but can also be characterised by its unique ECM. Substantial differences have been identified in ECM structure and molecular composition in the red pulp, white pulp and the marginal zone. Most significant are the variations in molecular composition of the reticular fibre networks in red pulp versus white pulp compartments, and the unique expression of laminin 521 isoform and the heparan sulfate proteoglycan, agrin, characteristic of the marginal zone. Differences in localisation of the various ECM molecules in the spleen suggests that the ECM plays a role in the compartmentalisation of the immune cells to their respective niches, an area which remains to be investigated. It is clear that future analyses of ECM animal models require consideration of possible immunology defects, an aspect rarely considered to date, while chemokine/immunological mouse models cannot overlook the need for analysis of stromal cells and the ECM.

References

[1] Mebius RE. Lymphoid organogenesis: educating stroma. Immunol Cell Biol 2007;85:79–80.

[2] Cupedo T, Mebius RE. Cellular interactions in lymph node development. J Immunol 2005;174:21–5.

[3] Cyster JG. Chemokines, sphingosine-1-phosphate, and cell migration in secondary lymphoid organs. Annu Rev Immunol 2005;23:127–59.

[4] Ushiki T. Collagen fibers, reticular fibers and elastic fibers. A comprehensive understanding from a morphological viewpoint. Arch Histol Cytol 2002;65:109–26.

[5] Steiniger B, Barth P, Hellinger A. The perifollicular and marginal zones of the human splenic white pulp: do fibroblasts guide lymphocyte immigration? Am J Pathol 2001;159:501–12.

[6] Drenckhahn D, Wagner J. Stress fibers in the splenic sinus endothelium in situ: molecular structure, relationship to the extracellular matrix, and contractility. J Cell Biol 1986;102:1738–47.

[7] Maatta M, Liakka A, Salo S, Tasanen K, Bruckner-Tuderman L, Autio-Harmainen H. Differential expression of basement membrane components in lymphatic tissues. J Histochem Cytochem 2004;52:1073–81.

[8] Bernfield M, Gotte M, Park PW, Reizes O, Fitzgerald ML, Lincecum J, et al. Functions of cell surface heparan sulfate proteoglycans. Annu Rev Biochem 1999;68:729–77.

[9] Ruhrberg C, Gerhardt H, Golding M, Watson R, Ioannidou S, Fujisawa H, et al. Spatially restricted patterning cues provided by heparin-binding VEGF-A control blood vessel branching morphogenesis. Genes Dev 2002;16:2684–98.

[10] Mulloy B, Rider CC. Cytokines and proteoglycans: an introductory overview. Biochem Soc Trans 2006;34:409–13.

[11] Handel TM, Johnson Z, Crown SE, Lau EK, Proudfoot AE. Regulation of protein function by glycosaminoglycans—as exemplified by chemokines. Annu Rev Biochem 2005;74:385–410.

[12] Timpl R. Macromolecular organization of basement membranes. Curr Opin Cell Biol 1996;8:618–24.

[13] Scheele S, Nystrom A, Durbeej M, Talts JF, Ekblom M, Ekblom P. Laminin isoforms in development and disease. J Mol Med 2007;85:825–36.

[14] Aumailley M, Bruckner-Tuderman L, Carter WG, Deutzmann R, Edgar D, Ekblom P, et al. A simplified laminin nomenclature. Matrix Biol 2005;24:326–32.

[15] Colognato H, Yurchenco PD. Form and function: the laminin family of heterotrimers. Dev Dyn 2000;218:213–34.

[16] Fleischmajer R, Jacobs 2nd L, Perlish JS, Katchen B, Schwartz E, Timpl R. Immunochemical analysis of human kidney reticulin. Am J Pathol 1992;140:1225–35.

[17] Fleischmajer R, MacDonald ED, Perlish JS, Burgeson RE, Fisher LW. Dermal collagen fibrils are hybrids of type I and type III collagen molecules. J Struct Biol 1990;105:162–9.

[18] Saito H, Yokoi Y, Watanabe S, Tajima J, Kuroda H, Namihisa T. Reticular meshwork of the spleen in rats studied by electron microscopy. Am J Anat 1988;181:235–52.

[19] Kumaratilake JS, Gibson MA, Fanning JC, Cleary EG. The tissue distribution of microfibrils reacting with a monospecific antibody to MAGP, the major glycoprotein antigen of elastin-associated microfibrils. Eur J Cell Biol 1989;50:117–27.

[20] Sixt M, Kanazawa N, Selg M, Samson T, Roos G, Reinhardt DP, et al. The conduit system transports soluble antigens from the afferent lymph to resident dendritic cells in the T cell area of the lymph node. Immunity 2005;22:19–29.

[21] Gretz JE, Anderson AO, Shaw S. Cords, channels, corridors and conduits: critical architectural elements facilitating cell interactions in the lymph node cortex. Immunol Rev 1997;156:11–24.

[22] Gretz JE, Kaldjian EP, Anderson AO, Shaw S. Sophisticated strategies for information encounter in the lymph node: the reticular network as a conduit of soluble information and a highway for cell traffic. J Immunol 1996;157:495–9.

[23] Kaldjian EP, Gretz JE, Anderson AO, Shi Y, Shaw S. Spatial and molecular organization of lymph node T cell cortex: a labyrinthine cavity bounded by an epithelium-like monolayer of fibroblastic reticular cells anchored to basement membrane-like extracellular matrix. Int Immunol 2001;13:1243–53.

[24] Karttunen T, Sormunen R, Risteli L, Risteli J, Autio-Harmainen H. Immunoelectron microscopic localisation of laminin, type IV collagen, and type III pN-collagen in reticular fibers of human lymph nodes. J Histochem Cytochem 1989;37:279–86.

[25] Hayakawa M, Kobayashi M, Hoshino T. Microfibrils: a constitutive component of reticular fibers in the mouse lymph node. Cell Tissue Res 1990;262:199–201.

[26] Fujita T, Ushiki T. Scanning electron microscopic observations of the immunodefensive systems with special reference to the surface morphology of the non-lymphoid cells. Arch Histol Cytol 1992;55(Suppl.):105–13.

[27] Fleischmajer R, Perlish JS, Burgeson RE, Shaikh-Bahai F, Timpl R. Type I and type III collagen interactions during fibrillogenesis. Ann N Y Acad Sci 1990;580:161–75.

[28] Braghetta P, Fabbro C, Piccolo S, Marvulli D, Bonaldo P, Volpin D, et al. Distinct regions control transcriptional activation of the alpha1(VI) collagen promoter in different tissues of transgenic mice. J Cell Biol 1996;135:1163–77.

[29] Kielty CM, Sherratt MJ, Shuttleworth CA. Elastic fibres. J Cell Sci 2002;115:2817–28.

[30] Kielty CM, Sherratt MJ, Marson A, Baldock C. Fibrillin microfibrils. Adv Protein Chem 2005;70:405–36.

[31] Hallmann R, Horn N, Selg M, Wendler O, Pausch F, Sorokin LM. Expression and function of laminins in the embryonic and mature vasculature. Physiol Rev 2005;85:979–1000.

[32] Liakka KA. The integrin subunits alpha 2, alpha 3, alpha 4, alpha 5, alpha 6, alpha V, beta 1 and beta 3 in fetal, infant and adult human spleen as detected by immunohistochemistry. Differentiation 1994;56:183–90.

[33] van den Berg TK, van der Ende M, Dopp EA, Kraal G, Dijkstra CD. Localization of beta 1 integrins and their extracellular ligands in human lymphoid tissues. Am J Pathol 1993;143:1098–110.

[34] Crivellato E, Mallardi F. Stromal cell organisation in the mouse lymph node. A light and electron microscopic investigation using the zinc iodide-osmium technique. J Anat 1997;190(Pt 1):85–92.

[35] Vega F, Coombes KR, Thomazy VA, Patel K, Lang W, Jones D. Tissue-specific function of lymph node fibroblastic reticulum cells. Pathobiology 2006;73:71–81.

[36] Balogh P, Horvath G, Szakal AK. Immunoarchitecture of distinct reticular fibroblastic domains in the white pulp of mouse spleen. J Histochem Cytochem 2004;52:1287–98.

[37] Gretz JE, Norbury CC, Anderson AO, Proudfoot AE, Shaw S. Lymph-borne chemokines and other low molecular weight molecules reach high endothelial venules via specialized conduits while a functional barrier limits access to the lymphocyte microenvironments in lymph node cortex. J Exp Med 2000;192:1425–40.

[38] Nolte MA, Belien JA, Schadee-Eestermans I, Jansen W, Unger WW, van Rooijen N, et al. A conduit system distributes chemokines and small blood-borne molecules through the splenic white pulp. J Exp Med 2003;198:505–12.

[39] Bajenoff M, Egen JG, Koo LY, Laugier JP, Brau F, Glaichenhaus N, et al. Stromal cell networks regulate lymphocyte entry, migration, and territoriality in lymph nodes. Immunity 2006;25:989–1001.

[40] Hataba Y, Kirino Y, Suzuki T. Scanning electron microscopic study of the red pulp of mouse spleen. J Electron Microsc (Tokyo) 1981;30:46–56.

[41] Kraal G, Schornagel K, Streeter PR, Holzmann B, Butcher EC. Expression of the mucosal vascular addressin, MAdCAM-1, on sinus-lining cells in the spleen. Am J Pathol 1995;147:763–71.

[42] Wang SL, Kutsche M, DiSciullo G, Schachner M, Bogen SA. Selective malformation of the splenic white pulp border in L1-deficient mice. J Immunol 2000;165:2465–72.

[43] Sasou S, Satodate R, Katsura S. The marginal sinus in the perifollicular region of the rat spleen. Cell Tissue Res 1976;172:195–203.

[44] Sasou S, Madarame T, Satodate R. Views of the endothelial surface of the marginal sinus in rat spleens using the scanning electron microscope. Virchows Arch B Cell Pathol Incl Mol Pathol 1982;40:117–20.

[45] Sasou S, Satodate R, Masuda T, Takayama K. Scanning electron microscopic features of spleen in the rat and human: a comparative study. Scan Electron Microsc 1986:1063–9.

[46] Tanaka H, Hataba Y, Saito S, Fukushima O, Miyasaka M. Phenotypic characteristics and significance of reticular meshwork surrounding splenic white pulp of mice. J Electron Microsc (Tokyo) 1996;45:407–16.

[47] Van Vliet E, Melis M, Foidart JM, Van Ewijk W. Reticular fibroblasts in peripheral lymphoid organs identified by a monoclonal antibody. J Histochem Cytochem 1986;34:883–90.

[48] Bender BL, Jaffe R, Carlin B, Chung AE. Immunolocalization of entactin, a sulfated basement membrane component, in rodent tissues, and comparison with GP-2 (laminin). Am J Pathol 1981;103:419–26.

[49] ten Dam GB, Hafmans T, Veerkamp JH, van Kuppevelt TH. Differential expression of heparan sulfate domains in rat spleen. J Histochem Cytochem 2003;51:727–39.

[50] Lo CG, Lu TT, Cyster JG. Integrin-dependence of lymphocyte entry into the splenic white pulp. J Exp Med 2003;197:353–61.

[51] Ocklind G, Talts J, Fassler R, Mattsson A, Ekblom P. Expression of tenascin in developing and adult mouse lymphoid organs. J Histochem Cytochem 1993;41:1163–9.

[52] Karttunen T, Alavaikko M, Apaja-Sarkkinen M, Autio-Harmainen H. An immunohistochemical study of laminin, type-IV collagen and type-III pN-collagen with relation to reticular fibres in Hodgkin's disease. Int J Cancer 1988;41:52–8.

[53] Katakai T, Hara T, Lee JH, Gonda H, Sugai M, Shimizu A. A novel reticular stromal structure in lymph node cortex: an immuno-platform for interactions among dendritic cells, T cells and B cells. Int Immunol 2004;16:1133–42.

[54] Lu TT, Cyster JG. Integrin-mediated long-term B cell retention in the splenic marginal zone. Science 2002;297:409–12.

[55] Dijkstra CD, Van Vliet E, Dopp EA, van der Lelij AA, Kraal G. Marginal zone macrophages identified by a monoclonal antibody: characterization of immuno- and enzyme-histochemical properties and functional capacities. Immunology 1985;55:23–30.

[56] Kraal G, Janse M. Marginal metallophilic cells of the mouse spleen identified by a monoclonal antibody. Immunology 1986;58:665–9.

[57] Crocker PR, Gordon S. Mouse macrophage hemagglutinin (sheep erythrocyte receptor) with specificity for sialylated glycoconjugates characterized by a monoclonal antibody. J Exp Med 1989;169:1333–46.

[58] Cinamon G, Matloubian M, Lesneski MJ, Xu Y, Low C, Lu T, et al. Sphingosine 1-phosphate receptor 1 promotes B cell localization in the splenic marginal zone. Nat Immunol 2004;5:713–20.

[59] Veerman AJ, van Ewijk W. White pulp compartments in the spleen of rats and mice. A light and electron microscopic study of lymphoid and non-lymphoid celltypes in T- and B-areas. Cell Tissue Res 1975;156:417–41.

[60] Satoh T, Takeda R, Oikawa H, Satodate R. Immunohistochemical and structural characteristics of the reticular framework of the white pulp and marginal zone in the human spleen. Anat Rec 1997;249:486–94.

[61] Saitoh K, Kamiyama R, Hatakeyama S. A scanning electron microscopic study of the boundary zone of the human spleen. Cell Tissue Res 1982;222:655–65.

[62] Luther SA, Tang HL, Hyman PL, Farr AG, Cyster JG. Coexpression of the chemokines ELC and SLC by T zone stromal cells and deletion of the ELC gene in the plt/plt mouse. Proc Natl Acad Sci USA 2000;97:12694–9.

[63] Gunn MD, Kyuwa S, Tam C, Kakiuchi T, Matsuzawa A, Williams LT, et al. Mice lacking expression of secondary lymphoid organ chemokine have defects in lymphocyte homing and dendritic cell localization. J Exp Med 1999;189:451–60.

[64] Benedict CA, De Trez C, Schneider K, Ha S, Patterson G, Ware CF. Specific remodeling of splenic architecture by cytomegalovirus. PLoS Pathog 2006;2:e16.

[65] Zhang M, Tang H, Guo Z, An H, Zhu X, Song W, et al. Splenic stroma drives mature dendritic cells to differentiate into regulatory dendritic cells. Nat Immunol 2004;5:1124–33.

[66] Svensson M, Maroof A, Ato M, Kaye PM. Stromal cells direct local differentiation of regulatory dendritic cells. Immunity 2004;21:805–16.

[67] Bertrand JY, Desanti GE, Lo-Man R, Leclerc C, Cumano A, Golub R. Fetal spleen stroma drives macrophage commitment. Development 2006;133:3619–28.

[68] Katakai T, Hara T, Sugai M, Gonda H, Shimizu A. Lymph node fibroblastic reticular cells construct the stromal reticulum via contact with lymphocytes. J Exp Med 2004;200:783–95.

[69] Cyster JG, Ansel KM, Reif K, Ekland EH, Hyman PL, Tang HL, et al. Follicular stromal cells and lymphocyte homing to follicles. Immunol Rev 2000;176:181–93.

[70] Balazs M, Horvath G, Grama L, Balogh P. Phenotypic identification and development of distinct microvascular compartments in the postnatal mouse spleen. Cell Immunol 2001;212:126–37.

[71] Balogh P, Balazs M, Czompoly T, Weih DS, Arnold HH, Weih F. Distinct roles of lymphotoxin-beta signaling and the homeodomain transcription factor Nkx2.3 in the ontogeny of endothelial compartments in spleen. Cell Tissue Res 2007;328:473–86.

[72] Parks WC, Wilson CL, Lopez-Boado YS. Matrix metalloproteinases as modulators of inflammation and innate immunity. Nat Rev Immunol 2004;4:617–29.

[73] Agrawal S, Anderson P, Durbeej M, van Rooijen N, Ivars F, Opdenakker G, et al. Dystroglycan is selectively cleaved at the parenchymal basement membrane at sites of leukocyte extravasation in experimental autoimmune encephalomyelitis. J Exp Med 2006;203:1007–19.

[74] Gustafsson E, Fässler R. Insights into extracellular matrix functions from mutant mouse models. Exp Cell Res 2000;261:52–68.

[75] Aszodi A, Legate KR, Nakchbandi I, Fassler R. What mouse mutants teach us about extracellular matrix function. Ann Rev Cell Dev Biol 2006;22:591–621.

[76] Mebius RE, Kraal G. Structure and function of the spleen. Nat Rev Immunol 2005;5:606–16.

[77] Gumati MK, Magyar A, Nagy N, Kurucz E, Felfoldi B, Olah I. Extracellular matrix of different composition supports the various splenic compartments of guinea fowl (Numida meleagris). Cell Tissue Res 2003;312:333–43.

[78] Jakubovsky J, Guller L, Cerna M, Balazova K, Polak S, Jakubovska V, et al. Fluorescence of hematoxylin and eosin-stained histological sections of the human spleen. Acta Histochem 2002;104:353–6.

[79] Liakka A, Karjalainen H, Virtanen I, Autio-Harmainen H. Immuno-electron-microscopic localization of types III pN-collagen and IV collagen, laminin and tenascin in developing and adult human spleen. Cell Tissue Res 1995;282:117–27.

[80] Abrahamson DR, Caulfield JP. Distribution of laminin within rat and mouse renal, splenic, intestinal, and hepatic basement membranes identified after the intravenous injection of heterologous antilaminin IgG. Lab Invest 1985;52:169–81.

[81] Murdoch AD, Liu B, Schwarting R, Tuan RS, Iozzo RV. Widespread expression of perlecan proteoglycan in basement membranes and extracellular matrices of human tissues as detected by a novel monoclonal antibody against domain III and by in situ hybridization. J Histochem Cytochem 1994;42:239–49.

[82] Till KJ, Zuzel M, Cawley JC. The role of hyaluronan and interleukin 8 in the migration of chronic lymphocytic leukemia cells within lymphoreticular tissues. Cancer Res 1999;59:4419–26.

Paper IV

Tim Lämmermann
Michael Sixt

The microanatomy of T-cell responses

Authors' address

Tim Lämmermann[1], Michael Sixt[1]

[1]Department of Molecular Medicine, Max Planck Institute of Biochemistry, Martinsried, Germany.

Correspondence to:

Michael Sixt
Max Planck Institute of Biochemistry
Am Klopferspitz 18, 82152 Martinsried
Germany
Tel.: 0049 89 8578 2849
Fax: 0049 89 8578 2024
e-mail: sixt@biochem.mpg.de

Summary: The priming of a T cell results from its physical interaction with a dendritic cell (DC) that presents the cognate antigenic peptide. The success rate of such interactions is extremely low, because the precursor frequency of a naive T cell recognizing a specific antigen is in the range of $1:10^5 - 10^6$. To make this principle practicable, encounter frequencies between DCs and T cells are maximized within lymph nodes (LNs) that are compact immunological projections of the peripheral tissue they drain. But LNs are more than passive meeting places for DCs that immigrated from the tissue and lymphocytes that recirculated via the blood. The microanatomy of the LN stroma actively organizes the cellular encounters by providing preformed migration tracks that create dynamic but highly ordered movement patterns. LN architecture further acts as a sophisticated filtration system that sieves the incoming interstitial fluid at different levels and guarantees that immunologically relevant antigens are loaded on DCs or B cells while inert substances are channeled back into the blood circulation. This review focuses on the non-hematopoietic infrastructure of the lymph node. We describe the association between fibroblastic reticular cell, conduit, DC, and T cell as the essential functional unit of the T-cell cortex.

Keywords: *lymph node, anatomy, conduit, stroma*

Adaptive immunity depends on secondary lymphatic tissues

Innate immune cells are constantly patrolling the body. Within minutes of local infection, they are recruited to the site of damage where they exert their defense function. The speed of such responses is possible because the innate immune cells are always available: some are resident within the tissue and some are quickly recruited from the bloodstream, where they are either freely circulating or patrolling along the endothelial lumen (1–4). As there are only few types of specialized innate immune cells, the copy number of each type is high, and supply is always guarantied. Adaptive immune responses are fundamentally different, because the number of specialized cell types is in the range of many millions, as lymphocytes of different specificity are randomly generated during somatic development. Naturally, the copy numbers of each specific cell type are extremely low. It was recently demonstrated that for an average antigen, the number of specific T cells is in the range of

a few hundreds (5, 6). Hence, the few specialized cells that recognize an antigen have to be expanded before they can effectively invade any tissue. The principle of lymphocyte activation/expansion is based on stochastic encounters between the antigen-presenting cells of the innate immune system, the dendritic cells (DCs), and T cells. Once the T cell physically contacts the DC presenting its cognate antigen, it is activated and expanded to a population size that is now sufficient to effectively invade the infected sites.

Secondary lymphatic organs are the solutions to solve the 'needle in the haystack' problem of identifying and expanding rare T cells within reasonable time frames. The prototypic example of a secondary lymphatic organ is the lymph node (LN), which we discuss in this review. LNs are compact immunological projections of the patch of peripheral tissue that they drain. DCs that collected information and antigens in the periphery migrate via the afferent lymphatic vessels into the draining LN. Once in the T-cell area, the immigrated DCs display, based on the information they received in the periphery, the antigen in a context that instructs the T cell to differentiate into the adequate effecter type (7). T cells recirculate through the LNs with the bloodstream that they leave via high endothelial venules (8). Within the T zone, the necessary high encounter rates between DCs and T cells are maintained by rapid cell locomotion that is effectively organized by chemokines (9). The big advantage of this system is that instead of scanning the whole periphery, naive T cells just visit the LN and receive all the instructions they need. Indeed, the adaptive immune system is so highly dependent on its organization centers that in the absence of secondary lymphatic organs, adaptive immunity is abolished (10).

Upon closer inspection, the schematic concept of immigrating DCs being the representation of the periphery is too simplified, and the reality is more complex. LNs are not only receiving DCs with the afferent lymph but also the whole stream of interstitial fluid with all its contents: soluble antigens, intact microbes, microbial particles, and locally produced extracellular signaling molecules like cytokines and chemokines. LNs are fluid filters that are providing the infrastructure to collect, select, and load soluble antigens on DCs that are permanently residing in the T zone. The filter function also physically prevents that replicable pathogens spread systemically via the blood circulation. LNs are also 'information hubs' that are quickly relaying soluble signals from the periphery toward the T cells in the blood circulation. Finally, it seems likely that LNs are critical regulators of the fluid balance between interstitium and blood.

The anatomy of LNs is complex, extremely dynamic, and until 2001, it was largely ignored by immunologists. Only the rise of intravital imaging technologies within the last years brought structural aspects of the lymphatic system back into the mind of the immunologist. Numerous excellent reviews are available that summarize the emerging knowledge of leukocyte motility patterns within LNs (11–13). However, the focus was largely on the hematopoietic fraction of the LN that is relatively easy to visualize. The mesenchymal infrastructure of the LN that supports and directs the blood cells is still poorly appreciated. Closely connected to the mesenchymal anatomy is the question of fluid dynamics within the lymphatic system. Although a detailed physiological knowledge of particle and solute transport will be necessary to understand the kinetics of infections at the organismic level, many aspects of these processes are not investigated.

In this review, we describe the non-hematopoietic infrastructure of the lymphatic system in the functional context of cell migration and fluid drainage. Our focus is the T-cell response, as the B-cell compartment has been reviewed recently (14), but we mention the B cells when necessary for comparative purposes. We use the skin and the draining LN as an example. For two reasons we also include an overview over the dermal microenvironment. First, almost every immune response is initiated in the periphery, and the dermal fluid and cell drainage system is critically involved in the initiation of adaptive immunity. Second, molecular composition and physiological characteristics of the dermal interstitium are well investigated and serve as a model to further discuss LN physiology that follows the same principles but is still an open field.

Circulation patterns of fluids

While cells and some microbes have the possibility to move autonomously, extracellular substances within vertebrates are either immobilized to cells or molecular components of the extracellular matrix (ECM) or they move with the bulk flow of fluid by convective forces, meaning that they are flushed (15). The interstitial fluid of vertebrates appears in several different forms while it is recirculating through the body. The plasma fraction of the blood is the most accessible variant. In the capillary bed, plasma is filtrated from the vasculature and becomes interstitial fluid, which is slowly percolating through the interstitium into the afferent lymphatic vessels (16). From there on it is termed afferent lymph. The afferent lymph is filtered through the draining LN, and once it has exited the LN is termed efferent lymph. In larger vertebrates and humans

(but not in mice), the efferent lymph is filtered through a hierarchy of second- and third-order LNs before it enters the cisterna chyli and is further actively transported via the thoracic duct back into the venous blood circulation (17, 18). All particles will passively follow the convective drag of the interstitial fluid if they are not immobilized or taken up by cells, trapped by binding to ECM, or filtered at a barrier due to size reasons. As a consequence of the different filtration steps, plasma, interstitial fluid, afferent lymph, and efferent lymph have quantitatively different molecular compositions, although they are in continuous exchange (19) (Fig. 1).

The peripheral tissues: dermis

After breaking the barrier of the epidermis, extracellular pathogens either spread laterally, grow into deeper areas, or
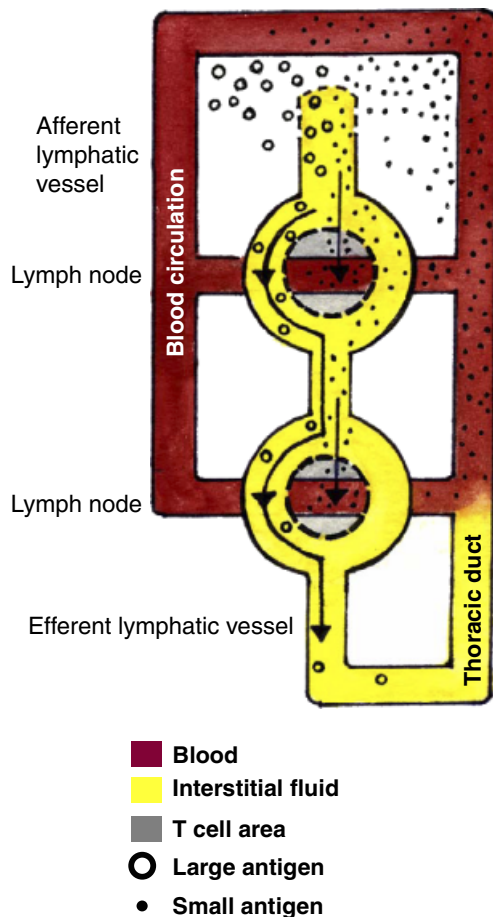

Blood
Interstitial fluid
T cell area
O **Large antigen**
• **Small antigen**

Fig. 1. Circulation patterns of fluids. Small particles (small dots) become filtrated from the blood stream (red) in the periphery, enter the afferent lymphatic vessel (yellow), and are transported into the draining LN. Here, they are directly reabsorbed into the bloodstream. Large particles (large, open dots) also enter the afferent lymphatic vessel but percolate through the sinus system of the LN and eventually (if they are not trapped in the sinus) are channeled via the efferent lymphatic vessel and the thoracic duct back into the blood circulation.

distribute systemically by accessing the blood vasculature. The molecular architecture and the hydrostatic conditions within the dermis dictate that the fluid and particle stream is strictly directed from the blood vessel into the lymph vessel (16, 19). This convective stream counteracts entry into the blood circulation by flushing particles away from blood vessels. Furthermore, the small pore size of the interstitium acts as a sterical barrier for active spreading. We start by describing general features of the dermal compartment, with focus on the questions of how molecular anatomy determines the transport of solutes, particles, and immune cells. The dermal stroma consists of two components: the stroma cell (typically a fibroblast) and the ECM that the stroma cell produces. The dermis is characterized by a wide extracellular space that is scaffolded by dense arrays of biopolymers. The fibroblasts are scattered within the tissue without forming cell–cell contacts. They are rather embedded as single cells into the surrounding ECM. Owing to the spacing, fibroblasts themselves do not form any significant barrier for solutes, cells, or particles (20). The ECM can be functionally divided into two categories: the fibrillar fraction that consists of arrays of fibrillar collagen bundles, elastic fibers, and microfibrils, and the non-fibrillar fraction that consists mainly of long-chained aminosugars (glycosaminoglycans) and proteoglycans. The fibrillar fraction is mechanically stable and counteracts the tension produced by the fibroblasts that contract the extracellular fibers via acto-myosin forces (21). The interplay between fibroblasts and fibers determines the mechanical characteristics of the skin. The non-fibrillar fraction fills the volume between the fibers. Unlike the fibrillar proteins, these extremely large sugars (chains of hyaluronic acid can reach a length up to 5 μm and a molecular weight of several million Daltons) are not tightly interconnected, and biophysically they rather behave like a very viscous fluid (22). Glycosaminoglycans are highly negatively charged and therefore bind ions and, as a consequence, attract and immobilize water. By sucking water, they act as 'expansion elements' that counteract the tensile force of the fibrillar ECM fraction (16).

Solute transport within the dermis

What are the driving forces of interstitial flow? The flow is a function of Starling's forces that set the capillary filtration rate: the local hydraulic pressure difference (blood pressure–interstitial pressure) across the blood vessel wall minus the colloid osmotic pressure difference between blood and interstitium (23). The hydraulic pressure of the dermal interstitium is actively kept low by the suction force of the lymphatic vessels that pump fluid away from the tissue and into the draining LN.

Under normal conditions the interstitial flow is slow, because the hydraulic conductivity of the interstitium is low. Conductivity is set by the pore size (the hydraulic radius) of the interstitium that is determined by the surface area of glycosaminoglycans and fibrillar ECM that is filling the interstitium. In the dermis, this radius is in the range of 100 nm, so that the interstitium is a sterical barrier for bigger particles like viruses or bacteria (24). The low mobility of interstitial water that is caused by the charged glycosaminoglycans prevents quick shifts of interstitial fluid upon pressure changes and restricts the diffusive or convective distribution of soluble molecules, even under mechanical stress. Only in the situation of peripheral lymphedema is the glycosaminoglycan fraction saturated with water. This dilution leads to the effect that the excess water moves freely (16, 25, 26). Therefore, edematous tissue can be easily 'squeezed out,' which is used as a simple clinical test: pushing into edematous skin but not into healthy skin leaves a pit. To our knowledge, the consequences of edema for particle transport have not been investigated systematically, but it is a clinical fact that peripheral edema predisposes for local infection (27) (Fig. 2).

There are two important implications for particle and solute transport within the dermis. (i) In principle, solutes and small molecules can freely diffuse, but their transport is dominated
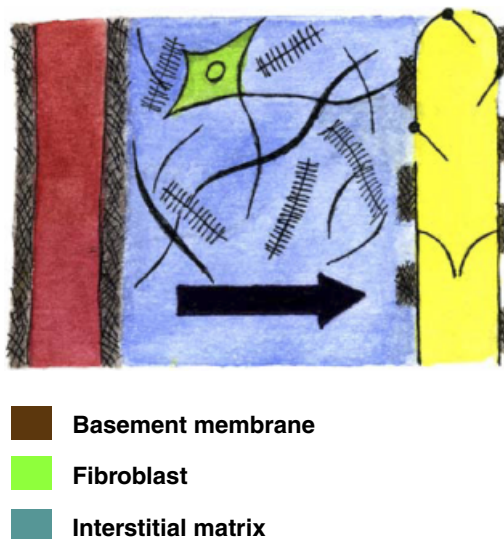

Basement membrane

Fibroblast

Interstitial matrix

Fig. 2. Interstitial flux within the dermis. Plasma becomes filtrated from the blood vessel (red). The endothelium and the endothelial basement membrane (brown) form a semi-permeable membrane. The interstitial flux (arrow) is strictly directed from the blood vessel toward the lymphatic vessel (yellow) that has no continuous basement membrane but flap valves opening toward the lumen. The interstitial matrix (blue) consists of collagen fibers (thick lines), microfibrils (thin lines), and glycosaminoglycans (brush like structures). Fibroblasts (green) associate with the interstitial matrix.

by the convection caused by the bulk fluid movement that is directed from the capillaries into the lymphatic vessels. The dermis is in a state of constant fluid secretion, and although this is frequently stated, re-absorption of fluid and solutes in the efferent capillary bed or across venules does not occur normally. (ii) For larger particles, the pore size of the interstitium is a sterical barrier. They 'become filtered,' and the only way to spread is by autonomous movement, digestion of the ECM, and subsequent increase of the pore size, or by 'hitchhiking' with cells.

Cell migration within the dermis
A soluble molecule or a particle can reach the draining LN via two principal routes: passively with the interstitial flow or carried by cells. The usual cell type that carries antigens into the LN is the DC. In the steady state, DCs are forming an area-wide network that constantly samples the tissue for internal (damage) or external (microbes) danger signals (7). Within the skin, there are two populations of resident DCs: the Langerhans cells of the epidermis that reside between the keratinocytes above the epidermal basement membrane (28, 29) and the dermal DCs that are scattered within the interstitium (30). Upon danger sensing, DCs undergo so-called maturation. DCs transiently become phagocytotic and subsequently acquire a state of high motility (7, 31). This metamorphosis from a rather static cell that adheres to the ECM via integrins to a very motile cell is associated with the upregulation of the chemokine receptor 7 (CCR7) that guides the cells toward the afferent lymphatics that are expressing the CCR7 ligand CCL21 (31). How do DCs migrate through the interstitial microenvironment? Considering the textbook paradigm that cell migration in metazoans relies on integrin-mediated coupling of cytoskeletal force to the ECM (32), it seems rather paradoxical that we and others found that upon maturation, DCs functionally inactivate their integrins (28, 29). However, we recently learned that DC migration in the interstitium is completely integrin independent. We rather found that DCs move through the fibrillar scaffold of the interstitium by a protrusive flowing of the actin cytoskeleton and by occasional contractions of the trailing edge that facilitates squeezing of the non-elastic nucleus through narrow areas (T. Lämmermann *et al.*, unpublished observations). Proteolytic digestion of fibrillar matrices is not required for this very quick mode of movement, and the spacing of the fibers is obviously large enough for the cells to squeeze through (33). Hence, leukocyte migration through the interstitium happens without causing permanent damage by remodeling or rearrangement of ECM; the cells move along the path of least resistance (34). It is currently

unclear how cells handle the tight network of glycosaminogly-cans that fills the space between the fibers. It is likely that these polymers are just pushed away. This is possible because the glycosaminoglycan network is not tightly crosslinked and is rather fluid.

The basement membrane as a specialized ECM

Although the interstitial matrix is not allowing unrestricted movement of particles, there is a variant of the ECM of much lower permeability: the basement membrane. Basement membranes underlie epithelia and endothelia and surround axons, fat, and muscle cells. Rather than a loose scaffold like the inter-stitial matrix, basement membranes are dense sheets of tightly interconnected glycoproteins of the laminin and the non-fibrillar collagen IV families that are coupled together by bridg-ing molecules like nidogens (35). Basement membranes do not only serve mechanical functions but also act as molecular sieves, anchoring structures and polarity signals for polarized cells, pathways or barriers for migrating cells, and, importantly, they harbor heparan sulfate proteoglycans like perlecan and agrin. These sulfated proteoglycans are again serving as mole-cular sinks, storage sites, or presentation platforms for the many heparan sulfate-binding growth factors and chemokines (36). Basement membranes strongly vary in their molecular composition, depending on the cell type they are produced by and associated with. Sixteen different laminin isoforms with distinct tissue-specific and developmental expression patterns and distinct cell-binding and biophysical characteristics are only one example of the highly specialized and not well-explored specializations of basement membranes (37).

Role of basement membranes for solute transport

The role of basement membranes in fluid filtration is not well investigated, except in the kidney where the primary urine is filtered through the basement membrane associated with the podocyte endfeet. Here, a dual role as a sterical and a charge filter for molecules above the size of albumin has been proposed (38). Three basement membranes transect the skin in a way that they might be relevant for fluid filtration: the basement membrane of the epidermal–dermal junction, of the blood vessel endothelium, and of the lymphatic endothelium. Although no functional studies are available, it appears likely that the endothelial basement membrane contributes to the semi-permeability of the blood vessel (39). The same is possible for the epidermal basement membrane, while the basement membrane of the lymphatic endothelium appears to be functionally different. It has long been doubted that lymph vessels have at all an underlying basement membrane and

lymphatic endothelial cells can be differentiated from blood endothelial cells by very low expression levels of collagen IV and laminins (40–42). Only recently it became clear that the basement membrane of lymph vessels exists but that it is very fragile and also fragmented (43, 44). This structural config-uration makes it unlikely that the lymphatic basement mem-brane is a significant barrier to fluid movement.

The role of basement membranes for cell migration

Basement membranes are structurally dense and as such require specialized mechanisms if they should be transmi-grated (45). Leukocytes can circumvent most dermal basement membranes, and the only sites where transmigration is neces-sary are the endothelial basement membrane of venules and the epidermal basement membrane. Cells have to penetrate these barriers to leave the bloodstream and the epidermis, respec-tively. Passing the epidermal basement membrane clearly requires proteolytic degradation and likely also integrin-mediated adhesion, as demonstrated for epidermal Langerhans cells and autoreactive T cells (45–48). For extravasating leukocytes that have traversed the endothelial monolayer and face the underlying basement membrane, this is less clear. Recently, it has been suggested that preformed openings (also called low expression sites as they show low levels of laminins and collagen IV) allow neutrophils to squeeze through the membrane without creating defects (49). Passing the rudimen-tary basement membrane of the lymphatics does not require active proteolytic mechanisms, and DCs likely enter via pre-formed openings (our unpublished data).

The lymphatic vessels

Entry of fluid into the lymphatic vessels

The lymphatic vessels actively pump interstitial fluid out of the tissue and thereby keep the interstitial pressure low and guarantee that flow is unidirectional away from the capillary bed. In most tissues, the lymphatic vessels are the only route of fluid absorption, and efferent capillaries and venules are not pathways of significant absorption (LNs and the gut are exceptions as we discuss below) (19). Unlike blood vessels, lymph vessels openly communicate with the interstitium. No tight endothelial barrier or continuous basement membrane restricts the movement of solutes. The suction force of the lymph vessel is generated by the interplay of four functional units: (i) the smooth muscle layer around the lymphatic collector vessels (the proximal part of the lymphatics) periodi-cally contracts and thereby pushes fluid toward the draining LN, (ii) backflush of fluid into the periphery during contractile phases is prevented by the semilunar valves between segments

of collector vessels, (iii) the lymphatic endothelial cells of the blind ending initial (distal) part of the lymphatics are arranged in an overlapping pattern that forms flap valves that allow entry but prevent exit of fluid, and (iv) the abluminal side of the lymph vessels are anchored to the interstitial fibrillar matrix via elastic filaments. Using the tensile force of the interstitial ECM, these filaments pull the lumen of the lymphatics open, even when interstitial pressure rises during edema. Edema rather enforces the opening of the lumen as it raises the tension within the interstitial matrix (50).

Cellular entry into the lymphatic vessels

How cells enter lymphatic vessels has not been thoroughly investigated *in vivo*. Several adhesion molecules have been implicated in this process based on *in vitro* assays or pharmacological inhibition. These molecules include the cell surface receptor clever 1 (51) and the interaction between leukocyte function-associated antigen-1 (LFA1) and very late antigen 4 (VLA4) on the DC and its counter ligands vascular cell adhesion molecule-1 (VCAM-1) and intracellular adhesion molecule-1 (ICAM-1) on the abluminal side of the lymphatic vessels (52). However, a recent report (and our own data) suggests that like for fluid transport, for cellular trafficking, the lymphatic vessels might not be a considerable barrier. The cell–cell contacts between the lymphatic endothelial cells at the level of initial lymph vessels are discontinuous. Instead of the continuous adherens junctions that are found between blood endothelial cells, the junctions between lymphatic endothelial cells are organized as 'buttons'. Within the buttons, the same molecular connectors, platelet-endothelial cell adhesion molecule-1 (PECAM-1) and VE Cadherin, are found as in the blood vessels. The spacing between the buttons is in the range of 3 μm (53). Although not formally demonstrated, the resulting gaps would be sufficient for DCs and lymphocytes to squeeze through without using specialized mechanisms of intravasation. Such a passive model would imply that lymphatic entry is only determined by the chemokine cue that guides the cells into the vessel. Lymphatic vessels express high levels of CCL21 (54), which could result in a diffusive gradient that attracts the leukocytes into the vessel. However, the mechanism of this process is far from clear, as the continuous interstitial flux would counteract a diffusive distribution of chemokine away from the lymphatic vessel and would instead suck CCL21 into the vessel. Recently, Swartz and colleagues (55, 56) suggested an alternative model for chemotactic migration within the dermis that was termed 'autologous chemotaxis.' Many cells expressing CCR7 also express the ligand CCL19, which seems paradox at first sight. However, within the interstitium, con-

vection will drag the secreted chemokine toward the lymph vessel and thereby create a gradient that can then be followed by the same cell. Autologous chemotaxis was demonstrated for metastatic tumor cells moving into lymph vessels and also was suggested as a driving force for DC migration into the lymphatics (55, 56). Although this concept appears appealing, it remains to be challenged *in vivo* by either testing if CCL19-deficient DCs migrate less or, more importantly, showing that even in the absence of CCL21 on lymphatic vessels DCs can move directionally into the lymph vessels.

Transport within the lymphatic vessels

It is beyond doubt that transport within the lymphatic vessels is the same for solutes and cells. It is a passive flowing with the stream of interstitial fluid that is powered by the periodic contractions of the lymphatic vessels. Cells and fluid are pumped directly into the subcapsular sinus of the node (50). Within the sinus, the sieving function of the LN starts. In the following we describe anatomy and physiology of the LN, and as in the previous section, we separately discuss the implications for the transport of solutes and the migration of cells.

The LN sinuses

Two anatomically distinct compartments of the LN are distinguished: the sinus and the cortex. Both consist of a stromal and a hematopoietic component. The most simplified view of a LN is that of an organ bathing within the lumen of a dilated lymphatic vessel. The sinuses represent the remaining lumen of the vessel, and the cortex represents the actual organ. Usually LNs mark sites where lymph vessels coming from different drainage areas meet, and therefore every LN has several afferent but most times only one efferent lymph vessel. The entry side of the LN that is close to the afferent vessels is called subcapsular sinus, and the one close to the efferent vessel is called the medullary sinus (57). As the sinus system surrounds the whole LN, the subcapsular and medullary sinuses are directly interconnected, and there is an open communication between them. Hence, cells, fluid, and soluble molecules can pass through the LN without contacting the cells of the cortex (58). In larger LNs, there are also intermediate sinuses that penetrate the parenchyma and constitute a direct route between afferent and efferent lymph (57, 59, 60). It has further been described that the deep cortex harbors a lymphatic labyrinth that is connected to the medullary sinus. These are blind ending sinuses that likely collect emigrating lymphocytes and lead them into the medulla (59, 60).

The subcapsular sinus is populated by different resident cell types. The stromal cell of the sinus is the sinus reticular cell or

retothelial cell (61–64). This cell type has morphological similarities with the fibroblastic reticular cell (FRC) of the T-cell area but is also carrying some typical surface markers of the lymphatic endothelial cell lineage (65). The retothelial cells constitute a three dimensional meshwork that is the backbone of the sinus and bridges the LN capsule with the LN cortex (60, 66). The retothelial cells are assembled around an ECM scaffold that appears different from the stroma of the periphery and already shows features of the conduit structures of the T-cell area. Bundles of fibrillar collagens transect the sinus and connect the fibrous capsule of the LN with the ECM of the conduits in the T-cell area (67). These collagen bundles are partially surrounded by a basement membrane and are completely enwrapped with stroma cells (59, 68–70). They form a structure that resembles the conduit of the T-cell stroma. Unlike in conduits, in the sinus the basement membrane is discontinuous and rather resembles rings or spirals. At some places where the basement membrane is more patchy, it takes the configuration of buttons that are connecting the cells with the interstitial matrix of the fibers (71). The functional significance of this ECM assembly has not been investigated. It appears likely that such a structure facilitates fluid drainage and at the same time gives structural support. The discontinuous nature of the basement membrane is also reminiscent of the button-like cell–cell adhesions of the initial lymphatics, with the exception that the retothelial cells build a three dimensional sponge-like structure instead of the two-dimensional sieve structure of the lymphatics. The interstitial matrix of the sinus is not qualitatively different from the interstitium of the dermis – it is just assembled in a more organized and condensed manner. The same is the case for the retothelial cells that appear like a condensed form of the dermal mesenchyme. While the dermal fibroblasts are scattered within the interstitium as single cells, the retothelial cells assemble a unique and complex type of cell–cell junctions that have been termed puncta adherentia (62).

The connective tissue of the sinus is not only populated by stroma cells, passaging lymphocytes, and DCs that wander through the sinus in search of danger; there is also a resident population of rather immobile subcapsular macrophages that settle between the retothelial cells. They constitute a big part of the cell mass of the sinus. It is unknown if subcapsular macrophages couple to the retothelial cells, if they bind to the ECM within the sinus, and if there are specific signals that localize these cells to the sinus. Interestingly, the subcapsular macrophages are not 100% restricted to the sinus but also leak into the first 10–30 μm of the cortex, which might support their function as antigen relays (72). The morphological details of the intermediate and medullary sinuses and the lymphatic labyrinth are poorly described. As there is a continuum between the subcapsular and the medullary sinus, the stroma of both areas has strong similarities. Additionally, the medullary sinus harbors antibody-secreting plasma cells.

The configuration of the sinuses is extremely flexible in inflammatory situations. It has been shown that during the course of a local LN activation by peripheral inflammation, the sinuses enlarge within hours and become more extended and also 'infiltrate the cortex.' This expansion has been interpreted as a consequence of proliferating lymphatic endothelial cells that invade the cortex and possibly make influx from the periphery more effective (73). However, how closely the retothelial cells indeed are related to the lymphatic lineage and if they respond to the same growth factors as lymphatic endothelia deserves further investigation. It is also possible that the stroma cell population within the sinus is not homogenous and that a population of lymphatic endothelial cells exists in parallel to the retothelial cells (Fig. 3).

A remarkable but rarely mentioned characteristic of the sinus is that it lacks blood vessels, and oxygenation has to be provided by the underlying cortex (60). Teleologically, a lack of blood vessels makes sense when viewing the sinus as the first level of particle filtration with large pore sizes. A direct connection to the blood circulation would bring along a high risk of hematogenic distribution of infectious particles. Consequently, all blood vessels in the LN are shielded from the permeable sinus and are embedded into the filtrating conduit system of the FRC network.

Solute transport within the sinus

Soluble molecules, particles, and cells periodically arrive with the pumping contractions of the lymphatic vessels. At pressure peaks, lymphatic fluid is actively pushed into the subcapsular sinus. Although direct measurements are lacking, intravital microscopy data suggest that fluid transport within the sinus is rather unrestricted (2). The hydraulic radius of the sinus is likely very large and allows not only soluble molecules but also particles and cells to float through the meshwork of resident cells. The solute distribution within the sinus can therefore be described as percolation: the resident cells are bathed within the unrestricted stream of afferent lymph. As the sinus system allows open communication between subcapsular and medullary areas, solutes can take a shortcut from afferent to efferent lymph. This route is preferentially taken by immunologically inert particles and larger molecules that are excluded from the cortex, as they do not have access to the conduit system of the T-cell cortex and further to the blood circulation.
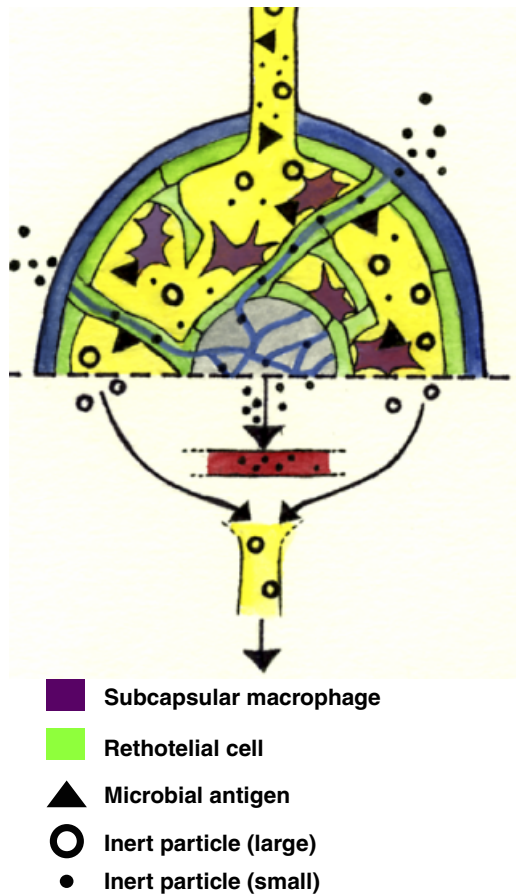
Subcapsular macrophage

Rethotelial cell

Microbial antigen

○ **Inert particle (large)**

• **Inert particle (small)**

Fig. 3. Particle movement within the sinus. The LN capsule consists of interstitial matrix (blue) that is continued within the sinus. Here, the matrix is surrounded by retothelial cells (green). Subcapsular macrophages (orange) are associated with the retothelial cells. Large particles percolate through the sinus and become trapped on macrophages and retothelial cells if they are immunologically relevant (triangles) and pass into the efferent lymph if they are inert (round dots). Small molecules can enter from the capsule and the sinus into the conduits of the T-cell cortex from where they access the blood.

The requirement for such a 'bypass route' becomes especially evident in the intestine, where the lymph does not only play a role in fluid drainage and immune surveillance but also transports the absorbed nutrients. Chylomicrons are collected in the initial lymphatic vessel of the villus (the lacteal), are channeled through the mesenteric nodes, and are transported via the thoracic duct into the blood circulation. Immunologically, all particles that pass through the sinus are irrelevant; they are not visible for DCs, T, or B cells if they are not trapped in the sinus. Selective trapping of solutes contained within the percolating lymph is achieved by the resident cells of the sinus. Both retothelial cells and macrophages catch soluble antigens and efficiently endocytose particles and microbes (29, 74). Accordingly, macrophages but also retothelial cells carry a rich surface repertoire of scavenger receptors (C-type lectins and many others) (65, 75) that unspecifically immobilize various

microbial antigens. How the retothelial cells contribute to immune responses after antigen trapping is unclear, while it has been recently shown that subcapsular macrophages can 'hand over' antigen and even whole virus particles to B cells through the floor of the subcapsular sinus (76–78). Junt *et al.* (77) demonstrated the important concept that the filtering capacity of subcapsular macrophages serves both innate and adaptive immune functions. First, it is essential to mount effective B-cell responses to viruses that arrive with the interstitial fluid. Second, it prevents the hematogenic spreading of the virus itself. When subcapsular macrophages were depleted from the sinus, virus passed the LN without accessing the parenchyma and recirculated via the efferent lymph and the thoracic duct into the blood circulation (77).

It is a widely ignored fact that an access route for small molecules into the sinus exists that is independent of afferent lymphatics. The interstitium of the sinus is directly connected to the ECM that constitutes the fibrous capsule of the node. The capsule consists of fibroblasts, their fibrillar collagen matrix, and likely many other components of a normal interstitium. Although the capsule encases and mechanically protects the LN, it does not shield it from interstitial fluids that surround the node. It was shown that tracers injected close to the node distribute along the capsular ECM and directly drain into the sinus and most likely also further into the conduit system of the T-cell cortex. This means that the ECM of the capsule forms a fluid exchange continuum with the ECM of the sinus and the parenchyma (79).

Cell movement within the sinus

Although histologically most areas of the sinus appear rather densely packed with cells, intravital microscopy studies showed that spacing of cells and interstitium is (at least in some areas of the sinus) obviously loose enough to allow free floating of single cells (2). Especially during pressure peaks caused by the peristaltic compressions of the afferent lymphatic pump, round cells are flushed through the sinus. However, other intravital microscopic studies also showed active amoeboid migration of DCs and T cells within the sinus (80, 81). Hence, both active migration and passive flowing occur in the sinus. Exit from the sinus has not been studied intensively. One intravital microscopy study suggested that the medullary sinus has preformed openings that allow active exit from the medullary sinus into the efferent lymphatics (82). Scanning electron microscopic studies favored the lymphatic labyrinth that continuously connects to the medullary sinus as the site of massive lymphocyte exit (59, 60).

It was shown by intravital microscopy that the sinus contains a population of motile DCs that wander between the static

retothelial cells and macrophages (80). It has not been addressed if these DCs are representing a specialized subset or if they are dermal DCs and Langerhans cells in steady state transit from the periphery toward the T-cell cortex. Independent of their origin, it is likely that these DCs are foraging for antigen and danger signals that are immobilized on the retothelial cells or macrophages. Once they detect a target, they likely go through their usual program: they transiently arrest and phagocytose, subsequently become motile, and actively enter the T-cell cortex to present the antigen.

The sinus–cortex interface

The floor of the sinus is demarcated by a basement membrane that has direct connections with the conduit system of the cortex. However, this basement membrane is not continuous and gaps allow cellular traffic without the need for proteolytic degradation. The stroma cell that is directly covering the floor of the sinus has been termed, describing its position, the sinus-lining cell. It has not been addressed if this cell is a morphological variant of the retothelial cell, a form of lymphatic endothelial cell, or a separate specialized cell lineage.

Penetration of fluid and small molecules into the parenchyma

Almost 50 years ago, tracer experiments demonstrated that there is no free exchange of small molecules between the sinus and the T-cell parenchyma (70). Although not widely acknowledged in textbooks, these findings clearly argued against free percolation being the principle of interstitial flux in the T-cell area. In their seminal tracer studies, the laboratories of Anderson and Shaw (58, 83) showed that rather than percolating through the parenchyma, small molecules are channeled through the conduit system of the T-cell area. Interestingly, molecules with a molecular weight above the size of albumin (70 kDa) were excluded from the parenchyma and were exclusively detectable within the sinus (58). Most large molecules and particles eventually exit the node via the efferent lymphatic vessel, without ever becoming immunologically visible. The fraction of large molecules that is not bypassing the T zone is trapped by retothelial cells or sinus macrophages and further processed.

The communication between the sinuses and the T-cell cortex is restricted for large soluble molecules and bigger particles. Small molecules can enter the cortex but remain confined to the conduit system instead of percolating between the T cells. The morphological correlate of the size-selective sinus-cortex barrier is not known. Below we put forward the idea that a physical barrier is not required to explain the exclusion of soluble molecules from the T-cell parenchyma but that this is just a consequence of a lacking interstitium between T cells.

Passage of cells through the sinus floor

Restricted movement of soluble molecules suggests that also cellular trafficking between sinus and cortex is restricted. However, this does not seem to be the case. It has been shown by intravital microscopy that T cells can effortlessly glide into the subcapsular sinus when exposed to artificial gradients of chemokine (81). Observations of DCs penetrating the subcapsular sinus suggested the same: locomotion kinetics of cells at the sinus cortex interface did not indicate that a barrier has to be traversed (84). If the sinus lining cells are discontinuous, if they 'open the gate' on demand, or if they are traversed transcellularly is unknown. Taken together, active cellular movement between sinus and cortex is possible while the passive movement of solutes and particles is restricted. Molecules, be it foreign antigens or endogenous factors dissolved in the interstitial fluid, with a size below 70 kDa can enter the T-cell cortex via the conduit. Larger molecules are excluded and have to enter as cellular cargo on the surface or inside incoming DCs or are relayed into the B-cell follicle by macrophages.

The T-cell cortex

The stromal backbone

The anatomy of the T-cell cortex is dominated by the densely packed T cells that constitute more than 95% of the cellular mass. The remaining space is occupied by resident DCs and the T-cell stroma cells. The stroma is the infrastructure that dictates shape and organization of the T zone. It is the only stable component while T cells are in continuous motion to maintain the high contact frequencies with DCs. The T-cell stroma is condensed to a minimal volume and has an extremely unusual appearance. It forms a filigrane three-dimensional network that is highly interconnected via cell–cell contacts and structurally resembles the skeleton of a sponge (67). The cells forming this network are called FRCs, and the ECM they assemble has been termed conduit, after its function to channel small molecules through the cortex. The stromal endoskeleton of the LN is therefore not only a structural backbone but also a complex system of tubes that forms one continuously interconnected fluid exchange system with physical connections to all sinuses and all blood vessels.

The conduit

The conduit, varying in diameter from 200 nm to 3 μm, contains all known types of ECM molecules from peripheral

tissues, with the decisive distinction that they are assembled in a highly ordered manner. The center of the conduit is formed by parallel bundles of fibrillar collagens (I, III). Associated with these bundles, depending on the size of the conduit, are the typical collagen-associated stabilizing and crosslinking molecules like fibromodulin, decorin, and lumican (our unpublished data). The collagen fibers vary in number from 20 to 200 per cross-section, and the individual thickness varies around 50 nm (57, 85). They are not tightly packed. Transmission electron microscopy studies demonstrated that an unordered meshwork of 5–10 nm fibrils, morphologically resembling microfibrils, fills the space between the collagen fibers (86). The whole array of collagen bundles is embedded in a coat of microfibrils. Accordingly fibrillins, the molecular constituents of microfibrils have been detected between and especially around the collagen fibers (29). Although not been thoroughly investigated, it is most likely that, as in the interstitium of the periphery, glycosaminoglycans are filling the gaps between fibers and fibrils. In human LNs, dermatan sulfate was detected in association with the conduit ECM, but studies of other sugars are missing (87). The fibrillar core is a cell-free compartment that is tightly enclosed by a basement membrane that forms a cylindrical cover, giving the conduit the ultrastructural appearance of a tube. The cell that produces and settles on the basement membrane is the FRC. It forms a cellular sleeve around the conduit by anchoring to the basement membrane. The FRC continuously enwraps the conduit, and by forming intracellular cell–cell contacts, they seal the conduit against the T-cell-containing parenchyma. Along the longitudinal axis, the individual FRCs connect with intercellular junctions (57). The exact nature of the cell–cell junctions between the FRCs remains to be determined. Although more than 95% of the conduit is covered with FRCs, gaps remain that are covered by hematopoietic cells (29, 88, 89). These cells are mainly resident DCs that are embedded in the FRC layer and extend processes into the lumen of the conduit.

The conduit as a compacted interstitium

The conduit structure by itself appears rather unusual, as basement membranes normally form two-dimensional sheets that separate mesenchymal from epithelial compartments. However, when envisaging the conduit core as a very condensed form of a conventional interstitium, the whole arrangement appears more familiar and could be viewed as a compacted and tiny version of the peripheral interstitium that we described for the dermis. It is compacted to an extent that it appears as a system of microchannels that are bordered by a basement membrane. To appreciate the similarity between peripheral interstitium, we suggest the following thought

experiment: imagine a vascularized mesenchymal tissue and extend the luminal surface of the endothelium until the interstitium almost disappears. The curvature of the endothelial lumen eventually bends backwards, and the interendothelial junctions reconnect without changing endothelial polarity. The endothelial cells would now 'internalize' their own interstitium, and by wrapping around the ECM, they will seal it against the 'luminal' surface that is in contact with the hematopoietic cells. Such a tissue would now resemble the T-cell cortex, where the blood cells occupy the labyrinthine 'lumen' formed by the FRCs, and the extravasacular space would be too tiny to contain any cells. In such a view, the T-cell cortex would rather be a specialized intravascular compartment than an extravascular space. In the T-cell cortex, FRCs take the function of both interstitial fibroblasts and endothelial (or epithelial) cells. FRCs clearly display features of epithelial and endothelial cells (apical basal polarity, cell–cell junctions, an underlying basement membrane, expression of cytokeratins) but also have characteristics of a fibroblast with myofibroblastic features (production of interstitial matrix, smooth muscle actin, expression of desmin and vimentin) (57, 90, 91).

LN anatomy during development and inflammation

The FRC network is an extreme variant of stromal differentiation that is already emerging in the sinus where a certain but not as extensive condensation of stroma and ECM occurs. This morphological continuity becomes obvious when looking at large collagen bundles that branch off the fibrous capsule, cross the subcapsular sinus (here they are loosely decorated with basement membrane patches and covered with retothelial cells), and enter the T-cell parenchyma, where they become incorporated into the conduit network. The view of a condensed interstitium is also consistent with the ontogeny of the FRC. During developmental and inflammatory lymphorganogenesis, FRCs are described as 'organizer cells' that are differentiating in a mutual crosstalk with hematopoietic 'inducer cells' that provide lymphotoxin signals. These lymphotoxin signals drive the transformation process of undifferentiated scattered mesenchymal cells into the FRC lineage (92, 93). The origin of undifferentiated mesenchyme in adult tissues is unclear, but the pericyte pool might be an interesting source. The FRC differentiation, which goes along with the formation of cell–cell junctions and polarization, resembles mesenchymal condensations or mesenchymal epithelial transitions that are well described in many other organogenetic processes like bone formation or kidney development (94).

In terms of anatomical features, the T-cell area is rather homogenous and does not show qualitatively distinct regions.

A quantitatively distinguishable area has been termed 'cortical ridge.' This is the T-cell area in close vicinity to the B-cell follicles. The cortical ridge shows a high density of high endothelial venules, and also the spacing of the reticular fibers was described as more densely packed (95).

The T-cell area shows enormous plasticity. During acute inflammation, LNs massively expand within hours, and the number of lymphocytes in the node multiplies. Theoretically, the sponge-like architecture of the T-zone stroma would allow for a certain swelling without increasing the surface area of the FRC network that could at the same time maintain structural integrity. However, mechanical expansion does not seem to be the critical factor, as it has been shown that during LN swelling the FRC surface expands. Although quantitative data on FRC spacing during LN expansion are lacking, qualitative data indicate that the FRC network grows with the increasing number of lymphocytes (96). It will be interesting to find out which factors keep the FRC to T-cell ratio constant. One possibility is that such a homeostatic balance might be regulated by factors that also regulate organogenesis like lymphotoxins.

Solute transport within the T-cell zone: entry into the conduit system

While in the periphery and in the sinus interstitial fluid and particles percolate around the cells through the interstitial space, the situation is radically different within the T zone. Large molecules are completely excluded from the parenchyma; they remain restricted to the sinus. Small molecules cannot be detected between the T cells either, but they have access to the conduit core. After subcutaneous injection, small molecular weight tracer molecules exclusively locate within the conduits, where they are sheltered from the T cells by the conduit basement membrane and the FRC layer around it (29, 57, 87). The conduit system is not a blind ending network but is highly connected with the capillaries and venules of the cortex (67). The conduits drain their fluid into the bloodstream: subcutaneously injected small molecules appear within the lumen of the high endothelial venules within minutes, demonstrating a shortcut between lymphatic fluid and blood at the level of the first draining LN (58, 83).

What is the physiological mechanism behind this size selective and directed transport? It has been proposed that flow within the conduit is active, meaning that sinus-lining cells at the sinus cortex interface (where the conduits start) pump the interstitial fluid into the conduits in a size-selective manner. Gretz et al. (57) suggested that a high transcytotic activity of the sinus-lining cells might support this function. However, it is entirely unclear how the conduit system could actively maintain pressure gradients that promote directed movement of fluid through such a complex and highly interconnected meshwork. A theory of active transport would also require an active exclusion mechanism that prevents entry of solutes into the T zone and a resulting percolation between the T cells. A recently published study showed that a small molecular tracer quickly distributed from the subcapsular sinus into the B-cell follicles, where it located diffusely between the lymphocytes. Interestingly, within the T zone the tracer distribution was restricted to the conduits (97). As there is clearly no anatomical barrier between T and B zone, such observations are difficult to include in a theory of active fluid transport through the conduits.

We propose that solute distribution within the T zone is a simple consequence of the biophysical characteristics of the T-zone interstitium. Instead of postulating that solutes are actively pushed into and confined within the conduit compartment, we propose that the conduit is the only space where interstitial fluid can distribute for reasons of hydraulic conductivity. As mentioned above, the FRCs are highly polarized, and on their apical side, they do not display or bind any ECM molecules (29). As T cells or DCs do not produce their own ECM, the T-cell compartment does not contain any interstitium that fills the intercellular space. This is a highly unusual situation and means that T cells are shielded from any ECM environment. Even the 'fluid phase ECM' of the blood, the serum proteins, are absent as the interstitial fluid is exclusively channeled through the conduit. This is indicated by tracer experiments where soluble molecules below 10 kDa were not visible between the T cells but restricted to the conduit (58). Hence, T cells move within a 'vacuum' and are packed at maximal density (98). As such, the T-cell compartment resembles a cell pellet after centrifugation. It is likely that the hematopoietic cells in the T zone are so tightly packed that they almost slide along each other in a membrane to membrane fashion, just separated by a layer of transmembrane proteins and cell surface glycosaminoglycans (that remain to be characterized in detail).

Although direct measurements of the hydraulic conductivity within the T-cell area are missing, it is likely that both diffusion and convection are extremely low between the T cells and that all significant fluid movements happen in the porous environment of the conduit core. Such a 'passive' view of the conduit system also explains that tracers continuously disperse from the LN capsule through the sinus into the conduit system. The continuity of the interstitial matrix allows for a free distribution within the interstitium, driven by Starling's forces that define the direction of flow.

The simple model of the conduit as a compact version of the dermal interstitium that is following the same physiological rules also implies that the B-cell area is behaving fundamentally differently, as it allows the free distribution of small soluble molecules. In this context, it is interesting that B-cell follicles show a diffuse staining for hyaluronic acid (our unpublished data) and are positive for the ECM molecule vitronectin (99). These findings open the possibility that B cells are surrounded by an interstitium with larger hydraulic conductivity than the T cells.

The driving force of solute distribution in the conduit system

In most peripheral tissues, the capillary system is in a state of continuous filtration, while the lymphatics absorb the filtered fluid volume. The situation changes in tissues where fluid enters via a separate route and creates a fluid excess. This is the case for submucosal tissues, where fluid enters across the gut epithelium, and for LNs, where interstitial fluid enters via the sinus (19). In gut and LN, Starling's forces result in an interstitial flux toward efferent capillaries and venules and cause a flow of fluid and small molecules into the blood system. Hence, LNs are in a continuous state of fluid absorption, which is reflected by measurements that show that the protein content of the afferent lymph is far below that of the efferent lymph (100–104). It is likely that absorption in the LN is as important for maintaining peripheral fluid homeostasis as the recirculation of interstitial fluid via the thoracic duct.

Unfortunately, comparative measurements of the molecular weight distribution of proteins within afferent and efferent lymph are lacking. Such data would allow to quantitatively test the 70 kDa size exclusion volume of the conduit. They might be further of pharmacological importance, as the lymph-blood shortcut at the level of the draining LN might be an important route for how subcutaneously applied substances enter the blood circulation. To understand the interstitial flow within the conduit, we further require a more detailed view of its molecular composition and biophysical properties. The extent to which sugars carrying fixed charges are embedded within the core region and the basement membrane will be required to estimate its swelling force and the hydraulic conductivity.

It will be interesting also to test the conduit function during altered physiological states like in the absence of afferent lymph drainage and elevated venous pressure. Under homeostatic conditions, the conduit system does not fill via the blood system, but this might change upon alterations of hydrostatic conditions. It has been shown that artificially increasing the venous pressure not only leads to a higher peripheral filtration rate of plasma but also causes dilution of the efferent lymph. This steeper decrease in protein content of the afferent versus the efferent lymph was due to decreased fluid absorption in the draining LN (100). High venous pressures might even lead to retrograde filling of the conduits via the blood. Studying the fluid balance of LNs in detail would tell us if the conduit system does indeed follow the rules of Starling or if active transport mechanisms, like water transport via aquaporin channels that are expressed in sinus-lining cells and LN endothelium (60), play a role.

When reflecting the physiology of fluid transport in LNs, it is interesting that the conduits of the spleen (105) and the thymic medulla (our unpublished data) fill via the blood system. In both cases, the conduits are solely connected to the blood vessels and the organs have no additional supply via lymphatics. Hence, these tissues should be in a state of continuous apillary filtration which matches the direction of interstitial flux within their conduits.

Small molecules and fluid are channeled through the conduit system of the T-cell cortex and drain into the vasculature. If access into the T-cell area is completely restricted and no solutes leak into the parenchyma, then where does the filtration take place and which sense does it make to channel all liquid through the T-cell cortex? It was demonstrated that the cell type that has best access to the content of the conduit is the resident DC that extends processes through the FRC layer into the lumen of the conduit (29, 30, 88, 106). Via this route, DCs can sample the content of the interstitial fluid like any other DC in the periphery can. Soluble antigens can be acquired and presented but also extracellular signaling molecules produced in the periphery can potentially be sensed. Via the conduit, the resident DCs of the LNs are rapidly informed about the state of the periphery. In other words, the soluble periphery is continuously projected into the conduits, and resident DCs can read out its condition. Immunologically, this principle is most effective, as the only cell that has to collect environmental information is the DC. T cells are not involved in 'decision making'; they just receive instructions from the DC (7). The anatomy of the T zone guaranties that they are not exposed to information they never need.

Functional implications of the conduit system

Even more enigmatic than these proximate aspects of conduit mechanisms is the ultimate question concerning the adaptive value of excluding large molecules from the conduit. We propose that size exclusion is a universal and efficient way to prevent that the lymph–blood shunt within the draining node

is exploited by infectious agents. By depleting subcapsular macrophages, Junt *et al.* (77) demonstrated that the filtering function of the sinus is essential for preventing the spread of virus particles via the blood circulation. In the absence of the scavenger function of the macrophages, virus arriving with the interstitial fluid quickly distributed via the thoracic duct into the blood and became systemic (77). Especially in bigger animals (and humans), many LNs are connected 'in row' (17), and it is likely that if virus is not cleared in the first node it becomes trapped in one of the following. If the conduits would not filter out large particles that have the potential to replicate, the lymph–blood shortcut would support hematogenic distribution and therefore would be a fatal distribution system for pathogens. In other words: as the LN blood vessels absorb fluid, a LN interstitium without a size exclusion volume would compromise the entire filtering concept of the LN.

We think that a larger exclusion size of the conduit would be dangerous for the organism. But what would be the consequence if the FRC network were to lack an interstitium, if the conduits would not exist? Why are they useful? The experiment to genetically eliminate the FRC interstitium has not been done, so we have to rely on indirect evidence. Immunologically, there seem to be two main functions of conduits: distribution of soluble antigens and endogenous signaling molecules toward resident DCs and information relay from the periphery into the lumen of high endothelial venules. In the absence of conduits, resident DCs would most likely have no access to soluble antigens or cytokines produced in the periphery − all the information would need to be (slowly) carried in by infiltrating DCs. Although this sounds like a dramatic change, it is far from clear what role soluble molecules have for the course of T-cell immune responses. Itano *et al.* (106) showed that soluble antigen presented on resident DCs can elicit T-cell responses. However, these responses were not sustained, and it is possible that they rather act as initiators that have to be consolidated by later incoming DCs. The only infectious model where immunity has been shown to be mainly triggered by soluble antigen is leishmaniasis (107). It remains to be shown how general such processes are and if soluble antigens are as important for the triggering of T-cell responses as they are for humoral immunity. Current data suggested that for tolerance induction, soluble antigens are not decisive, as maintaining tolerance is completely dependent on CCR7-mediated steady state migration of DCs (108). Much work has to be done on the role of soluble antigen.

The conduits as an information distribution system for resident DCs have not been addressed directly, and it would be interesting to see how resident DCs react to soluble cytokines or chemokines that arrive with the afferent lymph. Conduits as information superhighways have been studied in another context. It was demonstrated that chemokines produced in the periphery are rapidly (within seconds) channeled with the interstitial flux via the conduits into the lumen of high endothelial venules (109, 110). Here, they became immobilized to the luminal side of the endothelium, were sensed by circulating lymphocytes, and modulated their entry into the parenchyma. This system was interpreted as a remote control of the LN by the peripheral tissue and completes the picture of the LN as an immunological projection of the periphery that can rapidly adapt to peripheral threats (110).

A completely neglected context in which conduits might play a decisive role is fluid homeostasis. The fact that high amounts of fluids are resorbed into the blood circulation within the draining LN suggests that in the absence of conduits, interstitial fluid would either recirculate entirely via the efferent lymph and the thoracic duct or peripheral edema would develop. Unfortunately, data on the thoracic duct transport volume and the hydration state of peripheral tissues in mice lacking LNs for genetic reasons are not available.

Cell migration within the T-cell cortex

The functions of the FRC network are not entirely connected with the formation of conduits. As the only non-hematopoietic cells of the T-cell cortex, the FRCs are also organizing the migratory patterns of the blood cells. Cell migration patterns within the T-cell cortex were subjects of intense investigation during the last years, and many excellent reviews on this topic are available (9, 11–13). Here, we focus on the direct role of the stromal network for T-cell and DC migration. Although Gretz *et al.* (57) predicted that the FRC network plays a decisive role in guiding T cells through the LN, the reticular network was long ignored by intravital microscopists studying the swarming of T cells. The pathway taken by T cells was described as a random walk, and the encounters with DCs were regarded as random collisions (11, 57, 111). Bajenoff *et al.* (112) demonstrated that the opposite is the case: they showed that the routes of T-cell migration are not at all random but rather deterministic, as they lead preferentially along the FRC network. A theoretical model that tried to match experimental data on T-cell movement came to the same conclusion (113). By simultaneously visualizing T cells and FRCs *in vivo*, Bajenoff *et al.* (112) showed that the migration tracks of most T cells were aligned with the FRC scaffold. The migration direction of the T cells on the tracks was random. Hence, the FRCs appear to be an adhesive and chemokinetic surface that lack intrinsic

directional information (112, 114). FRCs are the producers of the homeostatic chemokines CCL19 and CCL21 that bind to the chemokine receptor CCR7 that is expressed on naive T cells (54, 115, 116). Both chemokines trigger and maintain the motile state of T cells and are essential for their swarming behavior. As CCL21 immobilizes to the FRC network, it is possible that the FRC network forms a chemokinetic surface that keeps the T cells dynamic and at the same time restricts their migration to the T-cell area. Such a system of chemokinetic surfaces has the attractive potential to generate high migration dynamics within sharp boundaries. In an independent study, the Germain laboratory (117) proved another important principle: cytotoxic T cells are able to respond quickly and flexibly to chemokines that are locally released by a successfully interacting pair of DC and helper T cell. Single cell tracking *in vivo* revealed that cytotoxic T cells actively chemotax toward the signal source (117). This finding means that the chemokinetic principle of swarming can be locally overcome by gradients that steer cells in a certain direction. If this directional migration is still guided along the FRC network or if T cells become autonomous from the chemokinetic scaffold once they follow soluble gradients is unknown. Many issues have to be resolved until a cell biological model of migration within the cortex will be available. Determining the role of soluble versus immobilized chemokines is one, while the question how T cells adhere to the FRC surface is another. It is also unclear how FRCs exactly handle the chemokines they produce. Interestingly, most of the CCL21 in the LN associates with the basement membrane of the conduit, where it likely immobilizes to the heparan sulfate residues (our unpublished data). Can the FRCs actively shuttle chemokine onto their apical surface where the T cells can sense it, and could such a step be flexibly regulated?

It is likely that DC migration within the cortex follows in principle similar rules: the population of resident DCs is partially embedded into the FRC layer, and it was shown also that antigen-carrying DCs immigrating from the periphery become incorporated into these networks (80). Like naive T cells, immigrating DCs respond primarily to CCR7 ligands (31). How the resident DCs couple to the FRC network is unknown, but it is most likely that they use cell surface receptors to interact with conduit and FRCs. One study showed that the DC population most tightly associated with conduits expresses high levels of a collagen-binding integrin (118). Importantly, migration along the FRC tracks leads the T cells directly into the DC networks and is therefore an ideal strategy to maximize encounters. However, testing the importance of these optimization strategies will require immunological

methods that challenge the detection limit of the adaptive immune system. Most of the common manipulations work with high doses of antigen and high frequencies of (transgenic) T cells that easily find each other, even in the absence of sophisticated guidance systems.

The functional unit of the T zone

We reviewed the anatomical and physiological features of a LN that define its function as a filter for soluble molecules and as an organizer of cellular encounters. We described in detail how the conduit, its FRC sleeve, the DCs embedded between the FRCs and the T cells gliding along the FRC surface form the functional unit of the T-cell zone. This functional unit is the
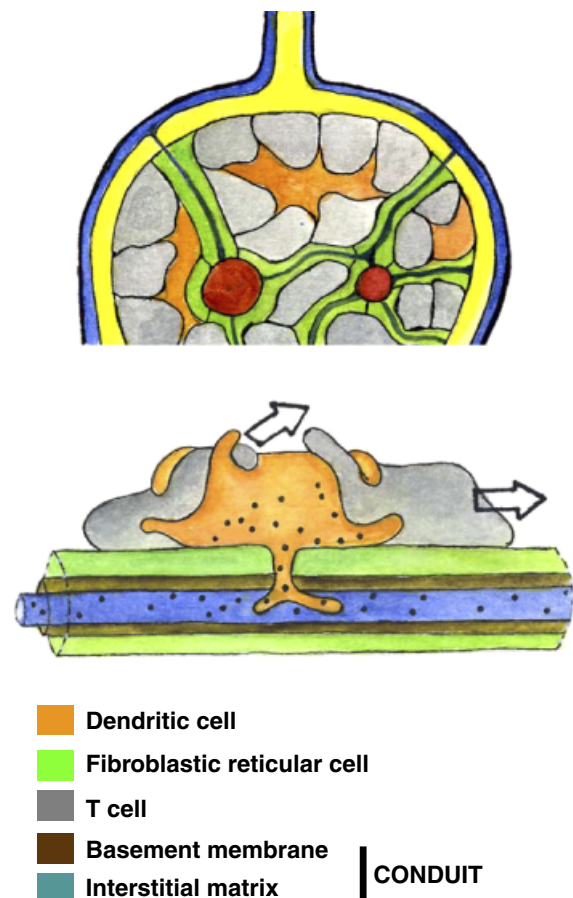

Dendritic cell
Fibroblastic reticular cell
T cell
Basement membrane
Interstitial matrix | **CONDUIT**

Fig. 4. **Functional unit of the T-cell cortex.** Upper schematic: the T-cell cortex is packed with T cells (gray) and dendritic cells (orange) and is interspersed with FRCs (green) that contain interstitial matrix in their lumen and connect with the blood vessels (red). Lower schematic: FRCs enwrap the conduit that consists of interstitial matrix and a surrounding basement membrane (brown). DCs associate with the FRCs and extend processes into the conduit lumen that can take up small molecules that are flushed through the conduit toward the blood vessels. T cells move on the surface of the FRCs and collide with the DCs.

essential environment that supports the principle of the adaptive immune system, where rare cell–cell encounters have to be selected. Accordingly, the functional unit characterizes not only all secondary lymphatic organs but it forms almost everywhere in the sustained presence of lymphocytes. Likely driven by cell surface lymphotoxin, the mesenchymal condensation is triggered that ultimately leads to the assembly of conduits, FRC networks, embedded DCs, and swarming T cells that are searching their cognate antigen. Accordingly, conduit-like structures are not only found in secondary but also in tertiary lymphatic organs and even in chronically inflamed areas like the perivascular space and the parenchyma of brains of multiple sclerosis patients (119, 120) (Fig. 4).

Conclusion

Although LNs gained much attention during the last years of intense dynamic imaging, they are still frequently viewed as simple containers for swarming and interacting blood cells. However, they are much more, and it is beyond doubt that the LN's complex stromal infrastructure is absolutely essential for organizing the dynamic state of order required for the high encounter rates between innate and adaptive immune cells. We are still far away from an integrated physiological concept of lymph nodes as the filter stations of the interstitium. It will be necessary to collect basic physiological data on LN fluid homeostasis under normal and inflammatory conditions and integrate them into the concept of adaptive immune priming.

References

1. Auffray C, et al. Monitoring of blood vessels and tissues by a population of monocytes with patrolling behavior. Science 2007;**317**:666–670.

2. Dustin ML. Stop and go traffic to tune T cell responses. Immunity 2004;**21**:305–314.

3. Phillipson M, Heit B, Colarusso P, Liu L, Ballantyne CM, Kubes P. Intraluminal crawling of neutrophils to emigration sites: a molecularly distinct process from adhesion in the recruitment cascade. J Exp Med 2006;**203**:2569–2575.

4. von Andrian UH, Mempel TR. Homing and cellular traffic in lymph nodes. Nat Rev Immunol 2003;**3**:867–878.

5. Blattman JN, et al. Estimating the precursor frequency of naive antigen-specific CD8 T cells. J Exp Med 2002;**195**:657–664.

6. Moon JJ, et al. Naive CD4(+) T cell frequency varies for different epitopes and predicts repertoire diversity and response magnitude. Immunity 2007;**27**:203–213.

7. Reis e Sousa C. Dendritic cells in a mature age. Nat Rev Immunol 2006;**6**:476–483.

8. Luster AD, Alon R, von Andrian UH. Immune cell migration in inflammation: present and future therapeutic targets. Nat Immunol 2005;**6**:1182–1190.

9. Bajenoff M, Egen JG, Qi H, Huang AY, Castellino F, Germain RN. Highways, byways and breadcrumbs: directing lymphocyte traffic in the lymph node. Trends Immunol 2007;**28**:346–352.

10. Karrer U, et al. On the key role of secondary lymphoid organs in antiviral immune responses studied in alymphoplastic (aly/aly) and spleenless (Hox11(−)/−) mutant mice. J Exp Med 1997;**185**:2157–2170.

11. Cahalan MD, Parker I. Imaging the choreography of lymphocyte trafficking and the immune response. Curr Opin Immunol 2006;**18**:476–482.

12. Germain RN, et al. An extended vision for dynamic high-resolution intravital immune imaging. Semin Immunol 2005;**17**:431–441.

13. Henrickson SE, von Andrian UH. Single-cell dynamics of T-cell priming. Curr Opin Immunol 2007;**19**:249–258.

14. Allen CD, Okada T, Cyster JG. Germinal-center organization and cellular dynamics. Immunity 2007;**27**:190–202.

15. Swartz MA. The physiology of the lymphatic system. Adv Drug Deliv Rev 2001;**50**:3–20.

16. Levick JR. Flow through interstitium and other fibrous matrices. Q J Exp Physiol 1987;**72**:409–437.

17. Pabst R. Plasticity and heterogeneity of lymphoid organs. What are the criteria to call a lymphoid organ primary, secondary or tertiary? Immunol Lett 2007;**112**:1–8.

18. Skobe M, Detmar M. Structure, function, and molecular control of the skin lymphatic system. J Investig Dermatol Symp Proc 2000;**5**:14–19.

19. Levick JR. Capillary filtration–absorption balance reconsidered in light of dynamic extravascular factors. Exp Physiol 1991;**76**:825–857.

20. Rutkowski JM, Swartz MA. A driving force for change: interstitial flow as a morphoregulator. Trends Cell Biol 2007;**17**:44–50.

21. Griffith LG, Swartz MA. Capturing complex 3D tissue physiology in vitro. Nat Rev Mol Cell Biol 2006;**7**:211–224.

22. Swartz MA, Fleury ME. Interstitial flow and its effects in soft tissues. Annu Rev Biomed Eng 2007;**9**:229–256.

23. Schmid-Schonbein GW. Microlymphatics and lymph flow. Physiol Rev 1990;**70**:987–1028.

24. Bert JL, Reed RK. Flow conductivity of rat dermis is determined by hydration. Biorheology 1995;**32**:17–27.

25. Guyton AC, Prather J, Scheel K, McGehee J. Interstitial fluid pressure. IV. Its effect on fluid movement through the capillary wall. Circ Res 1966;**19**:1022–1030.

26. Guyton AC, Scheel K, Murphree D. Interstitial fluid pressure. 3. Its effect on resistance to tissue fluid mobility. Circ Res 1966;**19**:412–419.

27. Rutkowski JM, Moya M, Johannes J, Goldman J, Swartz MA. Secondary lymphedema in the mouse tail: lymphatic hyperplasia, VEGF-C upregulation, and the protective role of MMP-9. Microvasc Res 2006;**72**:161–171.

28. De Vries IJ, et al. Effective migration of antigen-pulsed dendritic cells to lymph nodes in melanoma patients is determined by their maturation state. Cancer Res 2003;**63**:12–17.

29. Sixt M, et al. The conduit system transports soluble antigens from the afferent lymph to resident dendritic cells in the T cell area of the lymph node. Immunity 2005;**22**:19–29.

30. Itano AA, Jenkins MK. Antigen presentation to naive CD4 T cells in the lymph node. Nat Immunol 2003;**4**:733–739.

31. Randolph GJ, Angeli V, Swartz MA. Dendritic-cell trafficking to lymph nodes through lymphatic vessels. Nat Rev Immunol 2005;**5**:617–628.

32. Lauffenburger DA, Horwitz AF. Cell migration: a physically integrated molecular process. Cell 1996;**84**:359–369.

33. Wolf K, Muller R, Borgmann S, Brocker EB, Friedl P. Amoeboid shape change and contact guidance: T-lymphocyte crawling through fibrillar collagen is independent of matrix remodeling by MMPs and other proteases. Blood 2003;**102**:3262–3269.

34. Friedl P. Prespecification and plasticity: shifting mechanisms of cell migration. Curr Opin Cell Biol 2004;**16**:14–23.

35. Timpl R. Macromolecular organization of basement membranes. Curr Opin Cell Biol 1996;**8**:618–624.

36. Parish CR. The role of heparan sulphate in inflammation. Nat Rev Immunol 2006;**6**:633–643.

37. Sasaki T, Fassler R, Hohenester E. Laminin: the crux of basement membrane assembly. J Cell Biol 2004;**164**:959–963.

38. Jarad G, Cunningham J, Shaw AS, Miner JH. Proteinuria precedes podocyte abnormalities inLamb2 − / − mice, implicating the glomerular basement membrane as an albumin barrier. J Clin Invest 2006; **116**:2272–2279.

39. Levick JR. Fluid exchange across endothelium. Int J Microcirc Clin Exp 1997; **17**:241–247.

40. Hirakawa S, et al. Identification of vascular lineage-specific genes by transcriptional profiling of isolated blood vascular and lymphatic endothelial cells. Am J Pathol 2003;**162**:575–586.

41. Lymboussaki A, et al. Expression of the vascular endothelial growth factor C receptor VEGFR-3 in lymphatic endothelium of the skin and in vascular tumors. Am J Pathol 1998;**153**:395–403.

42. Podgrabinska S, Braun P, Velasco P, Kloos B, Pepper MS, Skobe M. Molecular characterization of lymphatic endothelial cells. Proc Natl Acad Sci USA 2002;**99**:16069–16074.

43. Sauter B, Foedinger D, Sterniczky B, Wolff K, Rappersberger K. Immunoelectron microscopic characterization of human dermal lymphatic microvascular endothelial cells. Differential expression of CD31, CD34, and type IV collagen with lymphatic endothelial cells vs blood capillary endothelial cells in normal human skin, lymphangioma, and hemangioma in situ. J Histochem Cytochem 1998;**46**:165–176.

44. Vainionpaa N, et al. Basement membrane protein distribution in LYVE-1-immunoreactive lymphatic vessels of normal tissues and ovarian carcinomas. Cell Tissue Res 2007;**328**:317–328.

45. Hotary K, Li XY, Allen E, Stevens SL, Weiss SJ. A cancer cell metalloprotease triad regulates the basement membrane transmigration program. Genes Dev 2006;**20**: 2673–2686.

46. Conrad C, et al. Alpha1beta1 integrin is crucial for accumulation of epidermal T cells and the development of psoriasis. Nat Med 2007;**13**:836–842.

47. Price AA, Cumberbatch M, Kimber I, Ager A. Alpha 6 integrins are required for Langerhans cell migration from the epidermis. J Exp Med 1997;**186**:1725–1735.

48. Ratzinger G, et al. Matrix metalloproteinases 9 and 2 are necessary for the migration of Langerhans cells and dermal dendritic cells

from human and murine skin. J Immunol 2002;**168**:4361–4371.

49. Wang S, et al. Venular basement membranes contain specific matrix protein low expression regions that act as exit points for emigrating neutrophils. J Exp Med 2006;**203**:1519–1532.

50. Witte MH, et al. Structure function relationships in the lymphatic system and implications for cancer biology. Cancer Metastasis Rev 2006;**25**:159–184.

51. Irjala H, Alanen K, Grenman R, Heikkila P, Joensuu H, Jalkanen S. Mannose receptor (MR) and common lymphatic endothelial and vascular endothelial receptor (CLEVER)-1 direct the binding of cancer cells to the lymph vessel endothelium. Cancer Res 2003;**63**: 4671–4676.

52. Johnson LA, Clasper S, Holt AP, Lalor PF, Baban D, Jackson DG. An inflammation-induced mechanism for leukocyte transmigration across lymphatic vessel endothelium. J Exp Med 2006;**203**:2763–2777.

53. Baluk P, et al. Functionally specialized junctions between endothelial cells of lymphatic vessels. J Exp Med 2007;**204**:2349–2362.

54. Luther SA, Tang HL, Hyman PL, Farr AG, Cyster JG. Coexpression of the chemokines ELC and SLC by T zone stromal cells and deletion of the ELC gene in the plt/plt mouse. Proc Natl Acad Sci USA 2000;**97**:12694–12699.

55. Fleury ME, Boardman KC, Swartz MA. Autologous morphogen gradients by subtle interstitial flow and matrix interactions. Biophys J 2006;**91**:113–121.

56. Shields JD, Fleury ME, Yong C, Tomei AA, Randolph GJ, Swartz MA. Autologous chemotaxis as a mechanism of tumor cell homing to lymphatics via interstitial flow and autocrine CCR7 signaling. Cancer Cell 2007;**11**:526–538.

57. Gretz JE, Anderson AO, Shaw S. Cords, channels, corridors and conduits: critical architectural elements facilitating cell interactions in the lymph node cortex. Immunol Rev 1997;**156**:11–24.

58. Gretz JE, Norbury CC, Anderson AO, Proudfoot AE, Shaw S. Lymph-borne chemokines and other low molecular weight molecules reach high endothelial venules via specialized conduits while a functional barrier limits access to the lymphocyte microenvironments in lymph node cortex. J Exp Med 2000;**192**:1425–1440.

59. He Y. Scanning electron microscope studies of the rat mesenteric lymph node with special reference to high-endothelial venules and hitherto unknown lymphatic labyrinth. Arch Histol Jpn 1985;**48**:1–15.

60. Ohtani O, Ohtani Y, Carati CJ, Gannon BJ. Fluid and cellular pathways of rat lymph

nodes in relation to lymphatic labyrinths and Aquaporin-1 expression. Arch Histol Cytol 2003;**66**:261–272.

61. Fujita T, Miyoshi M, Murakami T. Scanning electron microscope observation of the dog mesenteric lymph node. Z Zellforsch Mikrosk Anat 1972;**133**:147–162.

62. Hammerling B, Grund C, Boda-Heggemann J, Moll R, Franke WW. The complexus adhaerens of mammalian lymphatic endothelia revisited: a junction even more complex than hitherto thought. Cell Tissue Res 2006;**324**:55–67.

63. Schmelz M, Franke WW. Complexus adhaerentes, a new group of desmoplakin-containing junctions in endothelial cells: the syndesmos connecting retothelial cells of lymph nodes. Eur J Cell Biol 1993; **61**:274–289.

64. Wacker HH. Sinus lining cells. Immune accessory cells of lymph node sinuses. Veroff Pathol 1994;**143**:1–217.

65. Engering A, et al. Dynamic populations of dendritic cell-specific ICAM-3 grabbing nonintegrin-positive immature dendritic cells and liver/lymph node-specific ICAM-3 grabbing nonintegrin-positive endothelial cells in the outer zones of the paracortex of human lymph nodes. Am J Pathol 2004;**164**:1587–1595.

66. Fujita T, Ushiki T. Scanning electron microscopic observations of the immunodefensive systems with special reference to the surface morphology of the non-lymphoid cells. Arch Histol Cytol 1992;**55** (Suppl.): 105–113.

67. Ushiki T, Ohtani O, Abe K. Scanning electron microscopic studies of reticular framework in the rat mesenteric lymph node. Anat Rec 1995;**241**:113–122.

68. Clark SL Jr. The reticulum of lymph nodes in mice studied with the electron microscope. Am J Anat 1962;**110**:217–257.

69. Compton CC, Raviola E. Structure of the sinus-lining cells in the popliteal lymph node of the rabbit. Anat Rec 1985;**212**: 408–423.

70. Moe RE. Electron microscopic appearance of the parenchyma of lymph nodes. Am J Anat 1964;**114**:341–369.

71. Kramer RH, Rosen SD, McDonald KA. Basement-membrane components associated with the extracellular matrix of the lymph node. Cell Tissue Res 1988;**252**: 367–375.

72. Farr AG, Cho Y, De Bruyn PP. The structure of the sinus wall of the lymph node relative to its endocytic properties and transmural cell passage. Am J Anat 1980;**157**:265–284.

73. Angeli V, et al. B cell-driven lymphangiogenesis in inflamed lymph nodes enhances dendritic cell mobilization. Immunity 2006;**24**:203–215.

74. Glazyrin AL, et al. Distribution of colloidal gold tracer within rat parasternal lymph nodes after intrapleural injection. Anat Rec 1995;**241**:175–180.

75. Linehan SA, Martinez-Pomares L, Stahl PD, Gordon S. Mannose receptor and its putative ligands in normal murine lymphoid and nonlymphoid organs: in situ expression of mannose receptor by selected macrophages, endothelial cells, perivascular microglia, and mesangial cells, but not dendritic cells. J Exp Med 1999;**189**:1961–1972.

76. Carrasco YR, Batista FD. B cells acquire particulate antigen in a macrophage-rich area at the boundary between the follicle and the subcapsular sinus of the lymph node. Immunity 2007;**27**:160–171.

77. Junt T, et al. Subcapsular sinus macrophages in lymph nodes clear lymph-borne viruses and present them to antiviral B cells. Nature 2007;**450**:110–114.

78. Phan TG, Grigorova I, Okada T, Cyster JG. Subcapsular encounter and complement-dependent transport of immune complexes by lymph node B cells. Nat Immunol 2007;**8**:992–1000.

79. Sainte-Marie G, Peng FS. Diffusion of a lymph-carried antigen in the fiber network of the lymph node of the rat. Cell Tissue Res 1986;**245**:481–486.

80. Lindquist RL, et al. Visualizing dendritic cell networks in vivo. Nat Immunol 2004;**5**: 1243–1250.

81. Worbs T, Mempel TR, Bolter J, von Andrian UH, Forster R. CCR7 ligands stimulate the intranodal motility of T lymphocytes in vivo. J Exp Med 2007;**204**:489–495.

82. Wei SH, et al. Sphingosine 1-phosphate type 1 receptor agonism inhibits transendothelial migration of medullary T cells to lymphatic sinuses. Nat Immunol 2005;**6**:1228–1235.

83. Anderson AO, Anderson ND. Studies on the structure and permeability of the microvasculature in normal rat lymph nodes. Am J Pathol 1975;**80**:387–418.

84. Sumen C, Mempel TR, Mazo IB, von Andrian UH. Intravital microscopy: visualizing immunity in context. Immunity 2004;**21**:315–329.

85. Gretz JE, Kaldjian EP, Anderson AO, Shaw S. Sophisticated strategies for information encounter in the lymph node: the reticular network as a conduit of soluble information and a highway for cell traffic. J Immunol 1996;**157**:495–499.

86. Hayakawa M, Kobayashi M, Hoshino T. Microfibrils: a constitutive component of reticular fibers in the mouse lymph node. Cell Tissue Res 1990;**262**:199–201.

87. Kaldjian EP, Gretz JE, Anderson AO, Shi Y, Shaw S. Spatial and molecular organization of lymph node T cell cortex: a labyrinthine cavity bounded by an epithelium-like monolayer of fibroblastic reticular cells anchored to basement membrane-like extracellular matrix. Int Immunol 2001;**13**:1243–1253.

88. Anderson AO, Shaw S. Conduit for privileged communications in the lymph node. Immunity 2005;**22**:3–5.

89. Hayakawa M, Kobayashi M, Hoshino T. Direct contact between reticular fibers and migratory cells in the paracortex of mouse lymph nodes: a morphological and quantitative study. Arch Histol Cytol 1988;**51**: 233–240.

90. Link A, et al. Fibroblastic reticular cells in lymph nodes regulate the homeostasis of naive T cells. Nat Immunol 2007;**8**: 1255–1265.

91. Moll R, von Bassewitz DB, Schulz U, Franke WW. An unusual type of cytokeratin filament in cells of a human cloacogenic carcinoma derived from the anorectal transition zone. Differentiation 1982; **22**:25–40.

92. Mebius RE. Organogenesis of lymphoid tissues. Nat Rev Immunol 2003;**3**:292–303.

93. Okuda M, Togawa A, Wada H, Nishikawa S. Distinct activities of stromal cells involved in the organogenesis of lymph nodes and Peyer's patches. J Immunol 2007;**179**:804–811.

94. Thesleff I, Vaahtokari A, Partanen AM. Regulation of organogenesis. Common molecular mechanisms regulating the development of teeth and other organs. Int J Dev Biol 1995;**39**:35–50.

95. Katakai T, Hara T, Lee JH, Gonda H, Sugai M, Shimizu A. A novel reticular stromal structure in lymph node cortex: an immuno-platform for interactions among dendritic cells, T cells and B cells. Int Immunol 2004;**16**:1133–1142.

96. Katakai T, Hara T, Sugai M, Gonda H, Shimizu A. Lymph node fibroblastic reticular cells construct the stromal reticulum via contact with lymphocytes. J Exp Med 2004;**200**:783–795.

97. Pape KA, Catron DM, Itano AA, Jenkins MK. The humoral immune response is initiated in lymph nodes by B cells that acquire soluble antigen directly in the follicles. Immunity 2007;**26**:491–502.

98. Soderstrom N, Stenstrom A. Outflow paths of cells from the lymph node parenchyma to the efferent lymphatics – observations in thin section histology. Scand J Haematol 1969;**6**:186–196.

99. Castanos-Velez E, Biberfeld P, Patarroyo M. Extracellular matrix proteins and integrin receptors in reactive and non-reactive lymph nodes. Immunology 1995;**86**:270–278.

100. Adair TH, Guyton AC. Modification of lymph by lymph nodes. II. Effect of increased lymph node venous blood pressure. Am J Physiol 1983;**245**:H616–H622.

101. Adair TH, Guyton AC. Modification of lymph by lymph nodes. III. Effect of increased lymph hydrostatic pressure. Am J Physiol 1985;**249**:H777–H782.

102. Adair TH, Moffatt DS, Paulsen AW, Guyton AC. Quantitation of changes in lymph protein concentration during lymph node transit. Am J Physiol 1982; **243**:H351–H359.

103. Jacobsson S, Kjellmer I. Flow and protein content of lymph in resting and exercising skeletal muscle. Acta Physiol Scand 1964;**60**:278–285.

104. Quin JW, Shannon AD. The influence of the lymph node on the protein concentration of efferent lymph leaving the node. J Physiol 1977;**264**:307–321.

105. Nolte MA, et al. A conduit system distributes chemokines and small blood-borne molecules through the splenic white pulp. J Exp Med 2003;**198**:505–512.

106. Itano AA, et al. Distinct dendritic cell populations sequentially present antigen to CD4T cells and stimulate different aspects of cell-mediated immunity. Immunity 2003;**19**: 47–57.

107. Iezzi G, et al. Lymph node resident rather than skin-derived dendritic cells initiate specific T cell responses after Leishmania major infection. J Immunol 2006;**177**: 1250–1256.

108. Pabst O, Bernhardt G, Forster R. The impact of cell-bound antigen transport on mucosal tolerance induction. J Leukoc Biol 2007;**82**:795–800.

109. Larsen CG, Anderson AO, Appella E, Oppenheim JJ, Matsushima K. The neutrophil-activating protein (NAP-1) is also chemotactic for T lymphocytes. Science 1989;**243**:1464–1466.

110. Palframan RT, et al. Inflammatory chemokine transport and presentation in HEV: a remote control mechanism for monocyte recruitment to lymph nodes in inflamed tissues. J Exp Med 2001;**194**:1361–1373.

111. Wei SH, Parker I, Miller MJ, Cahalan MD. A stochastic view of lymphocyte motility and trafficking within the lymph node. Immunol Rev 2003;**195**:136–159.

112. Bajenoff M, et al. Stromal cell networks regulate lymphocyte entry, migration, and territoriality in lymph nodes. Immunity 2006;**25**:989–1001.

113. Beltman JB, Maree AF, Lynch JN, Miller MJ, de Boer RJ. Lymph node topology dictates T cell migration behavior. J Exp Med 2007;**204**:771–780.

114. Mempel TR, Junt T, von Andrian UH. Rulers over randomness: stroma cells guide lymphocyte migration in lymph nodes. Immunity 2006;**25**:867–869.

115. Asperti-Boursin F, Real E, Bismuth G, Traut-mann A, Donnadieu E. CCR7 ligands control basal T cell motility within lymph node slices in a phosphoinositide 3-kinase-independent manner. J Exp Med 2007;**204**:1167–1179.

116. Woolf E, et al. Lymph node chemokines promote sustained T lymphocyte motility without triggering stable integrin adhesive-ness in the absence of shear forces. Nat Immunol 2007;**8**:1076–1085.

117. Castellino F, Huang AY, Altan-Bonnet G, Stoll S, Scheinecker C, Germain RN. Chemokines enhance immunity by guiding naive CD8+T cells to sites of CD4+T cell–dendritic cell interaction. Nature 2006;**440**: 890–895.

118. Pribila JT, Itano AA, Mueller KL, Shimizu Y. The alpha 1 beta 1 and alpha E beta 7 integrins define a subset of dendritic cells in peripheral lymph nodes with unique adhesive and antigen uptake properties. J Immunol 2004;**172**: 282–291.

119. van Horssen J, Bo L, Dijkstra CD, de Vries HE. Extensive extracellular matrix depositions in active multiple sclerosis lesions. Neurobiol Dis 2006;**24**:484–491.

120. van Horssen J, Bo L, Vos CM, Virtanen I, de Vries HE. Basement membrane proteins in multiple sclerosis-associated inflammatory cuffs: potential role in influx and transport of leukocytes. J Neuropathol Exp Neurol 2005;**64**:722–729.

Paper V

ARTICLES

Rapid leukocyte migration by integrin-independent flowing and squeezing

Tim Lämmermann[1], Bernhard L. Bader[3], Susan J. Monkley[4], Tim Worbs[5], Roland Wedlich-Söldner[2], Karin Hirsch[1], Markus Keller[3], Reinhold Förster[5], David R. Critchley[4], Reinhard Fässler[1] & Michael Sixt[1]

All metazoan cells carry transmembrane receptors of the integrin family, which couple the contractile force of the actomyosin cytoskeleton to the extracellular environment. In agreement with this principle, rapidly migrating leukocytes use integrin-mediated adhesion when moving over two-dimensional surfaces. As migration on two-dimensional substrates naturally overemphasizes the role of adhesion, the contribution of integrins during three-dimensional movement of leukocytes within tissues has remained controversial. We studied the interplay between adhesive, contractile and protrusive forces during interstitial leukocyte chemotaxis *in vivo* and *in vitro*. We ablated all integrin heterodimers from murine leukocytes, and show here that functional integrins do not contribute to migration in three-dimensional environments. Instead, these cells migrate by the sole force of actin-network expansion, which promotes protrusive flowing of the leading edge. Myosin II-dependent contraction is only required on passage through narrow gaps, where a squeezing contraction of the trailing edge propels the rigid nucleus.

The current model of metazoan cell migration is frequently described as a multistep cycle: F-actin polymerization at the cell front pushes out a membrane protrusion that subsequently becomes anchored to an extracellular substrate by transmembrane receptors of the integrin family. Integrins are dynamically coupled to the cytoskeleton and transduce the internal force that is generated when myosin II contracts the actin network. Contraction imposes retrograde pulling forces on the integrins, which in turn facilitates forward locomotion of the cell body[1–3]. The mammalian integrin family consists of 24 different functional heterodimers with individual binding specificities for cellular and extracellular ligands[4]. The integrin repertoire of each cell type defines which substrate it can use for this 'haptokinetic' (adhesion driven) mode of migration. Such intimate linkage between substrate-specific adhesion and migration restricts the migrating cells to preformed pathways, and thereby creates the determinism that is essential for many of the precise cell trafficking and positioning processes underlying compartmentalization and patterning during development and regeneration. As all mammalian cells with the exception of erythrocytes carry integrins on their surface, it is reasonable to assume that haptokinesis is a universal phenomenon[4,5].

Leukocytes are outstanding cells, as they are scattered throughout the body and have the potential to infiltrate any type of tissue. Rather than following exact routes and being restricted to specific compartments, leukocytes frequently undergo stochastic swarming with single cell migration velocities that are up to 100 times faster than mesenchymal and epithelial cell types[6,7]. What makes leukocytes so quick and flexible? In contrast to slow cells, migrating leukocytes undergo frequent shape changes and were therefore morphologically described as ''amoeboid''[8]. How these shape changes relate to actual locomotion is poorly investigated, and it is currently unknown if amoeboid migration represents a specialized strategy or just an accelerated variant of the above introduced migration paradigm that is only well established for slow cells. We therefore studied the inter-dependency of adhesion, protrusion and contraction in inflammatory cells. We demonstrate

that integrin-mediated adhesion is only necessary to overcome tissue barriers like the endothelial layer, while interstitial migration is autonomous from the molecular composition of the extracellular environment. Such adhesion-independent migration is driven by protrusive flowing of the anterior actin network of the cell and supported by squeezing actomyosin contractions of the trailing edge to propel the rigid nucleus through narrow spaces.

Dendritic cells migrate without integrins

As a model system to study interstitial leukocyte migration *in vivo*, we focused on dendritic cells (DCs), phagocytes that reside within peripheral tissues such as skin. They become activated upon wounding or infection, sample antigens and quickly migrate via the afferent lymphatic vessels into the draining lymph node where they act as antigen presenting cells[9]. DC migration is primarily guided by the two chemokines CCL19 and CCL21; these are expressed in lymphatic endothelium and the lymph nodes' T-cell area, and bind the CC-chemokine receptor 7 (CCR7), which is upregulated on DCs upon activation[10].

Flow cytometric analysis of DCs generated from mouse bone-marrow-derived stem cells revealed expression of the β_1, β_2, β_7 and α_v integrin families (Fig. 1a). To investigate the role integrins play in DC migration *in vivo*, we used a combinatorial mouse genetics approach to delete all integrin heterodimers from the surface of DCs, thereby generating phenotypically normal pan-integrin-deficient (integrin$^{-/-}$) DCs (Fig. 1a, see Supplementary Material, Methods, and Supplementary Figs 1, 2, 4c). We co-injected 1:1 mixtures of differentially labelled integrin$^{-/-}$ and wild-type DCs into the dermis of mouse footpads and quantified their arrival in T-cell areas of the draining lymph nodes. Surprisingly, wild-type and integrin$^{-/-}$ DCs arrived and localized in the T-cell area in an indistinguishable manner (Fig. 1b, c, Supplementary Fig. 3), whereas CCR7$^{-/-}$ DCs, which cannot interpret the directional information, failed to enter the lymph node (Fig. 1c) as previously described[10]. We next targeted integrin functionality indirectly by deleting the talin1 gene in DCs

[1]Department of Molecular Medicine, [2]Junior Research Group Cellular Dynamics and Cell Patterning, Max Planck Institute of Biochemistry, 82152 Martinsried, Germany. [3]Department of Nutritional Medicine, Technische Universität München, Munich, 85350 Freising, Germany. [4]Department of Biochemistry, University of Leicester, Leicester LE1 9HN, UK. [5]Institute of Immunology, Hannover Medical School, 30625 Hannover, Germany.
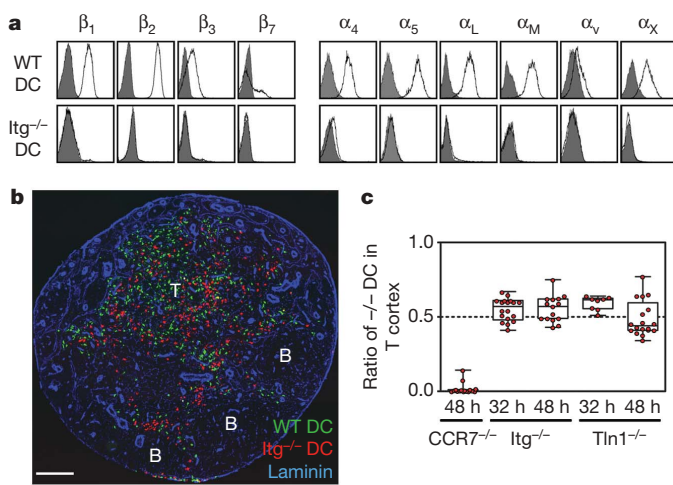
Figure 1 | Migration of integrin-deficient dendritic cells into lymph nodes.
a, Flow cytometric analysis of integrin subunits of wild-type (WT) and
integrin-deficient (Itg$^{-/-}$) dendritic cells (DCs) (integrin, unshaded; isotype
control, grey-shaded). **b, c**, *In vivo* migration of DCs after subcutaneous
injection into hind footpads of WT mice. At the time points indicated,
arrival of differentially labelled DCs in the lymph node was analysed.
b, Localization of DCs after 48 h. Composite of six separate images of a single
lymph node. Scale bar, 200 μm; B, B-cell follicle; T, T-cell cortex.
c, Quantitative histology. Dotted line at 0.5, 50% of DCs that migrated into
the lymph node are knockout DCs; Tln1, talin1. Red dots indicate single
experiments (1 lymph node); box shows median, 25%, 75% percentile;
whiskers show minimum, maximum.

(Supplementary Fig. 4a). The interaction of talin1 with integrin
cytoplasmic domains is required for integrin activation, ligand bind-
ing and coupling of F-actin to adhesion sites[11]. Accordingly, talin1
gene ablation in DCs did not affect the levels of integrin expression,
but completely abolished their ability to bind ligands (Supple-
mentary Fig. 4b–d). Again, arrival of talin1$^{-/-}$ DCs in lymph nodes
did not significantly differ from wild-type DCs (Fig. 1c).

To allow for a detailed comparison of the cellular dynamics of
wild-type and integrin$^{-/-}$ DCs within the different physiological
environments of their migration route, we employed two *in situ*
imaging approaches (Fig. 2). Representing the starting point of DC
migration, the interstitial space of the dermis is dominated by fibrillar
arrays of collagen bundles[12]. Using a newly developed set-up of *ex vivo*
live cell imaging within explanted ear dermis, we could directly visu-
alize DCs moving towards and entering the afferent lymphatic vessels
by wide-field microscopy (Fig. 2b, c, Supplementary Fig. 5). Single
cell tracking revealed no difference in the migratory behaviour of
wild-type, integrin$^{-/-}$ and talin1$^{-/-}$ DCs (Fig. 2c, d).

The lymph node constitutes a fundamentally different environment
for cellular migration, as it contains almost no freely accessible extra-
cellular matrix molecules but is densely packed with lymphocytes and
stroma cells[13,14]. To analyse the dynamics of intranodal DC migration
from the subcapsular sinus towards the T-cell area, we employed a
set-up of intravital two-photon microscopy of the popliteal lymph
nodes[15]. Evaluating a range of motility parameters, including cell
velocity, directional persistence, mean square displacement, motility
coefficients and morphology, we found that the movement behaviour
of wild-type and integrin$^{-/-}$ DCs was indistinguishable (Fig. 2e, f,
Supplementary Videos 1–3, data not shown).

2D but not 3D migration is integrin-dependent

On their way into the lymph node, DCs do not cross significant tissue
barriers, such as continuous endothelial or epithelial linings[12]. As
these processes have been shown to be integrin-dependent[16], we also
tested for extravasation of integrin$^{-/-}$ leukocytes from the blood
stream into the inflamed dermis, and found that it was indeed abo-
lished (Fig. 2g, Supplementary Fig. 6). This finding corroborates the
extravasation model in which integrin-mediated tight immobiliza-
tion of leukocytes to the luminal endothelial surface is necessary to
counteract the shear forces imposed by the blood flow[16]. In line with
this *in vivo* finding, we found that integrin$^{-/-}$ DCs were entirely
unable to adhere to and migrate on two-dimensional (2D) substrates.
Gravity was obviously not sufficient to confine the non-adherent cells
to planar surfaces and allow the transduction of traction forces

**Figure 2 | Integrin-independent
interstitial leukocyte migration
in vivo. a**, Scheme of the dendritic
cell (DC) migration path from the
skin via lymphatic vessels to the
lymph node; B, B-cell follicle; BV,
blood vessel; D, dermis; E, epidermis;
LN, lymph node; LV, lymphatic
vessel; T, T-cell cortex.
b–d, Migration of DCs within the
dermis of ear explants. **b**, Tracks of
DCs (red) entering LYVE-1$^+$ LVs
(green). **c**, Confocal images of whole
mount ear explants 2 h after addition
of DCs (red). DCs locate within the
lumen of LVs; all scale bars, 50 μm.
d, Speed and directional persistence
(DP, mean ± s.d.) of single cells (dots)
for wild-type (WT), integrin$^{-/-}$
(Itg$^{-/-}$) and talin1$^{-/-}$ (Tln1$^{-/-}$)
DCs. Red line, mean. **e, f**, Intravital
two-photon microscopy. **e**, 3D
tracking of WT (green, blue line) and
Itg$^{-/-}$ (red, yellow line) DCs
migrating in the interfollicular areas.
f, Quantification of the average speed
and DP (mean ± s.d.) of tracked
single cells (dots). Red line, mean.
g, Quantification of granulocytes
that extravasated from blood into ear
dermis (*n* = 6 for each mouse line).
Red line, median. *$P < 0.05$ (post hoc).

(Fig. 3a, b, Supplementary Fig. 4d, Supplementary Video 4). We conclude that extravasation requires integrin-mediated adhesion.

To better mimic the interstitial microenvironment, we established chemotaxis assays within artificial three-dimensional (3D) matrices of fibrin (a ligand for β_2 and β_3 integrins) and collagen I (a ligand for several members of the β_1 integrin subfamily). In this system, DCs persistently migrated along soluble gradients of CCL19 and showed amoeboid morphology and velocities that were comparable to our (and previously published[17]) *in vivo* observations. In agreement with our *in vivo* data and in contrast to 2D migration, integrin$^{-/-}$ and talin1$^{-/-}$ DCs migrated with speed and directional persistence that were indistinguishable from wild-type cells (Fig. 3c, Supplementary Fig. 7a, Supplementary Video 5). We also observed integrin-independent migration for chemotaxing B cells and granulocytes, suggesting a broader prevalence of this functional principle (Fig. 3d, Supplementary Fig. 7b).

Functional dissociation of front and back

To mechanistically understand how cells can move in the absence of integrin-mediated traction forces, we compared the integrin-dependent movement pattern of fibroblasts with that of leukocytes and found a striking difference. Leading edge protrusions of fibroblasts translocated collagen fibres towards the cell body, indicating the presence of rearward pulling forces and demonstrating that protrusion, adhesion and contraction are tightly coupled in this cell type (Supplementary Video 6)[18,19]. In contrast, chemotaxing DCs protruded without signs of anterior pulling forces while the trailing edge displayed an irregularly alternating contractile pattern. Contraction was characterized by shrinkage of the cell rear with concomitant forward-streaming of cytoplasmic matter (Supplementary Video 7). When we dynamically visualized activated myosin II, the motor system mediating contraction[1,2,20], by time-lapse imaging of DCs expressing a myosin light chain–GFP fusion protein, we found accumulation at the cell rear during contractile phases (Fig. 4a, Supplementary Fig. 8a, Supplementary Video 8). During non-contractile phases, the trailing edge remained motionless and

appeared to be passively dragged by the protruding cell front (Supplementary Video 7). These observations suggest that in contrast to slow moving cells, protrusion and contraction are spatio-temporally dissociated in leukocytes.

Receptor-mediated force transduction can only support forward movement if retrograde (contractile) but not anterograde (protrusive) forces are coupled to the environment[2,3]. To address how actomyosin contraction functionally contributes to leukocyte locomotion, we pharmacologically inhibited myosin II or its upstream-activator, Rho kinase. Irrespective of the presence of integrin function, either treatment severely reduced migration speeds of DCs, granulocytes and B cells (Fig. 4b, Supplementary Fig. 8e, data not shown). Nevertheless, the chemotactic gradient was still able to polarize the cell population. The leading edges of cells remained dynamic and protruded with normal speed towards the chemokine source. However, the cells were unable to move their trailing edges
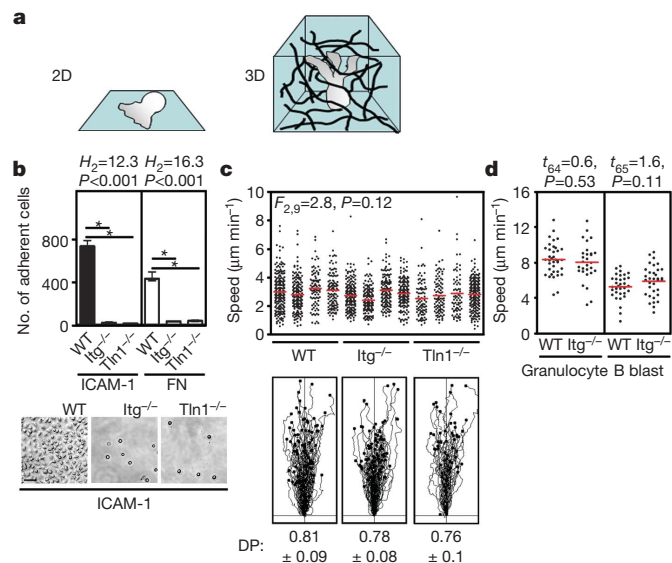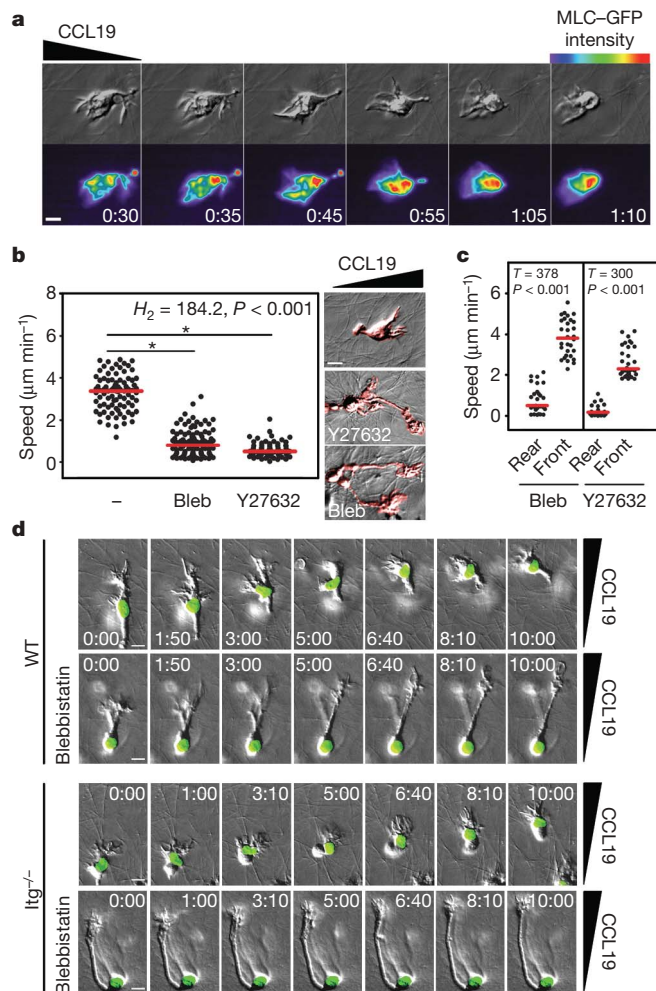

Figure 4 | Myosin II-dependent nuclear squeezing at the cell rear. a, Sequence of a myosin light chain (MLC)–GFP expressing wild-type (WT) dendritic cell (DC) migrating towards CCL19 in a 3D collagen gel; upper row, differential interference contrast (DIC) microscopy; lower row, MLC–GFP intensity profiles (encoded in pseudo-colours with red representing highest levels). Time in min:s. **b**, Left, velocities of single DCs (dots; red line, median), and right, DC morphology (coloured red, DIC microscopy), chemotaxing towards CCL19 in 3D collagen gels upon pharmacological inhibition. **c**, Speed of cell bodies (rear) versus cell protrusions (front) of DCs in the presence of inhibitor; red line, median. Bleb, blebbistatin; *$P < 0.05$ (post hoc). **d, e**, Time-lapse sequence of a WT (**d**) and integrin$^{-/-}$ (**e**) DC either with (lower row) or without (upper row) blebbistatin; DIC microscopy, nuclei (green). Time in min:s; scale bars, 5 µm (**a**), 10 µm (**b, d, e**).

Figure 3 | Integrin-independent leukocyte migration in 3D networks *in vitro*. a, 2D adhesion versus 3D migration of DCs. **b**, 2D adhesion on ICAM-1 and fibronectin (FN) 1 h after LPS stimulation. Top, quantification of the number of adherent cells (ICAM-1, $n = 6$; FN, $n = 8$ for each experiment). Bars, median values with interquartile range, *$P < 0.05$ (post hoc). Bottom, morphology of wild-type (WT), integrin$^{-/-}$ (Itg$^{-/-}$) and talin1$^{-/-}$ (Tln1$^{-/-}$) DCs. **c, d**, Velocities of chemotaxing leukocytes in 3D collagen matrices. **c**, Top, DCs (4 experiments per group); **d**, granulocytes, B cells. Dots, single cells; red line, mean. **c**, Bottom, single cell tracks of chemotaxing DCs; values indicate mean DP ± s.d.

(Fig. 4b–e, Supplementary Fig. 8b–d, Supplementary Video 9). This functional dissociation between front and back caused up to 30-fold cell elongation, and demonstrates that the leading edge migrates autonomously and without a need for receptor-mediated coupling of contractile forces to the extracellular matrix.

Trailing edge contraction propels the nucleus

How does trailing edge contraction contribute to cell body locomotion? In fibroblasts and leukocytes moving on 2D substrates, actomyosin contraction at the back is required to disassemble receptor binding-sites and subsequently retract the membrane[2,21,22]. Hence, blocking contraction causes membrane tethers at the trailing edge. Consistent with an adhesion-independent migration mode, we could not observe membrane tethers in myosin II-inhibited leukocytes migrating in 3D gels. We considered that the elongated phenotype with its rounded back was caused by the inability to move an internal resistance through narrow gaps within the gel. As the nucleus is the least elastic cellular compartment[23], we visualized DNA within chemotaxing DCs and granulocytes. In untreated cells, we observed continuous shape changes of nuclei, indicating deformation forces, while upon myosin II inhibition, spherical nuclei were immobilized at the rear ends of the cells (Figs 4d, e, Supplementary Fig. 8b–d, Supplementary Videos 10, 11).

Protrusion drives basal locomotion

Although 'locked' nuclei caused migration arrest in most cells, a few still showed locomotion. This residual migration was often characterized by cell body elongation and dragging of the nucleus (Fig. 5a, Supplementary Video 12). Such non-contractile movement was in line with our previous observations showing motile phases in the absence of trailing edge contractions. We hypothesized that such myosin II-independent migration might occur in areas of the collagen gel where external resistance was low due to increased spacing of the collagen fibres. To establish the relationship between internal contractile force and external resistance, we analysed DC chemotaxis in collagen gels of varying fibre spacing (Fig. 5b). In all collagen densities, myosin II-inhibited DCs were slower than untreated cells but importantly, they 'caught up' at lowest gel densities (Fig. 5b, Supplementary Video 13). A comparison of instantaneous velocities further showed that myosin II inhibition did not prevent DCs from reaching the same peak values as untreated cells (Supplementary Fig. 9a–c).

We conclude that, in contrast to the 'blebbing' model of amoeboid cell migration[24], cortical actin network contraction does not mediate locomotion itself but rather facilitates a protrusive mode of migration in confined environments where protrusion alone is unable to act against counter-forces. So in constricted areas, the cell overcomes internal and external resistance (rigidity of the nucleus and fibre density) by contraction (myosin II). Contractile force deforms the resistance and facilitates a purely protrusive mode of migration.

To challenge the concept of protrusive movement, we treated chemotaxing DCs with latrunculin B, which interferes with actin polymerization by depleting the pool of available functional G-actin monomers[25]. We found that this treatment reduced cell migration velocity in a dose-dependent manner (Fig. 5c). At intermediate concentrations, the trailing edge remained contractile and the nucleus was 'pushed' to the cell front (Fig. 5d, Supplementary Video 14). Consistent with a model where protrusion determines the speed of cell migration while contraction is only activated to overcome external resistances, the speed reduction of latrunculin B-treated cells was independent of gel density (Fig. 5b, c).

Discussion

We show that leukocytes migrate in the absence of specific adhesive interactions with the extracellular environment. This subversion of the metazoan principle makes them autonomous from the tissue context, and allows them to quickly and flexibly navigate through any organ without adaptations to alternating extracellular ligands. This strategy is in stark contrast to the haptokinetic migration principle that leads along preformed pathways and therefore promotes deterministic positioning. Adhesion independency better suits stochastic movement or chemotaxis where cells randomly migrate or follow soluble cues. Astonishingly, the protrusive flow of F-actin appears sufficient to drive rapid leukocyte locomotion in environments with large pore-size. This resembles the locomotion principle of nematode sperm cells that is entirely driven by treadmilling polymers of major sperm protein[26]. Only in narrow areas do leukocytes activate the contractile module to squeeze and propel the internal resistance of the nucleus in a manner resembling neuronal nucleokinesis[27]. This 'flowing and squeezing' migration model fulfils a central requirement for immune cell movement: the pericellular environment is transiently deformed but never digested[28] or
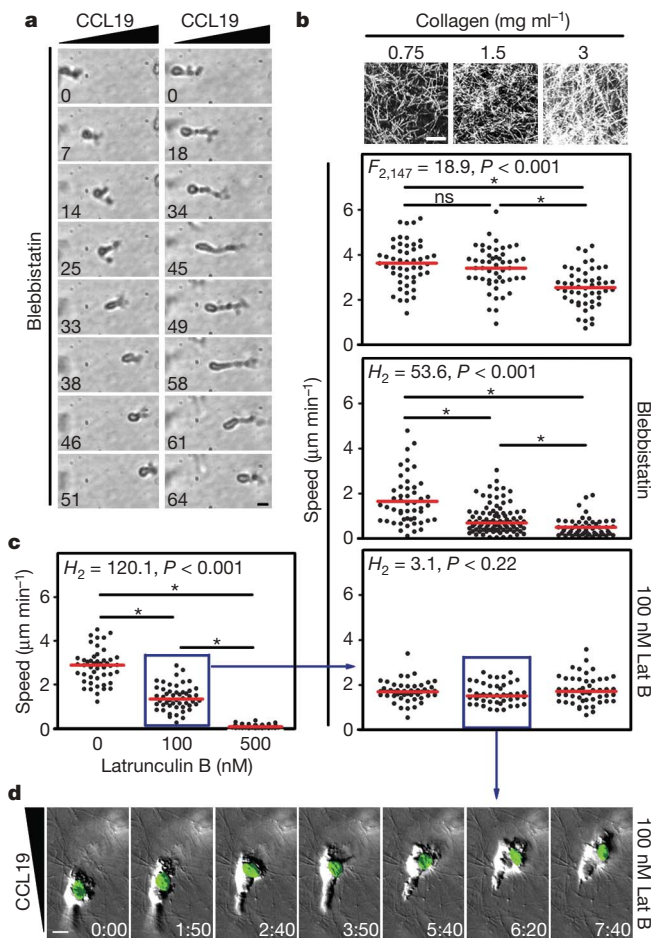
Figure 5 | Myosin II-independent protrusive migration of dendritic cells.
a, Two types of residual migration of wild-type (WT) dendritic cells (DCs) treated with blebbistatin in a standard 3D collagen gel. DCs either drag the nucleus behind with elongated appearance and low speed (right column) or appear morphologically normal with high speed (left column). Time in min. **b**, Top panel, confocal reflection microscopy of 3D collagen networks of different densities. Lower panels, velocities of single chemotaxing WT DCs (dots) in collagen gels with varying densities. Upper graph, no inhibitor; red line, mean. Middle graph, blebbistatin; red line, median. Bottom graph, 100 nM latrunculin B (partial actin depolymerization); red line, median. **c**, Velocity of single WT DCs (dots) in the presence of different concentrations of latrunculin B (1.6 mg ml^{-1} collagen); red line, median. In **b** and **c**, *P < 0.05 (post hoc). **d**, Time-lapse sequence of a 100 nM latrunculin B-treated WT DC; DIC microscopy, nuclei (green). Time, min:s. Blue boxes (in **b** and **c**) highlight experimental conditions that were used for follow-up experiments indicated by the blue arrow. Scale bars: 10 μm (**a**, **d**), 50 μm (**b**).

otherwise permanently remodelled which avoids 'collateral damage', caused by infiltrating cells.

The fact that leukocytes are able to move autonomously generates a new level of regulatory possibilities. Because surface bound chemokines and other immobilized extracellular signals do trigger integrin affinity[16] (unlike soluble chemokines), leukocyte integrins should no longer be viewed as force transducers during locomotion but as switchable immobilizing anchors that stop, slow down or confine high intrinsic motility to specifically assigned surfaces[29,30]. The role of integrins is therefore mostly to mediate retention, invasion, cell–cell communication and cell–cell adhesion[31].

METHODS SUMMARY

Generation of integrin-deficient leukocytes. Integrins and talin1 were targeted by generating mice with the genotype $\alpha_v^{flox/flox}$ (Supplementary Fig. 1), $\beta_1^{flox/flox}$ (ref. 32), $\beta_2^{-/-}$ (ref. 33), $\beta_7^{-/-}$ (ref. 34), Mx1Cre$^{+/-}$ (ref. 35) and talin1$^{flox/flox}$ (ref. 36), Mx1Cre$^{+/-}$, respectively. Cre expression in the haematopoietic system was induced by intraperitoneal injection of 250 µg Poly (I)·Poly (C) (Amersham Biosciences). 10–14 d after knockout induction DCs were generated from bone marrow suspension and matured with lipopolysaccharide (LPS). The DC culture was depleted for granulocytes and remaining integrin-positive contaminants by magnetic sorting (Miltenyi Biotech). DCs used for migration assays were >99% enriched for β_1 and α_v integrin knockout cells.

In situ live cell imaging. For dermal *ex vivo* microscopy, mouse ears were mechanically separated in dorsal and ventral halves, fluorescently stained with LYVE-1 antibody and immobilized with the epidermal side down. The dermis was overlaid with fluorescently labelled DCs and time lapse movies were recorded with an automated Leica MZ 16 FA stereomicroscope (Visitron Systems).

In vitro 3D chemotaxis assays. Cells were suspended in PureCol (INAMED) and cast in custom built migration chambers (standard collagen concentration: 1.6 mg ml^{-1}). After polymerization, gels were overlaid with culture medium containing the chemoattractant (CCL19, C5a and CXCL13 for DCs, granulocytes and B cells, respectively) and subsequently imaged using wide-field fluorescence video microscopes with differential interference contrast (Zeiss). For nucleus visualization, SYTO-dyes (Invitrogen) were used. For visualization of myosin light chain, DCs were nucleofected using Amaxa technology. Inhibitors were titrated and used 50 µm blebbistatin (Sigma) and 30 µm Y27632 (Calbiochem).

Statistical analysis. *t*-tests and analysis of variance (ANOVA) were performed after data were confirmed to fulfil the criteria of normal distribution and equal variance, otherwise Kruskal–Wallis tests or Mann–Whitney U-tests were applied. If overall ANOVA or Kruskal–Wallis tests were significant, we performed a post hoc test. Analyses were performed with Sigma Stat 2.03. For further statistical details, see Supplementary Table.

1. Giannone, G. *et al.* Lamellipodial actin mechanically links myosin activity with adhesion-site formation. *Cell* **128**, 561–575 (2007).
2. Lauffenburger, D. A. & Horwitz, A. F. Cell migration: A physically integrated molecular process. *Cell* **84**, 359–369 (1996).
3. Mitchison, T. J. & Cramer, L. P. Actin-based cell motility and cell locomotion. *Cell* **84**, 371–379 (1996).
4. Hynes, R. O. Integrins: Bidirectional, allosteric signaling machines. *Cell* **110**, 673–687 (2002).
5. Hynes, R. O. & Zhao, Q. The evolution of cell adhesion. *J. Cell Biol.* **150**, 89–96 (2000).
6. Friedl, P. Prespecification and plasticity: Shifting mechanisms of cell migration. *Curr. Opin. Cell Biol.* **16**, 14–23 (2004).
7. Pittet, M. J. & Mempel, T. R. Regulation of T-cell migration and effector functions: Insights from *in vivo* imaging studies. *Immunol. Rev.* **221**, 107–129 (2008).
8. de Bruyn, P. P. H. The amoeboid movement of the mammalian leukocyte in tissue culture. *Anat. Rec.* **95**, 117–192 (1946).
9. Reis e Sousa, C. Dendritic cells in a mature age. *Nature Rev. Immunol.* **6**, 476–483 (2006).
10. Förster, R. *et al.* CCR7 coordinates the primary immune response by establishing functional microenvironments in secondary lymphoid organs. *Cell* **99**, 23–33 (1999).
11. Calderwood, D. A. & Ginsberg, M. H. Talin forges the links between integrins and actin. *Nature Cell Biol.* **5**, 694–697 (2003).
12. Stoitzner, P., Pfaller, K., Stössel, H. & Romani, N. A close-up view of migrating Langerhans cells in the skin. *J. Invest. Dermatol.* **118**, 117–125 (2002).
13. Gretz, J. E., Anderson, A. O. & Shaw, S. Cords, channels, corridors and conduits: Critical architectural elements facilitating cell interactions in the lymph node cortex. *Immunol. Rev.* **156**, 11–24 (1997).
14. Lämmermann, T. & Sixt, M. The microanatomy of T-cell responses. *Immunol. Rev.* **221**, 26–43 (2008).
15. Mempel, T. R., Henrickson, S. E. & Von Andrian, U. H. T-cell priming by dendritic cells in lymph nodes occurs in three distinct phases. *Nature* **427**, 154–159 (2004).
16. Alon, R. & Dustin, M. L. Force as a facilitator of integrin conformational changes during leukocyte arrest on blood vessels and antigen-presenting cells. *Immunity* **26**, 17–27 (2007).
17. Lindquist, R. L. *et al.* Visualizing dendritic cell networks *in vivo*. *Nature Immunol.* **5**, 1243–1250 (2004).
18. Meshel, A. S., Wei, Q., Adelstein, R. S. & Sheetz, M. P. Basic mechanism of three-dimensional collagen fibre transport by fibroblasts. *Nature Cell Biol.* **7**, 157–164 (2005).
19. Vanni, S., Lagerholm, B. C., Otey, C., Taylor, D. L. & Lanni, F. Internet-based image analysis quantifies contractile behavior of individual fibroblasts inside model tissue. *Biophys. J.* **84**, 2715–2727 (2003).
20. Medeiros, N. A., Burnette, D. T. & Forscher, P. Myosin II functions in actin-bundle turnover in neuronal growth cones. *Nature Cell Biol.* **8**, 215–226 (2006).
21. Hogg, N., Laschinger, M., Giles, K. & McDowall, A. T-cell integrins: More than just sticking points. *J. Cell Sci.* **116**, 4695–4705 (2003).
22. Morin, N. A. *et al.* Nonmuscle myosin heavy chain IIA mediates integrin LFA-1 de-adhesion during T lymphocyte migration. *J. Exp. Med.* **205**, 195–205 (2008).
23. Hu, S., Chen, J., Butler, J. P. & Wang, N. Prestress mediates force propagation into the nucleus. *Biochem. Biophys. Res. Commun.* **329**, 423–428 (2005).
24. Paluch, E., Sykes, C., Prost, J. & Bornens, M. Dynamic modes of the cortical actomyosin gel during cell locomotion and division. *Trends Cell Biol.* **16**, 5–10 (2006).
25. Morton, W. M., Ayscough, K. R. & McLaughlin, P. J. Latrunculin alters the actin-monomer subunit interface to prevent polymerization. *Nature Cell Biol.* **2**, 376–378 (2000).
26. Bottino, D., Mogilner, A., Roberts, T., Stewart, M. & Oster, G. How nematode sperm crawl. *J. Cell Sci.* **115**, 367–384 (2002).
27. Schaar, B. T. & McConnell, S. K. Cytoskeletal coordination during neuronal migration. *Proc. Natl Acad. Sci. USA* **102**, 13652–13657 (2005).
28. Wolf, K., Müller, R., Borgmann, S., Bröcker, E. B. & Friedl, P. Amoeboid shape change and contact guidance: T-lymphocyte crawling through fibrillar collagen is independent of matrix remodeling by MMPs and other proteases. *Blood* **102**, 3262–3269 (2003).
29. Auffray, C. *et al.* Monitoring of blood vessels and tissues by a population of monocytes with patrolling behavior. *Science* **317**, 666–670 (2007).
30. Phillipson, M. *et al.* Intraluminal crawling of neutrophils to emigration sites: A molecularly distinct process from adhesion in the recruitment cascade. *J. Exp. Med.* **203**, 2569–2575 (2006).
31. Sixt, M., Bauer, M., Lämmermann, T. & Fässler, R. Beta1 integrins: Zip codes and signaling relay for blood cells. *Curr. Opin. Cell Biol.* **18**, 482–490 (2006).
32. Potocnik, A. J., Brakebusch, C. & Fässler, R. Fetal and adult hematopoietic stem cells require beta1 integrin function for colonizing fetal liver, spleen, and bone marrow. *Immunity* **12**, 653–663 (2000).
33. Wilson, R. W. *et al.* Gene targeting yields a CD18-mutant mouse for study of inflammation. *J. Immunol.* **151**, 1571–1578 (1993).
34. Wagner, N. *et al.* Critical role for beta7 integrins in formation of the gut-associated lymphoid tissue. *Nature* **382**, 366–370 (1996).
35. Kühn, R., Schwenk, F., Aguet, M. & Rajewsky, K. Inducible gene targeting in mice. *Science* **269**, 1427–1429 (1995).
36. Petrich, B. G. *et al.* Talin is required for integrin-mediated platelet function in hemostasis and thrombosis. *J. Exp. Med.* **204**, 3103–3111 (2007).

METHODS

Generation of integrin $\alpha_v^{+/flox}$ mice. To generate a conditional floxed α_v allele, a targeting vector spanning 8.2 kb of the murine α_v *integrin* locus[37] was constructed. First, the 2.2 kb genomic subclone pXB2.2 encoding the 5′ upstream region, exon 1 and part of the intron 1 of the α_v gene was used to introduce two *loxP*-sites. The 5′-*loxP1*-site including an EcoRI-restriction site to facilitate the identification of the targeted locus was cloned into the HindIII-site in the 5′-upstream region (nucleotide position, nt-pos., −310) of the α_v gene. The 3′-*loxP2*-site was introduced into the BamHI-site in intron 1 (nt-pos. +528). The genomic subclone pBS6 harbouring this BamHI-site at its 5′-end and ~6 kb 3′-downstream intron 1 sequences was used to clone a *pgk-neo;pgk-tk*-tandem gene selection-cassette (*neoTK*) flanked by two *frt*-sites (provided by G. R. Martin) into the BamHI-site. These two modified genomic regions of the α_v gene were then fused at the corresponding BamHI-site to obtain the α_v gene targeting vector. ES cell transfection, selection and screening was carried out as described[37] except that R1 ES cells[38] were used. Homologously targeted clones were identified by Southern blotting of EcoRI- or BamHI-digested DNA with 5′- or 3′-external probes A or B, respectively. To excise the neoTK selection cassette, targeted ES cells (*flneoTK*) were transiently transfected with the *CAGGS-FLPe*-expression construct[39] (provided by A. F. Stewart) and counterselected with ganciclovir. Loss of the selection cassette in the α_v floxed allele was then confirmed by Southern blotting. ES cell clones were injected into blastocysts of C57Bl/6 mice, and resulting germline transmitting male chimaeras were mated to C57Bl/6 females to generate heterozygous floxed α_v mice and wild-type F1 mice following protocols as described[37]. Two independent lines carrying the $\alpha_v^{+/flox}$ allele were established and initially maintained on a 129SV/C57BL/6 mixed background. $\alpha_v^{+/flox}$ and $\alpha_v^{flox/flox}$ mice show no obvious phenotype. Southern blot and PCR analyses: wild-type and mutant α_v alleles were assessed by Southern blot hybridization and/or PCR from DNA isolated from ES cells, mouse tail biopsies or from yolk sacs of embryos as described[37]. In brief, 10 µg of genomic DNA was digested with EcoRI or BamHI and analysed using radio-labelled 5′-external probe A (419 bp-EcoRI/XbaI DNA-fragment) or a 3′-external probe B (690 bp-SphI/EcoRI DNA-fragment), respectively (see Supplementary Fig. 1). Genomic DNA digested with EcoRI was used to confirm the presence or absence of the selection cassette with probe C encoding a 800 bp-PstI fragment of the neomycin-resistance gene. For genotyping wild-type (WT, +) and floxed α_v allele (flox) as well as the *cre*-mediated knockout allele ($\alpha_v^{\Delta ex1}$), PCR amplifications with genomic DNA and the specific primer set (see below) were performed. The positions of the primers are located in close vicinity to the *loxP*-sites. PCR amplifications using *Taq*-polymerase and standard reaction buffer adjusted to a final concentration of 1 mM $MgCl_2$ were carried out as follows. PCR samples were initially denatured at 94 °C for 3 min, followed by 35 cycles of amplification (94 °C for 1 min, 60 °C for 2 min, 72 °C for 3 min), and a final 10 min extension at 72 °C followed. PCR amplification products were separated through agarose gel electrophoresis. The allele-specific primer sequences, pairs and orientation (forward, Fw; reverse, Rev), the primer pairs and their corresponding PCR-product sizes are as follows: Primer-set (F30: 5′-AGGATGGAAGGGGAGGGAAATG-3′ (Fw; WT), F20: 5′-CTTGACCGCAA-GCGCACAGCACAG-3′ (Fw; WT), I2: 5′-CTGGATGCTGAGTGTCAGGT-3′ (Rev; WT)), PCR products (F20/I2: 499 bp (wild-type α_v allele, WT); F20/I2: 614 bp (floxed α_v allele, α_v^{flox}); F30/I2: 339 bp (*cre*-mediated α_v knockout allele, $\alpha_v^{\Delta ex1}$)).

Mouse strains. Mice with constitutive deletions of integrin β_7, integrin β_2, CCR7 and conditional $\beta_1^{flox/flox}$ mice were described[10,32–34]. All mice were kept on a mixed 129SV/C57BL/6 genetic background. The integrin targeted strains were inter-crossed with Mx1Cre transgenic mice to generate $\alpha_v^{flox/flox}$, $\beta_1^{flox/flox}$, $\beta_2^{-/-}$, $\beta_7^{-/-}$, Mx1Cre$^{+/-}$ animals. Talin1$^{flox/flox}$ mice[36] were crossed with Mx1Cre transgenic mice to obtain talin1$^{flox/flox}$, Mx1Cre$^{+/-}$ mice. All control animals were on a mixed 129SV/C57BL/6 genetic background. The mice were bred in a conventional animal facility at the Max Planck Institute of Biochemistry, and according to the local regulations.

Induction of the haematopoietic knockout. At an age between 8 and 12 weeks, mice of the desired genotype received a single intraperitoneal injection of 250 µg Poly (I)·Poly (C) (Amersham Biosciences), diluted in 0.5 ml phosphate buffered saline (PBS). Mice were killed 10–14 d after injection and knockout efficiency of haematopoietic precursors was estimated by flow cytometric analysis of peripheral blood platelets[40]. Bone marrow (BM) of mice with >85% integrin β_1-negative platelets was processed for dendritic cell (DC) culture or cell isolation. Platelet knockout efficiencies usually corresponded with knockout efficiencies of DCs and granulocytes, whereas peripheral B cells frequently showed lower efficiency.

Cell generation, separation and purification. DCs were generated from flushed BM suspension as described previously[41]. At day 8–10 of culture, 200 ng ml^{-1}

LPS (Sigma-Aldrich; *E. coli* 0127:B8) was added overnight and the pan-integrin-deleted DCs were subsequently depleted of remaining Gr-1$^+$ and integrin β_1^+ contaminants. For depletion, cells were incubated with biotinylated antibodies against Gr-1 (RB6-8C5) and integrin β_1 (Ha2/5) (both BD Pharmingen), followed by streptavidin-microbead separation according to the manufacturers protocol (Miltenyi Biotech). The negatively selected DCs used for migration assays were >99% enriched for β_1 integrin knockout cells and β_1-deficient cells were always 100% deleted for integrin α_v. After enrichment the cells are referred to as integrin$^{-/-}$ DCs. Talin1$^{-/-}$ DCs were generated identically and depleted of Gr-1$^+$ contaminants. To determine knockout efficiencies, DC lysates were loaded on 12–15% gradient gels for electrophoresis under reduced conditions and western blotting. Talin was detected with mouse anti-pan-talin antibody (T3287, Sigma), and the loading control was performed with rabbit anti-mouse actin antibody (A2066, Sigma). Integrin β_1 was detected with the rabbit poly-clonal anti-integrin β_1 antibody 1244[42]. Integrin α_v was detected with a rabbit polyclonal anti-integrin α_v antibody (Chemicon). Bound primary antibodies were detected with anti-mouse or anti-rabbit horse radish peroxidase (HRP) or anti-rabbit HRP (both Bio-Rad) as secondary antibodies, respectively. DCs with no detectable talin stain were chosen for experiments, guaranteeing that the cells were deleted for talin1 and that talin2 was neither expressed nor induced as a compensation mechanism in DCs. Granulocytes were isolated by staining whole bone marrow suspension with anti-Gr-1 PE or anti-Gr-1 PE/anti-β_1 FITC and subsequent fluorescent activated cell sorting using a FACSAria (BD Biosciences), revealing >96% purity. Before incorporation into the gels, granulocytes were treated for 30 min with 20 ng ml^{-1} TNF-α (Roche) at 37 °C. B lymphoblasts were generated by mincing spleens through a 70 µm nylon cell strainer (BD Pharmingen), lysing erythrocytes with ACK lysis buffer (0.15 M NH_4Cl, 1 mM $KHCO_3$, and 0.1 mM EDTA), and subsequent magnetic cell sorting (MACS) with mouse CD43 MicroBeads on LS columns (Miltenyi). The negatively sorted B cells were stimulated with 10 µg ml^{-1} LPS (Sigma) for 72 h at 37 °C, 5% CO_2. Streptavidin-microbead separation of integrin β_1^+ cells (see DCs) revealed >98% pan-integrin-deficient B lymphoblasts that we refer to as integrin$^{-/-}$ B lymphoblasts.

Flow cytometry. Mature DCs were identified as CD11c$^+$, MHCII^{high} cells for wild-type and talin1-deficient cells. For integrin$^{-/-}$ cells, MHCII^{high} cells corresponded to mature DCs as they carried enhanced levels of maturation markers CD86 and CD40. B lymphoblasts were identified as B220$^+$ cells, granulocytes as Gr-1$^+$ cells. Employed antibodies were against the mouse antigens: Gr-1 biotin and PE (RB6-8C5), B220 FITC (RA3-6B2), CD11c FITC and biotin (HL3), I-A/I-E biotin (2G9) and I-A/I-E PE (M5/114.15.2) (all from BD Pharmingen). For integrin expression profiles, the above cell markers were combined with anti-bodies raised against the mouse integrin chains: α_2 FITC (Ha 1/29), α_{IIB} FITC (MWReg30), α_M PE (M1/70), α_4 PE (9C10), α_5 PE (5H10-27), α_6 PE (GoH3), α_E PE (M290), α_v (RMV-7), β_1 biotin (Ha2/5), β_2 biotin (C71/16), β_3 biotin (2C9.G2), β_7 biotin (2C3.G2) (all from Pharmingen), α_1 FITC (HMalpha1), β_4 PE (346-11A) (both from Serotec), α_L biotin (M17/4) (eBiosciences) and β_1 PE (HMbeta1-1) (BioLegend). The following isotype-matched antibody controls were employed: rat IgG2a PE (B39-4, R35-95), rat IgG1 PE (R3-34), hamster IgG2 FITC (Ha4/8), hamster IgM FITC (G235-1) (all Pharmingen), rat IgG2a biotin, rat IgG2b FITC (eB149/10H5), rat IgG1 FITC (all eBiosciences), hamster IgG PE (HTK888), hamster IgM biotin (HTK204) (both BioLegend) and rat IgG2a PE (YTH71.3) (Serotec). Biotinylated antibodies were detected with secondary streptavidin-Cy5 (Jackson). Flow cytometric analysis was performed with a FACScalibur and CellQuest Pro Software (BD Biosciences).

Quantitative RT–PCR. RNA was isolated from sorted DCs (see above) using the Absolutely RNA Microprep Kit (Stratagene) and the RNeasy Mini Kit (Qiagen). One microlitre cDNA, generated from 15 ng RNA using the iScript cDNA Synthesis Kit (Bio-Rad), was subjected to real-time PCR with the iQ SYBR Green Supermix (Bio-Rad) on the iCycler (Bio-Rad). Primers for integrin β_1 5′-AGACTTCCGCATTGGCTTTG-3′ and 5′-GCTGGTGCAGTTTTGTTCAC-3′, and integrin α_v 5′-CAAGCTCACTCCCATCAC-3′ and 5′-GGGTGTCTT-GATTCTCAAAGGG-3′ were used. Integrin gene expression in wild-type and integrin$^{-/-}$ DCs was quantified with the Gene Expression Analysis Program for the iCycler iQ Real-Time PCR Detection System (Bio-Rad). GAPDH was used to normalize gene expression, and integrin expression levels in wild-type DCs were set to 1.

***In vivo* migration assay.** Gr-1-depleted wild-type and integrin$^{-/-}$ DCs were labelled with 3.5 µM cell-permeable 5-(and-6)-carboxyfluorescein succinimidyl ester (CFSE) or 1 µM tetramethylrhodamine (TAMRA) (both Invitrogen), respectively, and vice versa (the fluorescent labels did not influence DC migration (not shown)). 1×10^6 DCs at a 1:1 ratio were suspended in 20 µl PBS and injected subcutaneously into the hind footpads of C57BL/6 mice. 32 and 48 h after injection, mice were killed by CO_2 suffocation, popliteal lymph nodes frozen in cryomatrix (Thermo) and sectioned in 12 µm slices. To visualize the

lymph node compartments, methanol-fixed cryosections were stained after blocking with 1% BSA in PBS with pan-laminin antibody (L9393, Sigma) and secondary anti-rabbit Cy5 (Jackson). Three different layers of the T cell cortex of each lymph node were documented using an Axio Imager upright microscope (Zeiss). Quantification of DCs within the T cell cortex was performed with MetaMorph (Molecular Devices). Using inverse thresholding, the greyscale images of both fluorescence channels were separately binarized. DCs appeared as dots that were quantified using the morphometric analysis tool. The ratio of migrated knockout DCs was calculated as the number of knockout cells divided by the total number of DCs in the T cell cortex, with 0.5 as the value where 50% of knockout cells and 50% wild-type cells located in the centre of the lymph node. To confirm that fluorescent cells in the lymph node represent DCs that migrated from the injection site (Supplementary Fig. 3), DCs were labelled with 3 μM Cell Trace Oregon Green 488 (Invitrogen). 1×10^6 DCs of either wild-type or integrin$^{-/-}$ DCs were injected as described above and 48 h later DCs were identified as green cells expressing CD86 by flow cytometric analysis.

Ex vivo **wide-field microscopy in ear dermis.** Ears of killed C57BL/6 mice were removed and mechanically split into dorsal and ventral halves. During separation the dermis detached from the cartilage layer that remained on one of the halves. The cartilage free half was left unfixed and incubated with a rabbit polyclonal anti-LYVE-1 antibody (R&D Systems), washed with PBS and stained with a A488 conjugated anti-rabbit secondary antibody (Molecular Probes). The stained ears were mounted on custom-made migration chambers with the dermal surface exposed. LPS-matured BM-derived, MACS-purified, TAMRA-labelled DCs (see above) were re-suspended in culture medium, added on top of the dermis and incubated for 30 min at 37 °C, 5% CO_2. After gently washing away non-infiltrated DCs, the ear sheets were imaged in a custom-built climate chamber using a fully motorized upright Leica MZ 16 FA stereomicroscope equipped with a Spot camera and operated via MetaMorph software (system implemented by Visitron Systems). For multiple immunofluorescence stainings (Supplementary Fig. 5), ear sheets were fixed with 1% PFA after 120 min immigration of DCs and stained as described in the extravasation section. Cells were manually tracked using ImageJ as described below.

Two-photon intravital microscopy in lymph nodes. Intravital microscopy was performed as described previously[43]. Briefly, BM-derived DCs were matured overnight with LPS, purified and selected by MACS for the desired integrin deficiency (see above), differentially labelled with TAMRA and CFSE and subcutaneously injected into footpads of C57BL/6 mice. After 32 h popliteal lymph nodes were surgically exposed and imaged using an upright Leica DM LFSA microscope equipped with a ×20 0.95 NA water immersion objective (Olympus) and a MaiTai Ti:sapphire-pulsed laser (Spectra-Physics). 3D cell tracking was performed using Imaris software (Bitplane) as described.

In vivo **ear irritation in bone marrow chimaeric mice.** BM chimaera of talin1$^{flox/flox}$, Mx1Cre$^{+/-}$ and α$_v$$^{flox/flox}$, β$_1$$^{flox/flox}$, β$_2$$^{-/-}$, β$_7$$^{-/-}$, Mx1Cre$^{+/-}$ animals were generated by sublethal irradiation of wild-type mice and immediate reconstitution with 1×10^6 suspended BM cells of the indicated genotype. Six weeks after irradiation Poly (I)·Poly (C) was injected and 10 d later 20 μl of 1% croton oil (Sigma) in acetone[44] was applied on mouse ears. Mice were killed 12 h after application of croton oil. For histological analysis dorsal and ventral halves of ears were subjected to whole mount immunostaining. After fixation with 1% PFA, ear halves were blocked with 1% BSA (PAA) in PBS for 1 h at RT (while shaking), stained with anti-Gr-1 (RB6-8C5, Pharmingen) and anti-pan-laminin antibody (L9393, Sigma) in 1% BSA in PBS overnight at 4 °C (while shaking) and washed with 1% BSA in PBS. Primary antibodies were detected with a repeated cycle of staining with anti-rabbit A488 (Molecular Probes) and anti-rat Cy3 (Dianova) antibodies before tissue was embedded in elvanol and representative images taken with an Axio Imager (Zeiss) equipped with the Apotome. Concentration of granulocytes in blood was measured by staining peripheral blood with Gr-1 PE (BD Pharmingen) and counting all granulocytes per blood sample by flow cytometry using a FACSCalibur (BD Pharmingen). The numbers of granulocytes that extravasated into ear dermis were quantified by morphometric analysis employing MetaMorph imaging software (Molecular Devices).

3D collagen gel chemotaxis assay. For standard assays, PureCol (INAMED) in 1× minimum essential medium eagle (MEM, Sigma) and 0.4% sodium bicarbonate (Sigma) was mixed with cells in RPMI (Invitrogen), 10% fetal calf serum (FCS, Invitrogen) at a 2:1 ratio, resulting in gels with a collagen concentration of 1.6 mg ml^{-1}. Final cell concentrations in the assay were 1×10^6 cells per ml gel for DCs and 1.6×10^6 cells per ml gel for granulocytes and B lymphoblasts. For collagen titration experiments, above ratios were adapted. For gels with 3–5 mg ml^{-1} collagen concentration, Nutragen (INAMED) was employed. Collagen-cell mixtures were cast in custom-made migration chambers with a thickness of 0.5–1 mm. After 30 min assembly of the collagen fibres at 37 °C, the gels were overlaid with 50 μl of the following recombinant chemokines (all R&D Systems) diluted in RPMI, 10% FCS: CCL19 (0.6 μg ml^{-1}, DCs), C5a

(0.1 μg ml^{-1}, granulocytes) and CXCL13 (2.5 μg ml^{-1}, B cells). For inhibition studies, leukocytes were pre-incubated for 30 min with 50 μM blebbistatin (Sigma), 30 μM Y27632, 100 nM or 500 nM latrunculin B (both Calbiochem) before casting the gels. Inhibitors were also present in the same end-concentrations in the gel.

3D fibrin gel chemotaxis assay. Cells were taken up in 0.2% (w/v) human fibrinogen (IMCO) in RPMI, 10% FCS to a final concentration of 1×10^6 cells per ml gel. Before casting the gels in custom-made migration chambers, 0.125 U ml^{-1} thrombin (Calbiochem) was added. After 30 min polymerization of the fibrin gels at 37 °C, the gels were overlaid with 50 μl of 0.6 μg ml^{-1} CCL19 (R&D Systems) in RPMI, 10% FCS.

Analysis of chemotaxis assays. For comparison of DC velocities in collagen and fibrin gel assays in the absence of inhibitors (Fig. 3b and Supplementary Fig. 7a), movies were converted to kymographs using MetaMorph imaging software. Straight lines in the kymographs represent migrating cells and lead angles were measured to calculate single cell velocities. Manual single cell tracking of random samples employing ImageJ and the Manual Tracking Plugin revealed the same results. Manual tracking was applied to all other 3D chemotaxis assays. Here cells were tracked over 4 h (for DCs, 2 min per frame) or 15 min (for granulocytes, 15 s per frame). Speed and directionality parameters were calculated and visualized as plots and movies by analysing the acquired data with the Chemotaxis and Migration Tool Plugin (http://www.ibidi.de/applications/ap_chemo.html). For quantification of "resting" and "moving" phases in 0.75 mg ml^{-1} collagen gels (Supplementary Fig. 9) instantaneous velocities (distance per 2 min) were categorized as "resting" if velocity <1 μm per 2 min and "moving" if velocity ≥1 μm per 2 min. Average velocities during mobile phases were calculated by excluding the resting fraction. The percentage of resting phases was calculated as resting time / (resting time + moving time).

Time-lapse video microscopy. Low magnification bright-field movies of DCs in gels were recorded in indicated time intervals using inverted Axiovert 40 (Zeiss) cell culture microscopes, equipped with custom-built climate chambers (5% CO_2, 37 °C, humidified) and PAL cameras (Prosilica) triggered by custom-made software (SVS Vistek). High magnification DIC and fluorescence movies were recorded using a fully automated Axiovert 200M inverted fluorescence microscope with a 40× objective (Zeiss) and a CoolSNAP HQ CCD camera. The microscopic set-up (Visitron Systems) was controlled by MetaMorph software.

Transfection and labelling of cells. DCs were transfected with MLC-GFP (gift of M. Olson[45]) between days 8–10 of culture using the primary mouse T cell kit and the Amaxa nucleoporator (Amaxa). Cells were transfected according to the manufacturer's recommendations and immediately after transfection LPS was added for overnight maturation. For nucleus visualization of DCs and granulocytes nucleic acid dyes SYTO11 and SYTO13 (Invitrogen) were used, respectively, according to the manufacturers recommendations.

2D adhesion assays. Adhesion assays were performed in 24-well plates coated with 10 μg ml^{-1} fibronectin (Calbiochem) or 10 μg ml^{-1} recombinant mouse ICAM-1 (R&D). 3×10^5 DCs per well were seeded in RPMI medium containing 10% FCS in the presence of 200 ng ml^{-1} LPS and incubated for 30 min at 5% CO_2, 37 °C. Same cell numbers of LPS-maturated DCs were seeded in the presence of 200 ng ml^{-1} phorbol 12-myristate 13-acetate (Calbiochem) for 30 min. Cells were washed manually 3 times with PBS, 1% BSA and subsequently photo-documented and counted manually. Time-lapse video microscopy of chemokine-induced spreading of LPS-matured DCs (see Supplementary Video 4) was performed on 10 μg ml^{-1} mouse CCL21 (R&D)-coated plastic of cell culture dishes.

37. Bader, B. L., Rayburn, H., Crowley, D. & Hynes, R. O. Extensive vasculogenesis, angiogenesis, and organogenesis precede lethality in mice lacking all alpha v integrins. *Cell* **95**, 507–519 (1998).

38. Nagy, A., Rossant, J., Nagy, R., Abramow-Newerly, W. & Roder, J. C. Derivation of completely cell culture-derived mice from early-passage Embryonic stem cells. *Proc. Natl Acad. Sci. USA* **90**, 8424–8428 (1993).

39. Schaft, J., Ashery-Padan, R., van der Hoeven, F., Gruss, P. & Stewart, A. F. Efficient FLP recombination in mouse ES cells and oocytes. *Genesis* **31**, 6–10 (2001).

40. Bungartz, G. *et al.* Adult murine hematopoiesis can proceed without beta1 and beta7 integrins. *Blood* **108**, 1857–1864 (2006).

41. Lutz, M. B. *et al.* An advanced culture method for generating large quantities of highly pure dendritic cells from mouse bone marrow. *J. Immunol. Methods* **223**, 77–92 (1999).

42. Fässler, R. & Meyer, M. Consequences of lack of beta 1 integrin gene expression in mice. *Genes Dev.* **9**, 1896–1908 (1995).

43. Worbs, T., Mempel, T. R., Bolter, J., von Andrian, U. H. & Förster, R. CCR7 ligands stimulate the intranodal motility of T lymphocytes *in vivo. J. Exp. Med.* **204**, 489–495 (2007).

44. Berg, D. J. *et al.* Interleukin 10 but not interleukin 4 is a natural suppressant of cutaneous inflammatory responses. *J. Exp. Med.* **182**, 99–108 (1995).

45. Croft, D. R. *et al.* Actin-myosin-based contraction is responsible for apoptotic nuclear disintegration. *J. Cell Biol.* **168**, 245–255 (2005).

Paper VI

Proteinase 3 and neutrophil elastase enhance inflammation in mice by inactivating antiinflammatory progranulin

Kai Kessenbrock,[1] Leopold Fröhlich,[2] Michael Sixt,[3] Tim Lämmermann,[3]
Heiko Pfister,[1] Andrew Bateman,[4] Azzaq Belaaouaj,[5] Johannes Ring,[6,7]
Markus Ollert,[6] Reinhard Fässler,[3] and Dieter E. Jenne[1]

[1]Department of Neuroimmunology, Max-Planck-Institute of Neurobiology, Martinsried, Germany. [2]Institute of Pathophysiology,
University of Veterinary Medicine Vienna, Vienna, Austria. [3]Department of Molecular Medicine, Max-Planck-Institute of Biochemistry, Martinsried, Germany.
[4]Division of Experimental Medicine, McGill University and Endocrine Research Laboratory, Royal Victoria Hospital, Montreal, Quebec, Canada.
[5]INSERM UMR514, IFR 53, Hôpital Maison Blanche, CHU de Reims, Reims, France. [6]Department of Dermatology and Allergy,
Clinical Research Division of Molecular and Clinical Allergotoxicology, Technische Universität München, Munich, Germany.
[7]Division of Environmental Dermatology and Allergy, Helmoltz Zentrum München, German Research Center for Environmental Health, Neuherberg, Germany.

Neutrophil granulocytes form the body's first line of antibacterial defense, but they also contribute to tissue injury and noninfectious, chronic inflammation. Proteinase 3 (PR3) and neutrophil elastase (NE) are 2 abundant neutrophil serine proteases implicated in antimicrobial defense with overlapping and potentially redundant substrate specificity. Here, we unraveled a cooperative role for PR3 and NE in neutrophil activation and noninfectious inflammation in vivo, which we believe to be novel. Mice lacking both PR3 and NE demonstrated strongly diminished immune complex–mediated (IC-mediated) neutrophil infiltration in vivo as well as reduced activation of isolated neutrophils by ICs in vitro. In contrast, in mice lacking just NE, neutrophil recruitment to ICs was only marginally impaired. The defects in mice lacking both PR3 and NE were directly linked to the accumulation of antiinflammatory progranulin (PGRN). Both PR3 and NE cleaved PGRN in vitro and during neutrophil activation and inflammation in vivo. Local administration of recombinant PGRN potently inhibited neutrophilic inflammation in vivo, demonstrating that PGRN represents a crucial inflammation-suppressing mediator. We conclude that PR3 and NE enhance neutrophil-dependent inflammation by eliminating the local antiinflammatory activity of PGRN. Our results support the use of serine protease inhibitors as antiinflammatory agents.

Introduction

Neutrophils belong to the body's first line of cellular defense and respond quickly to tissue injury and invading microorganisms (1). In a variety of human diseases, like autoimmune disorders, infections, or hypersensitivity reactions, the underlying pathogenic mechanism is the formation of antigen-antibody complexes, so-called immune complexes (ICs), which trigger an inflammatory response by inducing the infiltration of neutrophils (2). The subsequent stimulation of neutrophils by C3b-opsonized ICs results in the generation of ROS and the release of intracellularly stored proteases leading to tissue damage and inflammation (3). It is therefore important to identify the mechanisms that control the activation of infiltrating neutrophils.

Neutrophils abundantly express a unique set of neutrophil serine proteases (NSPs), namely cathepsin G (CG), proteinase 3 (PR3; encoded by *Prtn3*), and neutrophil elastase (NE; encoded by *Ela2*), which are stored in the cytoplasmic, azurophilic granules. PR3 and NE are closely related enzymes, with overlapping and potentially redundant substrate specificities different from

those of CG. All 3 NSPs are implicated in antimicrobial defense by degrading engulfed microorganisms inside the phagolysosomes of neutrophils (4–8). Among many other functions ascribed to these enzymes, PR3 and NE were also suggested to play a fundamental role in granulocyte development in the bone marrow (9–11).

While the vast majority of the enzymes is stored intracellularly, minor quantities of PR3 and NE are externalized early during neutrophil activation and remain bound to the cell surface, where they are protected against protease inhibitors (12, 13). These membrane presented proteases were suggested to act as path clearers for neutrophil migration by degrading components of the extracellular matrix (14). This notion has been addressed in a number of studies, which yielded conflicting results (15–17). Thus, the role of PR3 and NE in leukocyte extravasation and interstitial migration still remains controversial.

Emerging data suggest that externalized NSPs can contribute to inflammatory processes in a more complex way than by simple proteolytic tissue degradation (18). For instance, recent observations using mice double-deficient for CG and NE indicate that pericellular CG enhances IC-mediated neutrophil activation and inflammation by modulating integrin clustering on the neutrophil cell surface (19, 20). Because to our knowledge no *Prtn3*$^{-/-}$ mice have previously been generated, the role of this NSP in inflammatory processes has not been deciphered. Moreover, NE-dependent functions that can be compensated by PR3 in *Ela2*$^{-/-}$ animals are still elusive.
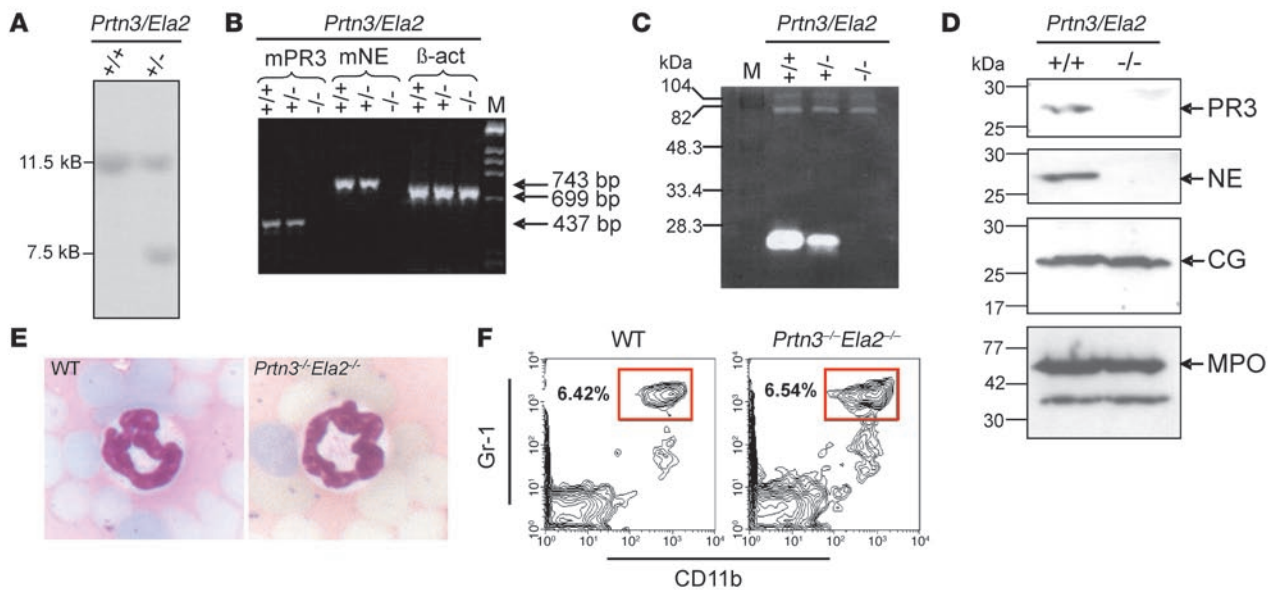
Figure 1
Generation and characterization of *Prtn3−/−Ela2−/−* mice. (**A**) Southern blot showing the WT (+/+) 11.5-kb band of the nontargeted allele and the presence of an additional 7.5-kb band in a heterozygous (+/–) PR3/NE-targeted embryonic stem cell clone. (**B**) RT-PCR revealed the complete lack of mouse PR3 (mPR3; 437 bp) and mouse NE (743 bp) transcripts in bone marrow cells from *Prtn3−/−Ela2−/−* mice (–/–), while expression of β-actin (699 bp) was normal. (**C**) Casein zymography showed prominent casein degradative activity at 27 kDa in WT neutrophil lysates, while intermediate degradation by heterozygous lines and no degradation by *Prtn3−/−Ela2−/−* lines was found at this size. M, marker. (**D**) Western blot analysis of granule enzyme expression in bone marrow–derived neutrophils. In *Prtn3−/−Ela2−/−* neutrophils, no signals for PR3 and NE were detected, while CG (~26 kDa), MPO (~59 kDa), and a smaller degradation product of MPO were detected at the same levels as in WT neutrophils. (**E**) Microscopic analysis of H&E-stained blood smears revealed normal granulocyte morphology in *Prtn3−/−Ela2−/−* mice, with a polymorphic nucleus (dark blue) identical to that of WT neutrophils. Original magnification, ×20. (**F**) Flow cytometry of peripheral blood with gating on Gr-1hiCD11b+ showed regular neutrophil populations (boxed regions) in *Prtn3−/−Ela2−/−* mice. Plots are representative of data obtained from 3 mice per group. Percentages denote percent cells in the boxed regions.

One mechanism by which NSPs could upregulate the inflammatory response has recently been proposed. The ubiquitously expressed progranulin (PGRN) is a growth factor implicated in tissue regeneration, tumorigenesis, and inflammation (21–23). PGRN was previously shown to directly inhibit adhesion-dependent neutrophil activation by suppressing the production of ROS and the release of neutrophil proteases in vitro (23). This antiinflammatory activity was degraded by NE-mediated proteolysis of PGRN to granulin (GRN) peptides (23). In contrast, GRN peptides may enhance inflammation (23) and have been detected in neutrophil-rich peritoneal exudates (24). In short, recent studies proposed PGRN as a regulator of the innate immune response, but the factors that control PGRN function are still poorly defined and its relevance to inflammation needs to be elucidated in vivo.

In the present study, we generated double-deficient *Prtn3−/− Ela2−/−* mice to investigate the role of these highly similar serine proteases in noninfectious neutrophilic inflammation. We established that PR3 and NE are required for acute inflammation in response to subcutaneous IC formation. The proteases were found to be directly involved in early neutrophil activation events, because isolated *Prtn3−/−Ela2−/−* neutrophils were poorly activated by ICs in vitro. These defects in *Prtn3−/−Ela2−/−* mice were accompanied by accumulation of PGRN. We demonstrated that PGRN represents a potent inflammation-suppressing factor that is cleaved by both PR3 and NE. Our data delineate what we believe to be a previously unknown proinflammatory role for PR3 and NE, which is accomplished via the local inactivation of antiinflammatory PGRN.

Results

Generation of Prtn3−/−Ela2−/− mice. To analyze the role of PR3 and NE in neutrophilic inflammation, we generated a *Prtn3−/−Ela2−/−* mouse line by targeted gene disruption in embryonic stem cells (see Supplemental Figure 1; supplemental material available online with this article; doi:10.1172/JCI34694DS1). Positive recombination of the *Prtn3/Ela2* locus was proven by Southern blotting of embryonic stem cell clones (Figure 1A). *Prtn3−/−Ela2−/−* mice showed no expression of mRNA for PR3 and NE in bone marrow cells, as assessed by RT-PCR (Figure 1B). The successful elimination of PR3 and NE was confirmed at the level of proteolytic activity in neutrophil lysates using a PR3/NE-specific chromogenic substrate (Supplemental Figure 3) as well as by casein zymography (Figure 1C). The substantially reduced casein degradation by heterozygous neutrophils indicates gene-dosage dependence of PR3/NE activities. Furthermore, PR3 and NE deficiency was proven by Western blotting using cell lysates from bone marrow–derived neutrophils, while other enzymes stored in azurophilic granula, such as CG and myeloperoxidase (MPO), were normally detected (Figure 1D). Crossing of heterozygous *Prtn3+/−Ela2+/−* mice resulted in regular offspring of WT, heterozygous, and homozygous genotype according to the Mendelian ratio. Despite the absence of 2 abundant serine proteases, and in contrast to expectations based on previous reports (9–11), we found unchanged neutrophil morphology (Figure 1E) and regular neutrophil populations in the peripheral blood of the mutant mice, the latter as assessed via flow cytometry to determine the differentiation markers CD11b and Gr-1 (Figure 1F)
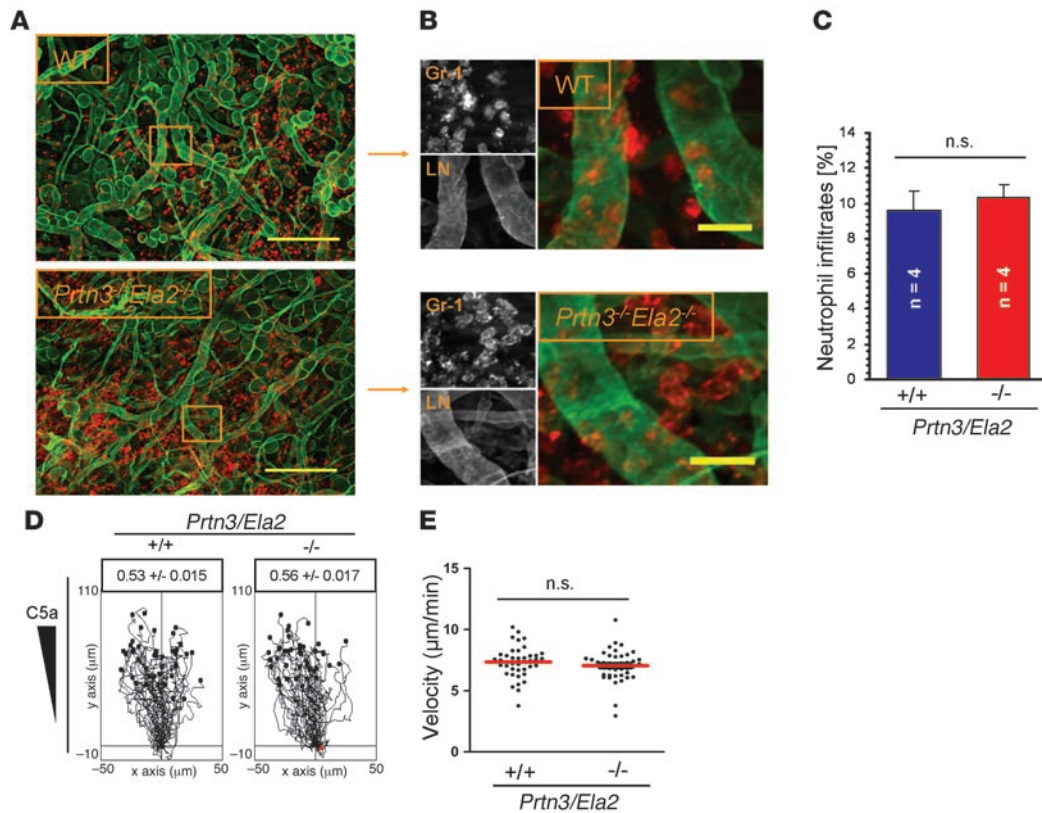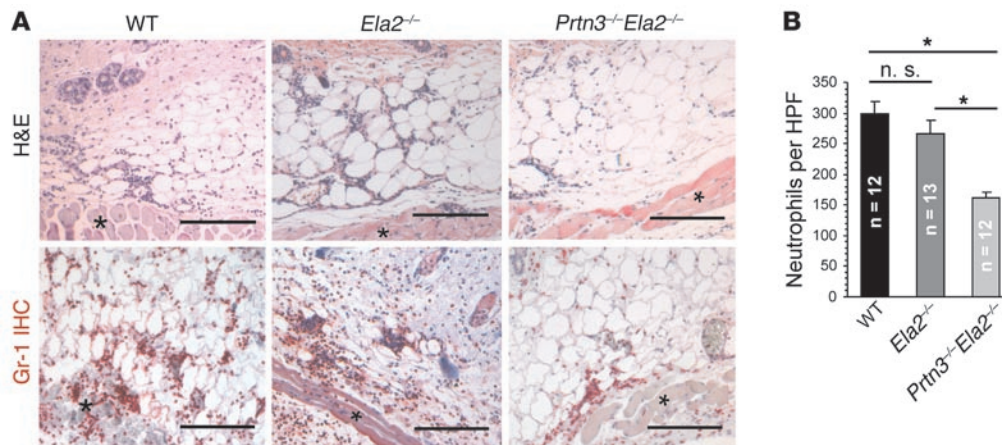
Figure 2

PR3 and NE are not principally required for neutrophil extravasation and interstitial migration. (**A** and **B**) Phorbol ester–treated ear tissues of WT and *Prtn3⁻/⁻Ela2⁻/⁻* mice were immunostained for laminin (LN; green) to visualize EBM and Gr-1 (red) to identify neutrophils. Lesions were examined 4 h after stimulus application by fluorescence microscopy as described in Methods. (**A**) Representative images of tissue from WT and *Prtn3⁻/⁻Ela2⁻/⁻* mice. Both genotypes developed strong and widespread neutrophil infiltrations. (**B**) Higher-magnification images of boxed regions in **A**. *Prtn3⁻/⁻Ela2⁻/⁻* neutrophils showed no retention at the EBM. Scale bars: 200 μm (**A**); 25 μm (**B**). (**C**) Overall neutrophil infiltrates were quantified as the percentage of Gr-1–positive cells per microscopic field. Data are mean ± SEM. Intravascular cells were excluded. No significant difference between WT and *Prtn3⁻/⁻Ela2⁻/⁻* mice was found (*P* = 0.63). In vitro migration of WT and *Prtn3⁻/⁻Ela2⁻/⁻* neutrophils directed by C5a through 3-dimensional collagen matrices was analyzed by time-lapse video microscopy (see Supplemental Video 1). (**D**) The tracks of WT (*n* = 41) and *Prtn3⁻/⁻Ela2⁻/⁻* (*n* = 42) neutrophils are shown, and the factor for directionality ± SEM is indicated. No impairment was observed regarding chemotactic directionality of *Prtn3⁻/⁻Ela2⁻/⁻* versus WT neutrophils (*P* = 0.19). (**E**) Velocities of single cells (individual points) were calculated and averaged (red bar). *Prtn3⁻/⁻Ela2⁻/⁻* neutrophils showed no significant difference versus WT cells (*P* = 0.30).

(25, 26). Moreover, *Prtn3⁻/⁻Ela2⁻/⁻* mice demonstrated normal percentages of the leukocyte subpopulations in the peripheral blood, as determined by the Diff-Quick staining protocol and by hemocytometric counting (Supplemental Figure 2, A and B). Hence, the proteases are not crucially involved in granulopoiesis, and ablating PR3 and NE in the germ line represents a valid approach to assess their biological significance in vivo.

PR3 and NE are dispensable for neutrophil extravasation and interstitial migration. To examine neutrophil infiltration into the perivascular tissue, we applied phorbol esters (croton oil) to the mouse ears. At 4 h after stimulation, we assessed the neutrophil distribution in relation to the extravascular basement membrane (EBM) by immunofluorescence microscopy of fixed whole-mount specimens (Figure 2A). We found that *Prtn3⁻/⁻Ela2⁻/⁻* neutrophils transmigrated into the interstitium without retention at the EBM (Figure 2B), resulting in quantitatively normal and widespread neutrophil influx compared with WT mice (Figure 2C). Moreover, we analyzed chemotactic migration of isolated neutrophils through a 3-dimensional collagen meshwork in vitro (Supple-

mental Video 1) and found unhampered chemotaxis toward a C5a gradient, based on the directionality (Figure 2D) and velocity (Figure 2E) of *Prtn3⁻/⁻Ela2⁻/⁻* neutrophils. These findings led us to conclude that PR3 and NE are not principally required for neutrophil extravasation or interstitial migration.

Reduced inflammatory response to ICs in Prtn3⁻/⁻Ela2⁻/⁻ mice. The formation of ICs represents an important trigger of neutrophil-dependent inflammation in many human diseases (2). To determine the role of PR3 and NE in this context, we induced a classic model of subcutaneous IC-mediated inflammation, namely the reverse passive Arthus reaction (RPA) (27). At 4 h after RPA induction, we assessed the cellular inflammatory infiltrates by histology using H&E-stained skin sections (Figure 3A). Neutrophils, which were additionally identified by Gr-1 immunohistochemistry, made up the vast majority of all cellular infiltrates (Figure 3A). We found that neutrophil infiltration to the sites of IC formation was severely diminished in *Prtn3⁻/⁻Ela2⁻/⁻* mice. Indeed, histological quantification revealed significantly reduced neutrophil influx in *Prtn3⁻/⁻Ela2⁻/⁻* mice compared with WT mice, while *Ela2⁻/⁻* mice

Figure 3
Impaired inflammatory response to locally formed ICs in *Prtn3⁻/⁻Ela2⁻/⁻* mice. (**A**) Representative photomicrographs of inflamed skin sections 4 h after IC formation. Neutrophils were identified morphologically (polymorphic nucleus) in H&E stainings and by Gr-1 staining (red). The cellular infiltrates were located to the adipose tissue next to the panniculus carnosus muscle (asterisks) and were primarily composed of neutrophil granulocytes. Scale bars: 200 μm. (**B**) Neutrophil infiltrates in lesions from *Prtn3⁻/⁻Ela2⁻/⁻* mice were significantly diminished compared with *Ela2⁻/⁻* mice and WT mice. Neutrophil influx in *Ela2⁻/⁻* mice was slightly, but not significantly, diminished compared with WT mice. Results are mean ± SEM infiltrated neutrophils per HPF. *$P < 0.05$.

showed marginally reduced neutrophil counts (Figure 3B). These results indicate that PR3 and NE fulfill an important proinflammatory function during IC-mediated inflammation.

PR3 and NE enhance neutrophil activation by ICs in vitro. Because PR3 and NE were required for the inflammatory response to IC (Figure 3), but not to phorbol esters (Figure 2), we considered the enzymes as enhancers of the neutrophil response to IC. We therefore assessed the oxidative burst using dihydrorhodamine as a readout for cellular activation of isolated, TNF-α–primed neutrophils in the presence of ICs in vitro. While both WT and *Prtn3⁻/⁻Ela2⁻/⁻* neutrophils showed a similar, approximately 20-min lag phase before the oxidative burst commenced, the ROS production over time was markedly reduced, by 30%–40%, in the absence of PR3 and NE (Figure 4A). In contrast, oxidative burst triggered by 25 nM PMA was not hindered in *Prtn3⁻/⁻Ela2⁻/⁻* neutrophils (Figure 4B), which indicated no general defect in producing ROS. We also performed a titration series ranging from 0.1 to 50 nM PMA and found no reduction in oxidative burst activity in *Prtn3⁻/⁻Ela2⁻/⁻* neutrophils at any PMA concentration used (Supplemental Figure 4). These data are consistent with our in vivo experiments showing that neutrophil influx to ICs was impaired (Figure 3), whereas the inflammatory response to phorbol esters was normal (Figure 2, A–C), in *Prtn3⁻/⁻Ela2⁻/⁻* mice. To compare neutrophil priming in WT and *Prtn3⁻/⁻Ela2⁻/⁻* neutrophils, we analyzed cell surface expression of CD11b after 30 min of incubation at various concentrations of TNF-α and found no difference (Supplemental Figure 5). Moreover, we observed normal neutrophil adhesion to IC-coated surfaces (Supplemental Figure 6A) and unaltered phagocytosis of opsonized, fluorescently labeled *E. coli* bacteria (Supplemental Figure 6, B and C) in the absence of both proteases. We therefore hypothesized that PR3 and NE enhance early events of adhesion-dependent neutrophil activation after TNF-α priming and binding of ICs. It is important to note that *Ela2⁻/⁻* neutrophils were previously shown to react normally in the same setup (20). Regarding the highly similar cleavage specificities of both proteases, we suggested that PR3 and NE complemented each other during the process of neutrophil activation and inflammation.

Antiinflammatory PGRN is degraded by PR3 and NE during IC-mediated neutrophil activation. This reasoning prompted us to search for substrates that are processed by both PR3 and NE and are thereby able to enhance neutrophilic activation. In a previous study, PGRN was described as a potent inhibitor of the adhesion-dependent oxidative burst of human TNF-α–primed neutrophils in vitro, which can be inactivated by NE (23). Because we observed a substantial reduction in ROS production in *Prtn3⁻/⁻Ela2⁻/⁻* neutrophils compared with WT cells (Figure 4A), we evaluated a potential link between PGRN cleavage and oxidative burst of neutrophils activated by ICs. We analyzed the culture supernatant as well as the cellular pellet of IC-activated neutrophils for the presence of PGRN by IB (Figure 4C). Indeed, the inhibitory, intact form of PGRN was detected in the supernatant of *Prtn3⁻/⁻Ela2⁻/⁻* neutrophils only. We also found a cellular pool of PGRN in all genotypes that was more abundant in *Prtn3⁻/⁻Ela2⁻/⁻* cells than in WT or *Ela2⁻/⁻* neutrophils. This led us to conclude that PGRN was released and degraded by PR3 and NE during neutrophil activation.

PGRN inhibits neutrophil activation by ICs in vitro. To show that the reduced oxidative burst of *Prtn3⁻/⁻Ela2⁻/⁻* neutrophils can be caused by defective PGRN degradation, we evaluated the amount of cell-associated and secreted PGRN detected by IB (Figure 4C). We tested whether these concentrations inhibited the IC-mediated oxidative burst of WT neutrophils when added to the cells in vitro. Indeed, when 100 nM PGRN was applied to WT granulocytes activated by ICs, the ROS response markedly decreased (Figure 4D). In positive control experiments, activation of neutrophils was unaffected by PGRN application when they were stimulated with PMA (Figure 4E). These data endorse the inhibitory effect of intact PGRN on innate immune cell activation and prove that defective PGRN degradation may cause the reduced activation and oxidative burst of *Prtn3⁻/⁻Ela2⁻/⁻* neutrophils triggered by ICs.

Both PR3 and NE process PGRN in vitro. In previous studies, NE was proposed as the principal PGRN-converting protease (23). Our experiments revealed an equally important role of PR3 in this pathway, because *Ela2⁻/⁻* neutrophils were not impaired in
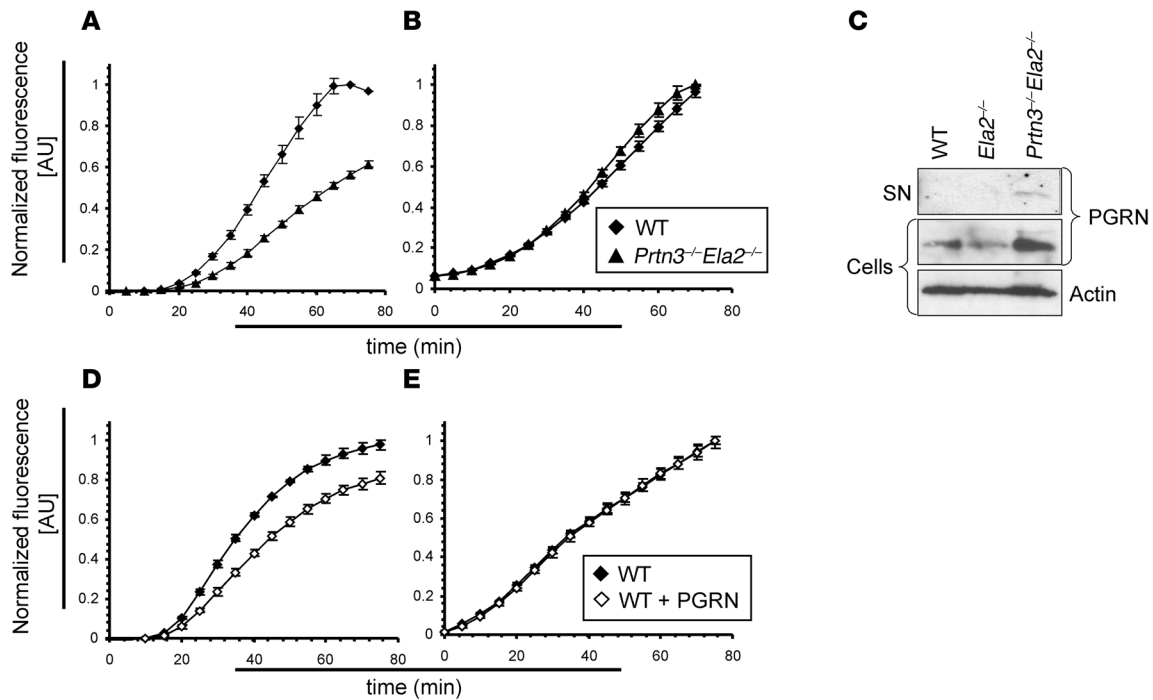
Figure 4
Impaired oxidative burst and PGRN degradation by IC-activated *Prtn3⁻/⁻Ela2⁻/⁻* neutrophils. Oxidative burst as the readout for neutrophil activation by ICs was measured over time. (**A**) While no difference was observed during the initial 20-min lag phase of the oxidative burst, *Prtn3⁻/⁻Ela2⁻/⁻* neutrophils exhibited diminished ROS production over time compared with WT neutrophils. (**B**) Bypassing receptor-mediated activation using 25 nM PMA restored the diminished oxidative burst of *Prtn3⁻/⁻Ela2⁻/⁻* neutrophils. Results are presented as normalized fluorescence in AU (relative to maximum fluorescence produced by WT cells). Data (mean ± SD) are representative of 3 independent experiments each conducted in triplicate. (**C**) Isolated mouse neutrophils were activated by ICs in vitro and tested for PGRN degradation by IB. In the cellular fraction, the PGRN (~80 kDa) signal was markedly increased in *Prtn3⁻/⁻Ela2⁻/⁻* cells compared with WT and *Ela2⁻/⁻* neutrophils. Intact PGRN was present in the supernatant (SN) of IC-activated *Prtn3⁻/⁻Ela2⁻/⁻* neutrophils only, not of WT or *Ela2⁻/⁻* cells. (**D** and **E**) Exogenous administration of 100 nM PGRN significantly reduced ROS production of neutrophils activated by ICs (**D**), but not when activated by PMA (**E**). Data (mean ± SD) are representative of 3 independent experiments each conducted in triplicate.

their degradation of PGRN (Figure 4C). We further substantiated this concept by incubating recombinant PGRN with the purified proteases in vitro. Both enzymes completely degraded PGRN as early as 5 min after incubation, although the pattern of lower–molecular weight cleavage products analyzed by silver-stained SDS-PAGE was not identical for both proteases (Figure 5, A and B). Hence, both PR3 and NE are potent converters of PGRN, indicating biological redundancy of the proteases in this process.

PR3 and NE are major PGRN-degrading enzymes of neutrophils. To evaluate the significance of PR3 and NE as PGRN-degrading enzymes, we next incubated recombinant mouse PGRN with neutrophil lysates from WT and protease-deficient mice. Anti-PGRN Western blot revealed that PGRN degradation was minimally reduced in the absence of NE, but strongly impaired when both PR3 and NE were lacking (Figure 5C). This observation demonstrates that PR3 and NE are major PGRN-converting enzymes of neutrophils, a finding supported by previous experiments showing that CG, the third NSP of primary granules, does not cleave PGRN (23).

PGRN inhibits IC-mediated inflammation in vivo. To provide in vivo evidence for the relevance of PGRN as an antiinflammatory mediator, we administered 2 μg recombinant PGRN to IC-mediated inflammation in mice. PGRN-treated lesions were directly compared with untreated lesions in the same mouse (Figure 6A). In both WT and *Prtn3⁻/⁻Ela2⁻/⁻* mice, neutrophil accumulation was diminished at the

PGRN-treated sites of IC-mediated inflammation, demonstrating that PGRN is a crucial inhibitory factor for neutrophilic inflammation. Neutrophil infiltration was reduced to a greater extent in *Prtn3⁻/⁻Ela2⁻/⁻* (40% reduction, $P < 0.01$; Figure 6C) than in WT mice (25% reduction, $P < 0.05$; Figure 6B), which likely reflected the impact of the PGRN-degrading proteases in this pathway.

PR3 and NE cleave PGRN during inflammation in vivo. Finally, we aimed to demonstrate defective PGRN degradation in *Prtn3⁻/⁻Ela2⁻/⁻* mice during neutrophilic inflammation in vivo. For practical reasons, we harvested infiltrated neutrophils from the inflamed peritoneum 4 h after casein injection and subjected the lysates of these cells to anti-PGRN Western blot. Intact, inhibitory PGRN was detected in *Prtn3⁻/⁻Ela2⁻/⁻* neutrophils, but not in WT cells (Figure 6D). These data prove that neutrophilic inflammation is accompanied by proteolytic removal of antiinflammatory PGRN and that the process of PGRN degradation is essentially impaired in vivo in the absence of PR3 and NE.

Discussion
Chronic inflammatory and autoimmune diseases are often perpetuated by continuous neutrophil infiltration and activation. According to the current view, the role of NSPs in these diseases is mainly associated with proteolytic tissue degradation after their release from activated or dying neutrophils. However, recent obser-
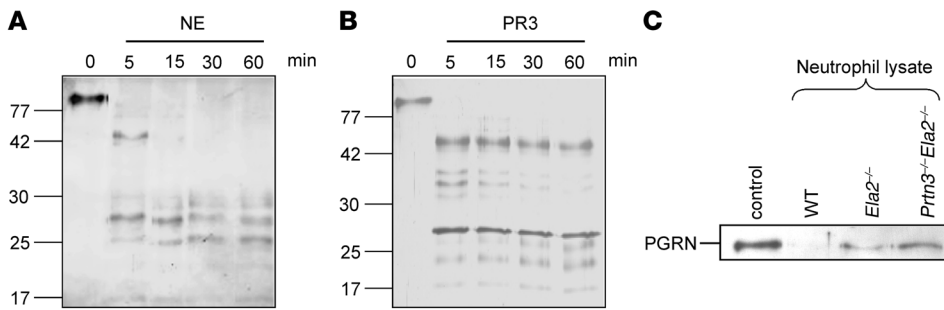
Figure 5
PR3 and NE are major PGRN processing enzymes of neutrophils. (**A** and **B**) Silver-stained SDS-PAGE analysis of recombinant human PGRN incubated at a 1:10 enzyme/substrate ratio with purified human NE (**A**) and recombinant mouse PR3 (**B**). Both NE and PR3 completely cleaved ~80-kDa PGRN to smaller molecular fragments within 5 min of incubation. (**C**) Recombinant mouse PGRN was incubated with neutrophil lysates from WT, *Ela2*−/−, and *Prtn3*−/−*Ela2*−/− mice for 1 h at 37°C and analyzed by anti-mouse PGRN Western blot. Compared with untreated PGRN (control), WT neutrophils completely degraded PGRN. In *Ela2*−/− neutrophils, a faint band of intact PGRN was detected, while in *Prtn3*−/−*Ela2*−/− neutrophils, a distinct PGRN band remained, comparable to control.

vations suggest that NSPs such as CG may contribute to noninfectious diseases in a more complex manner, namely as specific regulators of inflammation (18). Here, we demonstrate that PR3 and NE cooperatively fulfilled an important proinflammatory role during neutrophilic inflammation. PR3 and NE directly enhanced neutrophil activation by degrading oxidative burst–suppressing PGRN. These findings support the use of specific serine protease inhibitors as antiinflammatory agents.

Much attention has been paid to the degradation of extracellular matrix components by NSPs. We therefore expected that ablation of both PR3 and NE would cause impaired neutrophil extravasation and interstitial migration. Surprisingly, we found that the proteases were principally dispensable for these processes: *Prtn3*−/−*Ela2*−/− neutrophils migrated normally through a dense, 3-dimensional collagen matrix in vitro and demonstrated regular extravasation in vivo when phorbol esters were applied (Figure 2). This finding is in agreement with recent reports that neutrophils preferentially and readily cross the EBM through regions of low matrix density in the absence of NE (28).

Conversely, we observed that PR3 and NE were required for the inflammatory response to locally formed ICs (Figure 3). Even isolated *Prtn3*−/−*Ela2*−/− neutrophils were challenged in performing oxidative burst after IC stimulation in vitro (Figure 4A), showing that the proteases directly enhanced the activation of neutrophils also in the absence of extracellular matrix. However, when receptor-mediated signal transduction was bypassed by means of PMA, neutrophils from *Prtn3*−/−*Ela2*−/− mice performed normal oxidative burst (Figure 4B), indicating that the function of the phagocyte oxidase (phox) complex was not altered in the absence of PR3 and NE. These findings substantiate what we believe to be a novel paradigm: that all 3 serine proteases of azurophilic granules (CG, PR3, and NE), after their release in response to IC encounter, potentiate a positive autocrine feedback on neutrophil activation.

In contrast to CG, the highly related proteases PR3 and NE cooperate in the effacement of antiinflammatory PGRN, leading to enhanced neutrophil activation. Previous studies already demonstrated that PGRN is a potent inhibitor of the adhesion-dependent oxidative burst of neutrophils in vitro, which can be degraded by NE (23). Here, we showed that PR3 and NE play an equally important role

in the regulation of PGRN function. *Ela2*−/− neutrophils were sufficiently able to degrade PGRN. Only in the absence of both PR3 and NE was PGRN degradation substantially impaired, resulting in the accumulation of antiinflammatory PGRN during neutrophil activation in vitro (Figure 4C) and neutrophilic inflammation in vivo (Figure 6D). Moreover, we provided in vivo evidence for the crucial role of PGRN as an inflammation-suppressing mediator, because administration of recombinant PGRN potently inhibited the neutrophil influx to sites of IC formation (Figure 6, A–C). Hence, the cooperative degradation of PGRN by PR3 and NE is a decisive step for the establishment of neutrophilic inflammation.

The molecular mechanism of PGRN function is not yet completely understood, but it seems to interfere with integrin (CD11b/CD18) outside-in signaling by blocking the function of pyk2 and thus dampens adhesion-related oxidative burst even when added after the initial lag phase of oxidase activation (23). PGRN is produced by neutrophils and stored in highly mobile secretory granules (29). It was recently shown that PGRN can bind to heparan-sulfated proteoglycans (30), which are abundant components of the EBM and various cell surfaces, including those of neutrophils. Also, PR3 and NE are known to interact with heparan sulfates on the outer membrane of neutrophils, where the enzymes appear to be protected against protease inhibitors (12, 13, 31). These circumstantial observations support the notion that PGRN cleavage by PR3 and NE takes place at the pericellular microenvironment of the neutrophil cell surface.

Impaired outside-in signaling most likely reduced the oxidative burst in *Prtn3*−/−*Ela2*−/− neutrophils adhering to ICs. In support of this hypothesis, we excluded an altered response to TNF-α priming (Supplemental Figure 5) as well as reduced adhesion to immobilized ICs and defective endocytosis of serum-opsonized *E. coli* in *Prtn3*−/−*Ela2*−/− neutrophils (Supplemental Figure 6). MPO content and processing was also unchanged in *Prtn3*−/−*Ela2*−/− neutrophils (Figure 1D); hence, the previously discussed inhibitory effect of MPO on phox activity (32, 33) does not appear to be stronger in neutrophils lacking PR3 and NE. Because there was no difference in the lag phase of the oxidative burst, initial IC-triggered receptor activation was probably not affected by either PRGN or PR3/NE. Our concept is consistent with all these observations and takes into account that PGRN unfolds its suppressing effects in the second phase, when additional membrane receptors, endogenous PGRN, and some PR3/NE from highly mobile intracellular pools are translocated to the cell surface. The decline and cessation of ROS production suggested to us that outside-in signaling was not sustained and that active oxidase complexes were no longer replenished in the absence of PR3 and NE. Our present findings, however, do not allow us to exclude other potential mechanisms, such as accelerated disassembly of the active oxidase complex.

During cutaneous inflammation, PGRN is provided by multiple sources, including skin cells and neutrophils themselves, which produce and release PGRN as they infiltrate the tissue (21, 29).
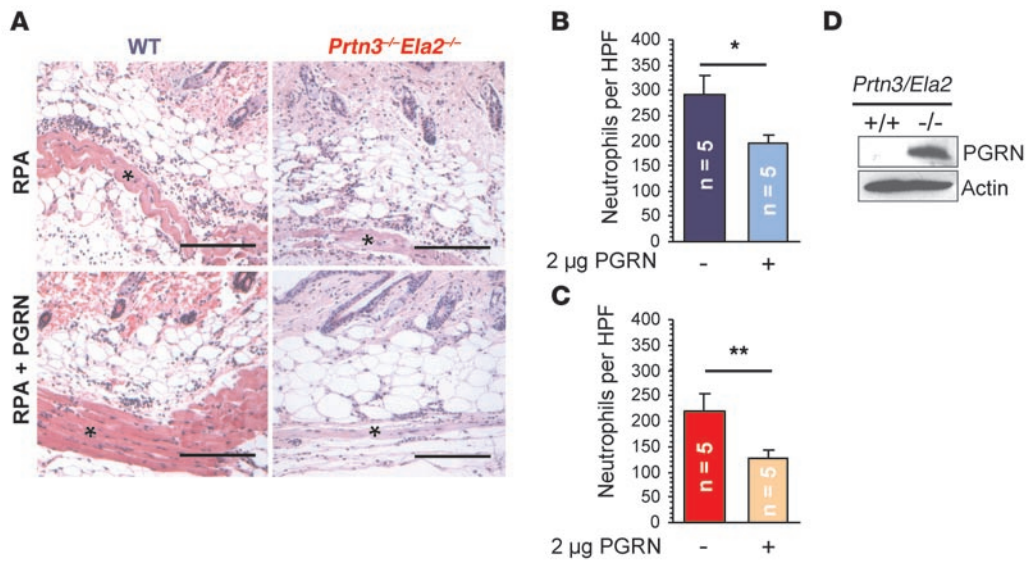
Figure 6
PGRN is a potent inhibitor of IC-stimulated inflammation in vivo. Recombinant mouse PGRN (2 μg) was intradermally applied with anti-OVA IgG, and the RPA was started in WT and *Prtn3⁻/⁻Ela2⁻/⁻* mice (n = 5 per group). (**A**) After 4 h, the effect of PGRN application was evaluated by histological analyses. Representative images show neutrophil infiltrates at the panniculus carnosus muscle (asterisks). Scale bars: 200 μm. (**B** and **C**) Effect of PGRN administration on neutrophil influx. In both WT (**B**) and *Prtn3⁻/⁻Ela2⁻/⁻* (**C**) mice, neutrophil infiltration was significantly diminished at PGRN-treated sites compared with untreated sites. This effect appeared to be more pronounced in the protease-deficient mice. Data are mean ± SEM infiltrated neutrophils per HPF. *$P < 0.05$; **$P < 0.01$. (**D**) Neutrophils isolated ex vivo from inflamed peritoneum of WT and *Prtn3⁻/⁻Ela2⁻/⁻* mice were analyzed by anti-mouse PGRN Western blot of concentrated neutrophil lysates. Intact PGRN was found abundantly in *Prtn3⁻/⁻Ela2⁻/⁻* but not WT neutrophils. Loading was controlled using anti-actin Western blot.

Thus, PGRN represents a prominent factor to control extravascular neutrophil function during skin inflammation. Proteolytic processing of PGRN was previously shown to generate GRN peptides that accumulate in inflammatory exudates, such as during casein-induced peritonitis (34). In contrast to the precursor PGRN, these GRN peptides might be proinflammatory and induce the release of neutrophil-attracting IL-8 from epithelial cells (23). In the absence of PR3 and NE, neutrophils are no longer able to provide the switch from inflammation-suppressing PGRN to proinflammatory GRN peptides. The activation of neutrophils by ICs is a decisive event in the cascade of reactions during the RPA. IC-activated neutrophils are known to release cytokines and chemokines and thus establish an inflammatory milieu. We hypothesize that the local persistence of PGRN dampens neutrophil activation and release of ROS as well as other inflammatory mediators in response to ICs, which results in diminished recruitment of further neutrophils in *Prtn3⁻/⁻Ela2⁻/⁻* mice. Hence, defective PGRN degradation can account for the impaired inflammation in the absence of PR3 and NE (Figure 7).

NSPs are strongly implicated as effector molecules in a large number of destructive diseases, such as emphysema or the autoimmune blistering skin disease bullous pemphigoid (14, 35–37). Normally, PR3/NE activity is tightly controlled by high plasma levels of α1-antitrypsin. This balance between proteases and protease inhibitors is disrupted in patients with genetic α1-antitrypsin deficiency, which represents a high risk factor for the development of emphysema and certain autoimmune disorders (38). The pathogenic effects of NSPs in these diseases have so far been associated with tissue destruction by the proteases after their release from dying neutrophils. Our findings showed that PR3 and NE were already involved in much earlier events of the inflammatory process, because the

enzymes directly regulated cellular activation of infiltrating neutrophils by degrading inflammation-suppressing PGRN. This concept is further supported by previous studies showing increased inflammation in mice lacking serine protease inhibitors such as SERPINB1 or SLPI (39, 40). Blocking PR3/NE activity using specific inhibitors therefore represents a promising therapeutic strategy to treat chronic, noninfectious inflammation. Serine protease inhibitors as anti-inflammatory agents can interfere with the disease process at 2 different stages, because they attenuate both early events of neutrophil activation and proteolytic tissue injury caused by released NSPs.

Methods
Mice. Simultaneous deficiency of the *Prtn3* and *Ela2* gene cluster in 129S6/SvEv mice was generated by homologous recombination in embryonic stem cells as detailed in Supplemental Methods. *Ela2⁻/⁻* mice on the 129S6/SvEv genetic background were previously generated (41) and were obtained as frozen embryos from the Medical Research Council Harwell (Oxford, United Kingdom). These and WT control mice were kept under pathogen-free conditions at the GSF Neuherberg (Munich, Germany). For most experiments, mice at 5–8 weeks of age were used. All animal experiments were performed with approval by the District Government of Upper Bavaria (Munich, Germany).

Characterization of Prtn3⁻/⁻Ela2⁻/⁻ mice. We analyzed the caseinolytic activity of neutrophil lysates from WT *Prtn3⁺/⁺Ela2⁺/⁺* mice, heterozygous *Prtn3⁺/⁻Ela2⁺/⁻* mice, and homozygous *Prtn3⁻/⁻Ela2⁻/⁻* mice by casein zymography. In short, 1.5 mg/ml casein (Sigma-Aldrich) was added to SDS polyacrylamide gels, and the lysate of $2.5 × 10^5$ cells per well was separated under nonreducing conditions at 4°C. Gels were then washed in PBS with 2.5% Triton X-100 followed by incubation overnight in Tris/HCl (pH 7.4), 10 mM CaCl₂, and 0.02% Brij 35. Gels were washed, stained with Coomassie blue, and destained in acetic acid.
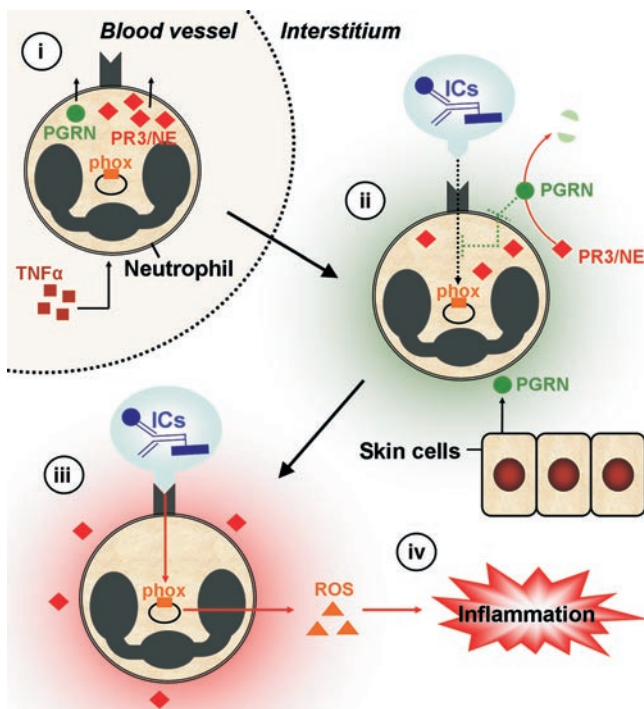
Figure 7
Proposed function of PR3 and NE in IC-mediated inflammation. TNF-α–primed neutrophils extravasate from blood vessels, translocate PR3/NE to the cellular surface, and discharge PGRN to the pericellular environment (i). During transmigration of interstitial tissues (ii), neutrophil activation is initially suppressed by relatively high pericellular levels of antiinflammatory PGRN (green shading), which is also produced locally by keratinocytes and epithelial cells of the skin. Until IC depots are reached, neutrophil activation is inhibited by PGRN. Surface receptors (e.g., Mac-1) recognize ICs, which results in signal transduction (black dotted arrow) and activation of the phox. The molecular pathway of PGRN-mediated inhibition is not completely understood, but it may interfere with integrin signaling after IC encounter (green dotted line inside the cell). Adherence of neutrophils to ICs (iii) further increases pericellular PR3 and NE activity. PR3 and NE cooperatively degrade PGRN in the early stage of neutrophilic activation to facilitate optimal neutrophil activation (red shading), resulting in sustained integrin signaling (red arrow) and robust production of ROS by the phox system. Subsequently, neutrophils release ROS together with other proinflammatory mediators and chemotactic agents, thereby enhancing the recruitment of further neutrophils and establishing inflammation (iv). In the absence of PR3/NE, the switch from inflammation-suppressing (ii) to inflammation-enhancing (iii) conditions is substantially delayed, resulting in diminished inflammation in response to ICs (iv).

To confirm the successful and specific knockout of PR3 and NE, we performed Western blot analyses of bone marrow–derived neutrophils. After reducing SDS-PAGE of neutrophil lysates and electrotransfer onto nitrocellulose, we probed the membranes with polyclonal rabbit sera specific for the granule serine enzymes PR3, NE, CG, and MPO as previously described (42).

To control normal neutrophil differentiation in *Prtn3$^{-/-}$Ela2$^{-/-}$* mice, peripheral blood neutrophils were characterized by flow cytometry using fluorescently labeled Gr-1– and CD11b-specific antibodies (BD Biosciences — Pharmingen) as previously described (25, 26). Blood smears were prepared and stained on glass slides according to the Diff-Quick protocol (Dade-Behring), and neutrophil morphology was analyzed by light microscopy. Differential blood leukocytes were identified by morphology and counted under the microscope to determine the percentage of each population. Moreover, the cell count per milliliter blood of each leukocyte population was determined using a hemocytometer (improved Neubauer chamber). For detailed descriptions of genetic characterization of *Prtn3$^{-/-}$Ela2$^{-/-}$* mice, see Supplemental Methods.

Recombinant and purified proteins. Recombinant mouse PR3 was produced and purified as previously described (43). Human NE was purchased from Elastin Products. Recombinant human PGRN was prepared as previously described (21). Recombinant mouse PGRN (aa 18–589) was produced with an N-terminal S-tag by transient expression into the supernatant of H5 insect cells using a modified pIEx-5 vector (Novagen; Merck) and the secretion signal of the adipokinetic hormone. Transfection of H5 insect cells cultured in TC-100 medium (Gibco; Invitrogen) was done using the Fugene HD transfection reagent (Roche) according to the manufacturer's instructions. At 6 days after transfection, the supernatant was harvested, and recombinant mouse PGRN was purified using an S-protein agarose column (Novagen; Merck). Following extensive washing of the column with PBS, the bound protein was eluted by 3 M magnesium chloride. Immediately thereafter, fractions were dialyzed against PBS and analyzed by silver-stained SDS-PAGE. Pure fractions were pooled and dialyzed against 20 mM ammonium bicarbonate, lyophilized, and stored at –80°C until use. For experiments, lyophilized protein was reconstituted in sterile PBS (Gibco; Invitrogen).

Skin inflammation models. Croton oil (Sigma-Aldrich) was diluted to 1% in acetone, and this dilution was topically applied to the ventral and the dorsal sides (20 μl each) of the ears of WT and *Prtn3$^{-/-}$Ela2$^{-/-}$* mice (n = 4 per group). After 4 h, mice were sacrificed by CO_2 inhalation. The earflap was split into 2 halves by carefully separating the dorsal and ventral skin. For histological analysis, dorsal and ventral halves of ears were subjected to whole-mount immunostaining. After fixation in paraformaldehyde, ear halves were blocked with 1% BSA (PAA Laboratories) in PBS for 1 h at room temperature, probed with biotin-labeled anti–Gr-1 (RB6-8C5; BD Biosciences — Pharmingen) to identify neutrophil granulocytes and anti–pan-laminin (L9393; Sigma-Aldrich) to visualize the EBM, diluted in 1% BSA in PBS overnight at 4°C (while shaking), and washed with 1% BSA in PBS. Antibodies were detected with a repeated cycle of staining with anti-rabbit Alexa Fluor 488 (Invitrogen) and anti-rat Cy3 (Dianova) before tissue was embedded in elvanol and representative images taken with a Zeiss Axio Imager equipped with an ApoTome (Zeiss). Location of neutrophils was analyzed in detail for potential accumulation at the basement membrane. For quantification of neutrophil influx, at least 3 images of the inflamed skin were taken using a ×10 objective to quantify total neutrophil infiltrates (calculated as the percentage of Gr-1 signal per microscopic field) using Metamorph software (Molecular Devices), while intravascular signal was excluded.

The RPA, a widely used model of IC-mediated inflammation, was induced in the skin of mice using OVA (grade V; Sigma-Aldrich) as the antigen and purified rabbit anti-OVA antibodies of the IgG class (Rockland Immunochemicals Inc.). Initially, the hair was removed from the ventral skin, and the area was cleaned with 70% alcohol. Anti-OVA IgG (2 μg/μl) was deposited intradermally in a volume of 30 μl using a 27-gauge needle. Intradermal injection of 30 μl unspecific polyclonal rabbit IgG (2 μg/μl; Sigma-Aldrich) served as a negative control in the same animal. Without delay, the antigen solution (OVA; 20 mg/kg body weight) was injected i.v. After 4 h, mice were sacrificed by CO_2 asphyxiation, and the inflammatory response was assessed by histology. Paraffin-embedded sections of the specimens were processed for H&E staining and analyzed by light microscopy for inflammatory cellular infiltrates. Neutrophils were additionally identified using Gr-1 immunohistochemistry. Briefly, deparaffinized tissue sections were incu-

bated with a rat anti–Ly-6G antibody (BD Biosciences — Pharmingen) followed by a biotinylated goat anti-rat antibody (BioGenex). Bound antibodies were labeled with streptavidin–alkaline phosphatase and visualized with fast red (BioGenex). Sections were counterstained with Mayer hematoxylin solution (Merck Eurolab). Random high-power fields (HPFs) of the lesions were photographed using a Leica DFC320 CCD camera (Leica) attached to a Zeiss Axioplan 2 microscope (Zeiss) with a ×10 objective. Digitized images were used to enumerate neutrophils as mean number per HPF in lesions from WT (n = 12), $Ela2^{-/-}$ (n = 13), and $Prtn3^{-/-}Ela2^{-/-}$ mice (n = 12).

To study the inhibitory capacity of PGRN on IC-stimulated inflammation, we deposited 2 μg recombinant mouse PGRN by intradermal injection together with 30 μl anti-OVA solution as described above. In the same mouse at different sites of the ventral skin, we intradermally applied anti-OVA alone and control IgG as positive and negative controls, respectively. The RPA was started by i.v. administration of OVA. Mice were sacrificed 4 h after initiation, and biopsies were taken to histologically quantify neutrophil infiltrates per HPF in PGRN-treated and untreated lesions from WT and $Prtn3^{-/-}Ela2^{-/-}$ mice (n = 5 per group).

Collagen gel chemotaxis assay. For migration assays, PureCol (INAMED) in 1× MEM (Sigma-Aldrich) and 0.4% sodium bicarbonate (Sigma-Aldrich) was mixed with cells in RPMI (Invitrogen) with 10% FCS (Invitrogen) at a 2:1 ratio, resulting in gels with a collagen concentration of 1.6 mg/ml. Neutrophils were primed by 10 ng/ml mouse TNF-α (Roche) for 15 min at 37°C. Final cell concentrations in the assay were 1.6×10^6 granulocytes per milliliter of gel. Collagen-cell mixtures were cast in custom-made migration chambers with a thickness of 0.5–1.0 mm. At 30 min after the assembly of the collagen fibers at 37°C, the gel surface was covered with 50 μl of 0.1 μg/ml C5a solution (R&D Systems). Pictures of migrating cells were taken every 20 s using a Zeiss Axioplan 2 light-field microscope (Zeiss), and stacks of images were used to generate time-lapse videos in .AVI format using Metamorph (Molecular Devices). Chemotactic parameters were calculated and visualized as plots by analyzing the acquired data with a Chemotaxis and Migration Tool plug-in (http://www.ibidi.de/applications/ap_chemo.html).

Isolation of mouse neutrophils. Mouse neutrophils were purified from the bone marrow using a discontinuous percoll gradient (Amersham Bioscience) as previously described (44). Neutrophil preparations were characterized by Gr-1 and CD11b (Mac-1) double immunostaining using flow cytometry and were found to be at least 80% pure. To isolate murine neutrophils ex vivo from an inflammatory environment, we injected 1 ml of a 9% sterile casein solution in PBS to induce peritonitis. At 4 h after injection, cells were harvested by peritoneal lavage using sterile PBS without Ca^{2+} or Mg^{2+} (Gibco; Invitrogen). Peritoneal cells were layered on a discontinuous histopaque 1119–1077 gradient (Sigma-Aldrich), and, after centrifugation for 30 min at 700 g, neutrophils were isolated from the 1.119–1.077 kg/l interphase. For anti-PGRN Western blots and PR3/NE activity assays, neutrophil lysates were prepared. In brief, neutrophils were lysed in 50 mM Tris/HCl (pH 7.4), 150 mM NaCl, 0.5 mM EDTA, and 0.5% nonidet by mechanical disruption using syringes with 27-gauge needles. Cell debris was pelleted by centrifugation. All steps were carried out at 4°C, and supernatant was frozen until used.

Neutrophil oxidative burst in vitro. To test neutrophil activation by ICs in vitro, we prepared immobilized ICs using an OVA/anti-OVA system as described previously (20). Isolated neutrophils were resuspended at a density of 2×10^6 cells/ml in phenol red–free RPMI (Gibco; Invitrogen) containing 10 ng/ml mouse TNF-α (Roche) and added to immobilized ICs. Activation by 25 nM PMA (Sigma-Aldrich) without TNF-α served as a positive control. We also determined the oxidative burst of neutrophils as a function of increasing PMA concentrations (0.1–50 nM) in order to define the concentrations that yield submaximal responses in mouse neutrophils. ROS production as the readout for neutrophil activation was detected using dihydrorhodamine 6G (catalog no. D633; Invitrogen) according to

the manufacturer's instructions, and the increase in fluorescence was measured over time with the fluorometer FLUOstar OPTIMA (BMG Labtech) at 37°C. For each time point, the IC-specific oxidative burst was determined by subtracting the mean fluorescence read on negative control coating from that on IC coating. To compare independent experiments, we normalized oxidative burst relative to maximum ROS production by WT neutrophils.

To examine the effect of PGRN on neutrophil activation in vitro, we first approximated the concentration of cell-associated and secreted PGRN in the absence of PR3/NE during IC-mediated neutrophil stimulation by comparison with the positive control band in anti-PGRN Western blot, estimated to be approximately 100 nM. We then added recombinant PGRN at a final concentration of 100 nM to isolated WT neutrophils stimulated by ICs or PMA. We compared the oxidative burst between PGRN-treated and untreated cells as described above.

Adhesion assay. Isolated neutrophils were labeled with Calcein AM (Invitrogen) and plated on ICs in the presence of 10 ng/ml TNF-α as previously described (20). In brief, wells were washed with PBS at the indicated time points, the number of adhering cells was determined using a fluorescence reader, and the percentage was calculated.

Phagocytosis assay. Neutrophil phagocytosis of opsonized, FITC-labeled *E. coli* was determined by flow cytometry using the Phagotest (Orpegen Pharma) according to the manufacturer's instructions, with some modifications. Briefly, 100 μl heparinized blood was incubated with 20 μl FITC-labeled *E. coli* suspension (10^9 bacteria/ml) and incubated for 30 min at 37°C. After washing and DNA staining (using DNA staining solution from the Phagotest kit), samples were analyzed by flow cytometry. Bacterial aggregates were excluded based on their lower DNA content, and neutrophil granulocytes were gated in the forward/side scatter analysis. Phagocytosis of FITC-labeled *E. coli* by neutrophil granulocytes was determined using the FL-1 channel regarding percentage as well as fluorescence intensity of phagocytosing cells.

Analysis of PGRN degradation. PGRN processing activity was tested with recombinant mouse PR3 and human NE each at a molar enzyme/substrate ratio of 1:10 according to the buffer conditions described by Zhu et al. (23). Recombinant human PGRN (2.5 μg) was added to enzymes and incubated at 37°C. At the time points indicated in the figures, samples were placed on ice, and the pattern of cleavage products was analyzed by reducing SDS-PAGE and subsequent silver staining.

To determine whether PGRN-degrading enzymes other than PR3 and NE existed in neutrophils, we incubated recombinant mouse PGRN with lysates from 3×10^4 WT, $Ela2^{-/-}$, and $Prtn3^{-/-}Ela2^{-/-}$ neutrophils for 1 h at 37°C. Samples were separated by SDS-PAGE and transferred onto nitrocellulose membranes. After incubation for 2 h in blocking buffer (5% fat-free dry milk in PBS/0.2% Tween-20), mouse PGRN was detected by Western blotting with sheep anti-mouse PGRN antibody (R&D Systems) at a concentration of 0.4 μg/ml and unspecific sheep IgG as a negative control (1 μg/ml; catalog no. I5131; Sigma-Aldrich). Bound antibodies were visualized using peroxidase-conjugated donkey anti-sheep Igs (1:10,000; Jackson ImmunoResearch Laboratories) and ECL reagents (Amersham Pharmacia). For actin detection, the membranes were incubated in a 1:5,000 dilution of anti-actin mouse monoclonal antibody (clone JLA-20; Calbiochem) followed by peroxidase-conjugated goat anti-mouse IgG and IgM incubation (1:10,000; Pierce) and subsequent ECL detection.

For detection of PGRN from neutrophils activated by ICs in vitro, we harvested the supernatant as well as the cellular pellet of isolated TNF-α–primed neutrophils after 3 h of IC stimulation. The concentrated supernatant as well as the cellular pellet of 2×10^5 IC-activated neutrophils was separated by reducing SDS-PAGE and subjected to anti-PGRN Western blotting as described above.

To analyze whether PGRN was cleaved by PR3/NE during inflammation in vivo, we harvested neutrophils from the inflamed peritoneum of WT

and *Prtn3*−/−*Ela2*−/− mice. Lysates were prepared from these cells as described above, but in the presence of 75 μg/ml PMSF and protease inhibitor cocktail (Calbiochem). Total lysates from 8×10^5 cells were subjected to anti-PGRN Western blotting, which was carried out as described above.

Statistics. All results are given as mean and SEM for data derived from different in vivo experiments and as mean and SD for data resulting from triplicate in vitro assays using isolated cells or cell lysates. Normal distribution of data sets was determined by the Kolmogorov-Smirnov test before we applied an unpaired Student's *t* test to compare 2 groups. Calculations were done using GraphPad Prism software. A *P* value less than 0.05 was considered statistically significant.

1. Nathan, C. 2006. Neutrophils and immunity: challenges and opportunities. *Nat. Rev. Immunol.* **6**:173–182.
2. Jancar, S., and Sanchez, C.M. 2005. Immune complex-mediated tissue injury: a multistep paradigm. *Trends Immunol.* **26**:48–55.
3. Ravetch, J.V. 1994. Fc receptors: rubor redux. *Cell.* **78**:553–560.
4. Belaaouaj, A., et al. 1998. Mice lacking neutrophil elastase reveal impaired host defense against gram negative bacterial sepsis. *Nat. Med.* **4**:615–618.
5. Belaaouaj, A., Kim, K.S., and Shapiro, S.D. 2000. Degradation of outer membrane protein A in Escherichia coli killing by neutrophil elastase. *Science.* **289**:1185–1188.
6. Reeves, E.P., et al. 2002. Killing activity of neutrophils is mediated through activation of proteases by K+ flux. *Nature.* **416**:291–297.
7. Segal, A.W. 2005. How neutrophils kill microbes. *Annu. Rev. Immunol.* **23**:197–223.
8. Weinrauch, Y., Drujan, D., Shapiro, S.D., Weiss, J., and Zychlinsky, A. 2002. Neutrophil elastase targets virulence factors of enterobacteria. *Nature.* **417**:91–94.
9. El Ouriaghli, F., et al. 2003. Neutrophil elastase enzymatically antagonizes the in vitro action of G-CSF: implications for the regulation of granulopoiesis. *Blood.* **101**:1752–1758.
10. Skold, S., Rosberg, B., Gullberg, U., and Olofsson, T. 1999. A secreted proform of neutrophil proteinase 3 regulates the proliferation of granulopoietic progenitor cells. *Blood.* **93**:849–856.
11. Bories, D., Raynal, M.C., Solomon, D.H., Darzynkiewicz, Z., and Cayre, Y.E. 1989. Down-regulation of a serine protease, myeloblastin, causes growth arrest and differentiation of promyelocytic leukemia cells. *Cell.* **59**:959–968.
12. Campbell, E.J., Campbell, M.A., and Owen, C.A. 2000. Bioactive proteinase 3 on the cell surface of human neutrophils: Quantification, catalytic activity, and susceptibility to inhibition. *J. Immunol.* **165**:3366–3374.
13. Owen, C.A., Campbell, M.A., Sannes, P.L., Boukedes, S.S., and Campbell, E.J. 1995. Cell surface–bound elastase and cathepsin-G on human neutrophils — a novel, nonoxidative mechanism by which neutrophils focus and preserve catalytic activity of serine proteinases. *J. Cell Biol.* **131**:775–789.
14. Shapiro, S.D. 2002. Neutrophil elastase - Path clearer, pathogen killer, or just pathologic? *Am. J. Respir. Cell Mol. Biol.* **26**:266–268.
15. Carden, D.L., and Korthuis, R.J. 1996. Protease inhibition attenuates microvascular dysfunction in postischemic skeletal muscle. *Am. J. Physiol.* **271**:H1947–H1952.
16. Hirche, T.O., Atkinson, J.J., Bahr, S., and Belaaouaj, A. 2004. Deficiency in neutrophil elastase does not impair neutrophil recruitment to inflamed sites. *Am. J. Respir. Cell Mol. Biol.* **30**:576–584.
17. Young, R.E., et al. 2004. Neutrophil elastase (NE)-deficient mice demonstrate a nonredundant role for NE in neutrophil migration, generation of proinflammatory mediators, and phagocytosis in response to zymosan particles in vivo. *J. Immunol.* **172**:4493–4502.
18. Pham, C.T. 2006. Neutrophil serine proteases: specific regulators of inflammation. *Nat. Rev. Immunol.* **6**:541–550.
19. Adkison, A.M., Raptis, S.Z., Kelley, D.G., and Pham, C.T. 2002. Dipeptidyl peptidase I activates neutrophil-derived serine proteases and regulates the development of acute experimental arthritis. *J. Clin. Invest.* **109**:363–371.
20. Raptis, S.Z., Shapiro, S.D., Simmons, P.M., Cheng, A.M., and Pham, C.T. 2005. Serine protease cathepsin G regulates adhesion-dependent neutrophil effector functions by modulating integrin clustering. *Immunity.* **22**:679–691.
21. He, Z., Ong, C.H., Halper, J., and Bateman, A. 2003. Progranulin is a mediator of the wound response. *Nat. Med.* **9**:225–229.
22. He, Z., and Bateman, A. 2003. Progranulin (granulin-epithelin precursor, PC-cell-derived growth factor, acrogranin) mediates tissue repair and tumorigenesis. *J. Mol. Med.* **81**:600–612.
23. Zhu, J., et al. 2002. Conversion of proepithelin to epithelins: roles of SLPI and elastase in host defense and wound repair. *Cell.* **111**:867–878.
24. Bateman, A., Belcourt, D., Bennett, H., Lazure, C., and Solomon, S. 1990. Granulins, a novel class of peptide from leukocytes. *Biochem. Biophys. Res. Commun.* **173**:1161–1168.
25. Fleming, T.J., Fleming, M.L., and Malek, T.R. 1993. Selective expression of Ly-6G on myeloid lineage cells in mouse bone-marrow — Rb6-8C5 Mab to granulocyte-differentiation antigen (Gr-1) detects members of the Ly-6 family. *J. Immunol.* **151**:2399–2408.
26. Hestdal, K., et al. 1991. Characterization and regulation of Rb6-8C5 antigen expression on murine bone-marrow cells. *J. Immunol.* **147**:22–28.
27. Arthus, M., and Breton, M. 1903. Cutaneous lesions produced by injections of horse serum in a rabbit anaphylactised by and for this serum. *C. R. Seances Soc. Biol. Fil.* **55**:1478–1480.
28. Wang, S., et al. 2006. Venular basement membranes contain specific matrix protein low expression regions that act as exit points for emigrating neutrophils. *J. Exp. Med.* **203**:1519–1532.
29. Lin, W.L., Zehr, C., Lewis, J., and Dickson, D.W. 2007. Progranulin is located in secretory granules and vesicles of neutrophils and macrophages by immunogold electron microscopy. *FASEB J.* **21**:A22.
30. Gonzalez, E.M., Mongiat, M., Slater, S.J., Baffa, R., and Iozzo, R.V. 2003. A novel interaction between perlecan protein core and progranulin — Potential effects on tumor growth. *J. Biol. Chem.* **278**:38113–38116.
31. Campbell, E.J., and Owen, C.A. 2007. The sulfate groups of chondroitin sulfate- and heparan sulfate-containing proteoglycans in neutrophil plasma membranes are novel binding sites for human leukocyte elastase and cathepsin G. *J. Biol. Chem.* **282**:14645–14654.
32. Locksley, R.M., Wilson, C.B., and Klebanoff, S.J. 1983. Increased respiratory burst in myeloperoxidase-deficient monocytes. *Blood.* **62**:902–909.
33. Rosen, H., and Klebanoff, S.J. 1976. Chemiluminescence and superoxide production by myeloperoxidase-deficient leukocytes. *J. Clin. Invest.* **58**:50–60.
34. Couto, M.A., Harwig, S.S., Cullor, J.S., Hughes, J.P., and Lehrer, R.I. 1992. eNAP-2, a novel cysteine-rich bactericidal peptide from equine leukocytes. *Infect. Immun.* **60**:5042–5047.
35. Shapiro, S.D., et al. 2003. Neutrophil elastase contributes to cigarette smoke-induced emphysema in mice. *Am. J. Pathol.* **163**:2329–2335.
36. Liu, Z., et al. 2000. The serpin alpha 1-proteinase inhibitor is a critical substrate for gelatinase B/MMP-9 in vivo. *Cell.* **102**:647–655.
37. Liu, Z., et al. 2000. A critical role for neutrophil elastase in experimental bullous pemphigoid. *J. Clin. Invest.* **105**:113–123.
38. Stoller, J.K., and Aboussouan, L.S. 2005. alpha 1-antitrypsin deficiency. *Lancet.* **365**:2225–2236.
39. Benarafa, C., Priebe, G.P., and Remold-O'Donnell, E. 2007. The neutrophil serine protease inhibitor serpinb1 preserves lung defense functions in Pseudomonas aeruginosa infection. *J. Exp. Med.* **204**:1901–1909.
40. Ashcroft, G.S., et al. 2000. Secretory leukocyte protease inhibitor mediates non-redundant functions necessary for normal wound healing. *Nat. Med.* **6**:1147–1153.
41. Tkalcevic, J., et al. 2000. Impaired immunity and enhanced resistance to endotoxin in the absence of neutrophil elastase and cathepsin G. *Immunity.* **12**:201–210.
42. Hirche, T.O., Gaut, J.P., Heinecke, J.W., and Belaaouaj, A. 2005. Myeloperoxidase plays critical roles in killing Klebsiella pneumoniae and inactivating neutrophil elastase: Effects on host defense. *J. Immunol.* **174**:1557–1565.
43. Pfister, H., et al. 2004. Antineutrophil cytoplasmic autoantibodies against the murine homolog of proteinase 3 (Wegener autoantigen) are pathogenic in vivo. *Blood.* **104**:1411–1418.
44. Lowell, C.A., Fumagalli, L., and Berton, G. 1996. Deficiency of Src family kinases p59/61(hck) and p58(c-fgr) results in defective adhesion-dependent neutrophil functions. *J. Cell Biol.* **133**:895–910.

Paper VII

Cdc42-dependent leading edge coordination is essential for interstitial dendritic cell migration

Tim Lämmermann, Jörg Renkawitz, Xunwei Wu, Karin Hirsch, Cord Brakebusch and Michael Sixt

---

Updated information and services can be found at:

http://bloodjournal.hematologylibrary.org/cgi/content/full/113/23/5703

Articles on similar topics may be found in the following *Blood* collections:

Plenary Papers (254 articles)
Phagocytes, Granulocytes, and Myelopoiesis (45 articles)

Information about reproducing this article in parts or in its entirety may be found online at:

http://bloodjournal.hematologylibrary.org/misc/rights.dtl#repub_requests

Information about ordering reprints may be found online at:

http://bloodjournal.hematologylibrary.org/misc/rights.dtl#reprints

Information about subscriptions and ASH membership may be found online at:

http://bloodjournal.hematologylibrary.org/subscriptions/index.dtl

Plenary paper

Cdc42-dependent leading edge coordination is essential for interstitial dendritic cell migration

Tim Lämmermann,[1] Jörg Renkawitz,[1] Xunwei Wu,[2] Karin Hirsch,[1] Cord Brakebusch,[2] and Michael Sixt[1]

[1]Hofschneider Group Leukocyte Migration, Department of Molecular Medicine, Max Planck Institute of Biochemistry, Martinsried, Germany; and [2]Biotech Research and Innovation Centre (BRIC), University of Copenhagen, Copenhagen, Denmark

Mature dendritic cells (DCs) moving from the skin to the lymph node are a prototypic example of rapidly migrating amoeboid leukocytes. Interstitial DC migration is directionally guided by chemokines, but independent of specific adhesive interactions with the tissue as well as pericellular proteolysis. Instead, the protrusive flow of the actin cytoskeleton directly drives a basal mode of locomotion that is occasionally supported by actomyosin contractions at the trailing edge to propel the cell's rigid nucleus. We here delete the small GTPase Cdc42 in DCs and find that actin flow and actomyosin contraction are still initiated in response to chemotactic cues. Accordingly, the cells are able to polarize and form protrusions. However, in the absence of Cdc42 the protrusions are temporally and spatially dysregulated, which leads to impaired leading edge coordination. Although this defect still allows the cells to move on 2-dimensional surfaces, their in vivo motility is completely abrogated. We show that this difference is entirely caused by the geometric complexity of the environment, as multiple competing protrusions lead to instantaneous entanglement within 3-dimensional extracellular matrix scaffolds. This demonstrates that the decisive factor for migrating DCs is not specific interaction with the extracellular environment, but adequate coordination of cytoskeletal flow. (Blood. 2009;113: 5703-5710)

Introduction

Cells of the hematopoietic lineage are fundamentally different from mesenchymal or epithelial cells. Many of them are not restricted to a specific tissue compartment, but rather circulate through the whole organism to perform surveillance or renewal functions. The difference between resident and mobile cells is reflected by the fact that mesenchymal and epithelial cells are constitutively adherent to specific extracellular substrates, whereas hematopoietic cells can flexibly accommodate their adhesive properties.[1] Dendritic cells (DCs) are excellent examples for both principles as their function relies on the switch from the sessile to the motile state.[2] The sessile immature DC samples antigens in peripheral tissues. Endogenous or exogenous danger signals trigger the differentiation into the motile state and at the same time induce the expression of the CC-chemokine receptor 7 (CCR7) that directionally guides the cells through the interstitium of the dermis and via the lymphatic vessels into the T-cell area of the lymph node.[3,4] In the T-cell area, DCs present the peripherally acquired antigens to naive T cells and upon cognate interaction instruct T-cell differentiation and proliferation. Acquisition of the motile state in DCs is accompanied by a functional deactivation of cell-cell adhesion and integrin receptors that allows the cells to detach from their substrates and move freely through the dermal interstitium.[5-7] Nonadhesiveness endows the cells with enormous flexibility as they become autonomous from the molecular composition of their environment and can directly follow soluble guidance cues like chemokines. We could recently show that nonadhesive DC migration in 3-dimensional (3D) environments can be driven solely by the protrusive flow of actin polymerization at the cell front, whereas actomyosin contractions of the trailing edge served to propel the nucleus through narrow

spaces.[7] Theoretic modeling confirmed that within confined environments actomyosin dynamics can directly drive cellular locomotion without requiring transmembrane force coupling via adhesion receptors.[8] The fact that 2-dimensional (2D) surfaces, as often used to study cell migration, cannot support such nonadhesive movement explains that cell biology has largely neglected the underlying mechanisms. The migration of leukocytes is likely to be more simplistic than that of adherent cells, as in 3D environments the sheer initiation and polarization of actin flow together with cortical shape changes likely explain most of its aspects.

The universally expressed small GTPases Rac, RhoA, and Cdc42 are commonly accepted to be the key switches determining cell shape.[9,10] One of their main functions is the coordination of the actin cytoskeleton and closely interrelated phenomena such as adhesion and microtubule dynamics. It is firmly established that the Rac family members are essential for actin polymerization and RhoA regulates actomyosin contractility.[10] Both effects have been demonstrated in DCs: Abolishing Rac activity in mature DCs by genetically deleting the 2 expressed isoforms Rac1 and Rac2 leads to rounding and concomitant immobility of the cells,[11] which is in line with completely abrogated actin polymerization dynamics. Blockade of RhoA downstream effectors leaves actin protrusion at the leading edge intact, but affects the trailing edge of mature DCs and neutrophils. Here, actomyosin contraction is required to perform squeezing contractions to propel the cell's rigid nucleus through small pores.[7]

The roles of Cdc42 are less clear cut and many functions such as filopodia formation appear to be cell type–specific.[12] The most conserved function of Cdc42 is the coordination of the polarity

module, and many cell types require Cdc42 to stabilize and maintain spatial and temporal asymmetries.[10,13] Morphologically, asymmetries usually manifest through the actin cytoskeleton, leading to diverse phenomena such as axon formation or apical basal orientation of epithelia.[14] In motile leukocytes, polarity determines the direction of movement, and accordingly loss of chemotactic path finding has been observed upon intervention with Cdc42 in neutrophils,[15,16] macrophages,[17] hematopoietic stem cells,[18] and *Drosophila melanogaster* hemocytes.[19]

The signaling pathways involved in Cdc42-dependent leukocyte polarization have been studied mainly in neutrophils. Here, a positive feedback loop has been described whereupon G protein–coupled receptor signaling the kinase PAK1 recruits the guanine nucleotide exchange factor αPIX, which activates Cdc42 that in turn positively regulates PAK1 activity.[20] In T cells, Cdc42 is activated by Rap1 and induces the Par polarity complex consisting of Par3, Par6, and PKCζ. This triggers Tiam1, which connects the Par polarity complex to Rap1 at sites of polarity initiation.[21] Although Cdc42 has not been deleted in DCs until now, studies using dominant-negative versions of the molecule revealed defects in the endocytotic pathway,[22] antigen presentation,[23] podosome formation,[24] and dendrite formation[25] of immature DCs.

Using DCs deficient for Cdc42, we here address the question of how coordination of actin flow influences migration. Whereas chemotactic movement of Cdc42-deficient DCs is only moderately impaired in 2D assays, it is completely abolished in the dermal interstitium. We show that the severe phenotype results from a defective coordination of multiple protrusions that leads to entanglement in the 3D fibrillar network. These findings demonstrate that the internal stabilization of polarity becomes increasingly important when the cells have to navigate through geometrically complex environments.

Methods

Animals

Conditional Cdc42[flox/flox] mice[26] were intercrossed with Mx1Cre transgenic mice[27] to generate Cdc42[flox/flox] Mx1Cre^{+/−} animals and kept on a mixed 129SV/C57BL/6 genetic background. Control animals were littermates (Cdc42[flox/flox] Mx1Cre^{−/−} or Cdc42[flox/+] Mx1Cre^{+/−}). At an age between 6 and 10 weeks, mice received a single intraperitoneal injection of 250 µg Poly (I)·Poly (C) (250 µg; GE Healthcare, Little Chalfont, United Kingdom), diluted in 0.5 mL phosphate-buffered saline (PBS). Mice were killed 10 to 14 days after injection. The mice were bred in a conventional animal facility at the Max Planck Institute of Biochemistry and according to the local regulations. Mouse breeding and all experimental procedures were approved by the Regierung von Oberbayern.

Dendritic cells

DCs were generated from flushed bone marrow (BM) suspension as previously described in detail.[7,28] At days 8 to 10 of culture, 200 ng/mL LPS (Sigma-Aldrich, Munich, Germany; *Escherichia coli* 0127:B8) was added for 24 hours, and subsequently the culture was depleted of remaining Gr-1^{+} contaminant cells. For depletion, cells were incubated with biotinylated antibodies against Gr-1 (RB6-8C5; BD Pharmingen, Heidelberg, Germany), followed by anti–biotin-microbead separation according to the manufacturer's protocol (Miltenyi Biotec, Bergisch Gladbach, Germany). The purified DCs were used for migration assays. To determine knockout efficiencies, DC lysates were loaded on 12% polyacrylamide gels for electrophoresis under reduced conditions and Western blotting. Cdc42 was detected with mouse anti–mouse Cdc42 antibody (clone 44; BD Transduction Laboratories, Heidelberg, Germany), and the loading control was

performed with rabbit anti–mouse actin antibody (A2066; Sigma-Aldrich). Bound primary antibodies were detected with anti–mouse or anti–rabbit horseradish peroxidase (HRP; both Bio-Rad, Hercules, CA) as secondary antibodies, followed by chemiluminescence with Western Lightning Reagent Plus (PerkinElmer, Boston, MA). Only DC batches without detectable Cdc42 signal were chosen for experiments. Maturation of DCs was analyzed by flow cytometry using antibodies against the mouse antigens: CD11c (HL3, FITC-conjugated), I-A/I-E (2G9), CD40 (3/23), CD86 (GL1; all PE-conjugated; all from BD Pharmingen), and CCR7 (PE-conjugated; eBiosciences, San Diego, CA) with the corresponding isotype controls.[7] Flow cytometric analysis was performed with a FACSCalibur and CellQuest Pro Software (BD Biosciences, San Diego, CA).

In vivo migration assay

Gr-1–depleted wild-type (WT) and Cdc42-deficient DCs were labeled with 3 µM cell-permeable Cell Trace Oregon Green 488 or 1 µM tetramethylrhodamine (TAMRA; both from Invitrogen, Karlsruhe, Germany), respectively, and vice versa. DCs (10^6) at a 1:1 ratio were suspended in 20 µL PBS and injected subcutaneously into the hind footpads of C57BL/6 mice. Forty-eight hours after injection, mice were killed by CO_2 suffocation, and popliteal lymph nodes were frozen in cryomatrix (Thermo, Pittsburgh, PA) and sectioned in 12-µm slices. To visualize the lymph node compartments, cryosections were methanol-fixed, blocked with 1% BSA in PBS, and stained with pan-laminin antibody (L9393; Sigma-Aldrich) and secondary antirabbit Cy5 (Dianova, Hamburg, Germany). Three different layers of the T-cell cortex of each lymph node were documented using an Axio Imager upright microscope (Zeiss, Jena, Germany). Quantification of DCs within the T-cell cortex was performed with MetaMorph (Molecular Devices, Ismaning, Germany). Using inverse thresholding, the greyscale images of both fluorescence channels were separately binarized. DCs appeared as dots that were quantified using the morphometric analysis tool. The ratio of migrated knockout DCs was calculated as the number of knockout cells divided by the total number of DCs in the T-cell cortex, with 0.5 as the value where 50% of knockout cells and 50% WT cells located in the center of the lymph node, and with 0 as the value where only WT cells located in the T-cell cortex of the lymph node.

Ex vivo migration assay

Ears of killed C57BL/6 mice were removed and mechanically split into dorsal and ventral halves. During separation, the dermis detached from the cartilage layer that remained on one of the halves. LPS-matured, BM-derived, magnetic-activated cell sorting (MACS)–purified, TAMRA-labeled DCs were resuspended in culture medium, added on top of the dermis, and incubated for 120 minutes at 37°C, 5% CO_2. For immunofluorescence stainings, ear sheets were then fixed with 1% paraformaldehyde, incubated with a rabbit polyclonal anti–LYVE-1 antibody (R&D Systems, Wiesbaden, Germany), washed with PBS, and stained with A488-conjugated anti–rabbit secondary antibody (Invitrogen). Images were obtained with a Leica DMIRE2 confocal microscope (objective HCX PL APO/40×/1.25-0.75 oil; Leica, Wetzlar, Germany). Merged z-stacks were generated with the Leica confocal software. For quantification of DC numbers within lymphatic vessels, z-stacks were 3D reconstructed, before the intersection of grayscale images from both fluorescence channels was determined, leaving only DCs within lymphatic vessels to be quantified by integrated morphometry analysis with MetaMorph.

In vitro migration assays

Three-dimensional collagen gel chemotaxis assays (Figure 6D) have been described earlier.[7] PureCol (INAMED, Fremont, CA) in 1× minimum essential medium eagle (Sigma-Aldrich) and 0.4% sodium bicarbonate (Sigma-Aldrich) was mixed with cells in RPMI (Invitrogen), 10% fetal calf serum (FCS; Invitrogen) at a 2:1 ratio, resulting in gels with a collagen concentration of 1.6 mg/mL. Final cell concentrations in the assay were 10^6 DCs/mL gel. Collagen-cell mixtures were cast in custom-made migration chambers with a thickness of 0.5 to 1 mm. After 30-minute assembly of the

collagen fibers at 37°C, the gels were overlayed with 50 μL of 0.6 μg/mL CCL19 (R&D Systems) diluted in RPMI/10% FCS.

For 3D collagen gel invasion assays (Figure 6A), 2.5 μg/mL CCL19 was added before polymerization of the 1.6 mg/mL collagen gel in a custom-made migration chamber. DCs (5×10^5) were placed on top of the collagen gel, and the chamber was incubated in an upright position for 8 hours at 37°C, 5% CO_2, before images were taken with an inverted Axiovert 40 (Zeiss).

Under-agarose chemotaxis assays (Figure 3A) have been performed as described elsewhere.[29] Briefly, 2.5% UltraPure agarose (Invitrogen) in distilled water was heated and mixed with 56°C prewarmed RPMI/20% FCS and 2× Hank buffered salt solution (Sigma-Aldrich) at a 1:2:1 ratio, resulting in an agarose concentration of 6.25 mg/mL. Two microliters of warm agarose-medium mixture was cast in 3.5-cm cell-culture dishes (BD Falcon, Franklin Lakes, NJ) and allowed to polymerize at room temperature. A responder hole (for DCs) was punched 1 mm from an attractor hole (for chemokine) into the agarose. After 30 minutes of equilibration at 37°C, 5% CO_2, 5×10^5 DCs were transferred into the responder hole and 1.2 μg/mL CCL19 was filled into the attractor hole. Time-lapse videomicroscopy was initiated when DCs started to migrate between the cell-culture plastic and the agarose. For under-agarose assays with homogenous chemokine (Figure 2A), 2.5 μg/mL CCL19 was added when the agarose-medium mixture cooled to 37°C before casting and polymerization. DC suspension (1 μL) was injected beneath the agarose with a fine pipette tip, and time-lapse videomicroscopy recording started immediately.

Low-magnification bright-field movies of 3D collagen chemotaxis assays and all agarose assays were recorded at indicated time intervals using inverted Axiovert 40 (Zeiss) cell-culture microscopes, equipped with custom-built climate chambers (5% CO_2, 37°C, humidified) and PAL cameras (Prosilica, Burnaby, BC) triggered by custom-made software (SVS Vistek, Seefeld, Germany). The objectives used were A-Plan 10×/0.25 Ph1 and LD A-Plan 20×/0.3 Ph1 (both Zeiss). Manual tracking was applied to 3D and under-agarose chemotaxis assays. DCs were tracked over 3 to 4 hours with ImageJ (National Institutes of Health [NIH], Bethesda, MD) and the Manual Tracking Plugin. Speed and directionality parameters were calculated and visualized as plots by analyzing the acquired data with the Chemotaxis and Migration Tool Plugin.

To visualize the 3D morphology of DCs migrating toward CCL19 in a 3D collagen gel (Figure 7A), DCs were labeled with 3.5 μM TAMRA (Invitrogen) and imaged with an inverted Zeiss Observer.Z1 microscope equipped with a Yokogawa spinning disc confocal scanhead, Coolsnap HQ2 camera (implemented by Visitron Systems, Pucheim, Germany) and a Plan-APOCHROMAT 40×/0.95 Korr oil objective (Zeiss). Images were 3D reconstructed in MetaMorph and processed with the Surpass Tool of the Imaris 4.0.6 software (Bitplane, Zürich, Switzerland).

Actin dynamics and total internal reflection microscopy

DCs were transfected with lifeact:GFP between days 8 and 10 of culture using the primary mouse T-cell kit and the Amaxa nucleoporator (Amaxa, Cologne, Germany).[30] Cells were transfected according to the manufacturer's recommendations, and immediately after transfection LPS was added for overnight maturation. The actin network of DCs migrating in an underagarose setting was visualized with an inverted Zeiss Axiovert 200M microscope equipped with a total internal reflection setup, Coolsnap HQ2 camera (both Visitron Systems) and a Plan-FLUAR 100×/1.45 oil objective (Zeiss). Images were taken every 2 seconds. Image analysis was performed with MetaMorph: protrusion and retraction of leading edge regions were presented as time montage after applying the background flattening tool. Actin dynamics were quantified by kymograph analysis, whereby the actin polymerization rate was calculated as the sum of the retrograde actin flow (as observed in some DCs) and the actin forward protrusion at the leading edge.

Statistics

After data were confirmed to fulfill the criteria, *t* tests were performed; otherwise, Mann-Whitney *U* tests were applied. Analyses were performed with Sigma Stat 2.03 (Systat, San Jose, CA).
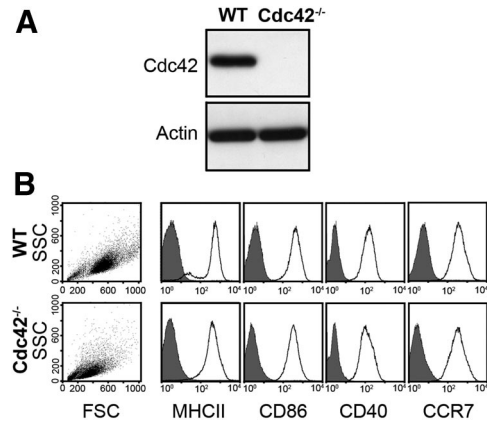

Figure 1. Knockout efficiency and maturation of Cdc42$^{-/-}$ dendritic cells. At day 8 of culture, bone marrow (BM)–derived dendritic cells (DCs) were matured with 200 ng/mL lipopolysaccharide for 24 hours and used for experiments. (A) Cdc42 expression was determined by Western blot analysis of wild-type (WT) and Cdc42$^{-/-}$ DC lysates. Actin expression was used as loading control. Cdc42$^{-/-}$ DCs with no detectable Cdc42 stain were chosen for experiments. (B) Size (dot plots) and maturation (histograms) of WT and Cdc42$^{-/-}$ DCs were analyzed by flow cytometric analysis. Expression of surface maturation markers on DCs (CD11c-positive cells) was detected with PE-labeled antibodies against MHCII, CD40, CD86, and CCR7 (white open curve) and corresponding isotype controls (gray closed curve). Representative result of independent DC cultures derived from BM of 4 WT and 4 Cdc42$^{-/-}$ mice.

Online supplemental material

Videos S1 through S6 and legends are available on the *Blood* website (see the Supplemental Materials link at the top of the online article).

Results

DC differentiation and maturation do not require Cdc42

We conditionally deleted Cdc42 in hematopoietic precursor cells by crossing mice carrying the conditional alleles with transgenics for the inducible Mx1 promoter–driven Cre recombinase.[26,27] We generated mature DCs in vitro from BM suspension of mice with induced knockout and obtained cells that were entirely negative for Cdc42 protein as tested by Western blotting (Figure 1A). The cells showed normal DC surface markers including high MHCII and costimulatory molecules and also normal expression levels of chemokine receptor CCR7 (Figure 1B). Cdc42-deficient (Cdc42$^{-/-}$) DCs had the typical veiled morphology, but were slightly smaller than WT DCs as revealed by the altered scatter profile in flow cytometry (Figure 1B). These findings show that Cdc42 deficiency does not prevent myelopoiesis and DC generation and maturation in vitro. Apart from their smaller size, immature Cdc42$^{-/-}$ DCs were severely impaired in the uptake of fluorescent dextran and also bacterial particles (data not shown), which is in agreement with previous reports that dominant-negative inhibition of Cdc42 function led to decreased endocytosis and phagocytosis.[22,31]

Symmetry-breaking in response to homogenous chemokine exposure

To observe the cells upon exposure to polarizing stimuli, we established an assay system that allowed us to follow the morphologic response of DCs by time-lapse video microscopy. As mature DCs are nonadherent,[6] we chose a setup where the cells are squeezed between a layer of agarose and a coverslip[29] (Figure 2A). The spatial constraint in this semi-3D setting caused flattening of the cells, leading to a "2D projection" that ideally suits to assess
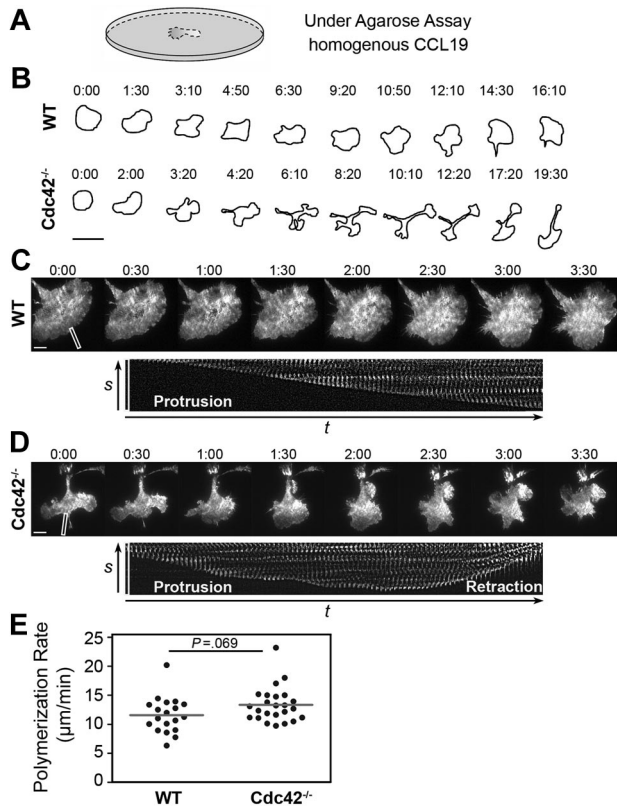
Figure 2. Actin polymerization and coordination at the leading edge of dendritic cells. (A) DCs were injected between a glass coverslip and a layer of agarose containing 2.5 μg/mL CCL19. This experimental setup served for studying the chemokinetic response and actin dynamics of DCs at 37°C, 5% CO_2 (in panels B-E). (B) Initial radial spreading, symmetry breaking, and subsequent polarization of DCs was recorded by time-lapse videomicroscopy. Morphology outlines of DCs were obtained by morphometric analysis (MetaMorph). A time sequence of a representative WT and Cdc42$^{-/-}$ DC is shown. Time (minutes:seconds). Scale bar represents 50 μm. Objective: LD A-Plan 20×/0.30 Ph1 (Zeiss). (C,D) WT (C) and Cdc42$^{-/-}$ (D) DCs were transfected with the actin marker lifeact:GFP and actin dynamics observed by TIRF microscopy over time. (Top panels) A time sequence of a representative entire cell is shown. Time (minutes:seconds). Scale bar represents 10 μm. Objective: Plan-FLUAR 100×/1.45 oil (Zeiss). (Bottom panels) Leading edge regions indicated by the white boxes were analyzed for phases of protrusion and/or retraction. After background flattening (MetaMorph), a time-lapse montage over 91 seconds (2 seconds/frame) presents the dynamics at the leading edge. (E) Quantification of the actin polymerization rate at the leading edge by kymograph analysis. Cells were derived from 2 independent BM DC cultures (of both WT and Cdc42$^{-/-}$ mice). Single cells (dots) were analyzed (line: mean, t test, $P = .069$, WT: n = 19, Cdc42$^{-/-}$: n = 24).

morphologic changes. When WT DCs were exposed to uniform concentrations of the CCR7-binding chemokine CCL19 (Figure 2B; Video S1), they underwent radial symmetrical expansion until after 2 to 3 minutes the disc shape was reached. This expansion was followed by sudden collapse of radial symmetry and segregation into a leading and a trailing edge, which was accompanied by locomotion. Although some WT cells developed multiple leading edges, the majority polarized along one randomly oriented axis. In Cdc42$^{-/-}$ DCs, expansion and symmetry breaking occurred equally, demonstrating that CCR7 signaling was intact and that polarization as such was not impaired. However, leading and trailing edge were rarely aligned along one axis. Instead, many cells developed multiple competing leading edges (Figure 2B; Video S1). These observations were in line with previous work demonstrating that Cdc42 regulates temporal and spatial stability of actin protrusions by either reinforcing one existing protrusion or suppressing the development of new protrusions.[32] This phenotype motivated us to

use Cdc42$^{-/-}$ DCs as a model system to study the role of actin flow polarization during locomotion.

Locally intact, but globally dysregulated, actin flow in Cdc42$^{-/-}$ DCs

Cdc42 is an upstream activator of Rac activity and was further shown to negatively affect RhoA activation in a neutrophil-like cell line.[16] Both effects might affect the protrusive and contractile aspects of the actin cytoskeleton. To characterize actin dynamics in Cdc42$^{-/-}$ DCs, we transfected the cells with lifeact:GFP, a recently described actin-binding peptide, that leaves actin dynamics unaffected and allows dynamic visualization of actin flow within the cells[30] (Figure 2C,D; Video S2). As an optical setup to image the cortical actin flow, we observed the transfected DCs under agarose with total internal reflection (TIRF) microscopy that excites exclusively the membrane-proximate 100 to 200 nm of the cell and allows high spatial and temporal resolution while phototoxic effects are minimized. In these assays, polarized WT DCs showed a continuous and expanding sheet of F-actin at the leading edge (Figure 2C), whereas retrograde flow was observed at the lateral aspects of the leading edge (data not shown). In line with our bright-field observations, the morphology of the actin cytoskeleton of Cdc42$^{-/-}$ DCs was altered, as many cells developed 2 and sometimes multiple competing leading edges (Figure 2D). Despite this global shape change, local actin flow at the leading edge did not significantly differ from WT cells: kymograph analysis showed that, on short timescale, polymerization rate and accordingly protrusion velocity were unaltered in the absence of Cdc42 (t test, $P = .069$; Figure 2E). As the persistence time of each protrusion was decreased, protrusion was frequently followed by phases of contraction and retrograde flow (data not shown). These findings show that locally actin protrusion and contraction can be initialized in the absence of Cdc42, meaning that a principal failure in Rac and RhoA activation is unlikely. It rather occurs that spatial and temporal coordination of actin dynamics is disturbed, leading to multiple competing, instead of one unifying, protrusions.

Chemotactic movement in Cdc42$^{-/-}$ DCs is moderately impaired in 2D

We next wanted to test whether this failure to coordinate protrusions affects chemotactic movement. A graded distribution of chemoattractant might preferentially trigger protrusion development toward the high concentration of attractant and, therefore, (partially) counteract the development of competing protrusions that we observed during spontaneous polarization.[33]

We exposed WT cells in the under-agarose assays to diffusion gradients of CCL19 (Figure 3A; Video S3), and observed directionally persistent chemotactic movement toward the chemokine source with single-cell velocities ranging between 5 and 15 μm/minutes and high directional persistence (Figure 3B-D). In Cdc42$^{-/-}$ DCs, median velocities were only moderately reduced (U test, $P < .001$) and cells still reached 80% of the WT values (Figure 3C). Although Cdc42$^{-/-}$ DCs still showed net movement toward the chemokine, directionality values dropped to 59% of the WT cells (t test, $P < .001$; Figure 3B,D). To test whether the decreased directionality was a consequence of impaired coordination of protrusions, we tracked the morphology of the chemotaxing DCs. To exemplify shape changes, we traced the outlines of single cells and displayed cellular morphology alongside instantaneous migration velocities (Figure 3E). Although chemotaxing WT DCs underwent constant shape change, the development of multiple
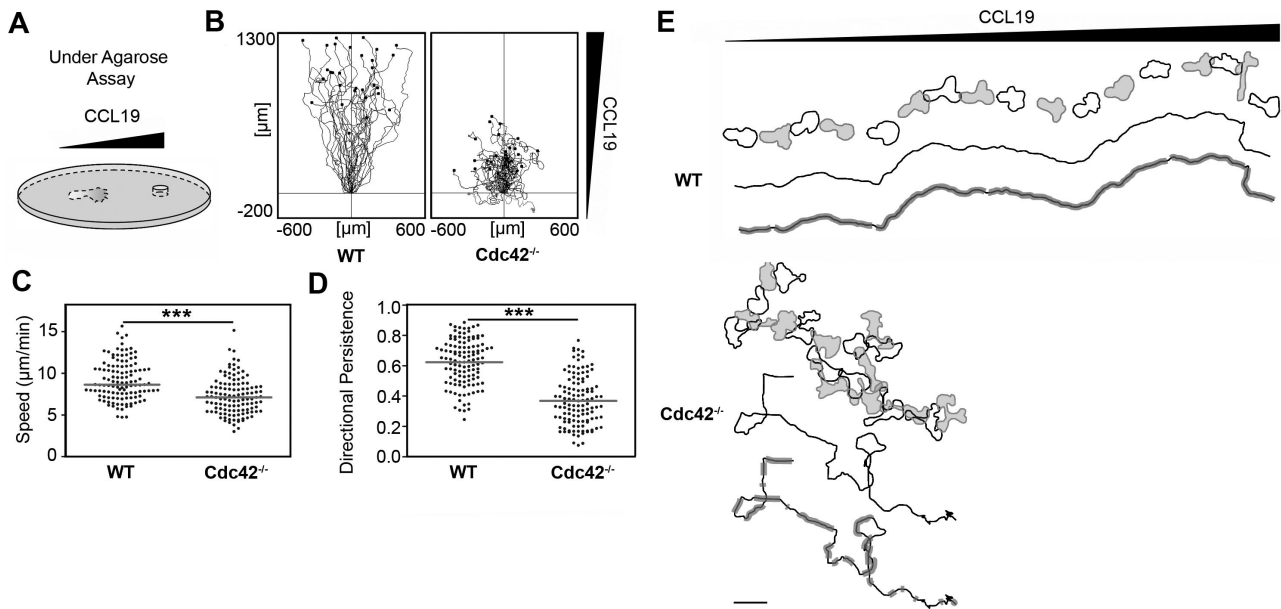
Figure 3. Directed migration of dendritic cells toward a CCL19 gradient in a planar under-agarose assay. (A) Analysis of DC chemotaxis in a planar under-agarose assay. DCs migrate beneath the agarose toward the 1-mm afar attractor hole containing 1.2 μg/mL CCL19. Directed migration at 37°C, 5% CO_2 was recorded by time-lapse videomicroscopy and analyzed with ImageJ software (in panels B-E). (B) Tracks of single DCs migrating toward a CCL19 gradient over 3 hours (n = 30 each). WT indicates wild-type. (C) Comparison of velocity (line: median, U test, $P < .001$) and (D) directionality (line: mean, t test, $P < .001$) of chemotaxing DCs. Cells were derived from 3 independent BM DC cultures (of both WT and Cdc42$^{-/-}$ mice) and applied to individual experiments. Forty single cells (dots) per experiment were tracked (WT: n = 120, Cdc42$^{-/-}$: n = 120). ***$P < .001$. (E) Correlation of morphology and migration tracks of representative single WT and Cdc42$^{-/-}$ DCs migrating along a CCL19 gradient. The top track shows outlines of DC morphology over time (WT: 82 minutes, Cdc42$^{-/-}$: 177 minutes). Morphology outlines of DCs were obtained by morphometric analysis (MetaMorph). The middle track (black line only) represents the migration track, whereas the bottom track indicates migration phases with instantaneous velocities over a threshold speed of 7 μm/minutes (gray shaded). Scale bar represents 50 μm. Objective: A-Plan 10×/0.25 Ph1 (Zeiss).

protrusions was rarely observed. Whenever protrusions branched, retraction of the deviating protrusion occurred almost instantaneously, leading to no significant deceleration of the cell. In addition, Cdc42$^{-/-}$ DCs showed phases of high velocities during which they resembled WT cells (Figure 3E, gray-shaded track phases). These phases were frequently interrupted by episodes where the cells displayed multiple competing leading edges, which caused either spinning behavior or complete migratory arrest. Occasionally, multipolar cells even underwent self-fragmentation when multiple protrusions migrated in different directions (data not shown).

Taken together, the graded distribution of chemokine could not compensate for the coordination defect of Cdc42$^{-/-}$ DCs, and the ability of chemotaxing cells to unify the actin flow in one protrusion was impaired. Importantly, this defect led only to slightly diminished migration velocities. Chemotactic migration was still possible in the vertically confined, but horizontally open, 2D setting of the under-agarose assay, albeit directionality was decreased due to the development of competing leading edges.

In vivo migration of Cdc42$^{-/-}$ DCs is completely abolished

Having defined the coordination defect of Cdc42$^{-/-}$ DCs in vitro, we wanted to test how the phenotype manifests in vivo. Bone marrow–derived DCs are well suited for this purpose, as injection into the dermis of mice results in in vivo migration toward the draining lymph node. In an internally controlled experiment, we injected Cdc42$^{-/-}$ DCs together with differentially labeled WT DCs into the footpads of mice and monitored their arrival in draining lymph nodes (Figure 4A). Strikingly, arrival in the T-cell area was completely abolished in the Cdc42$^{-/-}$ cells, and we could not detect even trace amounts of these cells either in the sinus area or in the T-cell cortex of the lymph node (Figure 4B,C). This drastic phenotype was somewhat in contrast with our under-agarose assay and raised the question at which level migration was blocked. This

could be movement in the dermal interstitium, entry into the lymphatic vessels, or transport toward the node.

To distinguish between a possible block of interstitial migration and impaired entry into the lymphatic vessels, we directly observed the DCs upon entry into the dermal compartment. To this end we used "crawl-in" assays where labeled BM-derived DCs were layered on exposed dermis of explanted murine ear sheets (Figure 5A). This technique allowed us to monitor dermal movement and lymphatic entry of DCs as the lymphatic vessels were visualized with fluorescent staining against LYVE-1. After 2-hour incubation, WT DCs localized within the lymphatic vessels, whereas Cdc42$^{-/-}$ DCs appeared randomly distributed (Figure 5B,C; Video S4). To
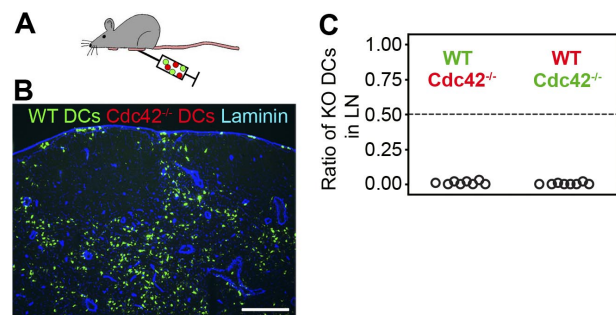

Figure 4. Analysis of in vivo dendritic cell migration from the skin via the lymphatic vessels to the lymph node. (A) Wild-type and Cdc42$^{-/-}$ DCs were labeled with TAMRA (red) or Oregon Green 488 (green), and a 1:1 mixture was injected subcutaneously into the hind footpads of C57BL/6 mice and arrival in the popliteal lymph node (LN) was analyzed 48 hours later. (B) Immunofluorescence microscopy (Axio Imager; Zeiss) of 12-μm-thick LN cryosections. Counterstaining against laminin (Cy5, blue) distinguishes B-cell follicles (B) and T-cell cortex (T). Scale bar represents 200 μm. Objective: EC Plan-NEOFLUAR 10×/0.3 (Zeiss). (C) Quantification of immunofluorescence analysis. Three different layers of the T-cell cortex of each LN were documented and quantified by morphometric analysis (MetaMorph). Dotted line at 0.5: 50% of DCs that migrated into the LN are Cdc42$^{-/-}$ DCs. Circles indicate single experiments (1 LN).
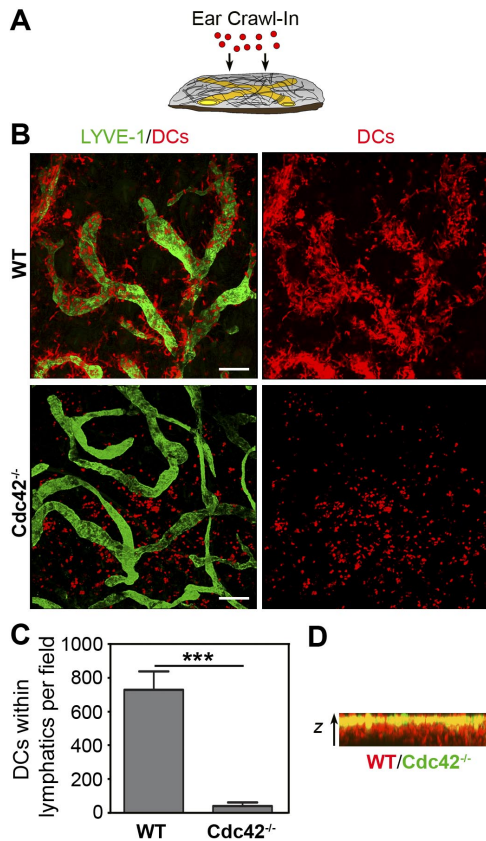
Figure 5. Analysis of ex vivo dendritic cell migration in a dermal ear explant. (A) Ears of C57BL/6 mice were separated into halves and mature DCs placed on top of the dermis. Two hours after addition of TAMRA-labeled DCs (red dots) and incubation at 37°C, 5% CO_2, entry of DCs into deep lymphatics was analyzed (in panels B-D). (B top row) Wild-type and (bottom row) Cdc42$^{-/-}$ DCs were placed on dermal ear explants in separate experiments. One percent PFA-fixed ear sheets were counterstained with anti–LYVE-1 antibody (green) to detect lymphatic vessels in the dermis. The images represent merged z-stacks (WT: 18 planes, 1.1 μm z-steps; Cdc42$^{-/-}$: 24 planes, 1.3 μm z-steps) obtained by confocal microscopy (Leica DMIRE2). Scale bars represent 100 μm. Objective: HCX PL APO/40×/1.25-0.75 oil (Leica). (C) Quantification of immunofluorescence analysis. Cells were derived from 2 independent BM DC cultures (of both WT and Cdc42$^{-/-}$ mice). Single DC cultures were applied to 3 C57BL/6 ears, confocal z-stacks 3-dimensional (3D) reconstructed, and the number of DCs within lymphatics calculated by morphometric analysis (mean ± SD; t test, $P < .001$, WT: n = 6, Cdc42$^{-/-}$: n = 6). ***$P < .001$. (D) Side view of the ear dermis (z = 50 μm) after addition of a 1:1 mixture of WT (red) and Cdc42$^{-/-}$ (green) DCs.

narrow down the anatomic site where migration was blocked, we recorded confocal z-stacks of the dermis. In an internally controlled experiment, we found that Cdc42$^{-/-}$ DCs remained on the surface of the tissue, whereas WT cells deeply penetrated the dermis where the lymphatic vessels are buried (Figure 5D). These data demonstrate the complete incapability of Cdc42$^{-/-}$ DCs to infiltrate the interstitial meshwork despite their principal ability to perform chemotactic movement.

Configuration, not molecular composition, of the environment leads to abrogated migration

Our previous data made it unlikely that the incapability to infiltrate the dermal interstitium was caused by a defect in chemokine sensing. Furthermore, the finding that DCs can migrate in the absence of adhesive interactions with the tissue[7] argued against Cdc42$^{-/-}$ DCs being unresponsive to other cues of the dermal interstitium, such as extracellular matrix molecules. Hence, we explored the option that not the composition but the geometry of the environment could prevent entry of Cdc42$^{-/-}$ DCs.
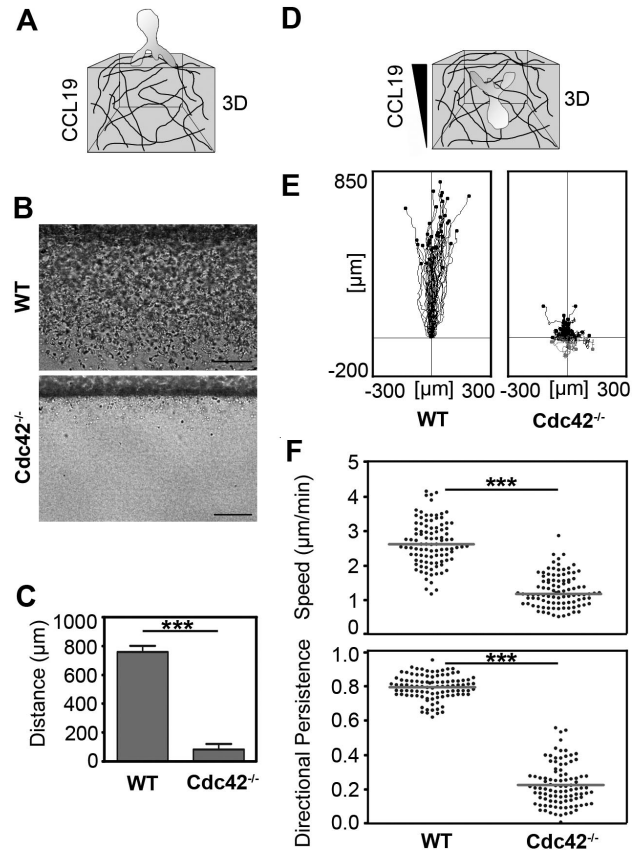

Figure 6. Directed migration of dendritic cells toward a CCL19 gradient in 3D collagen gels. (A) Three-dimensional in vitro setup to study DC tissue invasion (in panels B,C). DCs were layered on top of a polymerized 1.6 mg/mL collagen gel containing 2.5 μg/mL CCL19 and incubated at 37°C, 5% CO_2. After 8 hours, DC invasion into the gel was analyzed. (B) Images of WT and Cdc42$^{-/-}$ DC invasion were obtained by bright-field microscopy (inverted Axiovert 40; Zeiss). Scale bar represents 200 μm. Objective: A-Plan 10×/0.25 Ph1 (Zeiss). (C) Cells were derived from 2 independent BM DC cultures (of both WT and Cdc42$^{-/-}$ mice). Single DC cultures were applied on top of 6 collagen gels and the distance of DC migration into the gel was measured (mean ± SD, t test, $P < .001$, WT: n = 12, Cdc42$^{-/-}$: n = 12). ***$P < .001$. (D) Three-dimensional in vitro setup to study DC interstitial migration. DCs were added to 1.6 mg/mL collagen, followed by fiber assembly for 30 minutes at 37°C. Polymerized gels were overlaid with 0.6 μg/mL CCL19. DC migration at 37°C, 5% CO_2 was recorded for 4 hours by time-lapse videomicroscopy and analyzed with ImageJ software (in panels E,F). (E) Tracks of single DCs migrating toward a CCL19 gradient in 3D (n = 40 each). (F) Comparison of velocities (line: median, U test, $P < .001$) and directionality (line: mean, t test, $P < .001$) of DCs chemotaxing in 3D collagen matrices. Cells were derived from 2 independent BM DC cultures (of both WT and Cdc42$^{-/-}$ mice) and applied to individual experiments. Fifty single cells (dots) per experiment were tracked (WT: n = 100, Cdc42$^{-/-}$: n = 100). ***$P < .001$.

To simulate a complex fibrillar scaffold in the absence of the diverse dermal interstitial matrix molecules, we used 3D collagen gels as migration substrates. We showed previously that collagen gels are excellent substrates for chemotactic DC movement and that, like in vivo, the migration in these assays is independent of adhesion receptors.[7] We modified the previously described collagen gel chemotaxis assay to test for the invasive potential of DCs and layered WT and Cdc42$^{-/-}$ DCs on top of collagen gels that contained CCL19 (Figure 6A). Wild-type cells quickly invaded the gels, whereas Cdc42$^{-/-}$ DCs strictly remained on top of the gel and invasion was virtually abolished (t test, $P < .001$; Figure 6B,C). This indicated that the sheer configuration of the extracellular environment rendered the mutant cells unable to enter.

We next "forced" the cells into the gels by incorporation into the collagen scaffold before exposure to a CCL19 gradient (Figure 6D; Video S5). In line with the invasion assays, WT cells vigorously
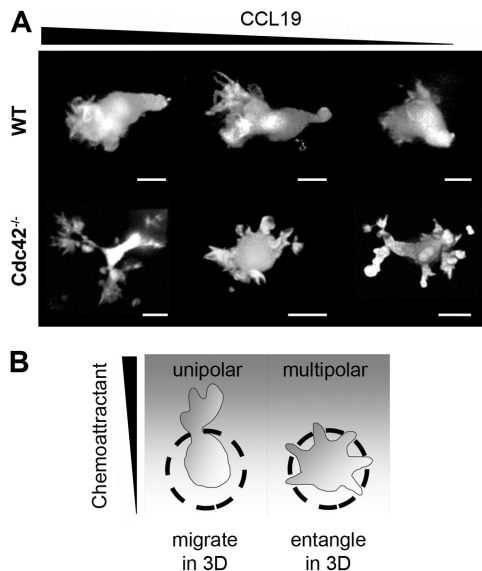
Figure 7. Morphology of migrating dendritic cells in 3D collagen gels and concluding scheme. (A) TAMRA-labeled DCs were added to 1.6 mg/mL collagen, followed by fiber assembly for 30 minutes at 37°C. Polymerized gels were overlaid with 0.6 μg/mL CCL19. After 60 minutes, snapshots of DCs migrating at 37°C, 5% CO_2 in the 3D collagen gel toward CCL19 were obtained by spinning disc confocal microscopy. DC morphologies result from 3D reconstruction of confocal stacks (MetaMorph) and Surpass processing with Imaris software. Scale bars represent 5 μm. Objective: Plan-APOCHROMAT 40×/0.95 Korr oil (Zeiss). (B) Concluding scheme about the decisive role of coordinated actin protrusions for leukocyte migration in complex 3D environments.

moved along the chemokine gradient, whereas Cdc42$^{-/-}$ DCs had a drastically reduced migration perimeter (Figure 6E). When we visualized the cells in high resolution within the gels, it became apparent that in the absence of Cdc42 the ability to move long distances was completely abolished as the cells simultaneously sent protrusions in all directions (Figure 7A; Video S6). Such behavior naturally leads to an entanglement of the cell in the dense meshwork. Accordingly, median migration velocities of Cdc42$^{-/-}$ DCs in collagen gels dropped to 44% compared with WT DCs (U test, $P < .001$) and directional persistence was reduced to 25% (t test, $P < .001$; Figure 6F).

Taken together, our 3D in vitro results completely resemble the severe in vivo migration defect and demonstrate that a loss of Cdc42-mediated coordination of protrusive actin flow leads to DC trapping in fibrillar networks. We interpret the data as the logical 3D extension of the moderate phenotype in the 2D context of the under-agarose assay, which permits unrestricted movement in the horizontal dimension as no physical barriers exist.

Discussion

Our previous findings showed that interstitial leukocyte migration is nonadhesive and driven mainly by shape changes of the cortical actin network and protrusive flowing of the leading edge.[7] Hence, it appears especially essential to gain more knowledge how cytoskeletal regulation affects locomotion in hematopoietic cells. We show here that depletion of Cdc42 in DCs results in a defect of global cytoskeletal coordination, whereas, locally, actin polymerization and actomyosin contraction remains intact. In cells migrating on 2D surfaces, this defect manifests as tumbling and 41% reduction of directional persistence, although the cells still reach 80% of the velocities of their WT counterparts. These findings are in line with

previous in vitro 2D migration studies that show intact chemokinesis, but impaired chemotaxis in macrophages,[17] neutrophil granulocytes,[15] and T lymphocytes[34] expressing dominant-negative mutants of Cdc42. The phenotype also resembles the phenotype of Cdc42$^{-/-}$ fibroblastoid cells, which show unimpaired migration speed during wound closure, while directionality is mildly affected.[35]

Surprisingly, the mild manifestation of the phenotype we observed in the 2D assays is qualitatively different in vivo where migration is almost completely arrested. As DCs migrate in the absence of adhesive interactions, it is unlikely that the different phenotypes result from distinct migration substrates in the 2D in vitro assays versus the interstitium of the dermis. We rather think that it is entirely due to the spatial configuration of the environment. This conclusion is supported by our finding that we also observed arrested migration in 3D collagen gels, which mimic the geometry of the dermis but not its complex molecular composition. This raises the question why increasing geometric complexity of the environment demands more tightly coordinated cytoskeletal protrusions. DCs and most other quickly migrating leukocytes do not use path-generating mechanisms such as pericellular proteolysis during migration in 3D environments.[36] They rather move along the path of least resistance and—if at all—they transiently deform their environment by squeezing contractions of the cell rear.[7] Hence, for a leukocyte, the interstitial environment can be described as a complex array of fixed pores (scheme, Figure 7B). The migratory process is a series of decisions to traverse the "most-promising" pore, which mechanistically means to funnel all actin flow into one cellular protrusion. In this scenario, indecisiveness is extremely problematic, as multiple protrusions lead to entanglement. The geometric complexity of the interstitium compared with the unrestricted environment of the 2D assay explains why the decision problem of Cdc42$^{-/-}$ DCs shows different manifestations in vivo and in vitro. In this study, we did not investigate in detail how Cdc42 regulates the decisive process of actin flow coordination. However, there is a large body of literature involving Cdc42 in molecular feedback loops that promote the stable formation of one leading protrusion while competing protrusions are suppressed.[37]

Interestingly, observations similar to our 2D findings were made in hemocytes of *Drosophila* embryos after blocking of Cdc42 activity by dominant-negative inhibition: when the chemotaxing cells were tracked in vivo, the inhibited cells reached velocities that were even higher than their WT counterparts but the directional persistence was diminished.[19] Although these observations in the 3D environment of a living fly embryo are contradictory with our 3D data at first sight, they are explainable, as animals with an exoskeleton lack an interstitial matrix scaffold.[38] Like in the unrestricted 2D assays, entanglement in the nonfibrillar environment appears unlikely, as a cellular or viscous tissue probably allows deformation by the cytoskeletal forces of the hemocyte.

So far, in vivo data on the effects of Cdc42 depletion in murine leukocytes are limited to a study showing that Cdc42$^{-/-}$ hematopoietic stem cells are severely impaired in their BM homing and retention capacity.[18] By investigating DC migration in a physiologic context, we show here that tight regulation of polarized actin is decisive for leukocyte migration in the interstitium. Our findings underline the importance of considering the extracellular context when investigating cell migration—even in cells locomoting independent of the molecular composition of the tissue. We further think that the cellular polarity module might be a promising target

to influence the interstitial migration of DCs or other types of leukocytes.

Acknowledgments

Authorship

Contribution: T.L. and M.S. designed experiments and wrote the paper; J.R. and K.H. helped with experiments; and X.W. and C.B. generated and contributed Cdc42$^{flox/flox}$ mice.

Conflict-of-interest disclosure: The authors declare no competing financial interests.

Correspondence: Michael Sixt, Max Planck Institute of Biochemistry, Am Klopferspitz 18, 82152 Martinsried, Germany; e-mail: sixt@biochem.mpg.de.

References

1. Friedl P. Prespecification and plasticity: shifting mechanisms of cell migration. Curr Opin Cell Biol. 2004;16:14-23.

2. Randolph GJ, Angeli V, Swartz MA. Dendritic-cell trafficking to lymph nodes through lymphatic vessels. Nat Rev Immunol. 2005;5:617-628.

3. Alvarez D, Vollmann EH, von Andrian UH. Mechanisms and consequences of dendritic cell migration. Immunity. 2008;29:325-342.

4. Förster R, Davalos-Misslitz AC, Rot A. CCR7 and its ligands: balancing immunity and tolerance. Nat Rev Immunol. 2008;8:362-371.

5. Schwarzenberger K, Udey MC. Contact allergens and epidermal proinflammatory cytokines modulate Langerhans cell E-cadherin expression in situ. J Invest Dermatol. 1996;106:553-558.

6. van Helden SF, Krooshoop DJ, Broers KC, Raymakers RA, Figdor CG, van Leeuwen FN. A critical role for prostaglandin E2 in podosome dissolution and induction of high-speed migration during dendritic cell maturation. J Immunol. 2006; 177:1567-1574.

7. Lämmermann T, Bader BL, Monkley SJ, et al. Rapid leukocyte migration by integrin-independent flowing and squeezing. Nature. 2008;453:51-55.

8. Hawkins RJ, Piel M, Faure-Andre G, et al. Pushing off the walls: a mechanism of cell motility in confinement. Phys Rev Lett. 2009;102:058103.

9. Etienne-Manneville S, Hall A. Rho GTPases in cell biology. Nature. 2002;420:629-635.

10. Heasman SJ, Ridley AJ. Mammalian Rho GTPases: new insights into their functions from in vivo studies. Nat Rev Mol Cell Biol. 2008;9: 690-701.

11. Benvenuti F, Hugues S, Walmsley M, et al. Requirement of Rac1 and Rac2 expression by mature dendritic cells for T cell priming. Science. 2004;305:1150-1153.

12. Wang L, Zheng Y. Cell type-specific functions of Rho GTPases revealed by gene targeting in mice. Trends Cell Biol. 2007;17:58-64.

13. Etienne-Manneville S. Cdc42: the centre of polarity. J Cell Sci. 2004;117:1291-1300.

14. Nelson WJ. Adaptation of core mechanisms to generate cell polarity. Nature. 2003;422:766-774.

15. Srinivasan S, Wang F, Glavas S, et al. Rac and Cdc42 play distinct roles in regulating PI(3,4,5)P3 and polarity during neutrophil chemotaxis. J Cell Biol. 2003;160:375-385.

16. Van Keymeulen A, Wong K, Knight ZA, et al. To stabilize neutrophil polarity, PIP3 and Cdc42 augment RhoA activity at the back as well as signals at the front. J Cell Biol. 2006;174:437-445.

17. Allen WE, Zicha D, Ridley AJ, Jones GE. A role for Cdc42 in macrophage chemotaxis. J Cell Biol. 1998;141:1147-1157.

18. Yang L, Wang L, Geiger H, Cancelas JA, Mo J, Zheng Y. Rho GTPase Cdc42 coordinates hematopoietic stem cell quiescence and niche interaction in the bone marrow. Proc Natl Acad Sci U S A. 2007;104:5091-5096.

19. Stramer B, Wood W, Galko MJ, et al. Live imaging of wound inflammation in Drosophila embryos reveals key roles for small GTPases during in vivo cell migration. J Cell Biol. 2005;168:567-573.

20. Li Z, Hannigan M, Mo Z, et al. Directional sensing requires G beta gamma-mediated PAK1 and PIX alpha-dependent activation of Cdc42. Cell. 2003; 114:215-227.

21. Gérard A, Mertens AE, van der Kammen RA, Collard JG. The Par polarity complex regulates Rap1- and chemokine-induced T cell polarization. J Cell Biol. 2007;176:863-875.

22. Garrett WS, Chen LM, Kroschewski R, et al. Developmental control of endocytosis in dendritic cells by Cdc42. Cell. 2000;102:325-334.

23. Shurin GV, Tourkova IL, Chatta GS, et al. Small rho GTPases regulate antigen presentation in dendritic cells. J Immunol. 2005;174:3394-3400.

24. Burns S, Thrasher AJ, Blundell MP, Machesky L, Jones GE. Configuration of human dendritic cell cytoskeleton by Rho GTPases, the WAS protein, and differentiation. Blood. 2001;98:1142-1149.

25. Swetman CA, Leverrier Y, Garg R, et al. Extension, retraction and contraction in the formation of a dendritic cell dendrite: distinct roles for Rho GTPases. Eur J Immunol. 2002;32:2074-2083.

26. Wu X, Quondamatteo F, Lefever T, et al. Cdc42 controls progenitor cell differentiation and beta-catenin turnover in skin. Genes Dev. 2006;20: 571-585.

27. Kühn R, Schwenk F, Aguet M, Rajewsky K. Inducible gene targeting in mice. Science. 1995;269: 1427-1429.

28. Lutz MB, Kukutsch N, Ogilvie AL, et al. An advanced culture method for generating large quantities of highly pure dendritic cells from mouse bone marrow. J Immunol Methods. 1999;223: 77-92.

29. Heit B, Kubes P. Measuring chemotaxis and chemokinesis: the under-agarose cell migration assay. Sci STKE. 2003;170:PL5.

30. Riedl J, Crevenna AH, Kessenbrock K, et al. Lifeact: a versatile marker to visualize F-actin. Nat Methods. 2008;5:605-607.

31. Caron E, Hall A. Identification of two distinct mechanisms of phagocytosis controlled by different Rho GTPases. Science. 1998;282:1717-1721.

32. Wedlich-Söldner R, Li R. Spontaneous cell polarization: undermining determinism. Nat Cell Biol. 2003;5:267-270.

33. Charest PG, Firtel RA. Feedback signaling controls leading-edge formation during chemotaxis. Curr Opin Genet Dev. 2006;16:339-347.

34. del Pozo MA, Vicente-Manzanares M, Tejedor R, Serrador JM, Sanchez-Madrid F. Rho GTPases control migration and polarization of adhesion molecules and cytoskeletal ERM components in T lymphocytes. Eur J Immunol. 1999;29:3609-3620.

35. Czuchra A, Wu X, Meyer H, et al. Cdc42 is not essential for filopodium formation, directed migration, cell polarization, and mitosis in fibroblastoid cells. Mol Biol Cell. 2005;16:4473-4484.

36. Wolf K, Müller R, Borgmann S, Bröcker EB, Friedl P. Amoeboid shape change and contact guidance: T-lymphocyte crawling through fibrillar collagen is independent of matrix remodeling by MMPs and other proteases. Blood. 2003;102: 3262-3269.

37. Wedlich-Söldner R, Li R. Yeast and fungal morphogenesis from an evolutionary perspective. Semin Cell Dev Biol. 2008;19:224-233.

38. Fessler JH, Fessler LI. Drosophila extracellular matrix. Annu Rev Cell Biol. 1989;5:309-339.